

Role of cyclooxygenase-2 in  
ischemia-reperfusion injury in the liver

PhD Thesis Marina Fuertes Agudo

PhD Thesis



2023

**ibv** INSTITUTO DE  
BIOMEDICINA DE  
VALENCIA CSIC



UNIVERSITAT  
POLITÈCNICA  
DE VALÈNCIA

# Role of cyclooxygenase-2 in ischemia-reperfusion injury in the liver

PhD Thesis  
**Marina Fuertes Agudo**

PhD Supervisors:  
Dr. Marta Casado Pinna  
Dr. Paloma Martín Sanz

April, 2023

**ibv**







UNIVERSITAT  
POLITÀCNICA  
DE VALÈNCIA



INSTITUTO DE  
BIOMEDICINA DE  
VALENCIA CSIC

Universitat Politècnica de València

PhD Program in Biotechnology

# **Role of cyclooxygenase-2 in ischemia- reperfusion injury in the liver**

PhD Thesis presented by

**Marina Fuertes Agudo**

PhD Supervisors

**Dr. Marta Casado Pinna**

**Dr. Paloma Martín Sanz**

April, 2023





UNIVERSITAT  
POLITÈCNICA  
DE VALÈNCIA



INSTITUTO DE  
BIOMEDICINA DE  
VALENCIA CSIC

Dr. Marta Casado Pinna, Principal Researcher at the Instituto de Biomedicina de Valencia (IBV) of the Consejo Superior de Investigaciones Científicas (CSIC), Dr. Paloma Martín Sanz, Principal Researcher at the Instituto de Investigaciones Biomédicas “Alberto Sols” (IIB), of the Consejo Superior de Investigaciones Científicas (CSIC) and the Universidad Autónoma de Madrid (UAM) and Dr. María Adelaida García Gimeno, Professor at the Universitat Politècnica de València (UPV),

CERTIFY:

That Marina Fuertes Agudo has completed the doctoral thesis entitled “Role of COX-2 in ischemia-reperfusion injury in the liver” at the Instituto de Biomedicina de Valencia (IBV) under their supervision (Dr. Marta Casado y Dr. Paloma Martín, co-directors) and tutoring (Dr. María Adelaida García), within the PhD programme in Biotechnology of the Universitat Politècnica de València (UPV).

Dr. Marta Casado  
Pinna

Director

Dr. María Adelaida  
García Gimeno

Tutor

Dr. Paloma Martín  
Sanz


Director



---

This work has been carried out with the financial support of the Spanish Ministry of Science and Innovation (SAF2016-75004R and PID2019-108977RB-100), the CIBERehd (Centro de Investigaciones Biomédicas En Red de Enfermedades Hepáticas y Digestivas) and the COST Action (CA15203 - Mitochondrial mapping: Evolution - Age - Gender - Lifestyle - Environment (MITOEAGLE)).

Marina Fuertes Agudo benefited from a pre-doctoral FPI contract (BES-2017-081928) associated with the SAF2016-75004R project. She spent 3 months in the laboratory of Dr. Pau Sancho Bru at the Institut d'Investigacions Biomèdiques August Pi I Sunyer (IDIBAPS, Barcelona, Spain) funded by a short stay grant awarded by the CIBERehd and 3 months in the laboratory of Dr. Anne Dubart Kupperschmitt and Dr. Jean Charles Duclos Vallée at the Institut Nationale de la Santé et la Recherche Médicale (INSERM, Villejuif, France) funded by a short stay grant awarded by the European Molecular Biology Organisation (EMBO, SEG\_9771).

*El trencadís de la portada representa un tall histològic d'una lesió isquèmica hepàtica; i és un homenatge a les ciutats de Barcelona i València, on m'he format i m'han vist créixer com a científica.* 



# ACKNOWLEDGEMENTS





Después de 5 intensos años, ha llegado el momento de hacer balance y poner en un mismo lugar no solo el resultado del trabajo de todo este tiempo, también mencionar a todos los que me han ayudado para llegar hasta aquí. Como dirían los *Manel*, “ens ha costat Déu i ajuda, arribar fins aquí”. Y yo no creo en Dios, pero ayuda sí he tenido. Y mucha. Creed a todo aquel que os diga que una tesis no se hace sola, porque, como voy a dejar claro en este apartado, no le falta ni una pizca de razón.

En primer lugar, quiero darle las gracias a Marta y a Paloma, mis directoras de tesis y las responsables de que me pase el día hablando de COX por donde vaya. Marta, gracias por acogerme en tu laboratorio, darme la oportunidad de crecer, creer en mí y en mis capacidades, aun cuando yo no creía mucho en ellas, y por darme siempre el punto de vista optimista que a mí me falta.

También quiero agradecer el apoyo al laboratorio UPME, pero muy especialmente a Carme. Has sido un apoyo increíble este tiempo, creo que has sido la persona en la que más he confiado ciegamente en el laboratorio, todas mis dudas (o la gran mayoría) se resolvían cuando iba a preguntarte. Si se me ha pegado una cuarta parte de tu pasión por la ciencia, tu rigor y tu profesionalidad en el trabajo, me doy por supersatisfecha. Ha sido un placer trabajar contigo.

Aunque el laboratorio ha sido siempre pequeñito, no solo he tenido a Carme de compañera. Gracias a todos los compis que habéis pasado por él, durante más o menos tiempo, todos me habéis aportado mucho y os recuerdo a todos con gran cariño. Víctor, has sido como un hermanito pequeño en el lab, me has acompañado en las tristezas y penurias del Oroboros y nos hemos acompañado en largas tardes de ordenador. ¡Te echo mucho mucho mucho de menos! Flavia, mi primera compi de labo, aunque coincidimos poco tiempo ha quedado claro que nuestra amistad caló fuerte. Fue un placer volver a reencontrarte en París después de tanto tiempo. Ya sabes que siempre va a haber una ración de paella valenciana esperándote. María, gracias por traer un poquito de sur al laboratorio. Ha sido un gusto compartir labo contigo, y te deseo lo mejor, ya verás que al final todo sale. Ana y tus visitas veraniegas, a veces para experimentos exprés, a veces solo para dejar unos alfajores, gracias por tus

consejos y ánimos. Rocío, un gran apoyo en la distancia, me hubiera encantado haber compartido más tiempo en el mismo lab, has sido una parte imprescindible de esta tesis y te agradezco mucho tu esfuerzo y dedicación. Y a Omar y Dani, gracias obviamente por vuestro trabajo, pero sobre todo por la última charla que hizo encajar todas las piezas. Eternamente agradecida.

La ciencia es un trabajo en equipo y la verdad, el equipo de todo el IBV es estupendo y os tengo que dar las gracias a todas y cada una de las personas que hacéis que el centro funcione y tire adelante. Es un gusto trabajar rodeada de gente amable y simpática que te saluda una, dos y tres veces al día si hace falta, que está dispuesta a echar una mano y devolver favores. Y, aunque quien más quien menos ha participado en algún momento de mi tesis, quiero hacer una especial mención a todo el equipo del laboratorio USN porque creo que han sido las que más me han aguantado pidiendo favores, aprendiendo técnicas con ellas, prestándome reactivos o simplemente escuchando mis quejas. Muchas gracias Mireia, Rosa, Ángela, Lorena, Teresa, Belén, Marcos y Eva. Y especialmente, gracias a mi tutora Ada. A ti un GRACIAS en mayúsculas. Porque más allá de tus tareas como tutora (imprescindibles, ha quedado claro), has sido un gran apoyo, me has escuchado en mis momentos de caos y desesperación y me has dado de los mejores consejos que he recibido para la tesis y para la vida. Estoy muy orgullosa de que hayas sido mi tutora y de haber recibido tu apoyo y entrega.

No quiero dejar de agradecer su trabajo a todo el servicio del animalario, el servicio de limpieza (especial gracias a Pili y Patri, qué buenos ratos echábamos en los almuerzos), seguridad, mantenimiento, informática y biblioteca. El IBV funciona gracias a vosotros.

Moltes gràcies al Pau Sancho, per haver-me acollit al seu laboratori durant la meva primera estada. No va ser una època fàcil (finals de 2020...), però vaig aprendre moltíssim i em vaig sentir molt ben acollida. I naturalment, gràcies al grup de “loquers”, Júlia, Raquel, Andrea, Celia, Bea i Sílvia. Tinc un molt bon record d’aquells dies tot i que només vam poder fer-nos un parell de birres en 3 mesos!!!!

Merci aussi à Anne DK, qui m'a ouvert les portes de son laboratoire pendant mon deuxième stage. Merci de m'avoir accueillie et enseignée, et de m'avoir donné l'occasion de découvrir d'autres façons de travailler. Merci à toute l'équipe, Eléonor, Meriem, Anne-Charlotte, Marwa et Nassima, je me suis sentie comme l'une d'entre vous dès le premier jour. And of course, thank you Antonietta, my favourite italian girl. I owe you all the good times I had in Paris. From the first coffee you offered me, the gym sessions, the hours on the L2 or in the office, you made me feel like home. You know you have Valencia and a race waiting for you. Grazie mille bellina.

El IBV me ha regalado grandes personas que me llevo ya para toda la vida. Miguel, hermano de tesis, gracias por tus tupperes, tus capacidades culinarias, tus *treats* y mensajes de ánimo y por estar siempre que lo he necesitado. Ana, gracias por convertirme en mi compi de piso, mi hombro en el que llorar (literal), mi cómica personal, mi bebesita y mi mejor amiga. Raquel, vas arrelar en mi i ja t'hi quedaràs per sempre. No em cansaré de dir-ho, però tant de bo la vida ens torni a fer coincidir en temps i espai. Y gracias a todos los demás con los que he compartido gran parte de estos años y que ya se han convertido en amigos para siempre: Carla, Rafa, Isabel, Alicia, Paco, Anmol, Juanju, Lúdia, David, Málina, Esther, Stefano, Lucía, Malu y Laura. Gracias por proponer incansablemente planes, cerves, cenas..., ¡necesitaría otra vida para que me diera tiempo a llegar a todo! Gracias porque le dais sentido a la locura esta que es la tesis.

Gracias a mis chumis, mis primeros amigos en Valencia. Aunque no sabíais a quién ibais a meter en el piso (la verdad, fuisteis demasiado confiados), al final parece que os convencí para que me adoptarais en vuestro grupito y ahora ya no hay marcha atrás. *Once a chumi, always a chumi*. Carlos, Alberto, Jordi, David y Álvaro, sois geniales y tenéis un sitio en mi corazoncito para siempre.

A la persona que em va regalar aquests primers amics i la raó per la qual soc una valenciana més, el meu estimat amic Nando, moltes gràcies. Ets la persona amb qui més ric i només puc dir-te que et vull sempre a la meva vida.

Y por supuesto, si agradezco a Nando sus risas, tengo que agradecer al grupo que hace que estas risas se multipliquen por mil cuando nos juntamos. Y es que es sorprendente cómo después de tantos años aún nos reíamos como el primer día, y lo que es peor, ¡¡de las mismas cosas!! Por favor, no cambies nunca porque como ya dije un día, y lo mantengo, me dais los años que el doctorado me quita. David, Carlos, Ana G, Ana D, Irene, Cris y Nando, que por muy lejos que estemos, os he sentido y os siento siempre cerca, gracias bonitos míos.

Gràcies a tots els meus amics d'Andorra, que encara que no ens veiem tant com m'agradaria, hi sou quan us necessito i quan ens ajuntem feu com si no hagués passat el temps. Laura, Olga, Noe, Mario, Arnau, Pere, Uri, Judith i Rosa. Gràcies Alba per compartir amb mi aquesta aventura que és la tesis, pels ànims i suport mutu. I també gràcies a les meves potentorres Ainoha, Marta i Natàlia. Gràcies per tots els bons moments, però sobretot pel viatge a Dènia. On hi hagi un arròs al senyoret, un matinar per agafar lloc a la platja, una bona sessió de postureig i un "o te unes o te apartas", que es tregui la resta. Sou la xarxa que em fa sentir segura.

Al grupo que me ha adoptado más recientemente, pero que me ha acogido como una más desde el primer día, también gracias. Ahora ya *desinfectados*, gracias por las paellitas, las muuuuuuchas cervezas y fiestecillas. Serena, Yuku, Fabry, Mara, Jose Carlos, Paco, Cristian, Silvia, Lorena y Félix. Como bien dijiste Félix, de esto se sale, y se ha salido. Gracias chicos!

A Irving, la persona que más me ha dado apoyo durante estos últimos años. Muchísimas gracias, por creer en mí siempre mucho más de lo que lo hago yo, celebrar mis éxitos y darme ánimos en mis momentos de bajón. Gracias por recorrer conmigo el camino, sin que nos importe cuál sea el destino. Te quiero 3000.

Por último, quiero agradecer a toda mi familia que claro está, sin ellos no estaría donde estoy ahora mismo. Gracias a mi hermana Elia, me has sacado las castañas del fuego más de una vez y sé que lo harías mil veces más. Gracias a Isaac, que es un cuñado de oro, por cuidarme como a su propia hermana. Y gracias a mis padres, Jesús y Juani,

por d armelo absolutamente todo, darme la oportunidad de estudiar lo que he querido, apoyarme en mis decisiones de irme a Barcelona, Valencia, Par s y Canad , y acompa arme en todos mis momentos de dudas y miedos (que han sido unos cuantos). Sois un apoyo esencial en mi vida y os estoy eternamente agradecida por ello. S  que est is orgullosos de m  y espero que pod is seguir est ndolo siempre.

Doncs ja ho tindriem!

*Gracias* ♥





# INDEX





---

<b>INDEX .....</b>	<b>1</b>
<b>ABBREVIATIONS.....</b>	<b>5</b>
<b>ABSTRACT .....</b>	<b>13</b>
<b>RESUMEN .....</b>	<b>19</b>
<b>RESUM .....</b>	<b>25</b>
<b>I. INTRODUCTION .....</b>	<b>31</b>
1. CYCLOOXYGENASE AND PROSTAGLANDINS .....	33
1.1 Cyclooxygenase description, function, and localisation.....	33
1.1 COX isoforms, expression, and regulation .....	34
1.2 Prostanoids and prostaglandins.....	36
2. PROSTAGLANDINS AND COX-2 IN HEPATIC PHYSIOPATHOLOGY .....	38
2.1 The liver: function and structure.....	38
2.2 Hepatic COX-2 expression .....	40
2.3 COX-2 in liver pathology .....	41
3. LIVER ISCHEMIA-REPERFUSION INJURY .....	43
3.1 Liver transplant.....	43
3.2 Ischemia-reperfusion injury.....	44
3.3 Inflammatory immune response.....	46
3.3.1 <i>Liver macrophages activation and recruitment</i> .....	47
3.3.2 <i>Neutrophil activation and recruitment</i> .....	48
3.4 Oxidative stress and antioxidant response .....	48
3.5 Endoplasmic reticulum stress .....	49
3.6 Cellular death.....	51
3.6.1 <i>Apoptosis</i> .....	51
3.6.2 <i>Necrosis</i> .....	52
3.7 Autophagy .....	53
4. MITOCHONDRIA.....	54
4.1 Mitochondrial respiration .....	56
4.1.1 <i>Electron transport chain and oxidative phosphorylation system</i> .....	56
4.1.1 <i>Supercomplexes</i> .....	57
4.2 Mitochondrial dynamics.....	60
4.3 Role of the mitochondria in ischemia-reperfusion injury .....	62
<b>II. OBJECTIVES .....</b>	<b>65</b>
<b>III. MATERIALS AND METHODS.....</b>	<b>69</b>
1. REAGENTS AND EQUIPMENT.....	71
2. ANIMAL MODELS AND EXPERIMENTAL DESIGN.....	72
2.1 Generation and maintenance of the <i>h-COX-2 Tg</i> mice.....	72

---

2.2	Pure genetic background <i>h-COX-2</i> Tg mice line generation (B6).....	74
2.3	F1 hybrid genetic background animals (B6D2 F1) .....	74
2.4	Mice genotyping .....	74
2.5	Experimental design.....	76
2.5.1	<i>Liver ischemia-reperfusion model</i> .....	76
2.5.2	<i>Ischemia preconditioning</i> .....	77
2.5.3	<i>Drug-inhibition of COX-2</i> .....	78
3.	SUBCELLULAR FRACTIONATION .....	78
3.1	Mitochondrial isolation .....	78
3.2	Nuclear fractionation.....	79
4.	HISTOLOGICAL ANALYSIS.....	80
4.1	Fixation, paraffin tissue inclusion, and sectioning.....	80
4.2	Deparaffination, rehydration, and dehydration of samples .....	80
4.3	Fixed paraffined tissue stains.....	80
4.3.1	<i>H&amp;E staining</i> .....	80
4.3.2	<i>Ly6G<sup>+</sup> staining</i> .....	81
4.4	Tissue cryopreservation and sectioning.....	82
4.5	Dihydroethidium staining.....	82
4.6	Transmission Electronic Microscopy (TEM) .....	82
5.	PROTEIN DETECTION .....	83
5.1	Protein extraction and quantification .....	83
5.2	Protein electrophoresis and immunoblotting .....	84
5.3	Protein native electrophoresis for supercomplex detection (BN-PAGE).....	85
5.4	Immunofluorescence .....	88
6.	GENE DETECTION AND EXPRESSION.....	88
6.1	Isolation of total DNA from frozen liver tissue .....	88
6.2	Determination of mitochondrial DNA content .....	89
6.3	RNA extraction, RT, and qPCR.....	90
6.4	Determination of <i>Xbp1</i> splicing.....	93
6.5	RNAseq and NGS analysis.....	94
7.	DETERMINATION OF METABOLITES AND CYTOKINES .....	94
7.1	Plasma collection .....	94
7.2	PGE <sub>2</sub> .....	94
7.3	Plasma transaminases.....	95
7.4	Plasma cytokines.....	95
7.5	Total NAD and NADH content determination .....	96
7.6	AMP and ATP determination .....	96
8.	ENZYMATIC ACTIVITIES .....	97
8.1	Caspase 3.....	97
8.2	Catalase .....	97
8.3	Superoxide dismutase.....	97
8.4	Glutathione reductase and Glutathione Peroxidase .....	98
8.5	Total glutathione and oxidised glutathione measurement.....	98
8.6	Myeloperoxidase activity .....	99
8.7	Indirect measurement of ROS production .....	99
9.	FUNCTIONAL ASSAYS.....	100
9.1	Measurement of mitochondrial membrane potential .....	100

---

9.2	High resolution respirometry .....	100
10.	PATIENTS .....	103
11.	STATISTICS .....	103
<b>IV.</b>	<b>RESULTS .....</b>	<b>105</b>
1.	CHARACTERIZATION OF THE ROLE OF COX-2 IN HEPATIC ISCHEMIA- REPERFUSION MODEL .....	109
1.1	Establishment of the ischemia-reperfusion injury pathology .....	109
1.2	Liver of <i>h-COX-2 Tg</i> mice have less tissue damage compared to the <i>Wt</i> animals .....	109
1.3	A mixed genetic background is required to reproduce the ischemia-reperfusion injury model in mice .....	112
1.4	Lower hepatic damage is due specifically to COX-2 expression .....	114
1.5	Hepatic preconditioning attenuates liver damage in <i>Wt</i> mice .....	115
1.6	The gene expression profile is altered after ischemia-reperfusion injury .....	117
2.	THE INFLAMMATORY RESPONSE IS ATTENUATED WHEN COX-2 IS EXPRESSED .....	119
2.1	Ischemia-reperfusion increases inflammatory markers that are lower in <i>h-COX-2 Tg</i> mice.....	119
2.2	Neutrophil infiltration is decreased with COX-2 expression .....	121
2.3	COX-2 expression attenuated NF- $\kappa$ B pathway .....	123
3.	CELLULAR STRESS IS REDUCED WHEN COX-2 IS EXPRESSED IN HEPATOCYTES .....	124
3.1	Constitutive hepatocyte COX-2 expression leads to decreased apoptosis .....	124
3.2	Hepatocyte COX-2 expression activates autophagy after ischemia-reperfusion.. .....	126
3.3	Unfolded protein response is activated in ischemia-reperfusion .....	127
3.4	The antioxidant response is enhanced when COX-2 is overexpressed .....	130
4.	STUDY OF THE MITOCHONDRIAL FUNCTION.....	134
4.1	Mitochondrial respiration is higher in <i>h-COX-2 Tg</i> livers after ischemia- reperfusion.....	134
4.2	Higher respiration in <i>h-COX-2 Tg</i> mitochondria is not due to an increase in ETC complexes expression .....	138
4.3	Ischemia-reperfusion causes lost in mitochondrial membrane potential and is prevented by COX-2 expression .....	140
4.4	Mitochondria number and phenotype are not altered because of the COX-2 expression.....	141
4.5	Mitochondrial dynamics is altered after ischemia-reperfusion .....	144
4.6	OPA1 processing is enhanced by a higher activity of OMA1 in <i>Wt</i> mitochondria after ischemia-reperfusion .....	146
5.	INCREASED PLASMATIC PGE <sub>2</sub> ARE ASSOCIATED WITH AN IMPROVEMENT IN LIVER FUNCTION .....	148

<b>V.</b>	<b>DISCUSSION.....</b>	<b>151</b>
<b>VI.</b>	<b>CONCLUSIONS .....</b>	<b>171</b>
<b>VII.</b>	<b>BIBLIOGRAPHY .....</b>	<b>175</b>
<b>VIII.</b>	<b>ANNEXES .....</b>	<b>203</b>
	ANNEX 1 – PATIENT INFORMATION TABLE .....	205
	ANNEX 2 – INDEX OF FIGURES .....	211
	ANNEX 3 – INDEX OF TABLES.....	215
	ANNEX 4 – PUBLICATIONS .....	217

# ABBREVIATIONS







---

$\Delta\psi_m$	Mitochondrial membrane potential
$\Delta p$	Proton motive force
$\Delta p H_m$	Mitochondrial pH gradient
15-PGDH	15-hydroxyprostaglandin dehydrogenase
AA	Arachidonic acid
ADP	Adenosine diphosphate
AKT	Protein kinase B
ALT	Alanine transaminase
AMP	Adenosine monophosphate
AMPK	5' AMP-activated protein kinase
<i>ApoB</i>	Apolipoprotein B-100
AST	Aspartate transaminase
ATF	Activating transcription factor (ATF4, ATF6...)
ATG	Autophagy related (ATG5, ATG7, ATG10, ATG12...)
ATP	Adenosine triphosphate
BAK	BCL-2 homologous antagonist/killer
BAX	BCL-2-like protein 4
BCL2	B-cell lymphoma 2
BN-PAGE	Blue native - polyacrylamide gel electrophoresis
BSA	Bovine serum albumin
C/EBP	CCAAT-enhancer-binding protein
$Ca^{2+}$	Calcium ion
cAMP	3',5'-cyclic adenosine monophosphate
CAT	Catalase
CCCP	Carbonyl cyanide chlorophenylhydrazone
CETF	Electron transfer flavoprotein complex
CHOP	CCAAT-enhancer-binding protein homologous protein
CI	Complex I (NADH dehydrogenase)
CII	Complex II (Succinate dehydrogenase)
CIII	Complex III (Coenzyme Q – cytochrome c reductase)
CIV	Complex IV (Cytochrome c oxidase)

## ABBREVIATIONS

---

CLEC4F	C-type lectin receptor 4F
CoQ	Ubiquinone
COX	Cyclooxygenase (COX-1, COX-2)
COXIB	COX-2 inhibitor
CV	Complex V (ATP synthase)
<i>Cybb</i>	Cytochrome b-245 heavy chain
CytC	Cytochrome C
DAMP	Damage-associated molecular patterns
DELE1	DAP3-binding cell death enhancer 1
DFU	5,5-dimethyl-3(3-fluorophenyl)-4-(4-methylsulfonyl) phenyl-2(5H)-furanone
DMEM	Dulbecco's modified eagle medium
DMSO	Dimethyl sulfoxide
DNA	Deoxyribonucleic acid
cDNA	Complementary DNA
dsDNA	Double stranded DNA
mtDNA	Mitochondrial DNA
nDNA	Nuclear DNA
DRP1	Dynamin-related protein 1
ECL	Electrogenerated chemiluminescence
EDTA	Ethylenediaminetetraacetic acid
EGTA	Ethylene glycol-bis ( $\beta$ -aminoethyl ether)-N,N,N',N'-tetraacetic acid
eIF2a	Eukaryotic translation initiation factor 2A
ER	Endoplasmic reticulum
ERK1/2	Extracellular signal-regulated kinases 1/2
ETC	Electron transport chain
FAD	Flavin adenine dinucleotide – quinone form
FADH <sub>2</sub>	Flavin adenine dinucleotide – hydroquinone form
Fe <sup>2+</sup>	Iron ion
FET	Forward electron transfer
FIS1	Fission protein 1
GAPDH	Glyceraldehyde 3-phosphate dehydrogenase (also G3PDH)

---

GPX	Glutathione peroxidase
GR	Glutathione reductase
GRP78	78 kDa glucose-regulated protein
GSH	Reduced glutathione
GSSG	Oxidised glutathione
H&E	Haematoxylin/eosin staining
H <sup>+</sup>	Hydrogen ion (proton)
H <sub>2</sub> O	Water
H <sub>2</sub> O <sub>2</sub>	Hydrogen peroxide
HCR	Hepatic control region
HEPES	4-(2-hydroxyethyl)-1-piperazineethanesulfonic acid
HMOX	Heme oxygenase 1
<i>Hprt</i>	Hypoxanthine phosphoribosyl-transferase
HRI	Eukaryotic translation initiation factor 2 alpha kinase 1, EIF2AK1
HSC	Hepatic stellate cell
HSP60	Heat shock protein 60
<i>Hspa5</i>	Endoplasmic reticulum chaperone BiP (GRP78 encoding gene)
IκBα	Nuclear factor of kappa light polypeptide gene enhancer in B-cells inhibitor, alpha
I/R	Ischemia-reperfusion
IL	Interleukin (IL-1, Interleukin 1; IL-1β, Interleukin 1β, IL-18, Interleukin 18)
IL-1R	Interleukin 1 receptor
IMM	Inner mitochondrial membrane
IMS	Intermembrane space
IRE1	Inositol-requiring enzyme 1
IRI	Ischemia-reperfusion injury
JNK	c-Jun N-terminal kinase
KC	Kupffer cell
KCl	Potassium chloride
LC3	Microtubule-associated protein 1A/1B-light chain 3
LDH	Lactate dehydrogenase

## ABBREVIATIONS

---

LPO	Lipid peroxidation
LSEC	Liver sinusoid endothelial cells
Ly6G	Lymphocyte antigen 6 complex locus
MAFLD	Metabolic (dysfunction) associated fatty liver disease
MFF	Mitochondrial fission factor
MFN	Mitofusin (MFN1, MFN2)
MgCl <sub>2</sub>	Magnesium chloride
MIEF/MID	Mitochondrial elongation factor/mitochondrial dynamics protein (MIEF1/MID51, MIEF2/MID49)
MPO	Myeloperoxidase
mPTP	Mitochondrial permeability transition pore
mTOR	Mammalian target of rapamycin
Na <sup>+</sup>	Sodium ion
NAD <sup>+</sup>	Nicotinamide adenine dinucleotide – oxidised
NADH	Nicotinamide adenine dinucleotide – reduced
NASH	Non-alcoholic steatohepatitis
NDUFA5	NADH dehydrogenase 1 alpha subcomplex subunit 5
NF-κB	Nuclear factor kappa-light-chain-enhancer of activated B cells
<i>Nfe2l2</i>	NRF2 coding gene
NLRP	Nucleotide-binding oligomerization domain, leucine-rich repeat-containing receptor (NLR) family pyrin domain-containing
NRF2	Nuclear factor erythroid 2-related factor 2
NSAID	Non-steroidal anti-inflammatory drug
O <sub>2</sub> • <sup>-</sup>	Superoxide anion
OCT	Optimal cutting temperature compound
OLT	Orthotopic liver transplant
OMA1	OMA1 zinc metallopeptidase
OMM	Outer mitochondrial membrane
OPA1	Optic atrophy-1
OXPHOS	Oxidative phosphorylation
PBS	Phosphate-buffered saline
PC	Preconditioning

PERK	PKR-like ER kinase
PFA	Paraformaldehyde
PG	Prostaglandin (PGD <sub>2</sub> , Prostaglandin D <sub>2</sub> ; PGE <sub>2</sub> , Prostaglandin E <sub>2</sub> ; PGF <sub>2α</sub> , Prostaglandin F <sub>2α</sub> ; PGG <sub>2</sub> , Prostaglandin G <sub>2</sub> ; PGH <sub>2</sub> , Prostaglandin H <sub>2</sub> )
PGC1α	Peroxisome proliferator-activated receptor-gamma coactivator (PGC)-1 alpha
PGI <sub>2</sub>	Prostacyclin (Prostaglandin I <sub>2</sub> )
PHGS	Prostaglandin G/H synthase
PI3K	Phosphoinositide 3-kinase
PINK	PTEN-induced kinase 1
PLA2	Phospholipase A2
PLC	Phospholipase C
PMSF	Phenylmethylsulphonyl fluoride
POX	Peroxidase
PRR	Pattern-recognition receptors
<i>Pppargc1a</i>	PGC1α coding gene
<i>Ptgs</i>	Prostaglandin-endoperoxide synthase, <i>PTGS</i> ( <i>Ptgs</i> ) -1/2 (COX coding gene)
PVDF	Polyvinylidene difluoride
QH <sub>2</sub>	Ubiquinol
RET	Reverse electron transfer
RNA	Ribonucleic acid
mRNA	Messenger RNA
ROS	Reactive oxygen species
<i>Rplp0</i>	60S acidic ribosomal protein P0
SC	Supercomplexes
SCSIE	Servicio central de soporte a la investigación experimental
SDS	Sodium dodecyl sulphate
SEM	Standard error of the mean
SOD	Superoxide dismutase (MnSOD, Manganese SOD)
TCA	Tricarboxylic acid

## ABBREVIATIONS

---

TEM	Transmission electron microscopy
TFAM	Transcription factor A, mitochondrial
Th2	T helper 2
TMPD	N,N,N',N'-tetramethyl-p-phenylenediamine dihydrochloride
TMRM	Tetramethylrhodamine methyl ester
TNB	5-thio-2-nitrobenzoic acid
TNF	Tumour necrosis factor (TNF $\alpha$ )
TRAF2	TNF receptor associated factor 2
TRAIL	TNF-related apoptosis-inducing ligand
TXA <sub>2</sub>	Thromboxane A2
UPR	Unfolded protein response
UCM	Universidad Complutense de Madrid
UV	Universitat de València
Wt	Wild type
XBP1	X-box binding protein 1
YME1L1	YME1 like 1 ATPase

# ABSTRACT







Hepatic ischemia-reperfusion (I/R) injury (IRI) is a major cause of mortality and morbidity in liver resection and liver transplantation. IRI causes up to 10% of early organ failure and predisposes to chronic rejection. During the period of hypoxia, the liver remains without oxygen supply, shifting its metabolism to anaerobic pathways that will lower intracellular pH in addition to the arrest of ATP synthesis. Paradoxically, the necessary restoration of oxygen flow causes the most damage with an activation of the immune system that will generate a burst of reactive species of oxygen (ROS) that will cause cell and tissue damage, leading to cell death and compromising tissue viability. Cyclooxygenase-2 (COX-2) is a key enzyme in prostaglandin biosynthesis and its importance in IRI is controversial. PGE<sub>2</sub>, prostaglandin E<sub>2</sub>, is the main product of COX-2, and is mainly involved in mediating pathological processes such as inflammation, fever and pain. While the use of NSAIDs, specific COX inhibitors, points to a beneficial effect of inhibition in the resolution of the inflammatory process, more and more studies now support the idea of an anti-inflammatory role of COX-2. In fact, previous studies have shown that COX-2 overexpression in hepatocytes protects mice from apoptosis and cellular stress, as well as reducing the inflammatory response, in different liver disease models (such as metabolic (dysfunction) associated fatty liver disease (MAFLD), and non-alcoholic steatohepatitis (NASH)).

In this PhD thesis, a hepatocyte-specific COX-2 transgenic mouse (*h-COX-2 Tg*) was used to elucidate the role and involvement of COX-2 in IRI. Wild type (*Wt*) and *h-COX-2 Tg* animals were subjected to 90 min of ischemia, followed by 4 or 24 h of reperfusion, and Sham surgery was used as a control in both groups of animals.

Comparing *h-COX-2 Tg* animals with their *Wt* littermates, cellular and tissue damage resulting from IRI is attenuated. Among these pathways, the inflammatory cascade is less activated, revealing less pro-inflammatory cytokine release with less hepatic recruitment and neutrophil infiltration. Necrosis and apoptosis pathways are also attenuated in *h-COX-2 Tg* mice after I/R, such as reduced endoplasmic reticulum stress, while autophagy is increased. The antioxidant response appears to be enhanced

in the context of COX-2 overexpression, by an increase in NRF2 and its antioxidant target genes. Total ROS production is also lower, contributing to less tissue damage. Interestingly, when livers from *Wt* animals are subjected to short ischemia prior to 90 min ischemia, termed preconditioning (PC), endogenous COX-2 is induced at higher levels than without PC, and these livers show less damage, attenuated inflammation, and an enhanced antioxidant response. The PC results validate those obtained with the overexpression model and shed light on why PC is beneficial when liver resection or transplant is required. Furthermore, the role of COX-2 in this observed protection has been shown to be specific, as its inhibition with DFU, a specific COX-2 inhibitor, reverses the observed effects, and matched the damage caused to *Wt* animals. Mitochondria are central players in the pathophysiology of IRI; on the one hand, they contribute to cell damage by modulating ROS generation, but on the other hand, they play an essential role in the antioxidant response through specific antioxidant enzymes. In this regard, mitochondrial function is preserved in COX-2-overexpressing livers, as can be demonstrated by a conserved mitochondrial membrane potential and a preserved respiratory rate associated with Complex I electron-feeding pathways. In addition, *h-COX-2 Tg*-derived mitochondria show a tendency to stabilise supercomplexes composed of Complex I, which may also contribute to the conservation of membrane potential and respiration. The maintenance of adequate mitochondrial membrane potential and respiratory rates, compared to *Wt*, can be explained by a stabilisation of mitochondrial cristae. Mitochondrial cristae, invaginations of the inner mitochondrial membrane (IMM), are maintained through interactions of various isoforms of OPA1, an IMM protein involved also in mitochondrial fusion. Its processing is mediated by proteases, such as OMA1, which acts under certain stimuli. In *h-COX-2 Tg* mice, there is a reduced OPA1 processing that correlates with attenuated OMA1 activity, showing a stabilisation of cristae in the context of COX-2 overexpression after I/R. On the other hand, as a validation of the study in mice, a retrospective study was conducted in patients who had undergone liver transplantation. In this part of the study, PGE<sub>2</sub> levels were analysed and correlated with liver functions after transplantation. This analysis

shows that the presence of PGE<sub>2</sub> in the plasma of recipients correlates with a better prognosis, while lower PGE<sub>2</sub> levels are associated with early graft dysfunction.

All these results present COX-2 as a new player in liver protection after I/R, showing an anti-inflammatory and antioxidant role, as well as reducing mitochondrial damage, cell stress and cell death. Furthermore, it is shown how COX-2-derived prostaglandins under physiological conditions can play a protective role in cases of liver transplant.



# RESUMEN





La lesión por isquemia-reperfusión (I/R) hepática (IRI, del inglés *ischemia-reperfusion injury*) es una causa importante de mortalidad y morbilidad en la resección hepática y el trasplante de hígado. La IRI causa hasta un 10% de los fallos orgánicos precoces y predispone al rechazo crónico. Durante el periodo de hipoxia, el hígado permanece sin aporte de oxígeno, cambiando su metabolismo a vías anaerobias que disminuirán el pH intracelular además del arresto de la síntesis de ATP. Paradójicamente, el restablecimiento necesario del flujo de oxígeno causa más daño, con una activación del sistema inmunitario que generará una gran cantidad de especies reactivas de oxígeno (ROS, del inglés *reactive oxygen species*) que causarán daño celular y tisular, provocando la muerte celular y comprometiendo la viabilidad tisular. La ciclooxigenasa-2 (COX-2) es una enzima clave en la biosíntesis de prostaglandinas y su importancia en la IRI es controvertida. La PGE<sub>2</sub>, prostaglandina E<sub>2</sub>, es el principal producto de la COX-2, y participa principalmente en la mediación de procesos patológicos como la inflamación, la fiebre y el dolor. Mientras que el uso de AINEs, inhibidores específicos de la COX, apunta a un efecto beneficioso de su inhibición en la resolución del proceso inflamatorio, cada vez más estudios apoyan actualmente la idea de un papel antiinflamatorio de la COX-2. De hecho, estudios previos han demostrado que la sobreexpresión de COX-2 en hepatocitos protege a los ratones de la apoptosis y el estrés celular, además de reducir la respuesta inflamatoria en diferentes modelos de enfermedad hepática (como la enfermedad del hígado graso asociada a disfunción metabólica (MAFLD, del inglés *metabolic (dysfunction) associated fatty liver disease*), y la esteatohepatitis no alcohólica (NASH, del inglés *non-alcoholic steatohepatitis*).

En esta tesis doctoral, se utilizó un ratón transgénico que sobreexpresa COX-2 específicamente en los hepatocitos (*h-COX-2 Tg*) para dilucidar el papel y la implicación de la COX-2 en la IRI. Los animales de tipo silvestre (*Wt*, del inglés *Wild type*) y *h-COX-2 Tg* fueron sometidos a 90 min de isquemia, seguidos de 4 o 24 h de reperfusión, y se usó la cirugía Sham (placebo) como control en ambos grupos de animales.

Comparando los animales *h-COX-2 Tg* con sus hermanos de camada *Wt*, el daño celular y tisular se atenúa tras la IRI. Entre las distintas vías modificadas, la cascada inflamatoria está menos activada, lo que revela una menor liberación de citoquinas pro-inflamatorias con menor reclutamiento hepático, e infiltración de neutrófilos. Las vías de la necrosis y la apoptosis también se atenúan en los ratones *h-COX-2 Tg* tras la I/R, como la reducción del estrés del retículo endoplásmico, mientras que aumenta la autofagia. La respuesta antioxidante parece potenciarse en el contexto de la sobreexpresión de COX-2, mediante un aumento de NRF2 y sus genes diana antioxidantes. La producción total de ROS también es menor, lo que contribuye a un menor daño tisular. Curiosamente, cuando los hígados de animales *Wt* se someten a una isquemia corta antes de la isquemia de 90 minutos, denominada precondicionamiento (PC), la COX-2 endógena se induce a niveles más altos que sin PC, y estos hígados muestran menos daño, una inflamación atenuada, y una respuesta antioxidante mejorada. Los resultados del PC validan los obtenidos con el modelo de sobreexpresión y arrojan luz sobre porqué el PC es beneficioso cuando se requiere una resección hepática o un trasplante. Además, se ha demostrado que el papel de la COX-2 en esta protección observada es específico, ya que su inhibición con DFU, un inhibidor específico de la COX-2, revierte los efectos observados e iguala el daño causado a los animales *Wt*. Las mitocondrias son actores centrales en la fisiopatología de la IRI; por un lado, contribuyen al daño celular modulando la generación de ROS, pero por otro, desempeñan un papel esencial en la respuesta antioxidante a través de enzimas antioxidantes específicas. En este sentido, la función mitocondrial está preservada en los hígados que sobreexpresan COX-2, como puede demostrarse por un potencial de membrana mitocondrial conservado y una tasa respiratoria preservada asociada a las vías de suministración de electrones del Complejo I. Además, las mitocondrias derivadas de *h-COX-2 Tg* muestran una tendencia a estabilizar los supercomplejos compuestos de Complejo I, lo que también puede contribuir a la conservación del potencial de membrana y la respiración. El mantenimiento de un potencial de membrana mitocondrial adecuado y de las tasas respiratorias, en comparación con las mitocondrias *Wt*, puede explicarse por una estabilización de las crestas mitocondriales. Las crestas mitocondriales, invaginaciones de la membrana



mitocondrial interna (IMM, del inglés *inner mitochondrial membrane*), se mantiene mediante interacciones de varias isoformas de OPA1, una proteína de la IMM implicada también en la fusión mitocondrial. Su procesamiento está mediado por proteasas, como OMA1, que actúa bajo determinados estímulos. En ratones *h-COX-2 Tg* hay un menor procesamiento de OPA1, que se correlaciona con una actividad atenuada de OMA1, mostrando una estabilización de las crestas en el contexto de la sobreexpresión de COX-2 tras I/R. Por otro lado, y como validación del estudio en ratones, se realizó un estudio retrospectivo en pacientes que habían sido sometidos a un trasplante hepático. En esta parte del estudio, se analizaron los niveles de PGE<sub>2</sub> y se correlacionaron con las funciones hepáticas tras el trasplante. Este análisis muestra que la presencia de PGE<sub>2</sub> en el plasma de los pacientes receptores se correlaciona con un mejor pronóstico, mientras que unos niveles más bajos de PGE<sub>2</sub> se asocian con una disfunción precoz del injerto.

Todos estos resultados presentan a la COX-2 como un nuevo actor en la protección del hígado tras I/R, mostrando un papel antiinflamatorio y antioxidante, así como reduciendo el daño mitocondrial, el estrés celular y la muerte celular. Además, se demuestra cómo las prostaglandinas derivadas de la COX-2 en condiciones fisiológicas pueden desempeñar un papel protector en casos de trasplante hepático.



# RESUM





La lesió per isquèmia-reperfusió (I/R) hepàtica (IRI, de l'anglès *ischemia-reperfusion injury*) és una causa important de mortalitat i morbiditat en la resecció hepàtica i el trasplantament de fetge. L'IRI causa fins a un 10% de les fallades orgàniques precoces i predisposa al rebuig crònic. Durant el període d'hipòxia, el fetge roman sense aportació d'oxigen, canviant el seu metabolisme cap a vies anaeròbies que disminuiran el pH intracel·lular a més de l'arrest de la síntesi d'ATP. Paradoxalment, el restabliment necessari del flux d'oxigen causa més danys, amb una activació del sistema immunitari que generarà una gran quantitat d'espècies reactives d'oxigen (ROS, de l'anglès *reactive oxygen species*) que causaran dany cel·lular i tissular, provocant la mort cel·lular i compromentent la viabilitat tissular. La ciclooxigenasa-2 (COX-2) és un enzim clau en la biosíntesi de prostaglandines i la seva importància a l'IRI és controvertida. La PGE<sub>2</sub>, prostaglandina E<sub>2</sub>, és el principal producte de la COX-2, i participa principalment en la mediació de processos patològics com la inflamació, la febre i el dolor. Mentre que l'ús d'AINEs, inhibidors específics de la COX, apunta a un efecte beneficiós de la seva inhibició en la resolució del procés inflamatori, cada cop més estudis donen suport a la idea d'un paper antiinflamatori de la COX-2. De fet, estudis previs han demostrat que la sobreexpressió de COX-2 en hepatòcits protegeix els ratolins de l'apoptosi i l'estrès cel·lular, a més de reduir la resposta inflamatòria, en diferents models de malaltia hepàtica (com la malaltia del fetge gras associada a disfunció metabòlica (MAFLD, de l'anglès *metabolic (dysfunction) associated fatty liver disease*), i l'esteatohepatitis no alcohòlica (NASH, de l'anglès *non-alcoholic steatohepatitis*).

En aquesta tesi doctoral, s'ha utilitzat un ratolí transgènic que sobreexpressa la COX-2 específicament en els hepatòcits (*h-COX-2 Tg*) per dilucidar el paper i la implicació de la COX-2 a l'IRI. Els animals de tipus silvestre (*Wt*, de l'anglès *Wild type*) i *h-COX-2 Tg* van ser sotmesos a 90 min d'isquèmia, seguits de 4 o 24 h de reperfusió, i es va usar la cirurgia Sham (placebo) com a control en tots dos grups d'animals.

Comparant els animals *h-COX-2 Tg* amb els seus germans de ventrada *Wt*, el dany cel·lular i tissular s'atenua després de l'IRI. Entre les diferents vies modificades, la cascada inflamatòria està menys activada, cosa que revela un menor alliberament de citocines proinflamatòries amb menor reclutament hepàtic i infiltració de neutròfils. Les vies de la necrosi i l'apoptosi també s'atenuen als ratolins *h-COX-2 Tg* després de la I/R, així com la reducció de l'estrès del reticle endoplasmàtic, mentre que l'autofàgia augmenta. La resposta antioxidant sembla potenciar-se en el context de la sobreexpressió de COX-2 mitjançant un augment de NRF2 i els seus gens diana antioxidants. La producció total de ROS també és menor, fet que contribueix a un menor dany tissular. Curiosament, quan els fetges d'animals *Wt* se sotmeten a una isquèmia curta abans de la isquèmia de 90 minuts, anomenada preconditionament (PC), la COX-2 endògena s'indueix a nivells més alts que sense PC, i aquests fetges mostren menys dany, una inflamació atenuada i una resposta antioxidant millorada. Els resultats del PC validen els obtinguts amb el model de sobreexpressió i donen llum sobre per què el PC és beneficiós quan es requereix una reseció hepàtica o un trasplantament. A més, s'ha demostrat que el paper de la COX-2 en aquesta protecció observada és específic, ja que la seva inhibició amb DFU, un inhibidor específic de la COX-2, reverteix els efectes observats i iguala el dany causat als animals *Wt*. Els mitocondris són actors centrals en la fisiopatologia de l'IRI; d'una banda, contribueixen al dany cel·lular modulant la generació de ROS, però de l'altra, tenen un paper essencial en la resposta antioxidant a través d'enzims antioxidants específics. En aquest sentit, la funció mitocondrial és preservada als fetges que sobreexpressen COX-2, com es pot demostrar per un potencial de membrana mitocondrial conservat i una taxa respiratòria preservada associada a les vies de subministrament d'electrons del Complex I. A més, els mitocondris derivats de *h-COX-2 Tg* mostren una tendència a estabilitzar els supercomplexos compostos de Complex I, cosa que també pot contribuir a la conservació del potencial de membrana i la respiració. El manteniment d'un potencial de membrana mitocondrial adequat i de les taxes respiratòries, en comparació amb els mitocondris *Wt*, pot explicar-se per una estabilització de les crestes mitocondrials. Les crestes mitocondrials, invaginacions de la membrana mitocondrial interna (IMM, de l'anglès *inner mitochondrial membrane*), es mantenen

mitjançant interaccions de diverses isoformes d'OPA1, una proteïna de la IMM implicada també en la fusió mitocondrial. El seu processament està mediat per proteasas, com OMA1, que actua baix determinats estímuls. En ratolins *h-COX-2 Tg* hi ha un menor processament d'OPA1, que es correlaciona amb una activitat atenuada d'OMA1, mostrant una estabilització de les crestes en el context de la sobreexpressió de COX-2 després d'I/R. D'altra banda, i com a validació de l'estudi en ratolins, es va fer un estudi retrospectiu amb pacients que havien estat sotmesos a un trasplantament hepàtic. En aquesta part de l'estudi es van analitzar els nivells de PGE<sub>2</sub> i es van correlacionar amb les funcions hepàtiques després del trasplantament. Aquesta anàlisi mostra que la presència de PGE<sub>2</sub> en el plasma dels pacients receptors es correlaciona amb un millor pronòstic, mentre que uns nivells més baixos de PGE<sub>2</sub> s'associen amb una disfunció precoç de l'empelt.

Tots aquests resultats presenten a la COX-2 com un nou actor en la protecció del fetge després d'I/R, mostrant un paper antiinflamatori i antioxidant, així com reduint la lesió mitocondrial, l'estrès cel·lular i la mort cel·lular. A més, es demostra com les prostaglandines derivades de la COX-2 en condicions fisiològiques poden exercir un paper protector en casos de trasplantament hepàtic.





# I. INTRODUCTION





## 1. CYCLOOXYGENASE AND PROSTAGLANDINS

### 1.1 Cyclooxygenase description, function, and localisation

The enzyme cyclooxygenase (COX), also known as prostaglandin G/H synthase (PHGS), is responsible for the limiting step in prostanoid biosynthesis, from arachidonic acid (AA) to the prostaglandin intermediate  $\text{PGH}_2$  [1]. It is characterised by having two enzymatic activities that act sequentially, cyclooxygenase (COX) activity and peroxidase (POX) activity. COX activity adds an oxygen molecule to AA converting it to prostaglandin  $\text{G}_2$  ( $\text{PGG}_2$ ), an endoperoxide intermediate. POX activity then reduces  $\text{PGG}_2$  to  $\text{PGH}_2$ .  $\text{PGH}_2$  is an unstable intermediate that will be further metabolised by tissue- and cell-specific isomerases to produce the final bioactive components, the different types of prostanoids (**Figure 1**).

The main cellular location of the COX enzyme is the luminal side of the endoplasmic reticulum (ER) membrane. However, it has also been detected in lipid bodies, mitochondria, and nuclear membrane [2][3][4]. The oxidative potential of the lumen of the ER is important for the function and folding of COX, allowing the formation of the disulphide bonds of the enzyme and the N-glycosylation that has as a post-translational modification [5]. In addition,  $\text{PGH}_2$ , the end product of COX, is sufficiently non-polar to diffuse across the ER membrane to be metabolised by isomerases located in the cytosol or on the cytosolic surface of the ER [6] (**Figure 1**).

COX enzymes are highly conserved between species. They are composed of around 600 amino acids, weigh  $\sim 70$  kDa, and have similar primary structures. Dimerisation of two COX monomers is necessary for its structural integrity and activity [7]. Each monomer has the same structure: a growth factor binding domain in the N-terminal, a membrane-binding domain and a globular catalytic domain in the C-terminal, where the two active sites of COX and POX are present [8]. The COX active site is a tunnel oriented towards the membrane-binding domain that accepts the AA coming from the lipid membrane. In contrast, the POX active site is located away from the membrane, in a surface groove facing the ER lumen [6] (**Figure 1**). Although

the dimer contains two catabolic sites for each reaction, only one monomer is active and it is thought that the second monomer plays an allosteric role.

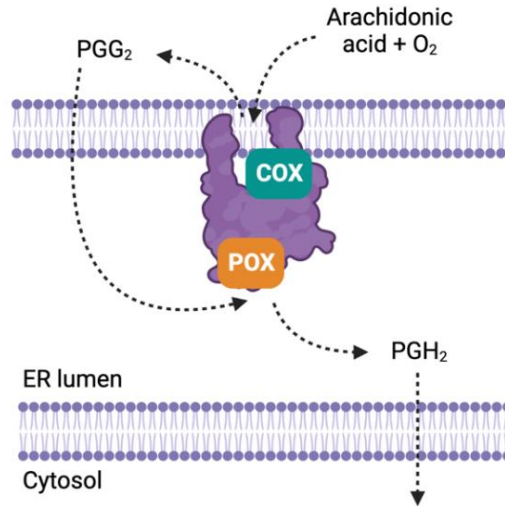


**Figure 1. Schematic representation of the cyclooxygenase enzyme.** Arachidonic acid is converted, together with an oxygen molecule, to PGG<sub>2</sub> by the action of the COX activity of the enzyme. Then, intermediate PGG<sub>2</sub> is converted, through the action of the POX activity, to PGH<sub>2</sub> which will exit the ER lumen into the cytosol. Figure adapted from *Chandrasekharan and Simons, 2004* [6]. *Created with Biorender.com*

### 1.1 COX isoforms, expression, and regulation

Two enzyme isoforms encoded by two different genes are described: COX-1 and COX-2. COX-1 is constitutively expressed in almost all tissues of the body and is involved in physiological processes such as platelet aggregation, maintenance of gastric mucosa, and renal function [9]. In contrast, COX-2 is inducible under certain stimuli like inflammatory stimuli, hormones and growth factors, and is related to both physiological situations (vasodilation and vasoconstriction, reproductive functions, pancreatic secretion) and pathological conditions (inflammation, fever, pain, thrombosis) [9].

As mentioned above, the two COX isoforms, COX-1 and COX-2 are encoded by two different genes: prostaglandin-endoperoxide synthase 1 and 2 (*PTGS1* and *PTGS2*) respectively. Although they are highly homogenous, they have some obvious sequence and motif differences. The promotor of *PTGS1* gene presents some elements close to the ones found in “housekeeping” genes, such as the lack of TATA or CAT boxes, and the presence of several transcriptional initiation sites and high GC content [10][11]. On the contrary, the *PTGS2* gene contains more regulatory elements in its promotor that control its transcription, making its expression inducible under determined circumstances. These regulatory elements in *PTGS2* promoter are, for example, nuclear factor kappa-light-chain-enhancer of activated B cells (NF- $\kappa$ B) binding sites, cyclic adenosine monophosphate (AMP) response element-binding (CREB), CCAAT-enhancer-binding proteins (C/EBP), E-box and TATA box, among others. These elements are found to be essential for COX-2 expression, induction, and regulation [10], in addition to the presence of multiple copies of the ATTTA destabilising element in the 3'-UTR, a determinant for messenger RNA (mRNA) instability through post-translational regulation [6]. Moreover, from a post-translational regulation point of view, the COX-2 protein presents an instability motive of 27 amino acids at the C-terminus, important for protein degradation [12].

The cyclooxygenase activity of the two COX isoforms is the target of non-steroidal anti-inflammatory drugs (NSAIDs) [13][14]. They are commonly used to treat inflammatory processes and to reduce fever and pain. Ibuprofen, flurbiprofen or naproxen, among other classic NSAIDs, act by competing with the substrate at the active site of COX [15], while aspirin covalently modifies the enzyme [16]. COX activity is not modified by the action of NSAIDs. Since the discovery that COX-2 expression is inducible and involved in inflammatory processes, selective COX-2 inhibitors (COXIB) have been developed. [17].

### 1.2 Prostanoids and prostaglandins

The primary product of COX enzymes was first detected in seminal fluids, and, thought to be synthesized by the prostate gland, they were termed prostaglandins (PGs) [18]. Subsequently, their production and secretion were detected in virtually all cell types and tissues, and various isomers of the product were described. Thus, PGs were included in a larger category encompassing all the different end products of the COX synthesis pathway, which are the prostanoids. Prostanoids are active lipid molecules that, together with the leukotrienes, are designated as eicosanoids, and act as mediators in multiple physiological pathways. They are derived from AA, a 20-carbon unsaturated fatty acid that is widely present in the phospholipids of all cell plasma membranes. AA is released from membranes by the action of membrane-bound phospholipases, such as phospholipase A<sub>2</sub> (PLA<sub>2</sub>) or C (PLC) [19], and is subsequently metabolised by both COX isoforms to form prostanoids, and by lipoxygenase to form leukotrienes. The PGH<sub>2</sub> intermediate is further metabolised into the different types of bioactive prostanoids by tissue- and cell type-specific isomerases and oxidoreductases, giving rise to the different types of prostaglandins (PGE<sub>2</sub>, PGD<sub>2</sub> and PGF<sub>2 $\alpha$</sub> ), prostacyclin (PGI<sub>2</sub>) and thromboxane (TXA<sub>2</sub>). They all bind to different receptors and perform different biological functions (**Figure 2**). For example, PGI<sub>2</sub>, a powerful vasodilator, is highly expressed in the lung and is essential for maintaining the lung in a dilated state [20]. PGF<sub>2 $\alpha$</sub>  is involved in the uterus contraction [21], while TXA<sub>2</sub>, produced mainly by platelets, exerts vasoconstrictive and angiotensin functions [22]. PGE<sub>2</sub> is the main product of cyclooxygenase in many tissues and is responsible for the control of salt and water excretion in the kidneys [23], the maintenance of gastric mucosa [24], as well as being involved in the reproductive system [25] and mediating inflammation [26][27].

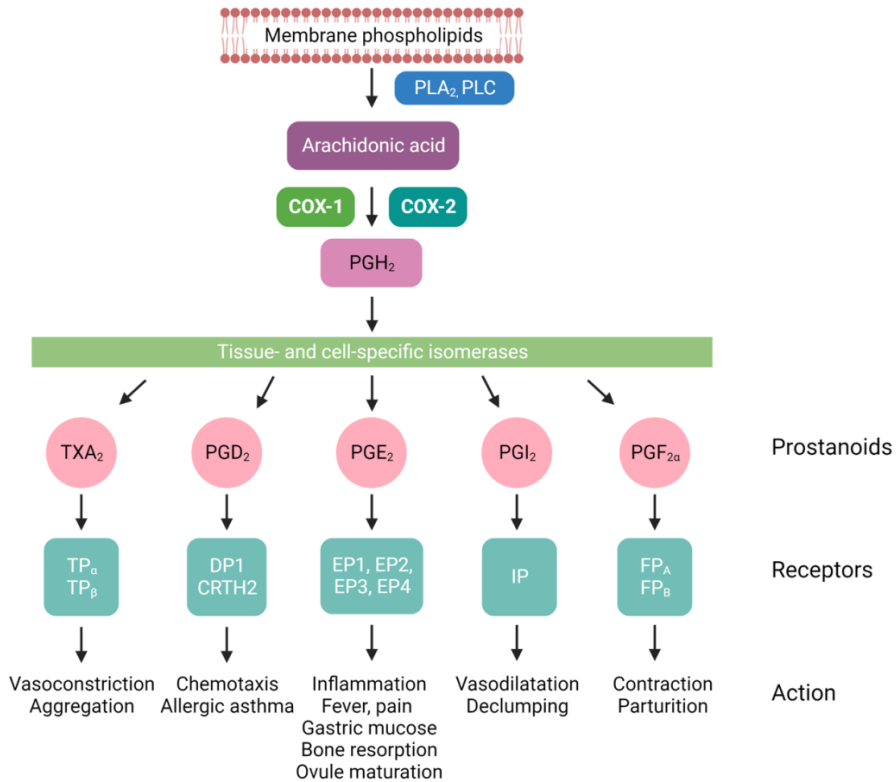


**Figure 2. Metabolic pathway of conversion of arachidonic acid (AA) into different types of prostaglandins.** AA is released from phospholipid membranes by the action of phospholipases and then converted to the  $PGH_2$  intermediate by the action of COX-1 or COX-2. Tissue- and cell-specific isomerases will convert this intermediate into the different type of prostaglandins, prostacyclin and thromboxane, which through interaction with specific receptors will lead to specific actions. Figure adapted from *FitzGerald et al, 2003* and *Funk, 2001* [15][31]. *Created with Biorender.com*

PGs, unlike hormones that are released into the circulation and take action systemically, act at the autocrine or paracrine level, i.e. they are synthesized and perform locally. Once produced and released into the extracellular space via specific PG transporters [28], PGs are internalised into the cells by binding to specific PG receptors. PG receptors are a family of rhodopsin-like 7-transmembrane-spanning G protein-coupled receptors, and each type of prostanoid will bind a specific one, like

PGE<sub>2</sub> that will bind receptors EP<sub>1-4</sub>, PGD<sub>2</sub> will bind DP and CRTH2, PGF<sub>2α</sub> will bind FP<sub>A</sub> and FP<sub>B</sub>, PGI<sub>2</sub> will bind IP-IP and IP-TP<sub>α</sub>, and TXA<sub>2</sub> will bind TP<sub>α</sub> and TP<sub>β</sub> [29]. All receptors will transduce the signal into the cell through different second messengers such as cAMP (cyclic AMP), calcium, and IP<sub>3</sub> (inositol triphosphate) that mediate the effects of receptors on cellular functions [29][30]. PGs have a short half-life and once synthesised and their action is performed, they are catabolised by the enzyme 15-hydroxyprostaglandin dehydrogenase (15-PGDH).

## 2. PROSTAGLANDINS AND COX-2 IN HEPATIC PHYSIOPATHOLOGY

### 2.1 The liver: function and structure

The liver is a vital organ in the body that handles for multiple essential functions, mainly related to metabolism. Among all its functions, it is responsible for the production of bile to process and facilitate absorption of fatty acids, the production of plasma proteins, the production of cholesterol and cholesterol transport proteins, the storage of glucose in the form of glycogen and the maintenance of glucose balance, detoxification of the blood of drugs, and other poisonous substances, among many others.

The hepatic portal vein, which originates from the pancreas, spleen, stomach, and intestines, supplies the liver with nutrient-rich blood while the hepatic artery supplies oxygenated blood. After passing through the liver, the de-oxygenated blood exits the organ through the hepatic vein into the cava vein. The bile duct collects bile from the liver and secretes its content into the duodenum, the first segment of the small intestine (**Figure 3**). Histologically, the liver can be divided into individual anatomical structures called hepatic lobules. These are hexagonal structures of hepatocytes, linked by sinusoidal capillaries that radiate into a hepatic vein in the centre, and with a portal triad at each corner consisting of a portal arteriole, a portal venule and a bile



duct. Blood and nutrients move from the portal triad towards the centre of the lobule in the direction of the hepatic vein, while bile flows backwards from the centre towards the periphery to be discharged into the bile duct.

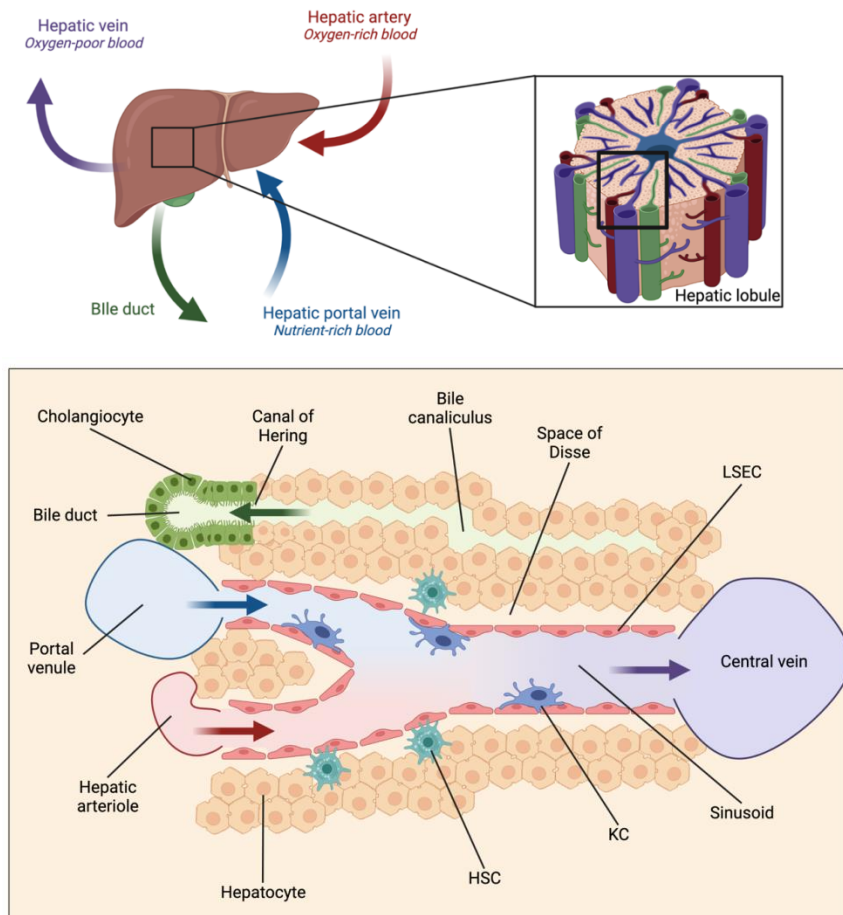


**Figure 3. Liver circulation and structure.** Oxygen-rich blood enters the liver through the hepatic artery and nutrient-rich blood through the hepatic portal vein. Oxygen-poor blood exits the liver through the hepatic vein, and bile through the bile duct. The liver is divided into lobules, hexagonal functional structures, composed of a portal venule and a hepatic arteriole that conduct blood flow to the central vein and, a bile duct that carries bile away from the liver. These lobules are composed of the different types of liver cells: hepatocytes, cholangiocytes, LSECs, KCs and HSCs. Abbreviations: LSECs, liver sinusoidal endothelial cells; KCs, Kupffer cells; HSCs, Hepatic stellate cells. *Created with Biorender.com*

Hepatocytes are the most abundant cells in the liver, accounting for around 80% of the liver volume [32]. They are the parenchymal cells of the tissue, responsible for the main functions of the liver (glucose storage, detoxification, production of plasma proteins, etc). The other 20% is composed of extracellular spaces (matrix, sinusoids...) and non-parenchymal cells that are responsible for vital functions as well. Cholangiocytes are biliary epithelial cells that form the Hering's canal and synthesise the bile acids that will make up bile. Liver sinusoidal endothelial cells (LSEC) form the sinusoidal plexus to facilitate blood circulation in a fenestrated fashion to allow transfer of molecules and proteins between serum and hepatocytes. Between the sinusoids and the hepatocytes there is a space called Disse's space where the hepatic stellate cells (HSC) are located, and inside the sinusoids are the Kupffer cells (KC). HSCs are of mesenchymal origin and are responsible for the storage of vitamin A and the production of extracellular matrix. KCs are the resident macrophages in the liver. They move between the sinusoids and, as agents in charge of the immune system in the liver, are responsible for defending the tissue from infection by phagocytosing any foreign particles and triggering the immune response [33] (**Figure 3**).

### 2.2 Hepatic COX-2 expression

COX-2 expression is, as mentioned, inducible thanks to the binding of different elements to the promoter region of the gene. The c-Jun N-terminal kinases (JNK), extracellular signal-regulated kinases 1/2 (ERK1/2) and p38 elements, as well as NF- $\kappa$ B element from transducer signalling pathways, are able to activate COX-2 expression. These elements are activated following a cascade of phosphorylation and de-phosphorylation of their elements when specific molecules bind to their receptors, especially inflammatory elements (Tumour necrosis factor alpha (TNF- $\alpha$ ), Interleukin 1 $\beta$  (IL-1 $\beta$ ), cytokines and growth factors) [6][10].

Under physiological conditions, adult livers do not express COX-2. In particular, although they express receptors for those ligands that stimulate its expression (IL-1 $\beta$ ,

TNF $\alpha$ , etc.), hepatocytes are not able to express COX-2. Its expression is limited to specific situations such as proliferation or dedifferentiation [34]. However, other liver cells can express COX-2 when stimulated, such as KCs and HSCs, as well as hepatocarcinoma cell lines used for *in vitro* studies. Nevertheless, this lack of COX-2 expression capacity is not absolute. In fact, foetal hepatocytes express COX-2 when subjected to proinflammatory stimuli [35]. This is because foetal hepatocytes lack expression of C/EBP $\alpha$ , a COX-2 repressor. Adult hepatocytes, in contrast, have high amounts of C/EBP $\alpha$ , thus repressing COX-2 expression. Only after prolonged aggression to hepatocytes or under proliferation/de-differentiation conditions, C/EBP $\alpha$  levels decrease and allow COX-2 expression [36][37].

### 2.3 COX-2 in liver pathology

As already stated, hepatic COX-2 expression is very rare. Its expression is only detected in models of partial hepatectomy in which part of the tissue is removed and the remaining tissue proliferates to recover part of the tissue mass. In these situations, hepatocytes undergo a process of de-differentiation, adopting a more foetal phenotype, and begin to proliferate, inducing COX-2 expression [34]. In fact, the use of COXIBs has been shown to delay tissue regeneration. In this regard, when the enzyme 15-PGDH is inhibited or disrupted in a partial hepatectomy model, regeneration is impaired [38].

Despite of uncommon expression of COX-2 in the liver, the use of NSAIDs to reduce inflammation appears to be effective, therefore, COX-2 inhibition in inflammatory processes appears to be beneficial. Many studies using COX-2 inhibitors in different models of liver injury have found a positive effect in reducing inflammation [39][40][41][42]. However, long-term COX-2 inhibition or even total depletion do not show any additional benefit, but seem to have detrimental effects [43][44]. Therefore, inhibition of COX-2 does not seem to be the best way to treat inflammation since its expression seems to be necessary to resolve pathological processes.

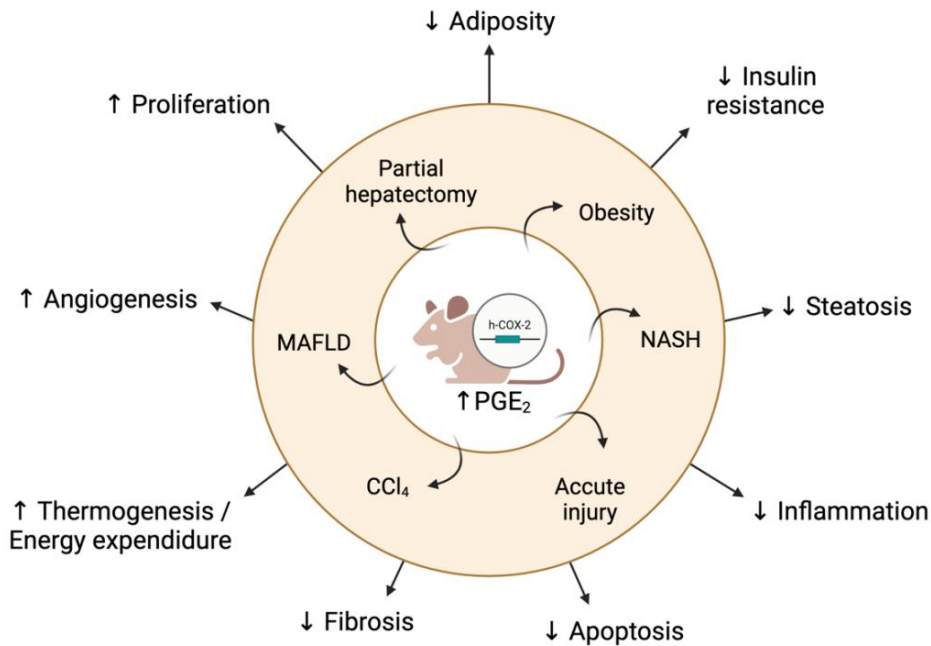


**Figure 4. Role of COX-2 in different liver pathology models.** COX-2 overexpression and its derived prostaglandins in hepatocytes confer protection and reduce markers of damage in multiple liver pathology models (within the yellow circle), such as partial hepatectomy, obesity, NASH, acute injury, CCl<sub>4</sub> and MAFLD. Abbreviations: NASH, Non-alcoholic steatohepatitis; CCl<sub>4</sub>, carbon tetrachloride; MAFLD, metabolic (dysfunction) associated fatty liver disease. *Created with Biorender.com*

Pharmacological induction of COX-2 has not yet been described, so to elucidate the role of COX-2 in liver pathologies, studies have been carried out using genetically modified animal models in a context of COX-2 overexpression specifically in the hepatocyte. In this way, the effect of the enzyme and/or its derived PGs in the establishment and resolution of different pathologies is evaluated. With these models, it has been possible to determine that the constitutive COX-2 expression offers multiple benefits and exerts a protective role (**Figure 4**). For example, a reduction in apoptosis, mediated by Fas (acute injury) [45] and by hyperglycaemia (chronic injury)

[46] has been demonstrated. Furthermore, COX-2 overexpression reduces steatosis, obesity and insulin resistance in mouse models of metabolic (dysfunction) associated fatty liver disease (MAFLD) [47], and in models of non-alcoholic steatohepatitis (NASH), in which mice show reduced steatohepatitis and fibrosis [48].

### 3. LIVER ISCHEMIA-REPERFUSION INJURY

#### 3.1 Liver transplant

Orthotopic liver transplantation (OLT) is a surgical procedure that involves the removal of a non-functional liver, resulting from liver failure, and its replacement with a healthy liver. OLT is an established therapeutic procedure for end-stage liver diseases, such as hepatocellular carcinoma, viral hepatitis infection, alcoholic liver disease and cirrhosis, metabolic diseases (non-alcoholic liver disease, steatosis and steatohepatitis), cholestatic disease, acute liver failure, and others [49].

The first attempts at liver transplantation date back to the 1960s. Francis D. Moore in Boston in 1963 and Jean Demirleau in Paris in 1964 performed liver transplants in humans, but the patients died within hours of the procedure [50]. The first successful transplant was performed by Thomas E. Starzl in Colorado in 1963. Although the patient died of a pneumonia infection within weeks, it was considered a breakthrough in transplant surgery, and after a lifetime of research into transplantation and rejection, it was considered the “father of transplantation”. Following these early attempts, medicine and surgery have been improving and benefiting from innovations that have made OLT a routine procedure to treat end-stage liver diseases today [49]. In 2018, the European Liver Transplant Registry (ELTR) reported that since data collection began in the late 1960s until 2016, 146.762 OLT have been performed in Europe [51]. Technical innovations and improved access to healthcare have increased survival rates of patients receiving liver transplants, to a survival rate of 86% after the first year and of 74% after fifth year [51].

Although OLT is the main therapeutic strategy to treat end-stage liver disease, and despite all the improvements in the surgical techniques, livers are subjected to risks that will determine transplant success or rejection. The main cause of rejection and dysfunction after OLT is ischemia-reperfusion (I/R) injury, which is responsible for 81% of primary non-function of liver allograft requiring re-transplantation and causes up to 10% of early organ failure and predisposes to chronic rejection [52].

In addition, the availability of healthy organs for transplantation is an added drawback. In today's society, where obesity has become the epidemic of the 21st century [53], the global population is increasing the risk of liver disease, to the extent that the prevalence of non-alcoholic liver disease is now considered to be 25% worldwide [54]. The shortage of healthy donor organs has led to increased use of marginal livers, which are more susceptible to damage generated by I/R [55], such as organs from elderly donors or steatotic livers. Indeed, the main cause of graft rejection after OLT is hepatic steatosis, which exacerbates the problem of organ shortage [56]. Therefore, the search for therapeutic strategies that can mitigate I/R derived damage is of interest both to improve clinical outcomes after transplantation, and to allow the use of marginal liver grafts to expand the pool of livers available for transplantation.

### 3.2 Ischemia-reperfusion injury

The term ischemia comes from the Latin *ischaemia*, and this one comes from the ancient Greek ἴσχαμιος *ischaimos* “that stops the blood”, ἴσχειν *íschein* “to hold” and αἷμα *háima* “blood”. It occurs when tissue is deprived of blood flow for a period of time, either accidentally (heart stroke or brain ictus) or as a consequence of surgical intervention (in the case of the liver, due to transplantation or resection). Dysfunction, injury, and cell death caused by oxygen deprivation vary according to the degree and duration of ischemia. Revascularisation and restoration of blood flow, called reperfusion, is the only therapeutic approach to resolve ischemia. Paradoxically, despite the need to restore oxygen and nutrient supply to the tissue, reperfusion exacerbates ischemia injury [57]. Therefore, since much of the damage is generated

at the time of reperfusion, the full name of the pathology is called ischemia-reperfusion injury (IRI).

During IRI, several mechanisms are activated that ultimately lead to cellular stress, cell death, and tissue damage. During the period of ischemia, due to the reduced availability of oxygen to the cellular machinery, several pathways are altered. When the electron transport chain (ETC) lacks oxygen as a final electron acceptor, a decrease in adenosine triphosphate (ATP) production is observed and is evident at several levels, including impaired mitochondrial function. For example, ion channels in the cell membrane are disrupted as they become depleted of ATP. This phenomenon causes an accumulation of intracellular calcium ions ( $\text{Ca}^{2+}$ ) that will trigger calcium signalling leading to cell death. In addition, the lack of oxygen pushes the cell into anaerobic metabolism. The end product of the anaerobic pathways is lactate, which will cause a drop in cytosolic pH. Calcium overload and the drop in pH will also cause mitochondria to swell due to the closure of the mitochondrial transition pore (**Figure 5, left**). In the reperfusion phase, oxygen levels are restored, causing different effects. On the one hand, the ETC function will be re-established, which will increase reactive oxygen species (ROS) production (discussed in more detail in section “4.3 Role of the mitochondria in ischemia-reperfusion injury”); on the other hand, pH will be corrected by reverting metabolism to glycolysis. Lipid peroxidation caused by ROS accumulation will facilitate membrane permeability and, together with the pH change and accumulated calcium, trigger the opening of the mitochondrial permeability transition pore (mPTP). This effect will cause a drop in the mitochondrial membrane potential, which will no longer be able to maintain the normal functionality of the ETC. The ion imbalance and ATP depletion will also contribute to cellular activation of the immune system, that in turn will release pro-inflammatory cytokines and more ROS contributing to cell death and tissue injury (**Figure 5, right**) [57][60][61][58].

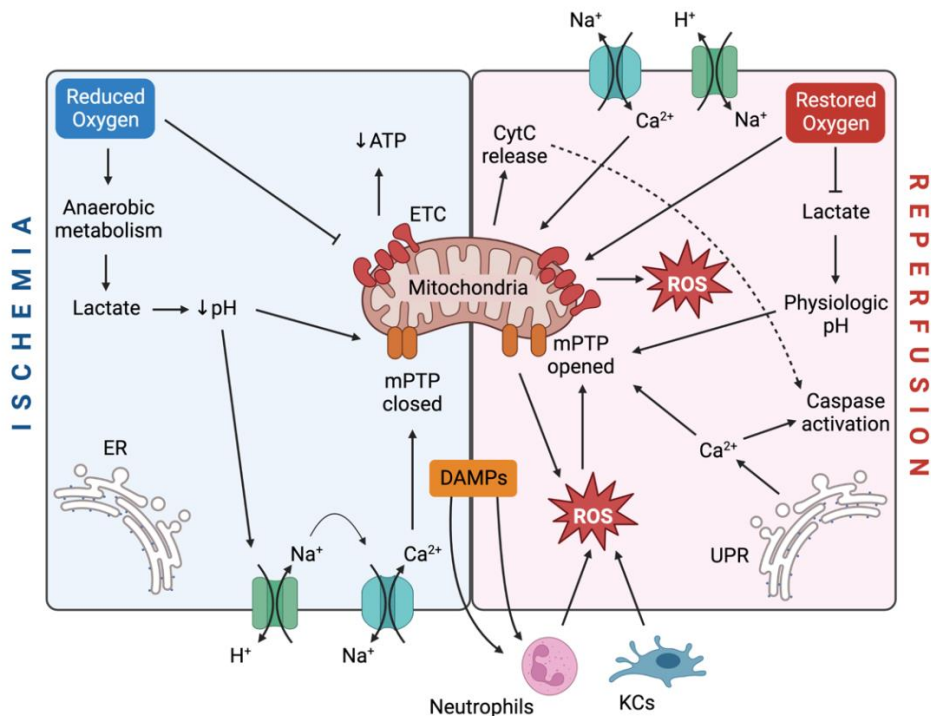


**Figure 5. Intracellular pathways activated during ischemia and during reperfusion that cause cellular and tissue damage.** Under reduced oxygen conditions, metabolic changes lead to ATP depletion, mitochondrial alterations and disruption of ionic exchange. When oxygen levels are restored, exacerbated ROS production occurs and the apoptotic and necrotic pathways are activated. Figure adapted from *Kalogeris et al, 2012; Mendez-Braz et al, 2012 and Xia et al, 2016* [57][58][59]. Abbreviations: ER, endoplasmic reticulum; UPR, unfolded protein response; CytC, cytochrome C; ETC, electron transport chain; mPTP, mitochondrial permeability transition pore; KCs, Kupffer cells; ROS, reactive oxygen species; DAMPs, damage-associated molecular patterns. *Created with Biorender.com*

### 3.3 Inflammatory immune response

IRI elicits what is known as sterile inflammatory response, in which an immune response is triggered by trauma, I/R or chemical-induced injury, in the absence of microbial infection [62]. Like microbial-induced inflammation, sterile inflammation is characterised by the recruitment of neutrophils and macrophages, and the



production of pro-inflammatory cytokines and chemokines, especially tumour necrosis factor (TNF) and interleukin-1 (IL-1) [62].

### *3.3.1 Liver macrophages activation and recruitment*

The macrophage-mediated immune response in the liver comprises distinct macrophage populations. KC are the resident macrophages in the liver, accounting for about 35% of non-parenchymal liver cells and 80-90% of the whole-body macrophage population in an adult mouse individual [63].

Kupffer cells reside in the luminal sites of the hepatic sinusoids and are responsible for sensing microenvironmental changes through long protrusions of their cytoplasmic membranes. They are characterized as CD45<sup>+</sup>, F4/80<sup>high</sup>, CD11b<sup>low</sup> and CLEC<sup>+</sup> cells in mice. In the context of IRI, damaged liver cells release damage-associated molecular patterns (DAMPs) that are detected by KC through pattern-recognition receptors (PRRs) and activate them, triggering the release of cytokines and chemokines. The release of these mediators promotes the recruitment of various immune cells such as monocytes, lymphocytes and neutrophils, which will promote tissue injury [64]. Activation of KC is also caused by ionic imbalance and ATP depletion [65], which results in their swelling and that of LSEC, causing narrowing of the sinusoidal lumen. This phenomenon contributes to the accumulation of neutrophils and increased activation of immune cells [58]. KC are also major producers of CCL2, a monocyte chemoattractant protein, which promotes neutrophil accumulation in livers under I/R stress [66].

Intracellularly, DAMP-PRR signaling leads to the activation of multiple signaling pathways that will initiate all immune responses (mainly cytokine and ROS release). The inflammasome is one of the targets of signaling pathways involved in the immune response. In activated immune cells, cytoplasmic PRRs can assemble into a supramolecular structure, called the inflammasome, and transduce downstream signals [67]. Activation of inflammasome, which is essential for initiating the inflammatory cascade, includes increased transcription of pro-inflammatory

cytokines, their subsequent processing and release (such as IL-1 $\beta$  or interleukin 18 (IL-18)), as well as activation of proinflammatory caspases, such as caspase 1 [61]. Caspase-activating inflammasomes can be classified according to their stimuli, like toxins activate the nucleotide-binding oligomerization domain, leucine-rich repeat-containing receptor (NLR) family pyrin domain-containing 1 (NLRP1), bacterial proteins activate NLRC4, double-stranded DNA (dsDNA) activates AIM2, and DAMPs and PAMPs (pathogen-associated molecular patterns) activate NLRP3 [68].

### 3.3.2 *Neutrophil activation and recruitment*

The release of DAMPs by stressed liver cells, together with the release of cytokines by activated KC, promotes neutrophil infiltration in the tissue. In addition, as mentioned above, chemoattractant proteins are detected by receptors on neutrophil cells that stimulate their recruitment. Once in the tissue, neutrophils promote tissue damage by releasing ROS and activating protease activity. Cytosolic myeloperoxidase (MPO), which catalyses the formation of hypochlorous acid/hypochlorite and oxidative species, is considered a reliable marker of neutrophil activity.

In the repair phase of sterile liver injury, neutrophil mobilisation is essential for the elimination of dead cells by forming a chemotactic gradient at the site of injury [69]. Neutrophils attract other immune cells, as well as other neutrophils, to maintain their presence in the wound healing process. This attraction is mediated by the release of cleaved proteins from damaged cells that bind to specific receptors present on neutrophils [61].

### 3.4 Oxidative stress and antioxidant response

Oxygen re-entry during reperfusion is, as aforementioned, necessary for re-establish oxygenation of the tissue, resume ATP production through ETC function and sustain aerobic metabolism. But paradoxically, this oxygen supply causes further damage, mainly due to the generation of ROS. ROS production is not intrinsically bad for the cell; indeed, they participate in several signalling pathways and are needed to

modify key regulatory proteins [70]. In physiological conditions, ROS production is balanced by a whole antioxidant machinery that ensures the presence of a minimum of these species for signalling purposes, avoiding further damage. Oxidative stress occurs when this antioxidant response is overwhelmed or inhibited, as well as when there is an increase in ROS production. This stress is characterised by direct damage to molecules such as proteins, lipids or DNA by ROS.

The major producer of ROS is the mitochondria, as by-products of mitochondrial respiration (reviewed in the section “4.1 Mitochondrial respiration”). The one-electron reduction of oxygen to superoxide anion ( $O_2^{\bullet-}$ ) is the most common reaction in the generation of ROS by the mitochondrial ETC [71].  $O_2^{\bullet-}$  is a highly toxic species but is rapidly demutated to hydrogen peroxide ( $H_2O_2$ ) by superoxide dismutase (SOD) enzymes, in either of its isoform (cytosolic, SOD1, or mitochondrial, SOD2 or MnSOD).  $H_2O_2$  is a very common signalling ROS, as it reversibly oxidises the thiol groups of proteins. In mitochondria,  $H_2O_2$  is detoxified by two groups of enzymes. On the one hand, catalase (CAT) can transform it into  $H_2O$ , and on the other hand, the coupled reaction of glutathione peroxidase (GPX) and glutathione reductase (GR) converts  $H_2O_2$  to water ( $H_2O$ ), oxidising and reducing glutathione [71]. If not processed by any antioxidant enzyme, one-electron reduction of  $H_2O_2$  produces the hydroxyl radical ( $\bullet OH$ ), an extremely harmful ROS, in the so-called Fenton reaction, involving ferrous ions ( $Fe^{2+}$ ) [72]. The transcription of all these antioxidant enzymes is regulated by one master regulator, the nuclear factor erythroid 2-related factor 2 (NRF2) transcription factor, that is activated under hypoxic conditions and oxidative stress [73]. Heme oxygenase 1 (HMOX1), involved in the catabolism of heme and considered the most sensitive and reliable marker of oxidative stress [74], is also regulated transcriptionally by NRF2 [73].

### 3.5 Endoplasmic reticulum stress

The ER is a membranous organelle that forms flattened sacs within the cytoplasm around the nucleus in eukaryotic cells. Its main functions are protein synthesis,

modification and folding, but it is also involved in calcium homeostasis and lipid biosynthesis. A variety of stressors disrupt the normal functioning of the ER, leading to calcium release and protein misfolding. The accumulation of unfolded and misfolded proteins is known as ER stress, and is detected by several transmembrane receptors, which will trigger the unfolded protein response (UPR). The purpose of UPR activation is to relieve the ER of these misfolded proteins by increasing chaperone synthesis, reducing protein translation and accelerating the degradation of misfolded proteins. However, if the UPR is unable to relieve this stress, the same response triggers apoptotic signals, ultimately leading to cell death.

The three main membrane receptors responsible for detecting unfolded proteins are PKR-like ER kinase (PERK), inositol-requiring enzyme 1 (IRE1), and activating transcription factor 6 (ATF6). Under physiological conditions, the chaperone 78 kDa glucose-regulated protein (GRP78) is bound to these three receptors, keeping them inactive, but as misfolded proteins accumulate, this chaperone is released to bind to them, facilitating receptor activation as a signal for initiation of the UPR.

On the one hand, once the ATF6 receptor is activated, it is internalised and undergoes proteolytic cleavage in the Golgi apparatus. A short form of the ATF6 then moves to the nucleus and act as a transcription factor to promote the transcription of more chaperones, as well as CCAAT-enhancer-binding protein homologous protein (CHOP), GRP94, and BiP that will enhance protein folding activity in the ER [75]. The transcription of CHOP in particular is related to induce apoptosis [76]. On the other hand, once activated, the PERK receptor will dimerise to induce the signal. This dimerization allows it to auto-phosphorylate and also induces the phosphorylation of eukaryotic translation initiation factor 2a (eIF2a). P-eIF2a will generally inhibit protein translation but at the same time induce translation of ATF4. ATF4 migrates to the nucleus and, like ATF6, induces transcription of chaperones, *Ddit3* (CHOP coding gene), among other genes. Finally, IRE1, like PERK, dimerises upon unbinding of GRP78 and becomes phosphorylated. Once activated, it also acts at different levels. It may contribute to inflammatory signalling by activating TRAF2 (TNF receptor

associated factor 2), which subsequently transduces the signal via JNK and NF- $\kappa$ B. It may also play a role in mRNA processing, as in the case of the X-box binding protein 1 (*Xbp1*) mRNA, which undergoes a cleavage producing a splicing variant that, once translated, will translocate to the nucleus and contribute to gene expression [75].

Cytokines and ROS produced during the reperfusion phase in IRI are stressful inducers of ER stress [77][78], as well as altered calcium homeostasis resulting from cytosolic overload and calcium depletion in the ER [79]. As mentioned above, the UPR is activated at early stages to ameliorate ER stress, but when the response is prolonged over time, apoptosis signalling is the ultimate fate.

Several examples show that when the UPR is activated by transgenic expression of one of its components [80] or by upregulating them [81] it is beneficial in I/R, promoting protective effects. But, in contrast, some other studies propose that UPR leads to I/R damage when other UPR factors are overexpressed or upregulated [82][83]. These controversies respond to this dual action over time of the UPR to alleviate ER stress.

### 3.6 Cellular death

There are many mechanisms that cause damage at a cellular level and that ultimately leads to cells, especially hepatocytes in the context of hepatic IRI, to die. Each mechanism can trigger whereas a programmed cell death (apoptosis), normally non-related with inflammation, or a more general and indiscriminate cell death (necrosis), usually related to inflammatory processes [61].

#### 3.6.1 Apoptosis

Apoptotic mechanisms can be divided into “extrinsic death receptor-dependent” and “intrinsic mitochondrial-dependent” pathways [61]. Activation of TNF $\alpha$ , Fas and TRAIL (TNF-related apoptosis-inducing ligand) receptors triggers the extrinsic cell death pathway, in which the receptors are internalised into the cell, trimerized and

oligomerised with many other proteins containing death domains. This death complex will activate caspase-8, which in turn cleaves and activates caspase-3 [84][57]. Intrinsic pathways are activated by different stressors, such as I/R-derived ROS, and induce the translocation of pro-death members of B-cell lymphoma 2 (BCL-2) family proteins (BCL-2-like protein 4 (BAX), BCL-2 homologous antagonist/killer (BAK), etc) to the outer mitochondrial membrane. Specifically, the function of the BAX protein is the formation of pores in the membrane causing membrane permeability, which favours the release of proteins from the intermembrane space, such as cytochrome C (CytC) [85]. Free CytC in the cytoplasm will bind to different partners that ultimately activate both caspase-9 and caspase-3. Caspase-3 acts as a cell executioner, proteolysing any type of protein. In the apoptotic process, there is no release of cellular contents to the outside, i.e. no rupture of the cell membrane, however, after induction of apoptosis, cells may also undergo secondary necrosis if the injury is too aggressive or the apoptotic process is not triggered in time [61], thus causing membrane rupture.

### 3.6.2 *Necrosis*

In contrast to apoptosis, cell death by necrosis is characterised by swelling of cells and organelles, disruption of the membrane and dissipation of cell contents. And also, unlike apoptosis, it was thought to be a type of uncontrolled cell death, leading to accidental cell death in response to overwhelming stress. However, this theory has been discarded as it has been shown that necrosis can also be induced by receptor signalling, a mechanism now known as necroptosis [86][87]. Along with this new term, two other types of necrosis have been described. Pyroptosis is characterised by the activation of caspase 1 [88], for example, via the NLRP3 inflammasome [89]; and ferroptosis is due to iron-dependent accumulation of lipid peroxides [90]. All types of necrosis result in the release of intracellular contents into the tissue environment, leaking DAMPs that will promote an inflammatory response and local inflammation [57][61].

### 3.7 Autophagy

Autophagy is a cellular mechanism by which cells can get rid of defective proteins, damaged parts or entire organelles and even cytosolic fractions, and allows the recycling of cellular materials for further utilisation. It provides cells with a “survival” pathway, when they suffer starvation, hypoxia, mitochondrial dysfunction, among other stress conditions that leave the cell depleted of amino acids and other building materials, or damage its components [57]. Autophagy is a highly regulated pathway that consists in the formation of autophagosomes, membrane structures that wrap around different cargoes and deliver them to the lysosome for degradation. The first step in autophagy is initiation, where 5' AMP-activated protein kinase (AMPK) signalling pathway promotes the formation of the ULK1 (Unc-51 like autophagy activating kinase) initiation complex [91], in coordination with inhibition of the mammalian target of rapamycin (mTOR), an inhibitor of autophagy [92]. Membrane nucleation and phagophore formation is the second step, which consists of the elongation of an isolated membrane around the tagged cargoes for degradation. The p62 factor acts as a marker of cargoes for degradation, especially misfolded or unfolded proteins. Several proteins of the autophagy related (ATG) family act in this step, such as ATG5, ATG7, ATG10 or ATG12. Next, the phagophore expansion step takes place, with the incorporation of the microtubule-associated protein 1A/1B-light chain 3 (LC3) tag. LC3 undergoes proteolytic cleavage when incorporated into the phagophore, from LC3-I in its full form to LC3-II in its processed form, and will be one of those in charge of detecting degradation-tagged cargoes. Once the phagophore is fully formed, it fuses with the lysosome, forming what is known as the autophagolysosome, where the cargoes will be degraded due to the acidic pH and lysosomal proteases [93][94].

After I/R, several stress pathways end up affecting different cellular compartments and structures, so autophagy is a good mechanism to prevent further cell damage by removing all these injured structures [95]. Furthermore, given that under hypoxic conditions tissues remain in a state of starvation, autophagy acts as a

good survival mechanism and is often upregulated [96]. Indeed, inhibition of autophagy has been reported to cause more damage after IRI [97], and pharmacological induction has a protective effect [98]. However, uncontrolled autophagy flux leads to cell death and contribute to I/R damage [99].

## 4. MITOCHONDRIA

Due to the lack of oxygen that occurs during the hypoxic period, mitochondria are the organelles most affected by ischemia [100]. Mitochondria are said to be the “powerhouse” of cells, providing cells with ATP through oxidative phosphorylation (OXPHOS), which transfers electrons from tricarboxylic acid (TCA) cycle metabolism to molecular oxygen, generating an electrochemical gradient that will be exploited by ATP synthase [71][101]. However, in addition to this energetic role, mitochondria are involved in many other vital functions, such as apoptosis and cell death, stem cell differentiation, activation of the immune response, and so on [71][101]. In addition, for example, mitochondria are responsible for the assembly of iron-sulphur clusters, which are essential enzyme cofactors; as well as for various catabolic and anaerobic reactions, such as fatty acid  $\beta$ -oxidation, biosynthesis of haem, of some phospholipids and other metabolites. Due to their essential functions, their regulation is tightly controlled, and respond and adapt to cellular demand, as well as being affected in certain circumstances, such as in the present case, under I/R [72]. In addition, mitochondria are the main generators of ROS during I/R, and are thus primarily responsible for ROS-induced cell damage and compromised cell viability after I/R. Therefore, mitochondria emerge as a central player in I/R.

Mitochondria are double-membraned organelles responsible for many vital functions. In the 1950s, an early study using transfer electron microscopy (TEM) images first described this double-membrane architecture [102], and the first mitochondrial compartments were described: an outer membrane, an inner membrane, a space between the two membranes and a matrix. The outer mitochondrial membrane



(OMM) is a smooth and permeable membrane (allowing diffusion of molecules up to 5000 Da) that borders the organelle and receives signals from the cytosol, where all the pathways converge, are decoded, and are transmitted into the mitochondria. In addition, the OMM establishes membrane contact sites with other structures and organelles, such as the ER, lysosomes, peroxisomes or lipid droplets [103]. The inner mitochondrial membrane (IMM) is a much less permeable membrane (freely permeable only to oxygen, carbon dioxide, and water), with several exchangers and pumps for ions, metabolites and small molecules, necessary to generate two essentially different environments: the intermembrane space (IMS), the space between the two membranes and the matrix, the inner mitochondrial lumen. The IMM can also be divided into two distinct compartments: the inner rim membrane, parallel to the OMM, and the cristae, deeply convoluted invaginations that extend the membrane surface and house the machinery necessary for mitochondrial respiration, held by cristae junctions, at their ends. The matrix is where most enzymatic and metabolic reactions take place, and act as a reservoir for calcium and ions.

Early TEM images showed mitochondria as static individual compartments in the cell cytosol, but as imaging techniques evolved, this assertion was increasingly discarded. In the 1980s, with the advent of live cell microscopy techniques, it was shown that mitochondria are highly dynamic organelles, and that they organise into large, interconnected intracellular networks [104]. These networks are coordinated by the antagonist function of fission and fusion events, and their balance determines mitochondrial number, size, positioning within the cell and mitochondrial elimination; all encompassed in what are termed mitochondrial dynamics [103][105][106]. In addition, the synthesis, import, and incorporation of proteins and lipids to existing mitochondria, plus the duplication of mitochondrial DNA (mtDNA), are comprised in the so-called mitochondrial biogenesis [107]. This process is highly regulated by different transcription factors, like transcription factor A, mitochondrial (TFAM), and co-activators, like PPAR $\gamma$  coactivator 1 alpha (PGC1 $\alpha$ ) [100][107].

### 4.1 Mitochondrial respiration

Mitochondrial respiration is defined as the set of metabolic reactions that convert the energy stored in macromolecules, such as glucose, fatty acids or amino acids, into ATP, the cell's universal energy donor, with a final consumption of oxygen. [71]. These metabolic reactions occur in coordination between the TCA cycle that happens in the mitochondrial matrix and the ETC located in the IMM, referred to as OXPHOS. Electrons donated from substrates originating from the TCA are transferred from one complex to another, causing a proton pumping that will generate an electrical and chemical gradient, which will be further utilised by ATP synthase (**Figure 6**) [101]. The production of ROS as a by-product of this mitochondrial respiration is often used by the cell as signalling mediators, when generated at low levels [108]. Any dysfunction in OXPHOS leading to exacerbated ROS production, accompanied by an overwhelmed antioxidant response, can propagate damage and cause cellular and tissue injury.

#### *4.1.1 Electron transport chain and oxidative phosphorylation system*

The catabolism of glucose, fatty acids and amino acids feeds the TCA, generating substrates for the ETC. Glucose, catabolised by glycolysis, and fatty acids catabolised in  $\beta$ -oxidation, generate pyruvate and acetyl-CoA, that will enter the TCA via the “first step”, the conversion of acetyl-CoA to citrate. Amino acids, such as glutamine, through oxidative deamination and transamination, enter the TCA at a different point with glutamate. The reducing equivalents, nicotinamide adenine dinucleotide hydrogen (NADH) and flavin adenine dinucleotide dihydrogen (FADH<sub>2</sub>), are generated in many reactions of the TCA cycle and will donate their electrons at the level of complex I (CI) and complex II (CII), respectively. The electrons from NADH are given up to CI (NADH dehydrogenase), inducing the pumping of protons (H<sup>+</sup>) from the matrix to the IMS. The electrons are then transferred to the Q-cycle, where ubiquinone (CoQ) is reduced to ubiquinol (QH<sub>2</sub>). CII (succinate dehydrogenase) is somewhat special, as it is part of both ETC and TCA. In its case, in the succinate to

fumarate step, it switches from FAD to FADH<sub>2</sub>, and electrons from FADH<sub>2</sub> pass immediately to the CoQ and the Q-cycle. Unlike CI, CII is not coupled to proton pumping. In IMM there are other enzymes that deliver FADH<sub>2</sub> electrons to the Q-cycle directly, like glyceraldehyde-3-phosphate dehydrogenase (G3PDH), that take the electrons from glycerol-3-phosphate [109]. Through Q-cycle, electrons are transferred to complex III (CIII, coenzyme Q - cytochrome c reductase), and then transferred to CytC, accompanied by additional H<sup>+</sup> pumping. CytC is a mobile element that moves in the IMS and delivers electrons from CIII individually to complex IV (CIV, cytochrome c oxidase).

In CIV, electrons will finally oxidise molecular oxygen, and together with two protons, a molecule of water will be formed, while more H<sup>+</sup> are also pumped into the IMS. All the H<sup>+</sup> accumulated in the IMS will generate an electrochemical gradient, called the mitochondrial membrane potential ( $\Delta\psi_m$ ). This potential gradient, together with a pH gradient ( $\Delta\text{pH}_m$ ) generates what is known as the proton motive force ( $\Delta\text{p}$ ), which will drive the re-entry of H<sup>+</sup> through the CV to ultimately synthesise ATP. The coupling of the ETC with the ATP synthesis process is collectively referred to as the OXPHOS system [71][101][109] (**Figure 6**).

#### 4.1.1 Supercomplexes

The first theory on the passage of electrons from each complex in the ETC to the next imply that the complexes “bump” into each other randomly, while moving freely in the IMM. This theory was termed the “fluid system”, and is supported by the experimental purification of individual active complexes [110]. However, a new theory emerges to challenge this fluid system, the so-called “solid system”, which proposes stable interactions within ETC complexes in a supra-molecular organisation called supercomplexes [111]. This model was supported by different experimental evidences such as electrophoretic resolution of supercomplexes with blue-native polyacrylamide gels (BN-PAGE), in-gel supercomplexes activity, electron microscopy observation of large entities comprising different ETC complexes,

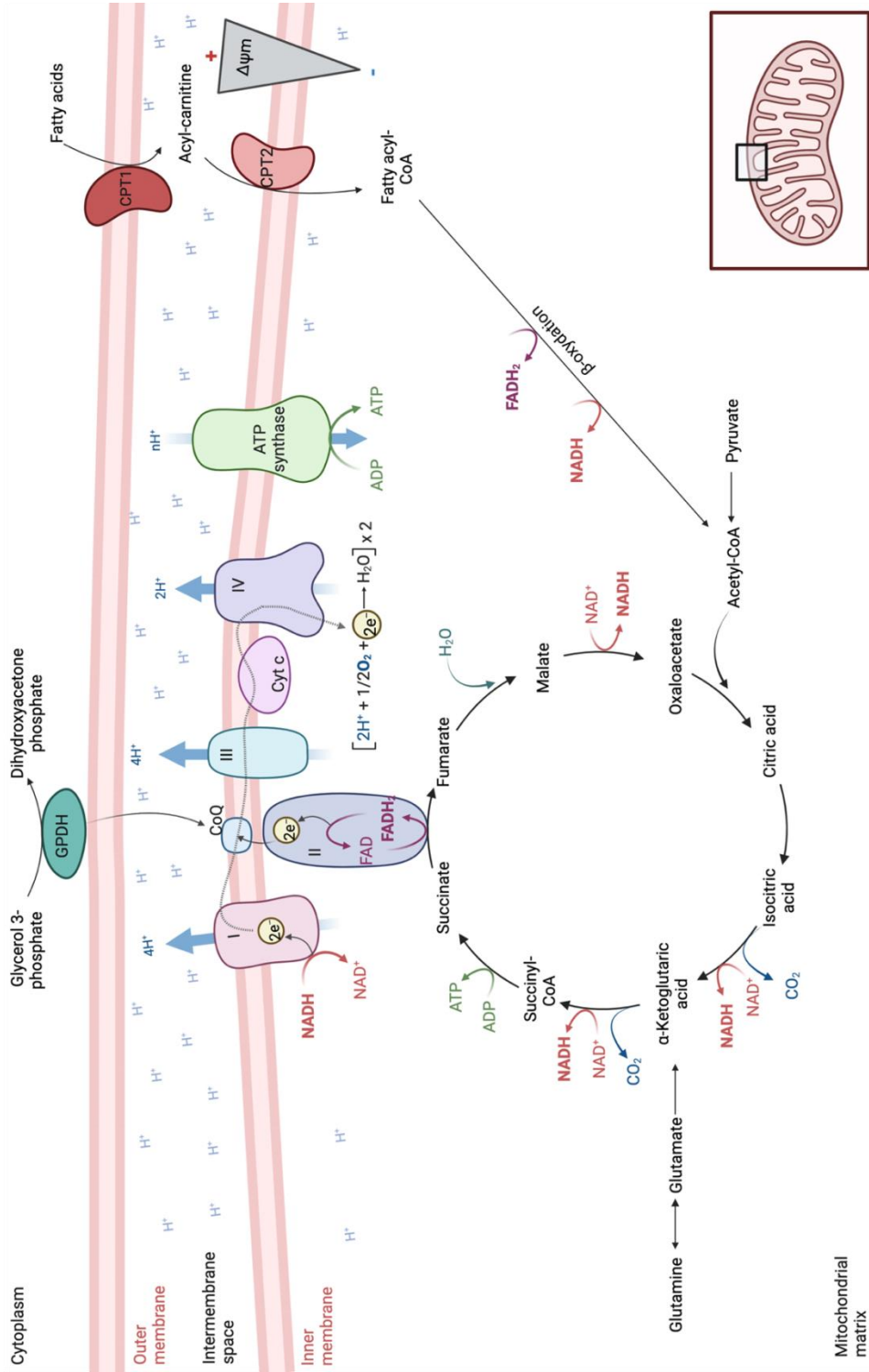


**Figure 6. Overview of the mitochondrial TCA cycle and OXPHOS.** The cofactors NADH and FADH<sub>2</sub>, the main electron donors to the ETC, are generated in multiple steps, from fatty acid  $\beta$ -oxidation to TCA cycle (through the input of multiple substrates such as pyruvate, glutamate). Electrons can also directly enter the ETC through the CoQ. Once electrons enter the ETC, they pass through the different complexes until they combine with oxygen and protons to form water, accompanied by proton pumping that will generate the proton motive force needed by ATP synthase to form ATP. *Created with Biorender.com*

respiratory flow experiments revealing that supercomplexes act as a single functional unit, or that point mutations in a single subunit of a complex can affect supercomplex formation [112]. Different combinations of individual complexes are described to form supercomplexes, as well as different stoichiometries. The most common combination is the “respirasome”: the stable interaction of CI+CIII<sub>2</sub>+CIV<sub>1-2</sub>, so called because it can autonomously carry out respiration in the presence of ubiquinone and CytC [112]. Other combinations of complexes can also be found, such as CI+CIII<sub>2</sub>+CII<sub>n</sub>, CI+CIII<sub>2</sub>+CIV<sub>3</sub>, or CI<sub>2</sub>+CIII<sub>2</sub> [113]. The proportion of each supercomplex found in each cell type or under different conditions, as well as the proportion of free complexes versus supercomplexes responds to metabolic needs and differences in the utilisation of mitochondrial respiration [114]. Indeed, a combination of free complexes within the membrane appear to coexist with supercomplexes, in a “dynamic system” [115], and helps mitochondria and the cell to adapt to different energy demands.

The functional arguments for the formation of supercomplexes are still under debate, but are beginning to be widely accepted. On the one hand, the close proximity between the different complexes helps electrons to move from one to the other in a shorter space, thus reducing electron leaking (and thus oxygen reduction and ROS formation) [111]. On the other hand, it was proposed that each complex needs to interact with the others to stabilise in the membrane [114][116][117].

Complex V is not part of supercomplexes because its higher organisation is exceptional; it organises into larger structures called *strings*, long oligomeric chains [112]. ATP synthase is composed of two domains; an intermembrane domain (F0) through which protons pass, and a matrix domain (F1), where the catalytic site is located. The CV monomers dimerise randomly through the interaction of F0 domains due to attractive forces, in a stable manner. This interaction produces a strong deformation in the IMM, which with the formation of larger CV chain-forming interactions, leads to the invaginations of the IMM, generating the characteristic mitochondrial cristae [118].

### 4.2 Mitochondrial dynamics

Mitochondria are highly dynamic organelles, constantly moving and undergoing structural changes to adapt and respond to ever-changing cellular and energetic demands [106][119]. While fusion promotes the formation of long and fused mitochondria, favouring the exchange of lipids and internal contents, fission drives the fragmentation of mitochondria into small individuals, favouring its transport, their division into dividing cells or their elimination (**Figure 7**) [106][120]. The balance between these two phenomena maintains mitochondrial function and responds to cellular needs by adapting the network to the availability of nutrients and the metabolic state of the cell [106].

Fusion is mediated by two mitofusins (MFN1 and MFN2) and the Optic atrophy-1 (OPA1), located in the OMM and the IMM respectively. MFN1 and MFN2 share a high degree of homology, although they are different and have distinct functions. In mitochondrial fusion, MFNs from two nearby mitochondria interact in both homotypic and heterotypic interactions. Although both MFNs are involved in fusion, MFN2 has been implicated more in mitochondrial-mitochondrial interactions, and mitochondrial contacts with other organelles, such as ER [103]. Internal mitochondrial fusion is carried out by OPA1, which is present in the IMM in different isoforms: a long form (L-OPA1), and a shorter form (S-OPA1). The interactions between L-OPA1 and S-OPA1 favour mitochondrial fusion, whereas the interaction

between two L-OPA1s has been linked more to the maintenance of cristae at cristae junctions. The presence of these two isoforms is largely due to the action of two proteases. YME1 like 1 ATPase (YME1L1), located in the IMM, acts basally, and is classically related to the maintenance of the balance between the two isoforms. OMA1 zinc metallopeptidase (OMA1) is also located in the IMM but, unlike YME1L1, it is an inducible protease (associated with mitochondrial dysfunction and pathology), and its cleavage of OPA1 favours the presence of the shorter form, obstructing both fusion and maintenance of the cristae [103]. In fact, the maintenance of the cristae, and thus of the internal mitochondrial structure, is also a dynamic process and is related to the mitochondrial metabolic state [105].

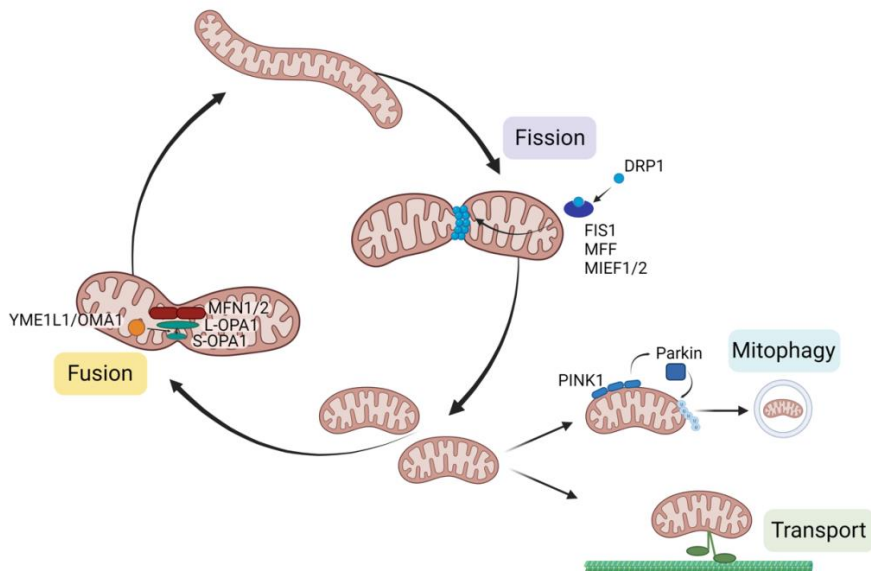


**Figure 7. Mitochondrial dynamics.** Two mitochondria fuse through the binding of MFN1/2 in the OMM and the action of L-OPA1 and S-OPA1 in the IMM. YME1L1 and OMA1 are responsible for processing OPA1. Long mitochondria divide by fission through the action of DRP1 which binds to its partners (FIS1, MFF, MIEF1/2) and forms a ring around the dividing mitochondrion. Small mitochondria are easily transported or marked for degradation (mitophagy) through the action of PINK1 and Parkin. Adapted from *Xie et al, 2020* [120]. *Created with Biorender.com*

Fission is carried out by dynamin-related protein 1 (DRP1), a cytosolic protein that is recruited on the OMM by interacting with its partners (receptors): fission protein 1 (FIS1), mitochondrial fission factor (MFF), mitochondrial elongation factor 1 (MIEF1/ MID51), and mitochondrial elongation factor 2 (MIEF2/MID49) [120]. Activated DRP1 oligomerises around a mitochondrion forming a ring that constricts and divides it. Different post-translational modifications drive DRP1 activation and interaction with its mitochondrial partners [103][120]. Sites of mitochondrial fission occur in the vicinity of the ER and ER contact sites, where the ER membrane participates in the mitochondrial fission process [103].

In addition, mitochondrial fission promotes two other important events related to mitochondrial dynamics: transport and mitophagy. Transport of small mitochondria appears to be easier than that of larger ones, and has a high impact on division events, ensuring the equal distribution of mitochondria in daughter cells. Furthermore, it is essential for driving and recruiting mitochondria to active regions of cells to meet their energy demands. Transport takes place via contacts between mitochondria and microtubules and actin filaments [120]. Mitophagy is the degradation of dysfunctional or damaged mitochondria by autophagy. It is mediated by the PTEN-induced kinase 1 (PINK) /Parkin system and results in ubiquitination of mitochondrial proteins for degradation and ultimately, encapsulation of mitochondria in an autophagophore for processing and recycling of element [120].

### 4.3 Role of the mitochondria in ischemia-reperfusion injury

As mentioned in the section “3.4 Oxidative stress and antioxidant response”, mitochondria are the main generator of ROS in the cell. Under physiological conditions, when  $\Delta p$  is not very high because CV is dissipating the  $\Delta\psi_m$ , while producing ATP, ROS production is low, and they are generated as by-products of ETC function in what is known as forward electron transfer (FET) [71]. This electron pathway is the physiological situation, when electrons flow through CI or CII to CIII, and finally to CIV, and is characterised by a minimal electron leakage at CI, CII and



CIII, which will generate small amounts of ROS, generally serving as signalling mediators.

During I/R, ROS production is exacerbated, mainly due to an imbalance in metabolism and ETC. Under conditions of hypoxia, such as during ischemia, molecular oxygen is not available and therefore the normal flow of ETC is blocked, as well as the TCA cycle. In this situation, substrates accumulate, in particular succinate, which accumulates significantly [121]. A reverse action of succinate dehydrogenase (CII), which transports electrons from accumulated QH<sub>2</sub> to fumarate, is responsible for the exceptional accumulation of succinate [122]. During reperfusion, the accumulated succinate acts as the main substrate providing reducing potential to the ETC. In addition, the Q pool is greatly reduced as a consequence of the hypoxic period and the  $\Delta p$  is restored from proton pumping by CIII and CIV at the onset of reperfusion. These three conditions trigger reverse electron transport (RET), in which electrons flow back from the Q-cycle to the CI, reducing NAD<sup>+</sup> to NADH, thus producing high amounts of O<sub>2</sub>•<sup>-</sup> [109][122][123].

The accumulation of ROS during I/R causes damage at many levels, such a protein, lipid and DNA damage. An example of protein oxidation leading to mitochondrial and cellular damage is the oxidation of thiol groups in CI subunits, which will contribute to further ROS formation [124]. Cardiolipin, an IMM specific phospholipid, is a lipid highly susceptible to peroxidation by ROS. Its oxidation is highly detrimental because it causes membrane destabilisation, affecting CIII and CIV activities [125].

In addition to the generation of ROS, mitochondria can undergo other alterations that damage the cell under I/R. One consequence of oxygen depletion and impaired OXPHOS function is ATP depletion: increased mitochondrial permeability and membrane potential dissipation following I/R lead to reduced OXPHOS activity and thus the impaired ATP supply to the cell [126]. Another intermediate that is altered is NAD<sup>+</sup>, which contributes to ATP depletion [100][127].

Mitochondrial calcium accumulation is also a hallmark of I/R damage [100]. During ischemia, the ATP depletion and the acidification of the cytosol due to lactate accumulation (due to anaerobic metabolism), drives the accumulation of sodium ions ( $\text{Na}^+$ ) through the  $\text{Na}^+/\text{H}^+$  membrane exchanger, which in turn will be pumped out through the  $\text{Na}^+/\text{Ca}^{2+}$  pump [128]. This  $\text{Ca}^{2+}$  will rapidly accumulate in the mitochondria when oxygen flow is restored. The  $\text{Ca}^{2+}$  accumulation will then trigger the opening of the mPTP [128], which will increase the permeability of the mitochondrial membrane, dissipating its membrane potential, releasing to the cytosol ROS and CytC that will cause damage and apoptosis signalling, as well as the release of other mitochondrial proteins and mtDNA, which will also signal as damage markers [129].

Finally, mitochondrial dynamics are also affected under oxygen deprivation [100][130]. Fission-induced mitochondrial fragmentation has been observed after I/R, contributing to ROS generation and  $\Delta\psi_m$  dissipation and ATP depletion [131]. Blocking fission, by genetic knock-out [132], dominant-negative transfection [133] or chemical inhibition [129] of fission-related proteins, promotes survival and protection after I/R. Conversely, fusion enhancement is associated with reduced damage and survival after I/R, by protecting mitochondria from mitophagy, and the release of ROS and pro-apoptotic signals [134][135][136]. In addition, mitochondrial biogenesis is also impaired in IRI. Initially, hypoxia can induce mitochondrial biogenesis in order to compensate ATP supply, however, when hypoxic conditions are maintained, *Ppargc1a* (PGC1 $\alpha$  encoding gene) and *Tfam* expression is reduced, leading to a reduced mitochondrial biogenesis [137][138].

## II. OBJECTIVES





Since COX-2 expression has been shown to be associated with several liver pathologies, and its overexpression triggers a protective function, the main aim of this thesis is to further investigate the role of COX-2 in liver pathophysiology. To this end, a general objective has been proposed:

- To study the role of the COX-2 enzyme in the context of hepatic ischemia-reperfusion injury.

In order to achieve this objective, more specific goals have been proposed, being these:

- a) Validation and characterisation of the I/R model in a transgenic mouse model overexpressing COX-2 in hepatocytes.
- b) To elucidate the molecular mechanism of COX-2 in the liver during ischemia and especially reperfusion.
- c) Assuming that mitochondria play a central role during I/R, both in the establishment of damage and during pathology resolution, determine whether COX-2 modulates mitochondria and whether it is involved in its mechanism of action.



# III. MATERIALS AND METHODS







## 1. REAGENTS AND EQUIPMENT

Instruments and devices used were from **Bio-Rad** (Hercules, CA, USA), **Eppendorf** (Hamburg, Germany), **Especialidades Médicas Myr S.L** (Tarragona, Spain), **GE Healthcare** (Chicago, IL, USA), **Invitrogen** (Thermo Fisher Scientific, Geel, Belgium), **Isogen Life Sciences** (De Meern, Utrecht, Netherlands), **Leica Microsystems** (Wetzlar, Germany), **Macrogen** (Geumchongu, Seoul, Korea), **Milteny Biotec** (Bergisch Gladbach, Germany), **Oroboros instruments** (Innsbruck, Austria), and **Thermo Fisher Scientific** (Geel, Belgium). General reagents and chemicals were from **Acros Organics** (Thermo Fisher Scientific (Geel, Belgium)), **BD Biosciences** (Franklin Lakes, New Jersey, U.S), **Biobasic** (Marham, Ontario, Canada), **Bio-Rad** (Hercules, CA, USA), **Biotium** (Fremon, CA, USA), **Calbiochem** (San Diego, CA, USA), **Electron Microscopy Sciences** (Hatfield, Pennsylvania, USA), **Invitrogen** (Thermo Fisher Scientific (Geel, Belgium)), **Karizoo** (Barcelona, Spain), **Merck Life Sciences S.L.U.** –**Sigma** (Darmstadt, Germany), **Milteny Biotec** (Bergisch Gladbach, Germany), **NZYtech** (Lisbon, Postugal), **Oroboros instruments** (Innsbruck, Austria), **Promega** (Madison, WI, USA), **Roche Diagnostics** (Basel, Switzerland), **Scharlab** (Barcelona, Spain), **Serva** (Heidelberg, Germany), **TCI** (Zwijndrecht, Belgium), **Thermo Fisher Scientific** (Geel, Belgium), and **Tocris** (Bristol, UK). Antibodies were from **Abcam** (Cambridge, UK), **Cayman Chemicals** (MI, USA), **Cell Signaling Technology** (Danvers, MA, USA), **Enzo Life Sciences** (Farmingdale, NY, USA), **Merck Life Sciences S.L.U.** –**Sigma** (Darmstadt, Germany), **MBL** (Sunnyvale, CA, USA), **Proteintech** (Rosemont, IL, USA), and **Santa Cruz Biotechnology** (Dallas, TX, USA). Kits were from **Arbor assays** (Ann Arbor, MI, USA), **BD Biosciences** (Franklin Lakes, NJ, USA), **Biosystems** (Wako Chemicals GmbH, Neuss, Germany), **Enzo Life Sciences** (Farmingdale, NY, USA), **Luminex** (Austin, TX, USA), **Merck Life Sciences S.L.U.** –**Sigma** (Darmstadt, Germany), **Promega** (Madison, WI, USA), **Roche Diagnostics** (Basel, Switzerland), and **Vector Laboratories** (Burlingame, CA, USA). Software was from **GraphPad Software** (San Diego, CA, USA), **Leica Microsystems** (Wetzlar, Germany), **Li-cor** (Lincoln, NE, USA), **Oroboros Instruments** (Innsbruck, Austria), **Rasband** (NIH, Bethesda, MD, USA), and **IBMCorp** (Armonk, NY, USA).

## 2. ANIMAL MODELS AND EXPERIMENTAL DESIGN

### 2.1 Generation and maintenance of the *h-COX-2 Tg* mice

The animal model used in this study is a transgenic mouse generated by the classical transgenesis method of pronuclear injection (1-cell state). A fragment of the *PTGS2* (*h-COX-2* coding gene) cDNA was cloned in a pLiv-Le6 vector that contains the constitutive human *APOE* gene promoter and its hepatic control region (HCR), and was injected into pronucleus of one-cell mouse embryos obtained from mating of hybrid (C57BL/6JRccHsd x DBA2JRccHsd) F1 mice. The resulting progeny were tested for the number of inserted copies in the genome by southern blot. One male with approximately 55 copies of the transgene was selected as founder. The colony was maintained by systematically mating heterozygous B6D2JRccHsd-Tg(*APOE-PTGS2*)4/Upme males expressing the *h-COX-2* enzyme with B6D2JRccHsd F1 females for more than 7 generations (B6D2) (**Figure 8A**). A full characterization of the model was performed and it was determined that no significant phenotypic differences were observed when comparing the livers of *h-COX-2 Tg* mice and their wild type (*Wt*) littermates at 12 weeks of age [45]. The colony was maintained at the IBV-CSIC animal facility in a 14-10 light-dark cycle, under a constant temperature of 23 °C, with chow and water *ad libitum* (SAFE A40 Rodent Maintenance Diet, Rettenmaier Iberica, Spain). The animals were housed in filter cages, with poplar bedding and nest material as enrichment. All experimental procedures were performed during the light cycle. All animal experimentation was controlled following the recommendations of the Federation of European Laboratory Animal Science Associations on health monitoring, European Community Law (2010/63/ UE), with approval of the Ethics Committee of the Spanish National Research Council, Spain and Spanish law (R.D. 53/2013; Projects approved 2016/VSC/PEA/00189 and 2020/VSC/PEA/0154).

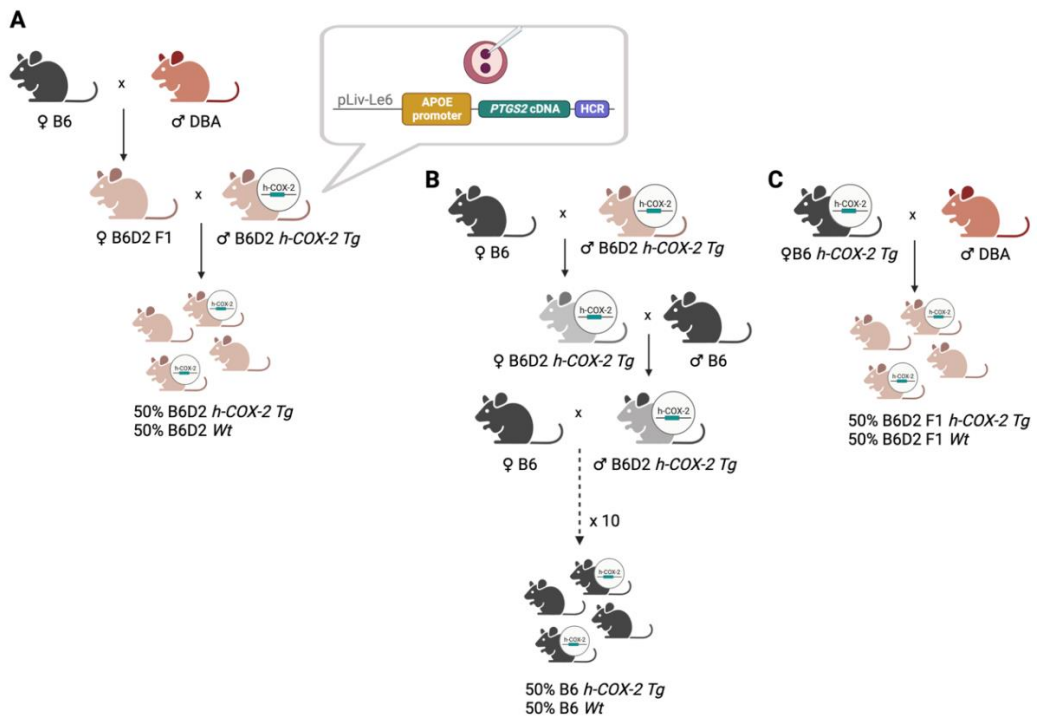


**Figure 8. Generation of the *h-COX-2* Tg mouse line and maintenance of the colony.** The *h-COX-2* Tg mice were generated using the classical transgenic method of pronuclear injection from B6DBA2JRcc embryos. The vector contains the *PTGS2* cDNA together with the APOE promoter and the hepatic control region (HCR) to express the enzyme specifically into hepatocytes. **(A)** To maintain the colony, heterozygous transgenic males are crossed with B6D2 F1 *Wt* females and 50% of the progeny carry the construct, while the other 50% are *Wt*. B6D2 F1 *Wt* females are obtained through the crossing of a B6 female and a DBA male. **(B)** The pure genetic background was obtained by backcrossing an *h-COX-2* Tg mouse from the mixed genetic background with a pure genetic background female. The cross of a male carrying the transgene in heterozygosity with a *Wt* female maintains the colony, and the progeny carry the transgene in a 50% proportion. **(C)** The F1 colony is obtained by crossing a pure genetic background female carrying the transgene in heterozygosity with a DBA male. The progeny is 50% *h-COX-2* Tg and 50% *Wt*. *Created with Biorender.com*

#### 2.2 Pure genetic background *h*-COX-2 *Tg* mice line generation (B6)

A pure C57BL/6JRccHsd (B6) genetic background mouse line (B6JRcc.B6D2JRccHsd-*Tg* (APOE/*PTGS2*)<sup>4</sup>/Upme) was also used. This line was obtained by crossing an *h*-COX-2 *Tg* male from the mixed genetic background line with a C57BL/6JRccHsd (B6) female (first cross). An *h*-COX-2 *Tg* female from the F1 was then crossed with a *Wt* B6 male (second cross) and then an *h*-COX-2 *Tg* male from the F2 with a *Wt* B6 female. From this moment, one male of each generation was crossed with a B6 female, until the 10th generation, when it is assumed that full passage to pure background has been achieved (**Figure 8B**).

#### 2.3 F1 hybrid genetic background animals (B6D2 F1)

To further study the influence of genetic background in the experiments, F1 hybrid animals were also used. These animals were obtained by crossing a B6JRcc-*Tg*(APOE/*PTGS2*)/Upme female with a DBA2JRccHsd male. Male mice carrying the transgene and their *Wt* littermates were used (B6D2 F1) (**Figure 8C**).

#### 2.4 Mice genotyping

To detect the presence of the *h*-COX-2 transgene, animals were genotyped before weaning. At day 10-12 mice were marked by toe tattooing and a tail biopsy was taken and incubated with 500  $\mu$ L of Lysis Buffer for DNA extraction (**Table 1**) with 100  $\mu$ g/ $\mu$ L Proteinase K (BioBasic) at 55 °C overnight. Once the tails were digested, the tubes were shaken, centrifuged at maximum speed for 5 min and the supernatant was transferred to new tubes. The DNA was precipitated with a volume of isopropanol, the tubes were shaken by inversion until the DNA strand was visualised and centrifuged at maximum speed for 5 min. Once the DNA pellet was formed, the supernatant was discarded, the pellet was washed twice with 70% ethanol and air dried at room temperature. The DNA was then dissolved in T.E. 10/0.1 (10 mM Tris, 0.1 mM EDTA) for 15 min at 55°C or overnight at 4°C.

When the DNA pellet was completely dissolved, DNA was quantified in a BioPhotometer (Eppendorf) and purity was determined. Conventional PCR was performed with *h-COX-2* specific primers (Table 2) and PCR Master Mix (Table 3, Promega). The PCR program was run (Table 4) and the PCR product was resolved in a 1% agarose gel (w/v) (in 1X TAE (40 mM Tris, 1mM EDTA, 0.1% Acetic Acid (v/v)) at 90 V for 30 min. The gel was then stained with Gel-red solution (1/20.000 dilution in distilled H<sub>2</sub>O, Biotium) for 10 min, and images were taken on a transilluminator (ULTima 16si Plus, Isogen Life Sciences).

**Table 1.** Lysis Buffer for DNA extraction

Compound	Concentration
Tris <i>pH</i> 8.5	100 mM
EDTA <i>pH</i> 8	5 mM
SDS	0,002 % (w/v)
NaCl	200 mM

**Table 2.** Primers for PCR genotyping of *PTGS2*

Gene	Primer pair
<i>PTGS2</i>	FP: 5' -CGCAGTACAGAAAGTATCACAGGC- 3' RP: 5' -GCGTTTGCGGTACTCATTAAAA- 3'

**Table 3.** PCR Master Mix

<b>Compound</b>	<b>Concentration</b>
GoTaq Green Buffer (5X)	1X
MgCl <sub>2</sub> (25 mM)	1,5 mM
Forward primer (10 μM)	0,2 μM
Reverse primer (10 μM)	0,2 μM
dNTPs (10 mM)	0,2 μM
Taq (5 u/μl)	1 u
DNA template	5 ng/μl
<i>Reaction volume</i>	<i>20 μl</i>

**Table 4.** PCR program for *PTGS2* detection

<b>Temperature</b>	<b>Time</b>	
95 °C	2 min	
95 °C	20 s	
60 °C	20 s	x 35 cycles
72 °C	30 s	
72 °C	3 min	

## 2.5 Experimental design

### 2.5.1 *Liver ischemia-reperfusion model*

Male *h-COX-2 Tg* mice aged 8 to 10 weeks and their *Wt* siblings were used. Only male mice were used in the procedures to avoid hormonal modulation of endogenous prostaglandin levels. Mice were randomly divided into 2 groups: Sham surgery group and hepatic ischemia-reperfusion (I/R) group. 30 min before surgery, 100 μL of an analgesic solution (Buprenorphine, 0,05 mg/kg) was injected subcutaneously. Animals were anesthetized with 1,2-2% isoflurane (Isoflutek, Karizoo), and a warm segmented (70%) hepatic I/R protocol was performed for 90 min, clamping the

hepatic triad (**Figure 9**) [139]. Reperfusion was initiated with the removal of the clamp and prolonged for 4 h or 24 h (**Figure 10**). 300  $\mu\text{L}$  of warm saline was injected subcutaneously before the animals were awakened. The animals were sacrificed by cervical dislocation, opened at the abdominal level and the livers were removed. The different lobes were divided and preserved according to future uses (frozen, fixed or used fresh). Whole blood was also collected by cardiac puncture just after the sacrifice.

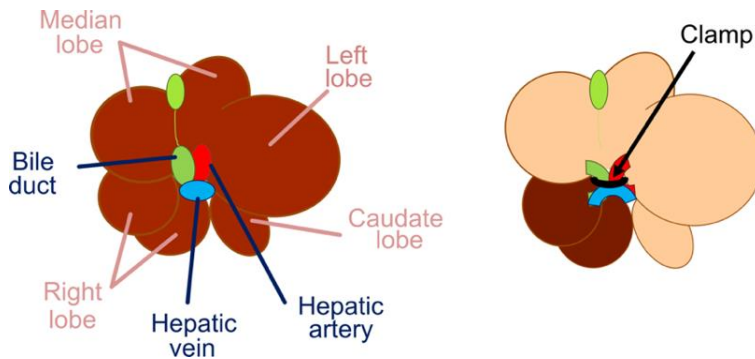


**Figure 9. Schematic representation of the 70% liver ischemia model in mouse liver.** The clamp is placed on the hepatic triad, interrupting hepatic artery supply as well as hepatic vein and bile duct flow. During ischemia, the median, left, and caudal lobes are deprived of blood supply and the right lobes remain hyperoxygenated.

### 2.5.2 Ischemia preconditioning

Prior to the ischemia-reperfusion model described above, a preconditioning (PC) is performed in some *Wt* animals. Once the animal is anesthetized, a short 20 min ischemia is performed clamping the hepatic triad. After this time, the clamp is removed, and a reperfusion of 30 min is allowed before the 90 min ischemia starts (**Figure 10**).

2.5.3 Drug-inhibition of COX-2

A group of *h-COX-2 Tg* and *Wt* PC mice were treated with the COX-2 inhibitor 5,5-dimethyl-3(3-fluorophenyl)-4-(4-methylsulfonyl)phenyl-2(5H)-furanone (DFU) prior to the ischemia surgery. Mice were injected intraperitoneally with 5 mg/kg DFU (reconstituted in dimethyl sulfoxide (DMSO) and diluted in saline) four times: once a day for 3 days and 45 min prior to surgery (Figure 10). Control mice were injected with DMSO diluted in saline.

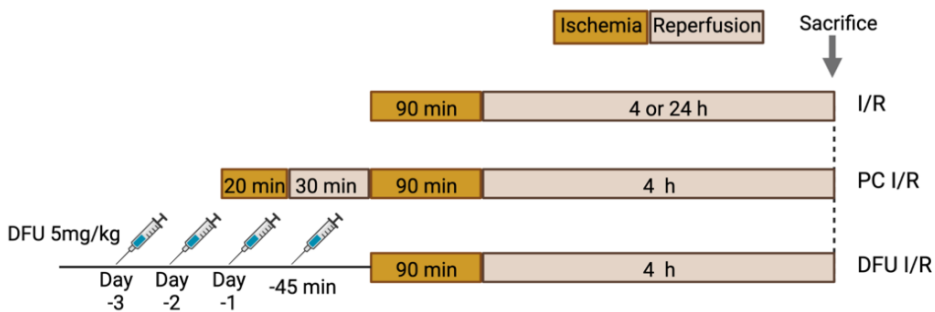


**Figure 10. Temporal diagram of the three different conditions of the experimental design.** The ischemia/reperfusion (I/R) consists of 90 min of ischemia, followed by 4 or 24 h of reperfusion before sacrifice. The PC condition consists of a short ischemia of 20 min, followed by 30 min of reperfusion, before I/R protocol. The DFU condition consists of 4 intraperitoneal injections of DFU at 5mg/kg prior to I/R. *Created with Biorender.com*

3. SUBCELLULAR FRACTIONATION

3.1 Mitochondrial isolation

Liver mitochondria were isolated following the method described by Frezza et al [140]. Briefly, a liver lobe (average weight 300-500 mg) was washed 3 times with cold Mitochondria Isolation Buffer (mIB, Table 5), cut into small pieces (~ 30 mg) and homogenised in a glass/Teflon Potter-Elvehjem homogenizer with 5 mL of cold



mIB at low revolutions. The homogenate was transferred to a 50 mL centrifuge tube and centrifuged at 600x *g* for 10 min at 4 °C. The pellet was discarded and the supernatant was transferred to a centrifuge tube and centrifuged at 7000x *g* for 10 min at 4 °C. The supernatant was discarded; the pellet was resuspended in 5 mL of cold mIB and centrifuged again at 7000x *g* for 10 min at 4 °C. The supernatant was discarded and the mitochondrial pellet was resuspended in 1 mL of mIB. Mitochondrial protein concentration was determined using the DC Protein Assay (Bio-Rad,) with bovine serum albumin (BSA) diluted in mIB for standard curve generation. Fresh mitochondria were used for functional assays (high-resolution respirometry) and frozen aliquots were used for protein assays (Western blotting and supercomplex resolution).

**Table 5.** Mitochondria Isolation Buffer (mIB)

<b>Compound</b>	<b>Concentration</b>
Sucrose	0,2 M
Tris-MOPS	10 mM
EGTA-Tris	1 mM
<i>pH</i>	7.4

### 3.2 Nuclear fractionation

Nuclear extract was isolated from 100 mg of liver tissue with 0,3 M sucrose solution. The tissue was homogenized in a glass/Teflon Potter- Elvehjem homogenizer and centrifuged at 1000x *g* for 10 min at 4 °C to separate the cytosolic fraction (supernatant) and nuclear fraction (pellet). The pellet was washed 4 times with 0,3 mM sucrose solution and centrifuged at 8000x *g* for 15 min at 4 °C. The pellet was then resuspended in Lysis buffer (**Table 6**) and shaken for 1 h at 4 °C. Finally, total protein concentration was determined using the DC Protein Assay (Bio-Rad), with BSA diluted in Lysis buffer for standard curve generation.

## 4. HISTOLOGICAL ANALYSIS

### 4.1 Fixation, paraffin tissue inclusion, and sectioning

Liver pieces were fixed in cold 4% PFA (v/v) overnight, then rinsed with 1X PBS and kept in cold 40% ethanol. Each piece of liver was then placed in a grating and processed in a Tissue Processor (Spin Tissue Processor STP 120, Especialidades Médicas). The protocol followed consists of 1 h in ethanol 70%, 3 h in ethanol 96% I, 1,5 h in ethanol 96% II, 2 h in ethanol 100% I, 6 h in ethanol 100% II, 1,5 h in xylene I, 2,5 h in xylene II, 2,5 h in paraffin I and 2 h in paraffin II. The tissues were then embedded in hot paraffin and allowed to cool to form the paraffin blocks. Sections of 4  $\mu$ m thick were then cut on a microtome (Leica Microsystems).

### 4.2 Deparaffination, rehydration, and dehydration of samples

The preparations were kept at 60 °C for 30 min, and then washed twice in xylene for 15 min. The tissues were then rehydrated in decreasing concentrations of ethanol (100% twice for 10 min, 90% for 5 min, 70% for 5 min and 50% for 5 min), washed with distilled H<sub>2</sub>O and maintained in distilled H<sub>2</sub>O before starting any staining protocol. After the staining, the preparations were dehydrated in increasing concentrations of ethanol (50% for 5 min, 70% for 5 min, 90% for 5 min and twice in 100% for 10 min) and xylene (twice in xylene for 15 min). A drop of mounting xylene-based DPX mounting solution (Scharlab) was then placed on the tissue sections and covered with a coverslip.

### 4.3 Fixed paraffined tissue stains

#### 4.3.1 *H&E staining*

After deparaffination and rehydration, the sections were immersed in Haematoxylin for 3 min, washed with distilled H<sub>2</sub>O<sub>2</sub> for 1 min and immersed in differentiator (soft acid) for 1 min. The sections were incubated with Eosin for 1 min and then dehydrated, mounted and scanned on a digital scanner (Aperio Versa 200,

Leica Microsystems). H&E stain was performed by the department of Animal Medicine and Surgery at the Veterinary Faculty, Universidad Complutense de Madrid (UCM) and by the Microscopy Facility at the Servicio Central de Soporte a la Investigación Experimental (SCSIE), Universitat de València (UV). Semi-quantitative analysis was used to estimate the extent of parenchymal necrosis, performed by a professional pathologist (Dr. Juana M. Flores (UCM) and Echervarne Laboratories, blinded to the features of animal group). At least five fields of each sample were examined at low power fields at 100X magnifications. To determine tissue lesion, the scores used were 0=none, 1=mild lesion (0-20% of necrosis), 2=moderate lesion (20-40% of necrosis), 3=severe lesion (more than 40% of necrosis) [141][142].

#### 4.3.2 *Ly6G<sup>+</sup> staining*

To estimate the degree of hepatic neutrophil infiltration, fixed paraffin-embedded liver sections were used. A standard immunohistochemistry protocol was followed using anti-mouse Ly6G (BD Pharmingen™). Briefly, after deparaffination and rehydration, an antigen retrieval step was performed by immersing the sections in Citrate Buffer (10 mM Sodium Citrate, 0,05% Tween-20 (v/v), pH 6) and microwaving for 5 min. The sections were then allowed to cool down and washed with 1X PBS. The sections were then incubated with Peroxidase Blocking Solution (10% methanol, 3% H<sub>2</sub>O<sub>2</sub> in 1X PBS) for 10 min to block the endogenous peroxidase, and later with Blocking Solution (6% BSA (w/v), 2% normal horse serum (v/v), 0.05% Tween-20 (v/v)) for 1 h to block any non-specific binding of the antibody. Sections were incubated with the primary antibody diluted in Blocking Solution overnight at 4 °C and the next day incubated with the secondary antibody for 1 h at room temperature. The signal was amplified incubating the slides in ABC solution for 45 min and was finally revealed by incubating the slides with DAB Peroxidase Substrate (Vector Laboratories) solution for 4 min. The reaction was stopped with tap water for 2 min; the slides were washed with 1X PBS and mounted with Prolong (Invitrogen).

#### 4.4 Tissue cryopreservation and sectioning

Liver pieces were washed in 1X PBS, kept overnight in 4 % PFA and then passed through increasing concentrations of sucrose in 1X PBS (1 h at 10 % and 20 % and overnight at 30 % (w/v)). Tissues were then briefly washed with 1X PBS, embedded in moulds with OCT embedding medium (LAMP/OCT, Thermo Fisher Scientific) and kept on dry ice until solidification. Sections of 8  $\mu\text{m}$  thick were cut on a cryostat (Leica Microsystems).

#### 4.5 Dihydroethidium staining

Superoxide content was determined in frozen liver sections following the protocol previously described [143]. Fresh liver pieces were washed in 1X PBS, immediately embedded in OCT and frozen in dry ice. 8  $\mu\text{m}$  sections of unfixed frozen liver samples were incubated for 15 min at 37 °C with 5  $\mu\text{M}$  dihydroethidium (Merck Life Sciences S.L.U. –Sigma) diluted in 1X PBS. Slides were washed with cold 1X PBS and covered with a coverslip. Sections were visualised with a Leica DM RXA2 fluorescence microscope. Fluorescence intensities in a minimum of five randomly selected areas (40X magnification) were quantified with Image J software (<https://imagej.nih.gov/ij/>).

#### 4.6 Transmission Electronic Microscopy (TEM)

For transmission electronic microscopy (TEM), tissues were fixed in 2% glutaraldehyde (v/v) (Electron Microscopy Sciences) in 0,1 M sodium cacodylate at pH 7.2, washed with cacodylate buffer containing 0,1 M sucrose and post-fixed with 1% osmium tetroxide (w/v) in phosphate buffer. After washing with H<sub>2</sub>O and dehydration with ethanol, the samples were embedded in epoxy resin. Ultra-thin slices (60 nm) were stained with 2% uranyl acetate (w/v) before TEM visualisation using a HITACHI HT7800 120Kv microscope at 60 Kv. Sample preparations was performed by the Microscopy Facility at the SCSIE, UV.

Images were acquired using an EMSIS XAROSA digital camera with Olympus image analysis software. Quantifications were performed at 12 k or 25 k magnification. An average of a minimum of five visual fields was assessed for each mouse liver. Quantifications were performed with Image J software (<https://imagej.nih.gov/ij/>) as described in [144].

## 5. PROTEIN DETECTION

### 5.1 Protein extraction and quantification

Protein extracts were obtained by homogenising a piece of frozen tissue (~ 50 mg) in cold Lysis Buffer (**Table 6**) with an Ultra Turrax. Homogenates were kept under orbital shaking for 2 h in cold and centrifuged at maximum speed for 20 min at 4 °C. Clear supernatants were collected and protein content was determined using the DC Protein Assay (Bio-Rad). BSA was used for the generation of the standard curve diluted in Lysis Buffer.

**Table 6.** Lysis Buffer for protein extraction

<b>Compound</b>	<b>Concentration</b>
NaCl	150 mM
NP-40	1 % (v/v)
Tris	50 mM
EDTA	5 mM
EGTA	5 mM
PMSF	0,1 mM
protease inhibitor cocktail (Roche)	1 tablet
<i>pH</i>	8

**Table 7.** Laemli sample Buffer

<b>Compound</b>	<b>Concentration</b>
SDS	4 % (w/v)
Glycerol	20 % (v/v)
Bromophenol blue	0,004 % (w/v)
Tris-HCl	0,125 M
DTT	200 mM
<i>pH</i>	<i>6.8</i>

## 5.2 Protein electrophoresis and immunoblotting

For detection of proteins by immunoblotting (Western blot), the same amount of protein for each sample was boiled in Laemli sample buffer (**Table 7**) for 5 min at 95 °C (50 µg for liver homogenates and 20 µg for isolated mitochondria). For detection of the OXPHOS proteins with the OXPHOS antibody cocktail detection, samples were heated at 50 °C for 5 min. Samples were loaded onto 8, 10, or 12% SDS-polyacrylamide (acrylamide/bisacrylamide, 29:1) electrophoresis gel (SDS-PAGE) and allowed to run for 90 min at 150 V in 1X Running Buffer (**Table 8**). Proteins were then transferred to PVDF membranes (Merck Life Sciences S.L.U. –Sigma) for 1 h with cold 1X Transfer Buffer (**Table 8**) at 100 V, and the blots were blocked with blocking solution (1X TBS (**Table 8**), 0,1% Tween-20 (v/v) and 5% milk (w/v) (Difco Skim Milk, BD Biosciences) for 1 h at room temperature. The blots were incubated overnight at 4 °C with the primary antibodies (**Table 10**) diluted in blocking solution. All blots were washed after and before incubations with antibodies with 1X TBS, 0,1% Tween-20 (v/v). After incubation with the corresponding secondary antibodies (anti-mouse IgG HRP, anti-rabbit IgG HRP or anti-goat IgG HRP diluted in blocking solution, 1:10.000 (Santa Cruz Biotechnology; Cayman Chemicals)) for 45 min at room temperature, the blots were washed with 1X TBS and developed with NZY Advanced ECL reagent (NZYTech). Images were acquired on a luminescent image analyser (LAS 4000 mini, GE Healthcare), and densitometric analysis of the bands,

expressed in arbitrary units, was performed with Image Studio Lite software (version 5.2.5, Licor). Band densities of target proteins were quantified and normalised with GAPDH or VINCULIN for cytosolic proteins and LAMIN B for nuclear proteins as loading controls. When isolated mitochondria were used, the loading control selected was CytC.

**Table 8.** Western blot buffers

	1X Running Buffer	1X Transfer Buffer	1X TBS
Compound	Concentration		
TRIS-base	25 mM	25 mM	50 mM
Glycine	0,2 M	0,2 M	-
SDS	3,5 mM	-	-
Methanol	-	20%	-
NaCl	-	-	150 mM
<i>pH</i>			7.6

### 5.3 Protein native electrophoresis for supercomplex detection (BN-PAGE)

Identification of mitochondrial supercomplexes was performed with blue-native gels (BN-PAGE). Briefly, the isolated mitochondria were centrifuged at 7000x g for 10 min at 4 °C. The mitochondrial pellet was resuspended in an appropriate volume of resuspension buffer (**Table 9**) to a final mitochondrial concentration of 10 µg/µL. 100 µg of mitochondria were incubated 5 min on ice with 10% digitonin (w/v) (**Table 9**), and then centrifuged at maximum speed for 30 min at 4 °C. The supernatant was collected in a new tube and blue sample buffer (5% (w/v) blue G dye, 1 M 6-aminohexanoic acid) was added (20% of the final volume). Samples were loaded in the XCellSureLock Mini-Cell Electrophoresis System (Thermo Fisher Scientific); dark blue Cathode buffer (20% (w/v) comassie brilliant blue G250 in 1X Anode

### III. MATERIALS AND METHODS

buffer) was loaded on the inside and 1X Anode buffer (NativePAGE 20X Running Buffer, Thermo Fisher Scientific) in the outside. The gel was run 30 min at 150 V at 4 °C, then the dark blue Cathode buffer was replaced with light blue Cathode buffer (1/10 dilution dark blue Cathode buffer : 1X Anode buffer), and run for further 150 min at 250V at 4 °C. At the end of the run, the gel was stained with blueSafe (NZYTech) and scanned or transferred to a PVDF membrane for immunoblotting assays.

**Table 9.** Buffers for the isolation of mitochondrial supercomplexes

Digitonin Buffer		Resuspension Buffer	
Compound	Concentration	Compound	Concentration
Digitonin	10 % (w/v)	6-amino-hexanoic acid	1 M
NaCl	50 mM	Bis-Tris/HCl	50 mM
Imidazole	50 mM	<i>pH</i>	7.0
6-amino-hexanoic acid	5 mM		
PMSF	4 mM		

**Table 10.** Primary Antibodies used for Western blot (WB) and Immunofluorescence (IF)

Antibody	Host specie	Dilution	Manufacturer	Cat. No.	Technique
ALBUMIN	goat	1:150	R&D Systems	AF-3329	IF
AKT	rabbit	1:1000	Cell Signaling Technology	9272	WB
p-AKT	rabbit	1:1000	Cell Signaling Technology	4060	WB
AMPK	rabbit	1:1000	Cell Signaling Technology	5832	WB
p-AMPK	rabbit	1:1000	Cell Signaling Technology	2535	WB
ATG7	mouse	1:1000	Santa Cruz Biotechnology	sc-376212	WB
BAX	rabbit	1:1000	Cell Signaling Technology	2772	WB
BCL-2	rabbit	1:1000	Cell Signaling Technology	2830	WB
CHOP	rabbit	1:1000	Santa Cruz Biotechnology	sc-793	WB



### III. MATERIALS AND METHODS

---

CLEC4F	goat	1:150	R&D Systems	AF-2784	IF
COX-1	rabbit	1:100	Cell Signaling Technology	4841	WB
COX-2 (monoclonal)	mouse	1:1000	Cayman Chemicals	160107	WB
COX-2 (polyclonal)	rabbit	1:1000	Cayman Chemicals	160106	IF
CytC	mouse	1:1000	Thermo Fisher Scientific	45-6100	WB
DRP1	rabbit	1:500	Abcam	ab184247	WB
eIF2 $\alpha$	rabbit	1:1000	Cell Signaling Technology	9722	WB
p-eIF2 $\alpha$	rabbit	1:1000	Cell Signaling Technology	9721	WB
FIS1	rabbit	1:1000	Proteintech	10956-1-AP	WB
GAPDH	mouse	1:1000	Ambion	AM4300	WB
GRP78	mouse	1:1000	Santa Cruz Biotechnology	sc-376768	WB
HSP60	rabbit	1:100	Abcam	ab46798	IF
I $\kappa$ B $\alpha$	rabbit	1:1000	Santa Cruz Biotechnology	sc-371	WB
p-I $\kappa$ B $\alpha$	mouse	1:1000	Santa Cruz Biotechnology	sc-8404	WB
JNK/SAPK	rabbit	1:1000	Cell Signaling Technology	9252	WB
p-JNK/SAPK	rabbit	1:1000	Cell Signaling Technology	9251	WB
LAMIN B	goat	1:1000	Santa Cruz Biotechnology	sc-6217	WB
LC3	rabbit	1:1000	Sigma-Merck	L7543	WB
MFN1	rabbit	1:1000	Proteintech	13798-1-AP	WB
MFN2	mouse	1:1000	Abcam	ab56889	WB
NDUFA5	rabbit	1:1000	Proteintech	16640-1-AP	WB
NRF2	rabbit	1:1000	Santa Cruz Biotechnology	sc-13032	IF, WB
OMA1	mouse	1:1000	Santa Cruz Biotechnology	sc-515788	WB
OPA1	rabbit	1:1000	Abcam	ab15457	WB
OXPHOS	mouse	1:250	Abcam	ab110413	WB
p62	rabbit	1:1000	MBL	PM045	WB
p65	rabbit	1:1000	Cell Signaling Technology	8242	WB
p65	rabbit	1:150	Santa Cruz Biotechnology	sc-109	IF
MnSOD	rabbit	1:1000	Enzo Life Sciences	ADI-SOD-110	IF, WB
VINCULIN	rabbit	1:2000	Proteintech	26520-1-AP	WB
YME1L1	rabbit	1:1000	Proteintech	11510-1-AP	WB

---

#### 5.4 Immunofluorescence

For cryopreserved tissues, sections were fixed with 4% PFA (v/v) at 4 °C for 30 min. For 4% PFA-fixed, paraffin-embedded tissues, sections were deparaffinised and rehydrated before starting the protocol. For the HSP60 immunostaining specifically, antigen retrieval was performed by incubating the tissues with 0,01% Trypsin (v/v) in 1X PBS at 37 °C for 10 min and microwave heating in Tris-EDTA buffer (10 mM Tris, 0,1 mM EDTA, pH 9) for 10 min. For all sections, non-specific binding was blocked with blocking solution (10% normal horse serum (v/v), 1% BSA (w/v), and 0,2% Triton X-100 (v/v) in PBS) for 1 h at room temperature and incubated overnight with primary antibodies diluted in blocking solution (**Table 10**). On the next day, the slides were washed with 1X PBS and incubated with secondary antibodies (Alexa Fluor 488 donkey anti-goat, Alexa Fluor 647 donkey anti-rabbit or Alexa 546 goat anti-rabbit diluted in blocking solution, 1:500 (Invitrogen, Thermo Fisher Scientific)) for 45 min at room temperature in the dark. Slides were washed with 1X PBS and nuclei were stained with Hoescht 33342 (at 160 µM in 1X PBS, Thermo Fisher Scientific) for 10 min at room temperature in the dark. Finally, the slides were mounted with Prolong (Invitrogen). Photographs (magnifications 40X and 63X) were taken with a confocal microscope (SP-8, Leica Microsystems) using the LAS AF software (Leica Application Suite Advanced Fluorescence, Leica Microsystem).

## 6. GENE DETECTION AND EXPRESSION

### 6.1 Isolation of total DNA from frozen liver tissue

Total DNA was isolated from small pieces of frozen liver tissues (~ 30 mg). The pieces were homogenized in 100 µL of DNA Isolation Homogenisation Buffer (**Table 11**) in a small glass/Teflon Potter-Elvehjem homogenizer manually. The homogenate was transferred to a 1,5 mL tube and 5 U/µL of RNase (NZYtech) was added. The tubes were incubated at 37 °C for 30 min. Next, 300 µL of DNA Isolation Lysis Buffer

(Table 11) plus 2% (v/v)  $\beta$ -mercaptoethanol were added. The tubes were vortexed briefly and incubated at 65 °C for 30 min. After this time, a volume of chloroform–isoamyl alcohol (24:1) was added, the tubes were shaken until the 2 phases were combined and centrifuged at 16000x *g* for 10 min at room temperature. The upper phase was then collected in new tubes and a volume of isopropanol was added. The tubes were kept at -20 °C for at least 1 h and then centrifuged at 16000x *g* for 25 min at 4 °C. The supernatant was discarded and the DNA pellet was washed twice with 70% ethanol, dried at room temperature and resuspended in T.E. 10/0,1 (10 mM Tris, 0,1 mM EDTA).

**Table 11.** DNA Isolation Buffers

DNA Isolation Homogenisation Buffer		DNA Isolation Lysis Buffer	
Compound	Concentration	Compound	Concentration
Tris-HCl	10 mM	CTAB	2% (w/v)
MgCl <sub>2</sub>	10 mM	Tris-HCl	100 mM
Triton X-100	5% (v/v)	EDTA	20 mM
<i>pH</i>	7.0	NaCl	1,4 M
		<i>pH</i>	8.0

## 6.2 Determination of mitochondrial DNA content

DNA quantification was performed with a Nanodrop 2000 (Thermo Fisher Scientific), and diluted to a final concentration of 10 ng/mL. The nuclear encoded gene *ApoB* was used as a nuclear genetic marker (nDNA) and mitochondrial encoded gene *CytB* as a mitochondrial genetic marker (mtDNA). Both genes were amplified by qPCR with Power SYBR Green Master Mix (Thermo Fisher Scientific) (Table 12) with specific primers (Table 14). The qPCR was performed with a QuantStudio 5 System (Thermo Fisher Scientific). Each sample was run in duplicate and mtDNA was normalized to nDNA. The biological replicates were then averaged and fold induction was determined in a  $2^{-\Delta\Delta C_t}$ -based fold-change calculation.

### 6.3 RNA extraction, RT, and qPCR

Total RNA from frozen liver pieces was extracted using TRI Reagent (Thermo Fisher Scientific) according to the manufacturer's indications. Briefly, frozen liver pieces (~30 mg) were homogenised with an Ultra Turrax in 1 mL of TRI Reagent and incubated at room temperature for 5 min. The tubes were centrifuged and the supernatants were collected in new tubes. 200  $\mu$ L of chloroform were added to the tubes, mixed vigorously and kept at room temperature for 15 min. After centrifugation at 12.000x *g* for 10 min at 4 °C, the aqueous phase (on top) was transferred to new tubes. 500  $\mu$ L of isopropanol were added; the tubes were shaken by several inversions and kept at room temperature for 10 min. RNA pellet was formed after centrifugation of 10 min at 12.000x *g* at 4 °C, and washed twice with cold 70% ethanol. Pellets were dried at room temperature for 5 min, resuspended in H<sub>2</sub>O (RNase-free), and stored at -80 °C for later use.

RNA was reverse transcribed using a Transcriptor High Fidelity cDNA Synthesis Kit according to the manufacturer's indications (Roche Diagnostic) ([Table 13](#)).

**Table 12.** Reverse Transcription (RT) program

Temperature	Time
65 °C	10 min
4 °C	-
25 °C	10 min
55 °C	30 min
85 °C	5 min
4 °C	-

**Table 13.** qPCR programs for SYBRGreen and TaqMan reagents

Fast SYBRGreen reagents			TaqMan reagents		
Temperature	Time		Temperature	Time	
95 °C	20 s		95 °C	10 min	
95 °C	1 s	x 40 cycles	95 °C	15 s	
60 °C	20 s		60 °C	60 s	x 45 cycles
95 °C	1 s	Melt curve stage	72 °C	1 s	
60 °C	20 s		40 °C	30 s	
95 °C	1 s				

The cDNA was used as a template for real-time qPCR. Specific genes were amplified using Fast SYBR Green Master Mix (Thermo Fisher Scientific) (Table 13) with specific primers (Table 14) or Eagle Taq Universal MMX w/ROX (Roche Diagnostic) (Table 13) master mix with specific primers and UPL probes (Table 14) in a real-time qPCR thermocycler. Each sample was run in duplicate and normalized to *Hprt* or *Rplp0* genes as housekeeping genes. The replicates were then averaged, and fold induction was determined in a  $2^{-\Delta\Delta C_t}$  based fold-change calculations.

**Table 14.** Primers for qPCR

<b>Gene</b>	<b>Primer pair</b>	<b>Technology</b>
<i>Atf4</i>	FP: 5'-CTCATGGGGCCTTTAGGACG-3' RP: 5'-GTGGTCACGTGATCCTACCG-3'	SYBRGreen
<i>Apob</i>	FP: 5' CGTGGGCTCCAGCATTCTA 3' RP: 5' TCACCAGTCATTTCTGCCTTTG 3'	SYBRGreen
<i>Cybb</i>	FP: 5' GCTTCCACTTCATCTTACCATTTA 3' RP: 5' TGTTGGGTTGTTTGATCCTG 3'	SYBRGreen
<i>Atf6</i>	FP: 5'-AGGTGTCTGTTTCGGGGAAG-3' RP: 5'-CAAACAACGTGCGACTCCCAGT-3'	SYBRGreen
<i>Ddit3</i>	FP: 5'-CCTGAGGAGAGAGTGTTCAG-3' RP: 5'-GACACCGTCTCCAAGGTGAA-3'	SYBRGreen
<i>Gpx</i>	FP: 5'-ATCGACATCGAACCTGACAT -3' RP: 5'-GAGTGCAGCCAGTAATCACC -3'	SYBRGreen
<i>Gsr</i>	FP: 5'-ATTGGCTGTGATGAGATGCT-3' RP: 5'-GGTAGGATGAATGGCAACTG-3'	SYBRGreen
<i>Hmox1</i>	FP: 5'-AGGCTAAGACCGCCTTCT -3' RP: 5'-TGTGTTCTCTGTGTCAGCATCA -3'	SYBRGreen
<i>Hprt</i>	FP: 5' -TCCTCCTCAGACCGCTTTT- 3' RP: 5' -CCTGGTTCATCATCGCTAATC- 3'	TaqMan (UPL probe #95)
<i>Hspa5</i>	FP: 5'-TGTGTGTGAGACCAGAACCG-3' RP: 5'-GCAGTCAGGCAGGAGTCTTA-3'	SYBRGreen
<i>Il-10</i>	FP: 5'-CTGGACAACATACTGCTAACCG- 3' RP: 5'-GGGCATCACTTCTACCAGGTAA-3'	SYBRGreen
<i>IL-1b</i>	FP: 5'-AGAAGCTGTGGCAGCTACCTG- 3' RP: 5'-GGAAAAGAAGGTGCTCATGTCC-3'	SYBRGreen
<i>Il-6</i>	FP: 5'-GAGGATACCACTCCCAACAGACC- 3' RP: 5'-AAGTGCATCATCGTTGTTTCATACA-3'	SYBRGreen
<i>Nlrp3</i>	FP: 5'-ATTACCCGCCCGAGAAAGG-3' RP: 5'-TCGCAGCAAAGATCCACACAG-3'	SYBRGreen
<i>Nfe2l2</i>	FP: 5'-TAGATGACCATGAGTCGCTTGC -3' RP: 5'-GCCAAACTTGCTCCATGTCC-3'	SYBRGreen
<i>Ppargc1a</i>	FP: 5' -AATTTTTCAAGTCTAACTATGCAGACC- 3' RP: 5' -CAAATCCAGAGAGTCATACTTGC- 3'	TaqMan (UPL probe #31)
<i>Ptgs1</i>	FP: 5'-ATGAGTCGAAGGAGTCTCTCG-3' RP: 5' GCACGGATAGTAACAACAGGGA-3'	SYBRGreen
<i>PTGS2</i>	FP: 5'- CGCAGTACAGAAAGTATCACAGGC-3' RP: 5'- GCGTTTGCGGTACTCATTAAAA -3'	SYBRGreen
<i>Rplp0</i>	FP: 5' -ACTGGTCTAGGACCCGAGAAG- 3' RP: 5' -TCCCACCTTGTCTCCAGTCT- 3'	SYBRGreen
<i>Sod1</i>	FP: 5'-TGTGTCCATTGAAGATCGTG-3' RP: 5'-CTTTGCCCAAGTCATCTTGT-3'	SYBRGreen
<i>Sod2</i>	FP: 5'-TCAGTGCTCACTCGTGTCAT-3' RP: 5'-ACACGATAGGTTTGGGCATA-3'	SYBRGreen
<i>Tfam</i>	FP: 5' -TGAGGCTTGGAAAAATCTGTCT- 3' RP: 5' -TCGTCCAACCTCAGCCATC- 3'	TaqMan (UPL probe #103)
<i>Tnf</i>	FP: 5'-CAGGCGGTGCCTATGTCTC- 3' RP: 5'-CGATCACCCCGAAGTTCAGTAG-3'	SYBRGreen

#### 6.4 Determination of *Xbp1* splicing

The cDNA was used as a template to detect splicing variants of the *Xbp1* gene. Splicing variants were amplified with conventional PCR with specific primers (Table 15) and PCR program (Table 16). The PCR product was loaded onto a 6% polyacrylamide (acrylamide/bisacrylamide, 29:1) electrophoresis gel for 90 min at 80 V. The gel was stained with ethidium bromide and visualised on a transilluminator. Densitometric analysis of the bands was performed with Image Studio Lite software (version 5.2.5, Licor) and expressed as percentages (spliced band to total).

**Table 15.** Primers for *Xbp1* cDNA PCR and splicing detection

Gene	Primer pair
<i>Xbp1</i>	FP: 5' -GAACACGCTTGGGAATGGACAC- 3' RP: 5' -AGAAAGGGAGGCTGGTAAGGAAC- 3'

**Table 16.** PCR program for *Xbp1* splicing detection

Temperature	Time	
95 °C	3 min	
95 °C	20 s	
62 °C	20 s	x 35 cycles
72 °C	30 s	
72 °C	3 min	

#### 6.5 RNAseq and NGS analysis

Briefly, total RNA was obtained using the mirVana miRNA Isolation Kit (Thermo Fisher Scientific,) and prepared for sequencing using the Illumina TruSeq RNA Sample Prep Kit v2 according to the manufacturer's instructions. RNA was sequenced on a Hiseq 4000 platform (Macrogen). The Illumina Hiseq 4000 generated raw images using HCS (HiSeq Control Software v3.3) for system control and base calling through an integrated primary analysis software called RTA (Real Time Analysis, v2.7.3). The Base Class Library (BCL) binary was converted into FASTQ using the Illumina package bcl2fastq (v2.17.1.14). Trimmed 100bp sequenced paired-end reads were mapped to a reference genome with HISAT2. After mapping the reads, Stringtie was used for transcript assembly. An expression profile was calculated for each sample and transcript/gene as fragments per kilobase of transcript per million mapped reads. Sequencing and analyse were performed by Macrogen.

## 7. DETERMINATION OF METABOLITES AND CYTOKINES

### 7.1 Plasma collection

Whole blood was obtained by cardiac puncture of the post-mortem left atrium with a heparinised syringe, and collected in 1,5 mL tubes containing 10  $\mu$ L of heparin (5% heparin solution (w/v) in saline). The tubes were centrifuged at 300x *g* for 30 min at 4 °C and the plasma (upper phase) was collected in new tubes.

### 7.2 PGE<sub>2</sub>

PGE<sub>2</sub> was determined in liver homogenates and plasma by means of a specific immunoassay (K051, Arbor Assays). Briefly, plasma and tissue homogenates were loaded onto a plate with a mouse IgG antibody conjugate at the bottom of the wells. PGE<sub>2</sub>-peroxidase conjugated and monoclonal antibodies to PGE<sub>2</sub> were then added to the samples. Incubation was performed to allow for the binding reaction before adding



the substrate. The substrate reacts with the bound peroxidase and after a short incubation the reaction is stopped. The intensity of the generated colour is detected in a microtiter plate reader at a wavelength of 450 nm. The concentration of PGE<sub>2</sub> in the samples is calculated using a standard curve supplied with the kit.

### 7.3 Plasma transaminases

Alanine transaminase (ALT) and aspartate transaminase (AST) activities were determined in plasma with specific kits from BioSystems (COD 11832 and COD 11830 respectively). For the ALT measurement, the kit is based on a two-step reaction. First, ALT present in the sample will transform alanine and 2-oxoglutarate into pyruvate and glutamate. Secondly, lactate dehydrogenase (LDH) catalyses the reaction between the pyruvate generated in the previous reaction with NADH and free protons to generate lactate and NAD<sup>+</sup>. ALT activity will be measured indirectly through the decrease of NADH at 340 nm. For the measurement of AST, the kit uses an approach very similar to that of ALT. In this case, AST present in the sample will transform aspartate together with the 2-oxoglutarate to generate oxaloacetate and glutamate. In a second reaction, the malate dehydrogenase enzyme catalyses the reaction between oxaloacetate, NADH, and free protons to generate malate and NAD<sup>+</sup>. AST activity will also be measured indirectly through the decrease of NADH at 340 nm. Samples are mixed with the appropriate reaction buffer containing all reagents and enzymes, incubated for 1 min and measured in a microtiter plate reader at 340 nm every min for 3 min. The absorbance increment per minute is calculated and the concentration of ALT and AST are calculated according to the manufacturer's instructions.

### 7.4 Plasma cytokines

LDH, IL-1 $\beta$ , TNF- $\alpha$  and IL-6 levels were assessed in plasma with a Luminex analysis kit (MCYTOMAG-70K, Millipore, Merck Life Sciences S.L.U. –Sigma). Parameters were measured by the Flow Citometry Facility at the Centro Nacional de Biotecnología (CNB-CSIC).

#### 7.5 Total NAD and NADH content determination

For determination of the total NAD and NADH content, the NAD/NADH Assay Kit (Colorimetric) was used (ab65348, Abcam). Briefly, frozen liver pieces (~20 mg) were homogenised in the corresponding NAD/NADH extraction buffer at a ratio of 400  $\mu$ L/20 mg in a glass Teflon homogeniser. Deproteinisation of the samples was performed with 10 kDa spin columns. Total NAD and NADH samples were loaded in duplicates into a 96-well flat-bottomed plate and the assay was performed according to the manufacturer's instructions. The absorbance was measured at 450 nm in a Spark TECAN microplate reader until the optical density stabilised (Tecan, Männedorf, Switzerland).

#### 7.6 AMP and ATP determination

The determination of AMP content was performed with the AMP Assay kit (Colorimetric) (ab273275, Abcam). Frozen liver tissue (minimum 10 mg) was homogenised in AMP assay buffer at a ratio of 100  $\mu$ L/10 mg in a glass Teflon homogeniser. Deproteinisation of the samples was performed with 10 kDa spin columns and the filtrate was loaded into a 96-well flat-bottomed plate in duplicate. The assay was performed according to the manufacturer's instructions and absorbance was measured at 560 nm in a Spark TECAN microplate reader.

Detection of total ATP was analysed with the ATP colorimetric/fluorometric assay (MAK190, Merck Life Sciences S.L.U. –Sigma). 10 mg of liver tissues were homogenised in 100  $\mu$ L ATP assay buffer in a glass Teflon homogeniser. Samples were diluted with ATP assay buffer and loaded into a black 96-well flat-bottomed plate, in triplicate. The assay was performed according to the manufacturer's instructions. Fluorescence was measured with a Spark TECAN microplate reader,  $\lambda_{Ex}$ =535 nm,  $\lambda_{Em}$ =587 nm.

## 8. ENZYMATIC ACTIVITIES

### 8.1 Caspase 3

Caspase-3 was determined by Caspase-3 Fluorogenic Substrate kit (556485, BD Biosciences) in plasma. A caspase-3 fluorogenic substrate (Ac-DEVD-AMC) is added to the samples and after an incubation for 1 h at 37 °C, fluorescence is measured in a microtiter plate reader,  $\lambda_{Ex}=380$  nm,  $\lambda_{Em}=420-460$  nm. Protease activity is represented by arbitrary units of fluorescence and normalised to protein content of the samples. Protein levels were determined using the DC Protein Assay (Bio-Rad). BSA was used for the generation of the standard curve.

### 8.2 Catalase

Catalase (CAT) activity was determined using a specific Enzo Life Sciences kit (ADI-907-027). The kit is based on the determination of the final amount of  $H_2O_2$  present in the medium after incubation with the CAT in the sample. Using a standard curve supplied by the kit with different concentrations of CAT, the CAT activity of the sample can be determined from the traces of  $H_2O_2$  that it does not metabolise. Briefly,  $H_2O_2$  is added to the samples, the reaction that converts  $H_2O_2$  to  $O_2$  and  $H_2O$  by the CAT present is allowed to occur, and then a detection reagent is added. This detection reagent will react with the remaining  $H_2O_2$  and emit fluorescence. The fluorescence intensity is measured in a microtiter plate reader,  $\lambda_{Ex}=570$  nm,  $\lambda_{Em}=590-600$  nm.

### 8.3 Superoxide dismutase

The superoxide dismutase (SOD) activity assay was based on the method of Donahue et al. [145], which measures the SOD inhibition of the photochemical reduction of nitroblue tetrazolium. Gel activity assays were performed on total extract fraction containing 35  $\mu$ g of protein separated by 12% non-denaturing PAGE at 4 °C. Gels were pre-equilibrated in 0,05 M potassium phosphate solution, pH 7.8, and 1

mM EDTA for 30 min, and then immersed in 0,24 mM nitroblue tetrazolium (NBT), 33,2 mM riboflavin, and 0,2% N,N,N',N'- tetramethylethylenediamine (TEMED) (v/v) in pre-equilibrating buffer for 30 min in the dark. In eukaryotic cells there are 2 types of SODs: Cu/Zn SOD and Mn SOD. Cu/Zn SOD is the predominant form present in cell cytosol (about 80% of total SOD), while the remainder is Mn SOD present in the mitochondrial matrix. To identify the individual isoforms, the gels were treated with or without 0,2 mM potassium cyanide in the pre-equilibration buffer. The Cu/Zn SOD isoform is inhibited by this way, but the activity of Mn SOD is not affected. Quantification, performed by densitometric analysis of the bands, was carried out with ImageJ software (Rasband, <http://imagej.nih.gov>) and expressed in arbitrary units.

#### 8.4 Glutathione reductase and Glutathione Peroxidase

Glutathione Reductase and Glutathione Peroxidase activities were monitored using specific colorimetric detection kits from Enzo Life Sciences (ADI-900-159 and ADI-900-158, respectively) according to manufacturer's indications.

In the assays, the oxidation of NADPH to NADP<sup>+</sup> is monitored by decreasing absorbance at 340 nm. This rate of decrease in absorbance at 340 nm is directly proportional to the enzymatic activities.

#### 8.5 Total glutathione and oxidised glutathione measurement

To determine the concentrations of total glutathione and oxidised glutathione in the samples, a specific kit from Enzo Life Sciences (ADI-900-160) was used. The assay is based on the principle of glutathione reductase reduction of oxidised glutathione (GSSG) to reduced glutathione (GSH). A detection agent, DTNB (5,5'-dithiobis-2-nitrobenzoic acid), reacts with GSH to produce a yellow 5-thio-2-nitrobenzoic acid (TNB) which absorbs at 405 nm. The detection of TNB is directly proportional to the concentration of glutathione in the sample. Liver samples were homogenised in 5% (w/v) meta-Phosphoric acid (20 mL/g tissue), centrifuged and the

clear supernatant was collected for the assay. Standards and samples were loaded into a 96-well plate, incubated with the reaction mix composed of glutathione reductase and DTNB and then absorbance was measured in a microtiter plate reader at 450 nm. For the detection of GSSG, the same assay was performed but with the addition of 4-vinylpyridine-treated to the samples and standards. The GSH measurement is calculated as total glutathione minus GSSG.

### 8.6 Myeloperoxidase activity

Myeloperoxidase (MPO) activity was determined using a fluorometric detection kit (ADI-907-029, Enzo Life Sciences) according to the manufacturer's instructions. Briefly, tissue samples were washed and homogenised, then loaded onto a 96-well plate. Next, a reaction cocktail containing H<sub>2</sub>O<sub>2</sub> and the detection agent was added to the samples and incubated to allow the reaction. The MPO present in the sample will react with the H<sub>2</sub>O<sub>2</sub> and the detection agent who will then emit fluorescence. Fluorescence signal was measured in a microtiter plate reader,  $\lambda_{Ex}$ = 530-571nm;  $\lambda_{Em}$ = 590-600nm.

### 8.7 Indirect measurement of ROS production

Lipid peroxidation (LPO) levels were determined as indirect measures of ROS production. The amount of aldehyde products generated by LPO was quantified *ex vivo* in liver tissue by TBA reaction according to the method of Ohkawa and colleagues [146]. Liver tissue (30 mg) was homogenised with 300  $\mu$ L of 0,15 M KCl, and 50  $\mu$ L of liver homogenate was incubated for 60 min at 95 °C with 0,3 % TBA (v/v) pH 3-3.5, 0,5 % SDS (w/v), and 7,5 % acetic acid (v/v). The mixture was centrifuged at 4000x *g* for 10 min. The amount of TBA reactants (TBARS) was expressed in terms of MDA using 1,1,3,3-tetramethoxypropane as a standard (nmol MDA/mg protein) [147].

## 9. FUNCTIONAL ASSAYS

### 9.1 Measurement of mitochondrial membrane potential

Mitochondrial membrane potential measurement was performed by flow cytometry. Briefly a fresh small liver lobe was washed in 1X PBS and minced with scissors. The small pieces were placed in a GentleMACS tube (Miltenyi Biotec) containing 5 mL of pre-warmed DMEM with 0,75 mg/mL collagenase A. Liver pieces were homogenised in the Octo Dissociator (Miltenyi Biotec) following a pre-set programme (37C\_m\_LIDK\_1), then the homogenate was filtered in a 100 µm filter, and the collagenase reaction was stopped with 5 mL of cold DMEM. The homogenate was centrifuged and the cell pellet was washed with 1X PBS once, and then resuspended in 10 mL of 1X PBS. A 200 µL aliquot of the cell suspension was treated with 10 µM cyclosporin H (1 mM stock in DMSO), labelled with 200 nM TMRM (20 µM stock, Invitrogen), and incubated at 37 °C for 30 min in the dark. After this time, 50 µL of cell suspension was passed through a flow cytometer (MACS Quant, Miltenyi Biotec) to determine the TMRM labelling with the 561 nm excitation filter (20.000 events analysed).

### 9.2 High resolution respirometry

For high-resolution respirometry assays, an Oroboros Oxygraph-2k Fluorescence Respirometry (O2k, Oroboros Instruments) was used. Chambers A and B were loaded with 2 mL of MiR05 medium ([Table 17](#)) and calibrated at 30 °C. 50 µg of fresh isolated mitochondria were loaded into each chamber. All experiments were performed comparing *Wt*- and *h-COX-2 Tg*-derived mitochondria. A substrate-uncoupler-inhibitor-titration protocol called SUIT-RP2 was performed ([Figure 11](#)) [148]. The substrates used can be found in [Table 18](#). ADP was added to initiate OXPHOS, 0,1 mM malate and 0,5 mM octanoyl-carnitine were then added to record the electron transfer flavoprotein complex (CETF) from fatty acid β-oxidation to CoQ (F pathway). Next, complex I substrates were added (2 mM malate, 5 mM pyruvate and 10 mM glutamate), to record OXPHOS at the N-junction. Succinate (50 mM) was

then added to record the OXPHOS capacity of the FNS state with convergent electron entry through complex I and II into the respiratory system. 10 mM glycerol-3-phosphate was added to activate the glycerol-3-phosphate dehydrogenase shuttle. To determine the state of ETS capacity at maximal oxygen flow, stepwise titrations with Carbonyl Cyanide Chlorophenylhydrazone (CCCP) in 0,5  $\mu$ M increments were performed. Inhibition of complex I was performed by the addition of rotenone. All respiratory coupling states were corrected for residual oxygen consumption (ROX), which was obtained after the addition of antimycin A. Finally, 2 mM ascorbate plus N,N,N',N'-tetramethyl-p-phenylenediamine dihydrochloride (0,5 mM TMPD) were used as substrates to assess complex IV activity [149]. All substrates were added when the flow stabilised after the addition of the previous substrate (approximately every 10 min), except for inhibitors, which were added after 5 min. CCCP titrations were added each time the flow reached a maximum (every 1,5 min).

Mitochondrial membrane integrity was verified after addition of CytC, and changes were always less than 10%. Oxygen concentrations (mM) and oxygen flux (pmol/s·mL) data were processed with DatLab 7.4.0.4 software (Oroboros Instruments) and specific flux (pmol/s·mg) data were obtained. All experiments were performed using instrumental background correction and after calibration of the polarographic oxygen sensors.

**Table 17.** MiR05 medium composition

<b>Compound</b>	<b>Concentration</b>
Sucrose	110 mM
k-lactobionate	60 mM
k-HEPES	20 mM
Taurine	20 mM
KH <sub>2</sub> PO <sub>4</sub>	10 mM
MgCl <sub>2</sub>	3 mM
EGTA	0,5 mM
BSA	1 mg/mL
<i>pH</i>	7.1

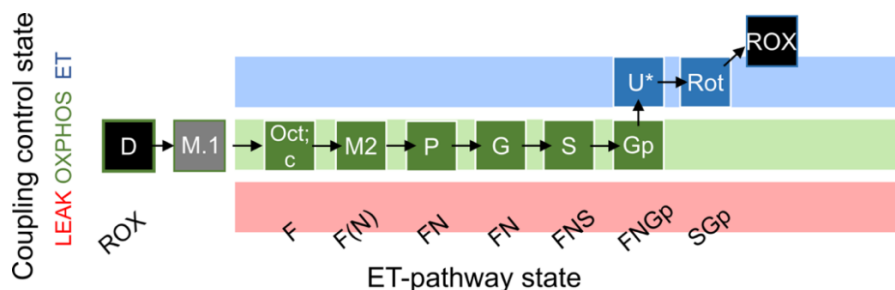


**Figure 11. Summary of the high respirometry SUIT2 protocol.** Sequentially added substrates and ET-pathway states are indicated. Figure adapted from Bioblast, Oroboros Instruments.

**Table 18.** Substrates, decoupling agents, and inhibitors for high-resolution respirometry protocols

Reagents	Abbreviation	Concentration in syringe (solvent)	Final concentration in 2ml O2k chamber	Injection volume (µl)
<b>Substrates</b>				
ADP	D	0,5 M	5 mM	20
DL-Octanoylcarnitine	Oct	0,1 M	0,5 mM	10
Cytochrome C	c	4 mM	10 µM	5
L-Malic Acid	M	0,05 – 0,4 mM	2 mM	4 – 9,5
Pyruvic Acid	P	2 M	5 mM	5
L-Glutamic Acid	G	2 M	10 mM	10
Succinate	S	1 M	50 mM	100
Glycerophosphate	Gp	1 M	10 mM	20
Ascorbate	As	0,8 M	2 mM	5
TMPD	Tm	0,2 M	0,5 mM	5
<b>Decoupling agents</b>				
CCCP	U	1 mM	steps of 0,5 µM	titrations of 1
<b>Inhibitors</b>				
Antimycin A	Ama	5 mM	2,5 µM	1
Rotenone	Rot	1 mM	0,5 µM	1
Sodium Azide	Azd	4 M	200 mM	100



## 10. PATIENTS

This study used plasma samples and patient data available from a cohort of 64 patients who had received OLT provided by Hospital Gregorio Marañón (Madrid). This analysis was approved by the Ethics Committee on Clinical Research of the Hospital Gregorio Marañón (Madrid, Spain; June 2016) and all patients had previously signed an informed consent allowing plasma collection and analysis. Patient information regarding gender, age, liver pathology, time of ischemia etc can be found in [Annex 1](#). Patient's plasma was obtained from cadaveric donors 60 min after reperfusion, and PGE<sub>2</sub> levels were measured with a specific kit ([section 7.2 of Materials and Methods](#)). Early graft function was assessed using the Toronto classification, which takes into accounts ALT elevation, coagulopathy and bile flow [150]. Patients were classified into good early graft function (grades 1 and 2) and poor early graft dysfunction (grades 3 and 4).

## 11. STATISTICS

Data are expressed as mean  $\pm$  standard error of the mean (SEM). The sample size (N) is indicated in each experiment. To assess the normality of the variables, a Shapiro–Wilk test was performed and all behave in a normal distribution. Therefore, statistical significance was tested by t-test when comparing two variables (*Wt* I/R to *h-COX-2 Tg* I/R, *Wt* I/R to *Wt* PC or *h-COX-2 Tg* I/R to *h-COX-2 Tg* DFU) or one-way ANOVA, followed by Tukey's posthoc test when multiple variables were compared (*Wt* Sham, *h-COX-2 Tg* Sham, *Wt* I/R and *h-COX-2 Tg* I/R; *Wt* I/R, *Wt* PC and *Wt* PC DFU; *Wt* Sham, *Wt* I/R and *Wt* PC). For patients, the Kolmogorov-Smirnov test was used to assess the normality of the distribution of numerical variables. In this case, samples follow a non-normal distribution. To compare means between independent samples, the Mann-Whitney rank-sum test was used. To assess a significant relationship between two variables, Spearman's correlation was

calculated. The analysis was performed with the statistical software SPSS (IBM Corp; Version 27.0). Graphs and additional statistical tests were performed with GraphPad Prism (GraphPad Software, Version 7).

\*  $p < 0,05$  versus *Wt Sham*; #  $p < 0,05$  versus *Wt I/R*; \$  $p < 0,05$  versus *Wt PC*; †  $p < 0,05$  versus *h-COX-2 Tg I/R*; &  $p < 0,05$  versus *h-COX-2 Tg Sham*.

## IV. RESULTS





The results presented in sections 1, 2 and 3 below were done in collaboration with Dr. Omar Motiño and Dr. Daniel E. Francés; Dr. Carme Cucarella performed the splicing-variant detection PCR of *Xbp1*. The results presented in section 4 were obtained entirely by the PhD candidate. The results presented in section 5 were elaborated from data provided by the Hospital Gregorio Marañón and laboratory measurements.



## 1. CHARACTERIZATION OF THE ROLE OF COX-2 IN HEPATIC ISCHEMIA-REPERFUSION MODEL

### 1.1 Establishment of the ischemia-reperfusion injury pathology

The mouse model used in this study is a transgenic mouse that constitutively expresses the human COX-2 enzyme (h-COX-2) specifically in the hepatocyte. The generation of this transgenic model is already described [45]. Male *h-COX-2 Tg* mice and their *Wt* siblings were subjected to a 90 min hepatic ischemia by clamping the hepatic triad, followed by 4 or 24 h of reperfusion (I/R) or a laparotomy without clamping (Sham). First, *h-COX-2* mRNA and h-COX-2 protein expression were analysed, and there is no change in either protein (**Figure 12A**) or mRNA (**Figure 12D**) expression in the *h-COX-2 Tg* mice after ischemia and 4 or 24 h of reperfusion. The expression of the endogenous *Ptgs1* mRNA isoform and its protein mCOX1 is also not altered under any condition (**Figure 12A-C**).

Hepatic prostaglandins are, as expected, significantly increased in the livers of *h-COX-2 Tg* mice, and are maintained under all conditions (**Figure 12B**). *Wt* mice only showed an increase in PGE<sub>2</sub> expression after 90 min of ischemia and 24 h of reperfusion.

### 1.2 Liver of *h-COX-2 Tg* mice have less tissue damage compared to the *Wt* animals

After 4 and 24 h following the initiation of reperfusion, the animals were sacrificed and tissue and blood samples were collected. Plasma ALT and AST transaminases were analysed as markers of hepatic damage (**Figure 13A**). The presence of these markers is higher after I/R in all conditions, reflecting the presence of liver damage, although after 24 h of reperfusion, these levels are lower compared to 4 h of reperfusion. In addition, *h-COX-2 Tg* animals have lower levels of transaminases compared to *Wt* animals, indicating less liver damage in the transgenic mice. LDH was measured as a marker of necrosis.

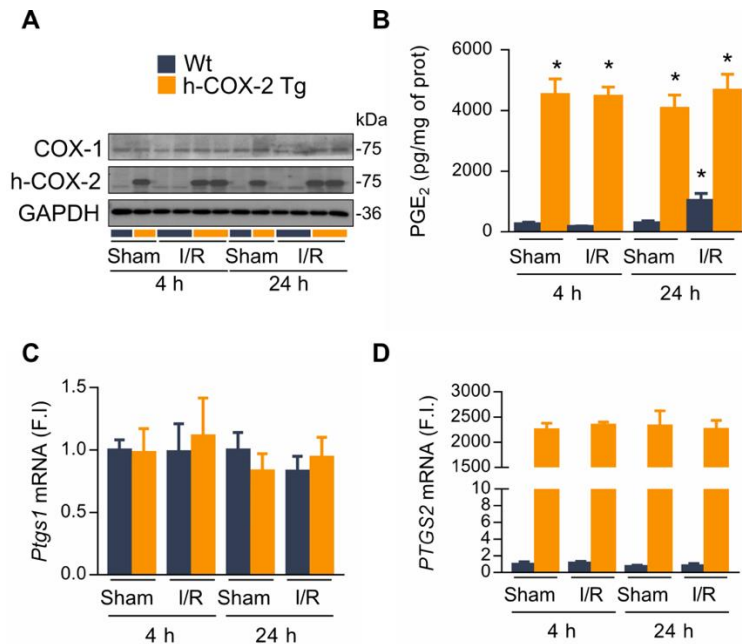


**Figure 12. h-COX-2 expression evaluation in h-COX-2 Tg mice. (A)** Representative Western blot of endogenous COX-1 and human COX-2 proteins expression in livers from *Wt* and *h-COX-2 Tg* mice under Sham and I/R conditions, after 4 and 24 h. **(B)** Measurement of hepatic PGE<sub>2</sub> levels of *Wt* and *h-COX-2 Tg* mice under Sham and I/R conditions after 4 and 24 h. **(C)** Measurement of mRNA levels of *Ptgs1* gene (endogenous COX-1-encoding gene) and **(D)** *PTGS2* gene (human COX-2-encoding gene) expression from livers of *Wt* and *h-COX-2 Tg* mice under Sham and I/R conditions, after 4 and 24 h. Data are represented as mean  $\pm$  SEM (n=5-8 per group). \*p<0,05 versus *Wt* Sham. Abbreviations: GAPDH, glyceraldehyde 3-phosphate dehydrogenase, F.I., fold induction.

Like transaminase levels, plasma LDH is higher after I/R, compared to the Sham condition (**Figure 13B**). In this case, LDH levels are higher at 24 h of reperfusion, compared to 4 h of reperfusion. LDH levels increase after a few hours after the onset of injury because necrosis is a phenomenon that occurs later in the injury [151]. Plasma LDH levels in *h-COX-2 Tg* animals are significantly lower than those in *Wt* animals, after 4 and 24 h of reperfusion, in agreement with transaminase levels. Less necrotic areas are also observed in *h-COX-2 Tg* livers when histological samples are analysed. Liver sections were stained with H&E stain (**Figure 13D**), and different



grades of necrosis were assigned according to necrotic areas (**Figure 13C**). Liver IRI causes liver damage and necrosis, but COX-2 expression attenuates its severity in *h-COX-2 Tg* mice.

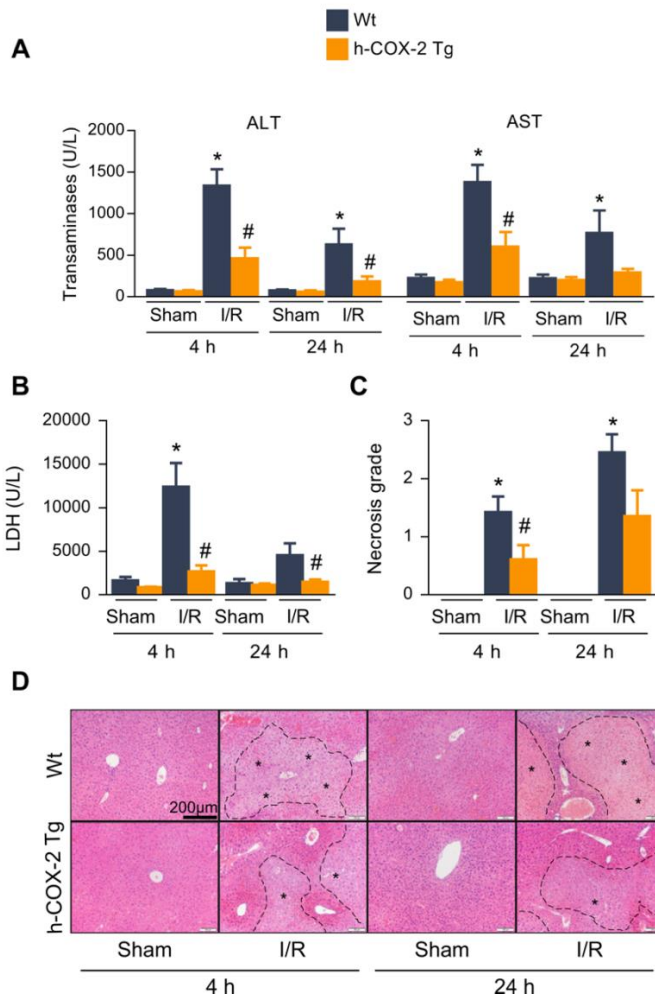


**Figure 13. Assessment of the liver damage after I/R.** (A-B) Plasma transaminases (A) and LDH (B) levels of *Wt* and *h-COX-2 Tg* mice under Sham and I/R conditions after 4 and 24 h. (C) Degree of necrosis assessed by histological examination. Scores used were 0=none, 1=mild lesion (0-20% of necrosis), 2=moderate lesion (20-40% of necrosis), 3=severe lesion (more than 40% of necrosis). (D) Representative H&E images of liver sections from *Wt* and *h-COX-2 Tg* mice from Sham and I/R conditions after 4 and 24 h. Necrotic areas are marked with asterisks. Data are represented as mean  $\pm$  SEM (n=5-8 per group). \*p<0,05 versus *Wt* Sham; #p<0,05 versus *Wt* I/R. Abbreviations: ALT, alanine transaminase; AST, aspartate transaminase; LDH, lactate dehydrogenase; H&E, haematoxylin-eosin staining.

### 1.3 A mixed genetic background is required to reproduce the ischemia-reperfusion injury model in mice

Due to the technique used in the generation of the transgenic model, the genetic background of the mouse strain is a combination of two backgrounds: DBA2JRcHsd (D2) and C57BL/6JRccHsd (B6). Hence, it could be assumed that this mouse line will be highly heterogeneous, and this genetic mixture could affect the results. Therefore, two more homogenous lines were generated to compare the above results and to determine the effect of genetic background on the establishment of the lesion after I/R and the role of the COX-2 enzyme. First, a pure genetic background line (B6) was generated by several crosses, known as backcrossing, with the C57BL/6JRccHsd strain, until the 10<sup>th</sup> generation, when pure background is assumed to be reached. Secondly, once the pure genetic background strain is established, an F1 generation is obtained (B6D2 F1) by crossing a B6 *h-COX-2 Tg* female with a DBA2JRcc male (described in “2.2 and 2.3 of Materials and Methods”). These F1 hybrid animals are more similar to the original line (B6D2) but all these animals have the same amount (50%) of contribution from the two genetic backgrounds in a stable way. It is assumed that these two new mice will have a more homogenous response to the experiments as the genetically variability is avoided.

Therefore, with these two new animals, the 90 min ischemia model was performed, followed of 4 h of reperfusion. After sacrifice of the animals, blood and tissue samples were collected and analysed. First, the expression of the COX-2 enzyme was analysed. Both lines correctly express the h-COX-2 protein in the livers of *h-COX-2 Tg* mice (**Figure 14A**), reflecting that the correct expression of the transgene is not affected by the change of the genetic background. Interestingly, plasma levels of transaminases are lower compared to the mixed line (B6D2) in both mouse lines (**Figure 14B**).

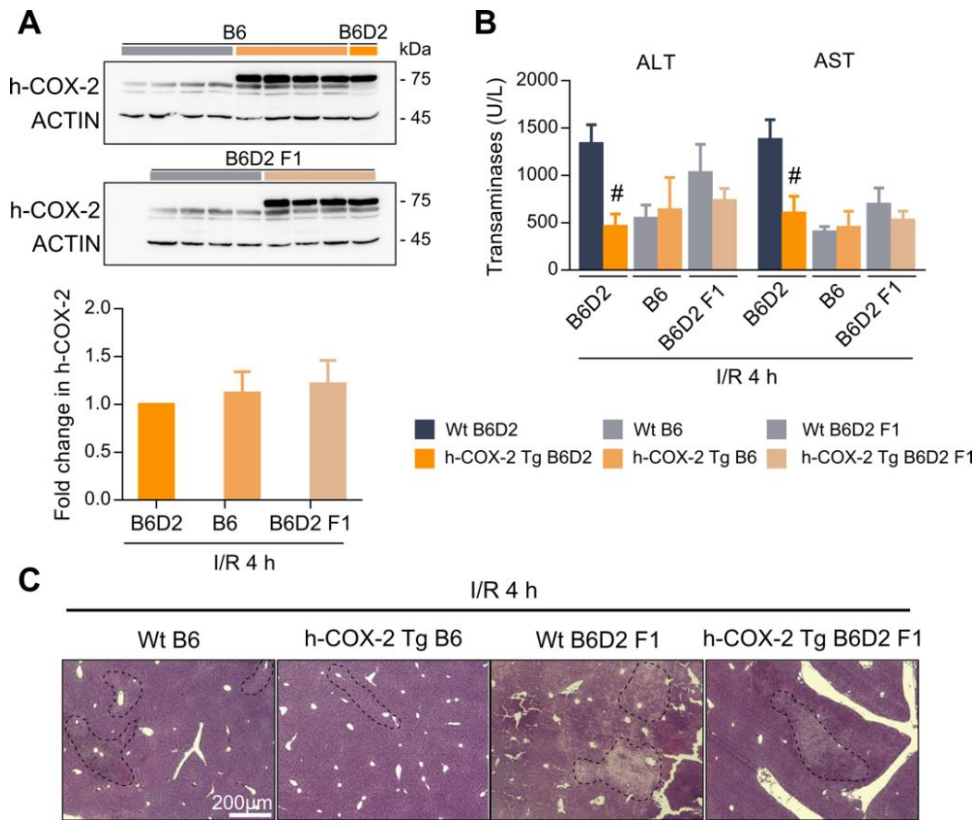


**Figure 14. Pure genetic and F1 hybrid backgrounds don't reproduce the I/R model.** (A) Representative Western blot and densitometric analysis of h-COX-2 protein expression (normalised to ACTIN), in liver extracts from B6 and B6D2 F1 genetic backgrounds mice, in both *Wt* and *h-COX-2 Tg* mice, after I/R 4 h. (B) Plasma transaminases levels of *Wt* and *h-COX-2 Tg* mice in the three different genetic backgrounds after I/R 4 h. (C) Representative H&E images of liver sections of *Wt* and *h-COX-2 Tg* mice from B6 and B6D2 F1 genetic backgrounds after I/R 4 h. Data are represented as mean  $\pm$  SEM (n=7-9 per group). # $p < 0,05$  versus *Wt* I/R. Abbreviations: ALT, alanine transaminase; AST, aspartate transaminase; H&E, haematoxylin-eosin staining.

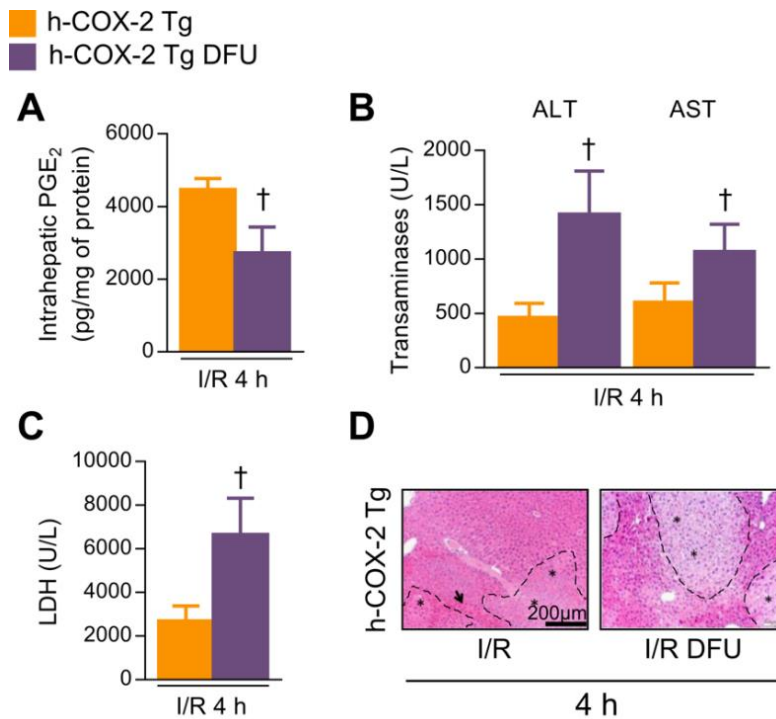
Furthermore, the observed differences in I/R between *Wt* and *h-COX-2 Tg* samples in the mixed background are not present in the B6 and B6D2 F1 mice. This decrease in damage, observed by the detection of the small increase in plasma transaminases, is also observed in histological analyses, where necrotic areas are hardly visible in either mouse strain under any condition (Figure 14C). These results

led to the continuation of the study with the mixed genetic background (B6D2) mouse strain as is the only one reflecting liver damage after I/R and the overexpression of COX-2 enzyme appear to have an effect in the pathology.

#### 1.4 Lower hepatic damage is due specifically to COX-2 expression

To demonstrate that the COX-2 enzyme is responsible for less liver damage after I/R, selective inhibition of the enzyme was performed. To perform this experiment, a new group of *h-COX-2 Tg* mice was selected and half of them were injected with the COX-2 specific inhibitor DFU four times prior to ischemia surgery. All animals were then subjected to 90 min ischemia followed by 4 h of reperfusion. Hepatic prostaglandin levels are lower in DFU-injected *h-COX-2 Tg* mice (**Figure 15A**), indicating effective inhibition of the drug at the functional level of the enzyme. Plasma transaminase levels in DFU-injected *h-COX-2 Tg* mice are significantly increased, compared to *h-COX-2 Tg* samples (**Figure 15B**), revealing increased tissue damage. Necrosis is also increased, as seen in increased LDH levels (**Figure 15C**) and histological analysis, where larger necrotic areas are observed (**Figure 15D**). Therefore, reduced liver damage is closely related to the specific expression of *h-COX-2* in the hepatocytes.

**Figure 15. Damage protection in *h-COX-2 Tg* mice is due to COX-2 activity. (A)** Measurement of hepatic PGE<sub>2</sub> in *h-COX-2 Tg* mice and *h-COX-2 Tg* mice injected with DFU, after I/R 4 h. **(B-C)** Plasma transaminases **(B)** and LDH **(C)** levels measured in *h-COX-2 Tg* and *h-COX-2 Tg* DFU mice after I/R 4 h. **(D)** Representative H&E images of liver sections from *h-COX-2 Tg* and *h-COX-2 Tg* DFU mice after I/R 4 h. Necrotic areas are marked with asterisks and vascular congestion with arrowheads. Data are represented as mean ± SEM (n=5-8 per group). †p<0,05 versus *h-COX-2 Tg* I/R. Abbreviations: ALT, alanine transaminase; AST, aspartate transaminase; LDH, lactate dehydrogenase; H&E, haematoxylin-eosin staining. (next page)



### 1.5 Hepatic preconditioning attenuates liver damage in *Wt* mice

To test the role of the endogenous COX-2 enzyme, preconditioning (PC) was performed in the liver to activate *Ptgs2* expression. This experiment was carried out with a new group of *Wt* mice. They were divided in 4 groups: Sham condition, I/R, PC and preconditioning injected with DFU (PC-DFU). The PC group was subjected to a shorter 20 min liver ischemia followed by 30 min of reperfusion before the 90 min ischemia model, followed by 4 h reperfusion. The PC-DFU group was injected four times prior to ischemia surgery with DFU to inhibit COX-2 enzyme activity, then subjected to PC and I/R. The mRNA analysis shows that the expression of the endogenous *Ptgs2* gene increases when ischemia is performed, compared to the Sham condition in *Wt* animals, and this increase is greater when animals are preconditioned (Figure 16A). This induction of expression is also observed at the protein level (Figure 16B-C).

## IV. RESULTS

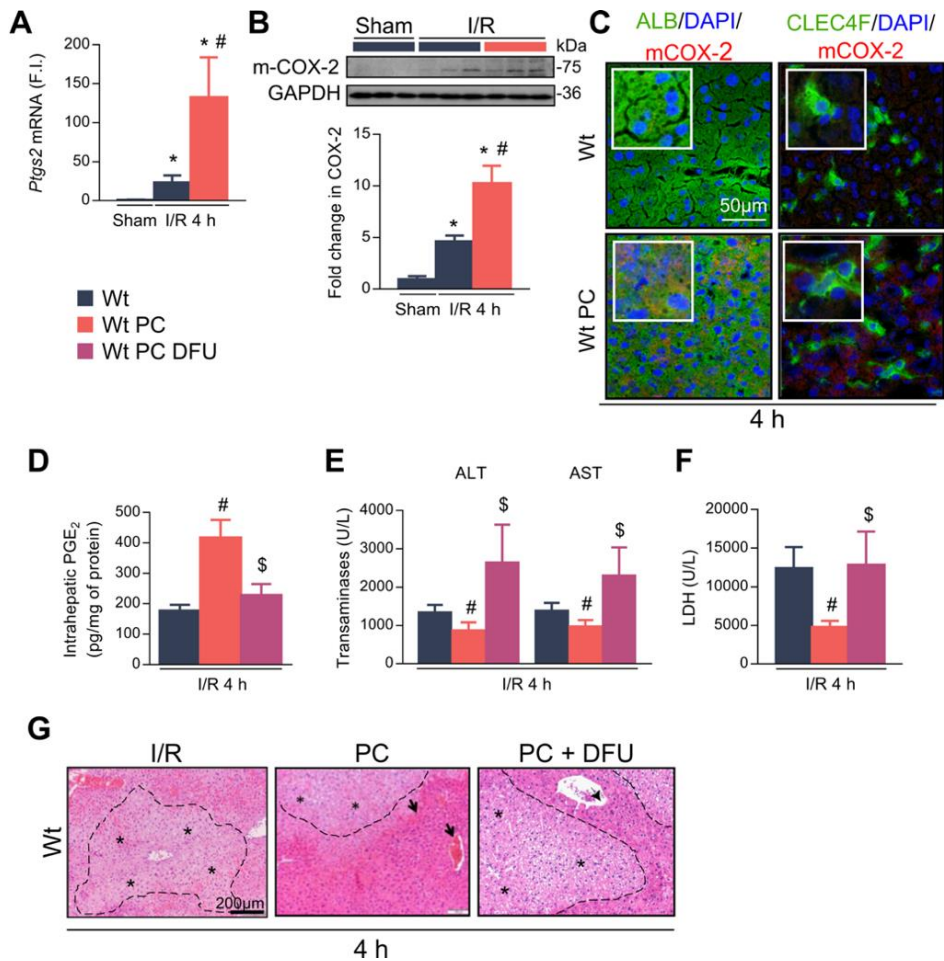


**Figure 16. Endogenous expression of COX-2 confers protection to *Wt* mice following I/R.** (A) Measurement of mRNA levels of the *Ptg2* gene (endogenous gene encoding COX-2) in *Wt* mice under Sham, I/R and PC conditions. (B) Representative Western blot and densitometric analysis of endogenous (m, mouse) COX-2 protein expression in liver extracts from *Wt* mice after Sham, I/R and PC conditions. (C) Representative immunofluorescence images of liver sections from *Wt* mice after I/R and PC of endogenous COX-2 in red, ALBUMIN (hepatocyte marker) or CLEC4F (macrophage marker) in green and DAPI (nucleus marker) in blue. (D) Measurement of hepatic PGE<sub>2</sub> in *Wt* mice after I/R, PC and PC+DFU. Plasma transaminases (E) and LDH (F) levels measured in *Wt* mice after I/R, PC and PC+DFU. (G) Representative H&E images of liver sections from *Wt* mice after I/R, PC and PC+DFU. Necrotic areas are marked with asterisks and vascular congestion with arrowheads. Data are represented as mean ± SEM (n=5-8 per group). \*p<0,05 versus *Wt* Sham; #p<0,05 versus *Wt* I/R; \$ p<0,05 versus *Wt* PC. Abbreviations: PC, preconditioning; ALB, albumin; DAPI, 4', 6-diamidino-2-phenylindole; ALT, alanine transaminase; AST, aspartate transaminase; LDH, lactate dehydrogenase; H&E, haematoxylin-eosin staining; F.I., fold induction.

Prostaglandins assessment shows increased intrahepatic PGE<sub>2</sub> levels in preconditioned *Wt* animals, compared to normal I/R *Wt* mice (Figure 16D), revealing increased activity of endogenous COX-2. In addition, preconditioned *Wt* mice injected with DFU had reduced PGE<sub>2</sub> levels (Figure 16D), demonstrating effective inhibition of endogenous COX-2 activity. When analysing liver damage, preconditioned *Wt* mice show lower levels of plasma transaminases compared to the *Wt* animals that has undergone the common I/R model (Figure 16E). Moreover, plasma LDH is lower in preconditioned *Wt* mice (Figure 16F), and they show smaller necrotic areas (Figure 16G), reflecting less necrosis. Furthermore, as observed by immunofluorescence staining, the expression of endogenous COX-2 when the tissue is preconditioned is localised in hepatocytes, not in inflammation-mediating KCs, which parallels the idea that the COX-2 expression in the hepatocyte is beneficial in attenuating the onset of inflammation (Figure 16C). These results demonstrate that preconditioning is effective in stimulating endogenous COX-2 expression and that this expression protects the tissue from liver damage after I/R.

### 1.6 The gene expression profile is altered after ischemia-reperfusion injury

Based on the evidence that COX-2 is conferring a protection in front of IRI in mouse liver, it is assumed that there will be changes in different cellular pathways and signalling responses. Therefore, a whole transcriptome analysis was performed to determine the differences in gene expression profiles in *h-COX-2 Tg* mice after IRI and compare them to *Wt* mice. Whole RNA was extracted from livers after 90 min of ischemia and 4 h of reperfusion, and subjected to transcriptomic analysis. Up to 70 genes had significant differential expression between *Wt* and *h-COX-2 Tg* samples (false discovery rate  $\leq 0,05$ ,  $\log_2 \geq 2$ ), 18 of them were up-regulated and the remaining 52 were down-regulated (Figure 17A-B). Gene ontology analysis was performed to determine the biological functions in which these genes were involved. The pathways that were highly altered after IRI comparing *Wt* and *h-COX-2 Tg* samples were the inflammatory response, the stress response, as well as several pathways related to



## IV. RESULTS

metabolic processes (Figure 17C). Therefore, these were the main pathways investigated in this study, focusing on the establishment of the inflammation, the response to different cellular stress pathways such as apoptosis or oxidative stress and, finally, the mediation of the mitochondria as a central player between cellular response to stress and metabolism.

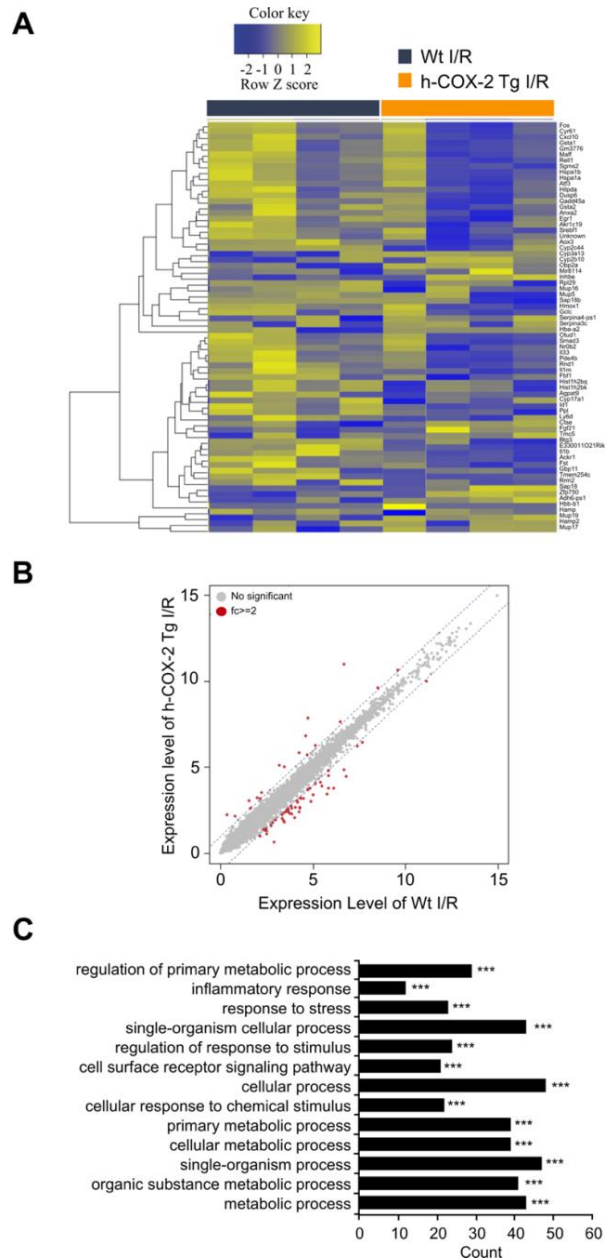




**Figure 17. Whole transcriptome sequencing shows a differential gene expression profile in *h-COX-2 Tg* mice after I/R.** Total RNA was obtained from *Wt* and *h-COX-2-Tg* mice after I/R at 4 h (n = 4 in each experimental group). **(A)** Unsupervised heatmap of 70 genes with fold change  $\geq 2$  using Z score for normalised values (log<sub>2</sub>-based). **(B)** Scatter plot of expression levels comparing *Wt* and *h-COX-2 Tg* samples. Red dots mark genes with fold change  $\geq 2$ . **(C)** A gene ontology-based gene enrichment test was performed with a list of significant genes. The most significantly enriched biological processes are shown (P < 0,001 by modified Fisher's exact test).

## 2. THE INFLAMMATORY RESPONSE IS ATTENUATED WHEN COX-2 IS EXPRESSED

### 2.1 Ischemia-reperfusion increases inflammatory markers that are lower in *h-COX-2 Tg* mice

Ischemia-reperfusion initiates a cascade of different signals involving not only the hepatocytes, but all the cell types present in the liver. Their combined action promotes different signals that affect the outcome of the pathology. One important pathway initiated during the reperfusion event is the inflammatory response [152]. The expression of different genes involved in this inflammatory response was analysed in liver samples of *h-COX-2 Tg* and *Wt* mice, after 4 and 24 h of reperfusion. Genes encoding the pro-inflammatory cytokines *Tnf*, *Il-1b* and *Il-6* are highly expressed after I/R in *Wt* and *h-COX-2 Tg* livers, although in *h-COX-2 Tg* samples the increase is significantly lower, compared to *Wt* (**Figure 18A**). The expression of the inflammasome gene *Nlrp3* is also increased in the I/R, with an attenuated increase in *h-COX-2 Tg* samples. In contrast, the gene encoding the anti-inflammatory cytokine *Il-10* is upregulated in *h-COX-2 Tg* samples, with a discrete increase in *Wt* samples, after I/R. Consistent with these results, the presence of these cytokines in plasma is higher after I/R, especially after 24 h of reperfusion in the *Wt*, while *h-COX-2 Tg* samples have an attenuated increase (**Figure 18B**).

IV. RESULTS

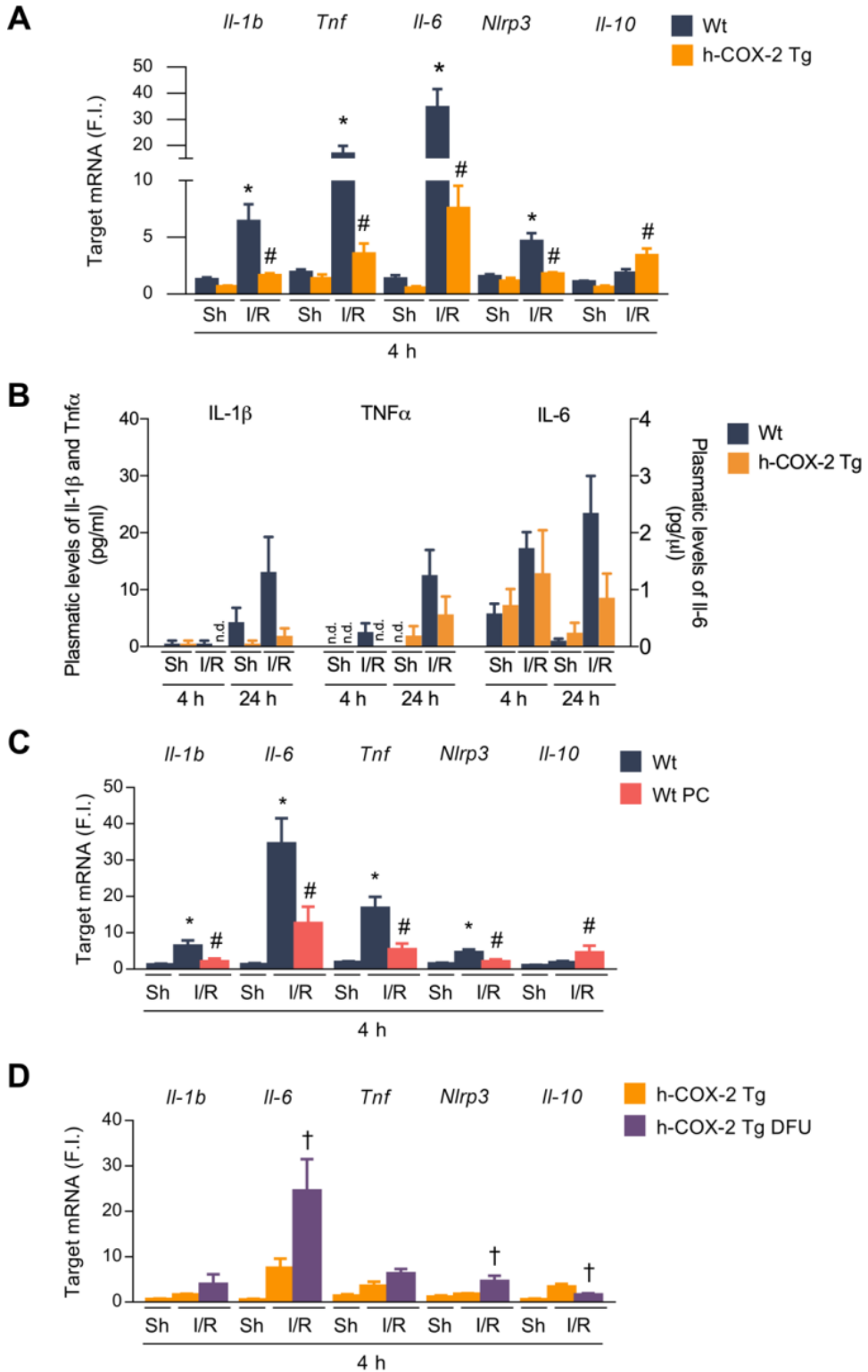


**Figure 18. Analysis of inflammatory-related genes and cytokines after I/R.** (A) Measurement of mRNA levels of inflammation-related genes (*Il-1b*, *Tnf*, *Il-6*, *Nlrp3*, *Il-10*) in liver extracts from *Wt* and *h-COX-2 Tg* mice under Sham and I/R 4 h conditions. (B) Plasma levels of IL-1 $\beta$ , TNF $\alpha$  and IL-6 cytokines in *Wt* and *h-COX-2 Tg* mice under Sham and I/R conditions after 4 and 24 h. (C) Measurement of mRNA levels of inflammation-related genes in liver extracts from *Wt* and *Wt* PC mice and (D) *h-COX-2 Tg* and *h-COX-2 Tg* DFU mice, under Sham and I/R 4 h conditions. Data are represented as mean  $\pm$  SEM (n=5-8 per group). \*p<0,05 versus *Wt* Sham; #p<0,05 versus *Wt* I/R; †p<0,05 versus *h-COX-2 Tg* I/R. Abbreviations: PC, preconditioning; Sh, Sham; F.I., fold induction; n.d., not detectable.

The attenuation of the inflammatory response by COX-2 action is supported by the results obtained with preconditioned animals and COX-2 inhibition. When livers from preconditioned *Wt* animals are analysed, the expression of pro-inflammatory genes is shown to be decreased, compared to non-preconditioned *Wt* mice (Figure 18C). In addition, endogenous COX-2 expression observed in *Wt* PC animals decreases *Nlrp3* gene expression and increases *Il-10* gene expression. In contrast, when COX-2 activity is inhibited with DFU, all pro-inflammatory markers increase, and the expression of the anti-inflammatory marker *Il-10*, decreases (Figure 18D). These results demonstrate that COX-2 is involved in mitigating the inflammatory response.

## 2.2 Neutrophil infiltration is decreased with COX-2 expression

Neutrophils are key players in mediating the inflammatory response [153]. Therefore, two analyses were performed to assess the presence and activity of neutrophils. On the one hand, the MPO activity was analysed as an index of neutrophil infiltration. The MPO enzyme is expressed mainly in neutrophils and acts as an antimicrobial defence mechanism and in other defence responses. The reactive species generated by MPO activity causes tissue damage, thus contributing to inflammation. The detection of elevated MPO activity translates into elevated inflammation. MPO activity was analysed in all conditions and increases significantly in *Wt* samples after ischemia, but only after 24 h of reperfusion (Figure 19A). There is no evidence on neutrophil accumulation after 4 h of reperfusion. On the other hand, another marker

## IV. RESULTS

for neutrophil infiltration, Ly6G<sup>+</sup> cell staining, was analysed. Ly6G is a neutrophil plasma membrane biomarker, so the presence of these cells in tissues reveals neutrophil infiltration. Immunohistochemical analysis of this marker reveals a lower presence of neutrophils in *h-COX-2 Tg* samples compared to *Wt* mice after 24 h (**Figure 19B**). Both results point to an attenuated accumulation of neutrophils when COX-2 is expressed, in agreement with the results presented above revealing less inflammation.

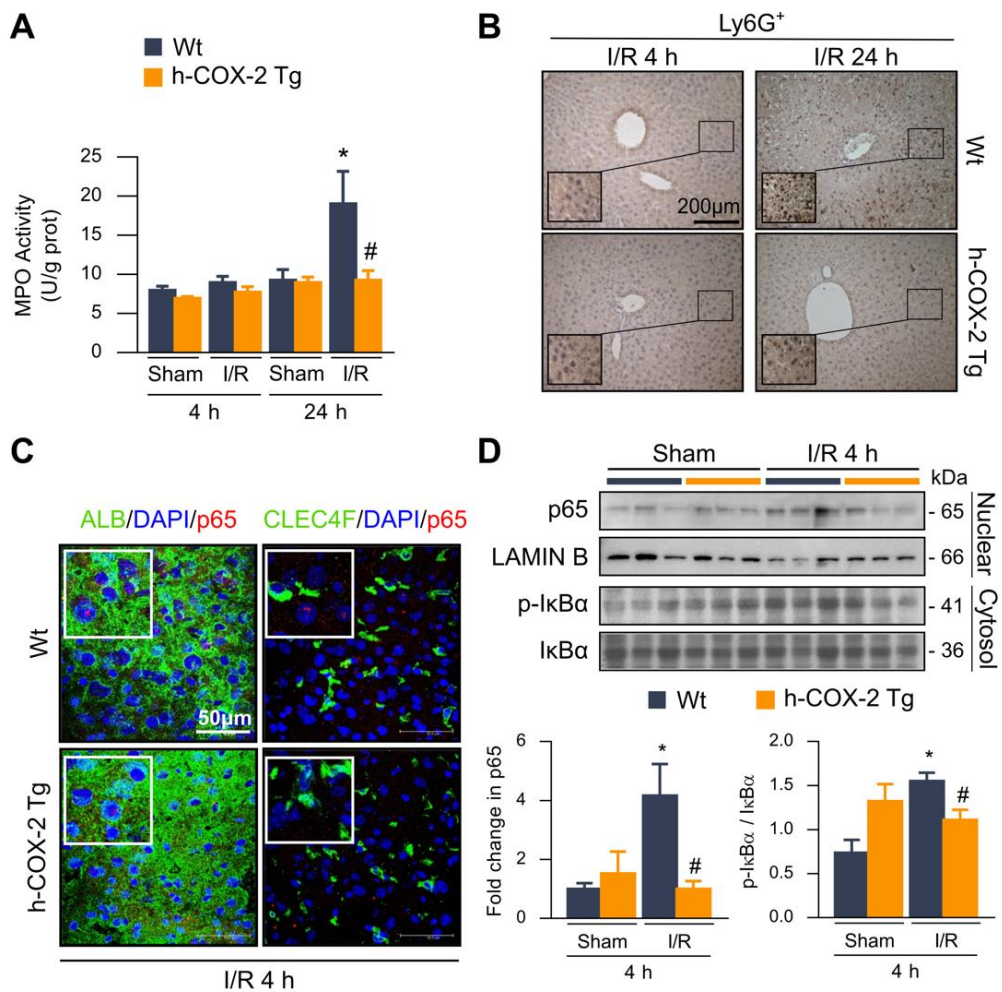


**Figure 19. Analysis of pro-inflammatory markers after I/R. (A)** MPO activity measured in livers of *Wt* and *h-COX-2 Tg* mice under Sham and I/R 4 h conditions. **(B)** Representative immunohistochemistry of Ly6G<sup>+</sup> staining in livers sections from *Wt* and *h-COX-2 Tg* mice after I/R 4 and 24 h. **(C)** Representative immunofluorescence images of liver sections from *Wt* and *h-COX-2 Tg* mice after I/R 4 h of p65 in red, ALBUMIN (hepatocyte marker) or CLEC4F (Kupffer cell marker) in green and DAPI (nucleus) in blue. **(D)** Representative Western blot and densitometric analysis of p65 protein (normalised to LAMIN B) and p-I $\kappa$ B $\alpha$  protein (normalised to I $\kappa$ B $\alpha$ ), in nuclear and cytosolic extracts of *Wt* and *h-COX-2 Tg* livers under Sham and I/R 4 h conditions, respectively. Data are represented as mean  $\pm$  SEM (n=5-8 per group). \*p<0,05 versus *Wt* Sham; #p<0,05 versus *Wt* I/R. Abbreviations: MPO, myeloperoxidase; ALB, albumin; DAPI, 4', 6-diamidino-2-phenylindole.

### 2.3 COX-2 expression attenuated NF- $\kappa$ B pathway

One of the canonical pathways involved in the establishment of inflammation is the NF- $\kappa$ B pathway [154]. Through the binding of different components to the cell surface receptors, for example via the IL-1R, a signalling cascade involving different factors such as I $\kappa$ B or p65 is activated, culminating in the translocation of certain transcription factors to the nucleus and promoting the expression of genes encoding for cytokines, chemokines and other genes mediating inflammation. A marker of NF- $\kappa$ B pathway activation, p65 expression, was analysed. The expression of p65 increases after I/R, and its increase is higher in *Wt* samples, compared to *h-COX-2 Tg* mice (**Figure 19D**). Moreover, as can be seen in immunofluorescence images, its expression is localised in the nucleus of *Wt* tissues after I/R, while is hardly present in the nuclei of *h-COX-2 Tg* liver cells (**Figure 19C**). In addition, phosphorylation of the I $\kappa$ B $\alpha$  factor was also analysed. Like with p65, phosphorylation of the I $\kappa$ B $\alpha$  factor, i.e. its activation, is increased in *Wt* livers after I/R, and attenuated when COX-2 is expressed (**Figure 19D**). All these data suggest a strong activation of the NF- $\kappa$ B pathway in *Wt* mice after IRI, whereas this effect was attenuated in *h-COX-2-Tg* mice.

### 3. CELLULAR STRESS IS REDUCED WHEN COX-2 IS EXPRESSED IN HEPATOCYTES

#### 3.1 Constitutive hepatocyte COX-2 expression leads to decreased apoptosis

Ischemia-reperfusion injury ultimately leads to cell death when cellular mechanisms fail to cope with different types of cellular stress [155]. Cell death leads to further tissue damage. COX-2 expression in hepatocytes has previously been shown to have an anti-apoptotic role [45][46], therefore different apoptotic markers were analysed in this study. Caspase 3 is a protease that is activated during apoptotic cell death; so, its activity was measured after I/R. Its activity appears to increase after I/R compared to the Sham condition, but only in the *Wt* samples, after 4 and 24 h of reperfusion (**Figure 20A**). BAX and BCL2 are two other markers of apoptosis. As a general convention, BAX protein is a pro-apoptotic maker, while BCL2 is anti-apoptotic, so when the BAX/BCL2 ratio is high, it indicates favoured apoptosis. Indeed, this is the result observed when comparing the different conditions. The BAX/BCL2 ratio is higher after 24 h of reperfusion in the *Wt* samples compared to the *h-COX-2 Tg* samples, which maintained the ratio as when there is no damage (Sham condition) (**Figure 20B**). In addition, analysis of Protein kinase B (AKT) and 5' AMP-activated protein kinase (AMPK $\alpha$ ) pathways are often used as markers of survival. Here, both pAKT/AKT and pAMPK $\alpha$ /AMPK $\alpha$  ratios were increased in *h-COX-2 Tg* samples compared to *Wt* after 4 h of reperfusion (**Figure 20C-D**), indicating increased activation of these pathways. Taken together, these results demonstrate reduced apoptosis after I/R when COX-2 is expressed in hepatocytes.

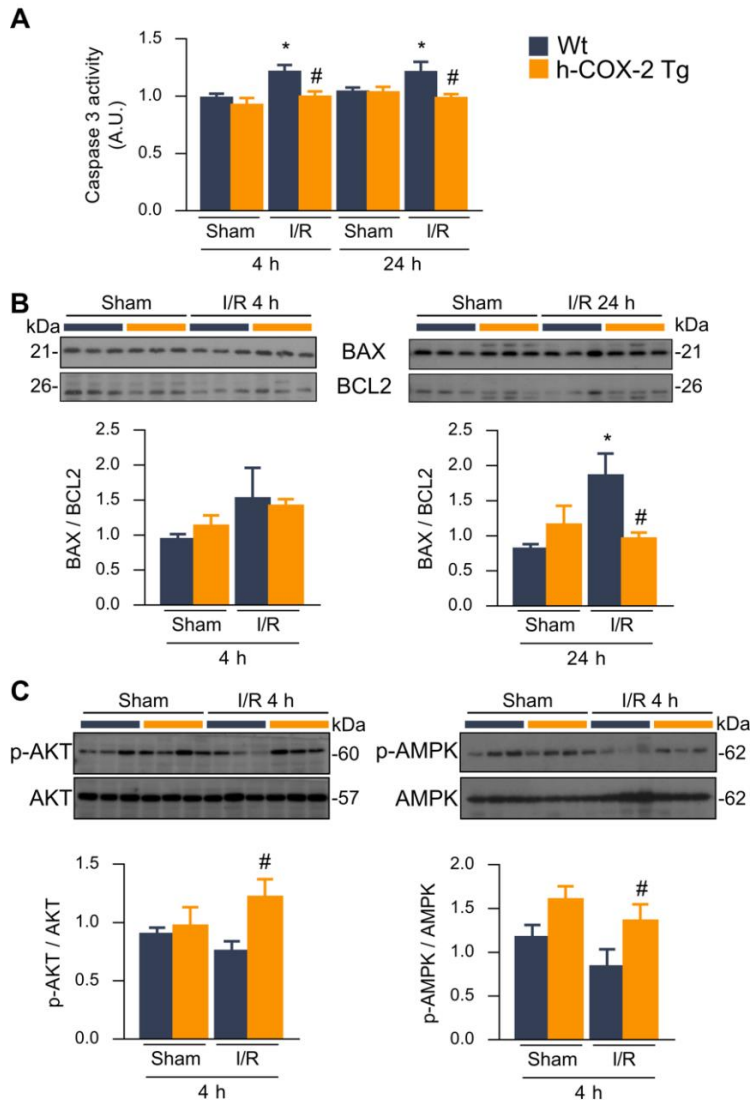


**Figure 20. Apoptotic markers analysis after I/R.** (A) Caspase-3 activity in liver extracts from *Wt* and *h-COX-2 Tg* mice under Sham and I/R 4 and 24 h conditions. (B) Representative Western blot and densitometric analysis of BAX protein (normalised to BCL2 protein), in liver extracts from *Wt* and *h-COX-2 Tg* mice under Sham and I/R 4 and 24 h conditions. (C) Representative Western blot and densitometric analysis of p-AKT and p-AMPK normalised to AKT and AMPK respectively, in liver extracts from *Wt* and *h-COX-2 Tg* mice under Sham and I/R 4 h conditions. Data are represented as mean  $\pm$  SEM ( $n=5-8$  per group). \* $p<0,05$  versus *Wt* Sham; # $p<0,05$  versus *Wt* I/R. Abbreviations: A.U., arbitrary units.

### 3.2 Hepatocyte COX-2 expression activates autophagy after ischemia-reperfusion

Autophagy is characterised by the recycling of different cellular components, from damaged or misfolded proteins to large organelles, in order to continue to reuse its components, amino acids, fatty acids, etc. It is especially active under conditions of starvation, or when stressful pathways affect and damage cellular compartments, such as I/R [95]. In this process, several proteins and factors regulate the different steps of the process, so the analysis of the presence of these factors is a marker of the good state of the process and, therefore, of the cellular state. The autophagy-initiating factor ATG7 is analysed to assess the general status of autophagy. In this case, ATG7 is down-regulated in *Wt* mice after I/R, but its expression is conserved in *h-COX-2 Tg* mice (**Figure 21A**). LC3 is mainly involved in autophagosome formation, undergoing proteolytic processing from LC3-I to LC3-II when incorporated into the autophagosome membrane. Expression of high amounts of LC3-II correlates with increased autophagy. After 4 h of reperfusion, *h-COX-2 Tg* mice have increased LC3-II levels, compared to *Wt* mice that remain as in control conditions.

However, after 24 h of reperfusion, both *h-COX-2 Tg* and *Wt* mice have increased LC3-II levels, compared to Sham (**Figure 21B**). The p62 marker, which labels the cargo for degradation, is less expressed in *h-COX-2 Tg* mice compared to *Wt* animals after ischemia and 4 and 24 h of reperfusion (**Figure 21C**). Moreover, it is upregulated in *Wt* samples, increasing significantly after 24 h of reperfusion. All these results point to a decrease in autophagy after I/R in control conditions, and that COX-2 expression in hepatocytes promotes autophagy, despite the fact that under control conditions there would be more marked cargoes for its degradation, as indicated by the increase in p62 protein. The electron microscopy images also show a greater presence of autophagosome structures in the *h-COX-2 Tg* liver sections (**Figure 21D**), which reinforces the idea of activated autophagy.



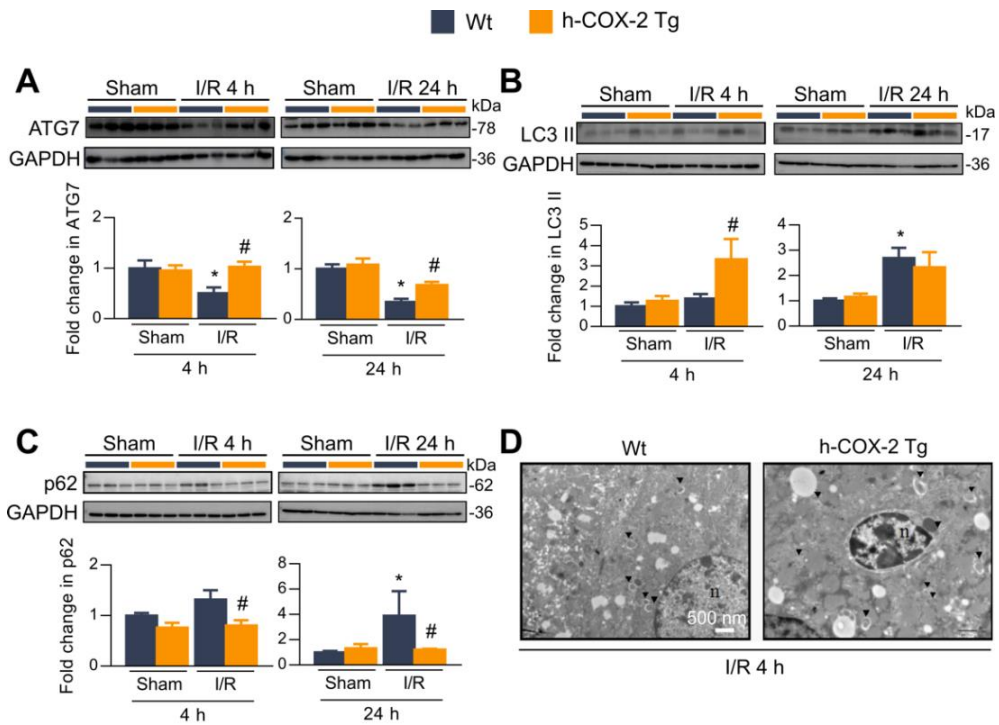


**Figure 21. Analysis of autophagy markers after I/R.** Representative Western blot and densitometric analysis of (A) ATG7, (B) LC3 II, and (C) p62 proteins (normalised to GAPDH), in liver extracts from *Wt* and *h-COX-2 Tg* mice under Sham and I/R 4 and 24 h conditions. (D) Representative transmission electron microscopic micrographs of liver sections from *Wt* and *h-COX-2 Tg* mice after I/R 4 h. Original magnification  $\times 4,000$ . Autophagosomes are marked with arrowheads. n means nucleus. Data are represented as mean  $\pm$  SEM ( $n=4-6$  per group). \* $p<0,05$  versus *Wt* Sham; # $p<0,05$  versus *Wt* I/R. Abbreviations: GAPDH, glyceraldehyde 3-phosphate dehydrogenase.

### 3.3 Unfolded protein response is activated in ischemia-reperfusion

Another pathway that is typically affected during ischemia-reperfusion is the unfolded protein response (UPR) [156]. This pathway is activated as a stress signal from the endoplasmic reticulum (ER) to respond to unfolded proteins and initiates a signalling pathway that results in the synthesis and release of several chaperones, autophagy-related genes, as well as an arrest of the translation machinery. The UPR is mediated by 3 main sensors: ATF6, IRE1 and PERK. Each sensor transduces the

## IV. RESULTS

signal that will ultimately lead to the activation of the response. In general, all major players involved in the UPR are attenuated in *h-COX-2 Tg* livers after I/R, compared to the *Wt* mice, and therefore, the ER stress is lower. ATF6 protein is an ER membrane protein that when activated is internalised, processed by proteolytic cleavage in the Golgi apparatus and translocated to the nucleus to act as a transcription factor. Following I/R, *h-COX-2 Tg* cells have this gene up-regulated, compared to the *Wt* cells (**Figure 22A**).

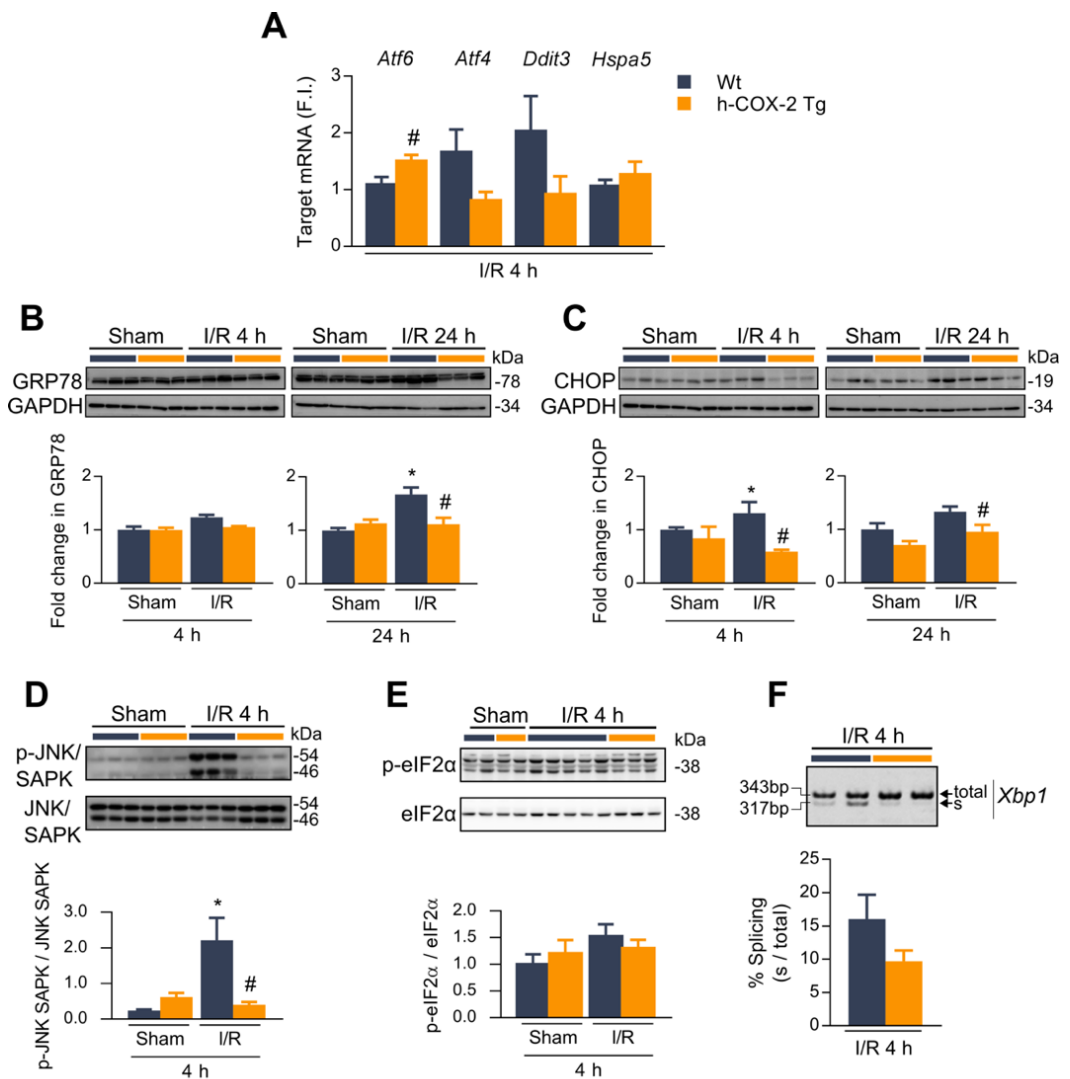


**Figure 22. Unfolded protein response (UPR) markers analysis after I/R. (A)** Measurement of mRNA levels of genes involved in UPR (*Atf6*, *Atf4*, *Ddit3*, *Hspa5*) in liver extracts from *Wt* and *h-COX-2 Tg* mice after I/R 4 h. **(B-C)** Representative Western blot and densitometric analysis of GRP78 **(B)** and CHOP **(C)** proteins (normalised to GAPDH), from liver extracts of *Wt* and *h-COX-2 Tg* mice under Sham and I/R 4 and 24 h conditions. **(D-E)** Representative Western blot and densitometric analysis of p-JNK/SAPK **(D)** and p-eIF2 $\alpha$  **(E)** proteins (normalised to JNK/SAPK and eIF2 $\alpha$  respectively), from liver extracts of *Wt* and *h-COX-2 Tg* mice under Sham and I/R 4 h conditions. **(F)** Representative gel of PCR product after *Xbp1* specific amplification and densitometric analysis. Spliced (s) and total forms of *Xbp1* are marked with arrows. Data are represented as mean  $\pm$  SEM (n=4-9 per group). \*p<0,05 versus *Wt* Sham; #p<0,05 versus *Wt* I/R. Abbreviations: F.I., fold induction.

Like ATF6, IRE1 is a membrane protein that under normal conditions binds to the chaperone GRP78. When there is an accumulation of misfolded proteins, GRP78 detaches from IRE1 and binds the misfolded proteins. The release of IRE1 will allow its dimerisation, autophosphorylation and initiation of its own signalling cascade. This cascade will promote alternative splicing of the *Xbp1* mRNA, resulting in a shorter form of the protein that will internalise into the nucleus and promote chaperone transcription and others related genes. In addition, IRE1 pathway will activate the JNK pathway that will ultimately lead to apoptosis and cell death. In this sense, the alternative splicing of *Xbp1* is slightly enhanced in the *Wt* livers after I/R as it is shown by a higher presence of spliced form of *Xbp1* mRNA (**Figure 22F**), favouring the synthesis and translocation to the nucleus of the short form of XBP1. Meanwhile the JNK pathway is highly active in *Wt* after I/R (**Figure 22D**). Finally, the last sensor of the UPR is PERK which, like IRE1, under normal conditions binds to GRP78 but in the presence of unfolded proteins it is released, dimerised and autophosphorylated. This active dimer will phosphorylate the eIF1 $\alpha$  factor that will act at two levels: on the one hand it will stop the synthesis of new proteins, and on the other hand it will promote the synthesis of the ATF4 factor which will promote the transcription of genes related to autophagy and apoptosis, such as *Ddit3* (encoding gene for CHOP). *Atf4* gene expression shows no difference after I/R comparing *Wt* and *h-COX-2 Tg*

samples (**Figure 22A**); on the other hand, both gene and protein expression of *Ddit3*/CHOP is decreased in *h-COX-2 Tg* samples after I/R compared to *Wt* (**Figure 22A-C**). However, the p-eIF2 $\alpha$ /eIF2 $\alpha$  ratio shows no differences (**Figure 22E**). The chaperone GRP78 (encoded by the gene *Hspa5*), the first sensor of unfolded protein response, is unaltered after ischemia and 4 h of reperfusion in *Wt* and *h-COX-2 Tg* samples, both mRNA (**Figure 22A**) and protein (**Figure 22B**). While after 24 h of reperfusion, its presence expressed in protein is higher in *Wt* samples, compared to *h-COX-2 Tg* that remain unaltered (**Figure 22B**). Taken together, these results show an impaired unfolded protein response, in particular that *h-COX-2 Tg* livers exhibit decreased ER stress after I/R, compared to when COX-2 is not expressed.

### 3.4 The antioxidant response is enhanced when COX-2 is overexpressed

Since the role of reactive oxygen species (ROS) in ischemia-reperfusion injury is well defined [157], an extensive study of the ROS levels and the oxidative stress was performed to understand the effect of COX-2 in the model. Using dihydroethidium staining, which labels the ROS present in tissue, it is clear that large amounts of ROS are generated after I/R, and that they are significantly lower when COX-2 is overexpressed (**Figure 23A**). This lower presence of ROS in *h-COX-2 Tg* samples after I/R is also observed when lipid peroxidation is measured (**Figure 23B**), as an indirect measure of ROS production. The lower ROS accumulation could be due to lower ROS production or higher antioxidant activity. In this regard, several antioxidant genes were measured and indeed their expression is higher in *h-COX-2 Tg* livers after I/R compared to *Wt* livers. The transcription factor NRF2, encoded by the gene *Nfe2l2*, which regulates the expression of several antioxidant response proteins, was analysed in depth. Its mRNA expression appears to be higher, as well as that of other antioxidant enzymes, such as *Gpr*, *Gsx*, *Sod1* and *Sod2* (**Figure 23C**). Moreover, when subcellular fractionation was performed, NRF2 protein is found to be more present in nucleus in the *h-COX-2 Tg* samples (**Figure 23D**). It is even found more enriched in the nucleus of hepatocytes, rather than KCs, in *h-COX-2 Tg* sections after I/R than in *Wt* sections observed by immunofluorescence staining (**Figure 23E**). Other important antioxidant enzymes are those of the superoxide dismutase (SOD)

group. The *Sod1* and *Sod2* genes code for different isoforms of SOD proteins, which are either cytosolic (SOD1) or mitochondrial (SOD2). Both *Sod1* and *Sod2* mRNAs are highly increased in the *h-COX-2 Tg* samples (Figure 23C). The mitochondrial form of SOD, SOD2, also known as Manganese SOD (MnSOD), is responsible for the transformation of the superoxide ion to hydrogen peroxide in the mitochondrial matrix. Both its expression (Figure 23G) and activity (Figure 23H) are increased in *h-COX-2 Tg* samples after I/R, especially its presence after 4 h of reperfusion. Moreover, immunofluorescence staining shows that it is the hepatocytes that express SOD2 (Figure 23F), at least when COX-2 is overexpressed, just like NRF2. Other antioxidant enzyme activities are also increased in *h-COX-2 Tg* samples, such as CAT, GR and GPX, compared to *Wt* after I/R (Table 19).

Finally, glutathione is also a classical marker for assessing oxidative stress. Total glutathione decreases in *Wt* samples after I/R and 4 h of reperfusion, whereas *h-COX-2 Tg* samples remain unchanged (Figure 23I). The ratio GSSG/GSHt (oxidised glutathione to total glutathione) is higher in *Wt* samples (Figure 23I), indicating a higher presence of oxidised glutathione, a marker of oxidative stress. The higher expression of antioxidant genes, higher antioxidant enzymes activity and lower presence of ROS are indicators of an enhanced antioxidant response after I/R in hepatocytes in the presence of the COX-2 enzyme.

The relationship between COX-2 and the antioxidant response is also demonstrated when endogenous COX-2 is induced. In preconditioned *Wt* animals, the expression of some genes related to antioxidant response is increased. In contrast, in *h-COX-2 Tg* animals injected with DFU, the expression of these genes does not decrease compared to *h-COX-2 Tg* after I/R 4 h, and they remain at the same levels (Figure 24).

# IV. RESULTS

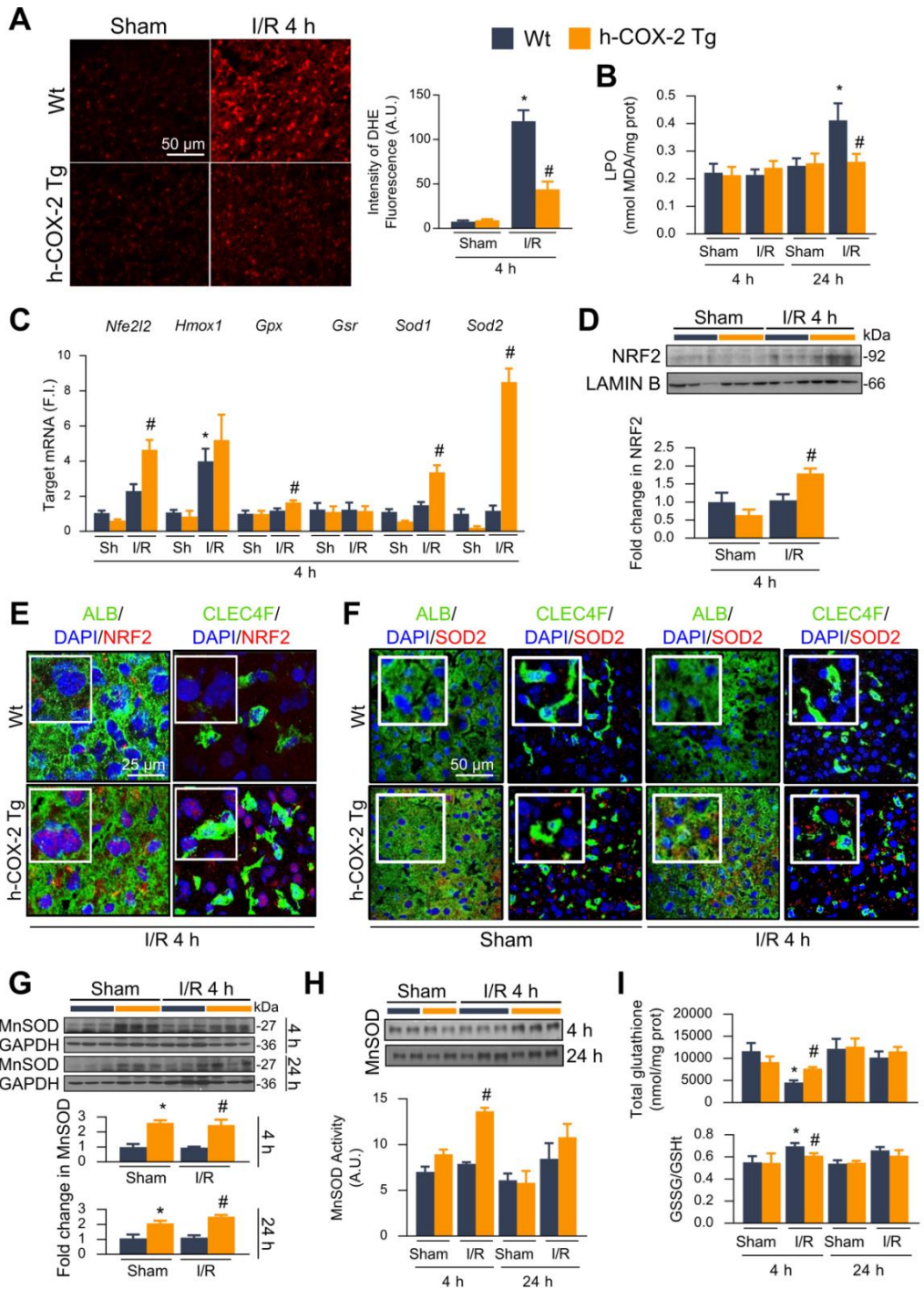




**Figure 23. Oxidative stress and antioxidant response after I/R.** (A) Representative images of DHE staining and quantification in liver sections from *Wt* and *h-COX-2 Tg* mice under Sham and I/R conditions. (B) Measurement of lipid peroxidation in liver homogenates from *Wt* and *h-COX-2 Tg* mice under Sham and I/R 4 and 24 h conditions. (C) Measurement of mRNA levels of genes related to the antioxidant response (*Nfe2l2*, *Hmox1*, *Gpx*, *Gsr*, *Sod1*, *Sod2*) in livers of *Wt* and *h-COX-2 Tg* under Sham and I/R 4 h conditions. (D) Representative Western blot and densitometric analysis of NRF2 protein (normalised to LAMIN B), from nuclear extracts of livers from *Wt* and *h-COX-2 Tg* mice under Sham and I/R 4 h conditions. (E) Representative immunofluorescence images of *Wt* and *h-COX-2 Tg* liver sections after I/R 4 h of NRF2 in red, ALBUMIN (hepatocyte marker) or CLEC4F (Kupffer cell marker) in green and DAPI (nucleus) in blue. (F) Representative immunofluorescence images of liver sections from *Wt* and *h-COX-2 Tg* mice from Sham and I/R 4 h conditions, of SOD2 in red, ALBUMIN (hepatocytes) or CLEC4F (Kupffer cells) in green and DAPI (nucleus) in blue. (G) Representative Western blot and densitometric analysis of liver extracts of MnSOD protein (normalised to GAPDH), from *Wt* and *h-COX-2 Tg* mice under Sham and I/R 4 and 24 h conditions. (H) MnSOD activity assessed by reduction inhibition assay with nitro blue tetrazolium chloride in native polyacrylamide gel electrophoresis, and densitometric analysis, of *Wt* and *h-COX-2 Tg* liver extracts under Sham and I/R 4 and 24 h conditions. (I) Measurement of total glutathione and GSSG/GSht ratio of *Wt* and *h-COX-2 Tg* liver extracts under Sham and I/R 4 and 24 h conditions. Data are represented as mean  $\pm$  SEM (n=4-8 per group). \*p<0,05 versus *Wt* Sham; #p<0,05 versus *Wt* I/R. Abbreviations: DHE, Dihydroethidium; LPO, lipid peroxidation; F.I., fold induction; ALB, albumin; SOD2, superoxide dismutase 2 (mitochondrial); MnSOD, manganese superoxide dismutase; GSSG, oxidised glutathione; GSht, total glutathione.

**Table 19.** GR, GPX and CAT enzymatic activities.

	4 h				24 h			
	Sham		I/R		Sham		I/R	
	<i>Wt</i>	<i>h-COX-2 Tg</i>	<i>Wt</i>	<i>h-COX-2 Tg</i>	<i>Wt</i>	<i>h-COX-2 Tg</i>	<i>Wt</i>	<i>h-COX-2 Tg</i>
<b>GR Activity (U/mg)</b>	0,0122 $\pm$ 0,0006	0,0110 $\pm$ 0,0007	0,0097 $\pm$ 0,0006*	0,0110 $\pm$ 0,0006#	0,0139 $\pm$ 0,0013	0,0128 $\pm$ 0,0009	0,0139 $\pm$ 0,0012	0,0128 $\pm$ 0,0004
<b>GPX Activity (U/mg)</b>	1703,83 $\pm$ 163,13	1707 $\pm$ 16,62	1387,60 $\pm$ 61,82	1755,67 $\pm$ 66,92#	1529,29 $\pm$ 144,39	1709,76 $\pm$ 123,41	1048,65 $\pm$ 241,37	1798,81 $\pm$ 179,36#
<b>CAT Activity (U/mg)</b>	319,2 $\pm$ 100,2	410 $\pm$ 41,3	323,4 $\pm$ 49,8	308 $\pm$ 33,9	319,2 $\pm$ 57	274 $\pm$ 30,5	311,2 $\pm$ 73	299,1 $\pm$ 9,2

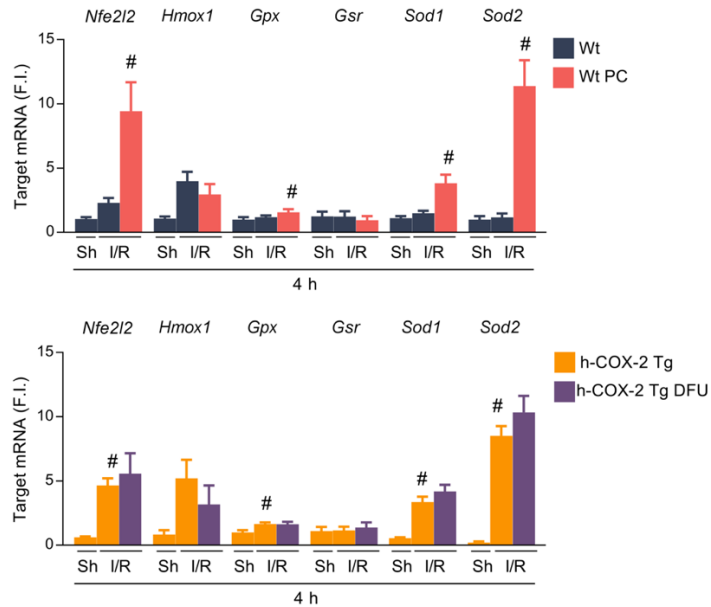


**Figure 24. Antioxidant response is increased in COX-2 expressing tissues.** Measurement of mRNA levels of genes related to the antioxidant response (*Nfe2l2*, *Hmox1*, *Gpx*, *Gsr*, *Sod1*, *Sod2*) in livers of *Wt*, *Wt PC*, *h-COX-2 Tg* and *h-COX-2 Tg DFU* mice under Sham and I/R 4 h conditions. Data are represented as mean  $\pm$  SEM (n=5-8 per group). # $p < 0,05$  versus *Wt* I/R. Abbreviations: PC, preconditioning, Sh, Sham.

## 4. STUDY OF THE MITOCHONDRIAL FUNCTION

### 4.1 Mitochondrial respiration is higher in *h-COX-2 Tg* livers after ischemia-reperfusion

The lower presence of ROS in *h-COX-2 Tg* livers after I/R could be due to an increased antioxidant response in hepatocytes. However, a lower production of ROS in the cells could contribute to the lower ROS accumulation in the tissue. To this end, an in-depth study of mitochondrial function was performed. First, analyses of mitochondrial function were assessed. Fresh, intact mitochondria were isolated from *Wt* and *h-COX-2 Tg* livers after Sham surgery or ischemia and followed by 4 h of reperfusion. These mitochondria were loaded into an O2k oxygraph (Oroboros) and



fed with the different substrates that contribute to the generation of electrons that will move through the different ETC complexes, and finally will be accepted by molecular oxygen. Therefore, the measurement of the concentration of oxygen available in the chambers and the rate of oxygen consumption are indicators of mitochondrial respiration. The response of all the complexes after injection of their specific substrates is very similar between mitochondria derived from *Wt* and *h-COX-2 Tg* mice, but not in all pathways (**Figure 25A**). Observed in detail, the injection of a low concentration of malate and octanoyl-carnitine, that will initiate fatty acid oxidation, shows a lower specific flux, i.e. a lower respiration, in the *Wt* samples after I/R (**Figure 25B**). The same lower respiration is seen in the *Wt* samples after I/R when substrates that generate NADH and thus feed complex I (pyruvate, malate and glutamate) are added to the system (**Figure 25B**). However, the *h-COX-2 Tg*-derived mitochondria respond to all substrates like mitochondria in the Sham condition, acting as if they were not damaged at all. All other substrates feeding the other complexes (succinate, glycerol-3-phosphate) show no significant difference; complex IV shows no change (**Figure 25B**).

Surprisingly, the increase in respiration due to increased efficiency of the F- and N- pathways is not reflected in a change in NADH or NAD<sup>+</sup> levels in the livers of *Wt* and *h-COX-2 Tg* animals after I/R (**Figure 25C**). When AMP and ATP levels were analysed to see if the increased activity translated into increased ATP production, it was observed that AMP levels did not change and ATP levels showed a slight tendency to increase in the transgenic animal's samples (**Figure 25C**).

Mitochondrial respiration is linked to ROS production, so H<sub>2</sub>O<sub>2</sub> production was also measured in parallel to respiration. In this case, the ratio between ROS production and respiration is lower in mitochondria isolated from I/R livers, but there was no difference when comparing *Wt* and *h-COX-2 Tg* samples (**Figure 25D**). These results indicate that although there is a higher substrate utilisation of ETC complex I, it does not translate into a higher ROS generation, or into significantly higher ATP production.

## IV. RESULTS

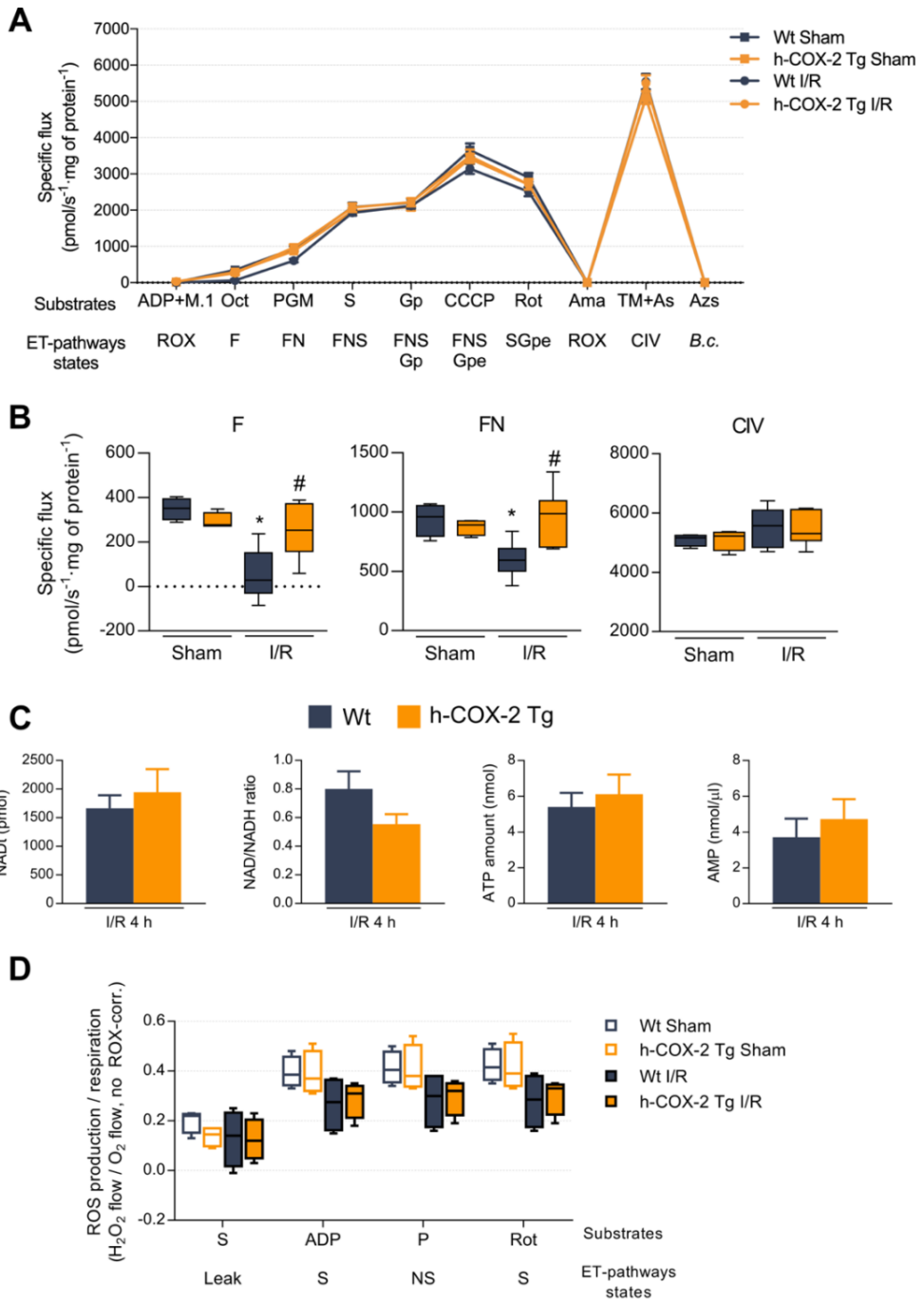


**Figure 25. High-resolution mitochondrial respirometry analysis.** (A) Complete SUIT2 protocol profile of isolated liver mitochondria from *Wt* and *h-COX-2 Tg* mice under Sham and I/R 4 h conditions. The different substrates added (ADP, malate (M), octanoyl-carnitine (Oct), pyruvate (P), malate, glutamate (G), succinate (S), glycerol-phosphate (Gp), CCCP and rotenone (Rot)) and ET-pathways states (ROX, residual oxygen consumption; F, F-junction pathway; N, N-junction pathway; S, succinate pathway; Gp, glycerol-phosphate pathway; e, uncoupled state, maximal respiration), are indicated. After the addition of CI inhibitor rotenone, the respiration was inhibited by addition of complex III inhibitor antimycin A (Ama), and complex IV was fed with ascorbate (As) and TMPD (TM). Subsequently, the whole system was inhibited with sodium azide and complex IV was measured after calibration of the chemical background (b.c., background correction). (B) Specific flux of ET-pathway states F, FN and CIV are shown in detail. (C) Measurement of NADt, NADH, ATP and AMP cofactors in livers from *Wt* and *h-COX-2 Tg* mice after I/R 4 h. (D) Combined determination of oxygen consumption and H<sub>2</sub>O<sub>2</sub> flux by O2k-Fluorometry in isolated liver mitochondria from *Wt* and *h-COX-2 Tg* mice under Sham and I/R 4 h conditions, using succinate as initial substrate. The H<sub>2</sub>O<sub>2</sub> flow/O<sub>2</sub> flow ratio was calculated. Fluorescence signals were calibrated using the H<sub>2</sub>O<sub>2</sub> titrations at the corresponding state. Bar graphs represent mean ± SEM (n=4-9 per group). \*p<0,05 versus *Wt* Sham; #p<0,05 versus *Wt* I/R. Abbreviation: SUIT, substrate-uncoupler-inhibitor titration; F, F-junction pathway; N, N-junction pathway; CIV, complex IV.

Mitochondria isolated from *Wt* mice show a lower respiration rate compared to Sham condition, indicating that the damage generated by I/R is affecting the mitochondrial respiration chain. Furthermore, *h-COX-2 Tg* mitochondria have similar respiration rate to the control conditions, indicating that they are protected and IRI does not cause a decrease in respiratory activity. When mitochondria isolated from B6 (Figure 26A) and B6D2 F1 (Figure 26B) animals were analysed in high-resolution respirometry, the previously observed difference between *Wt*-derived and *h-COX-2 Tg*-derived mitochondria is lost, as they respond equally to all substrates. These results are consistent with the idea mentioned above that these animals, although they are more homogenous in terms of genetic background, are not damaged after I/R, so their mitochondria behave unchanged at the level of respiration.

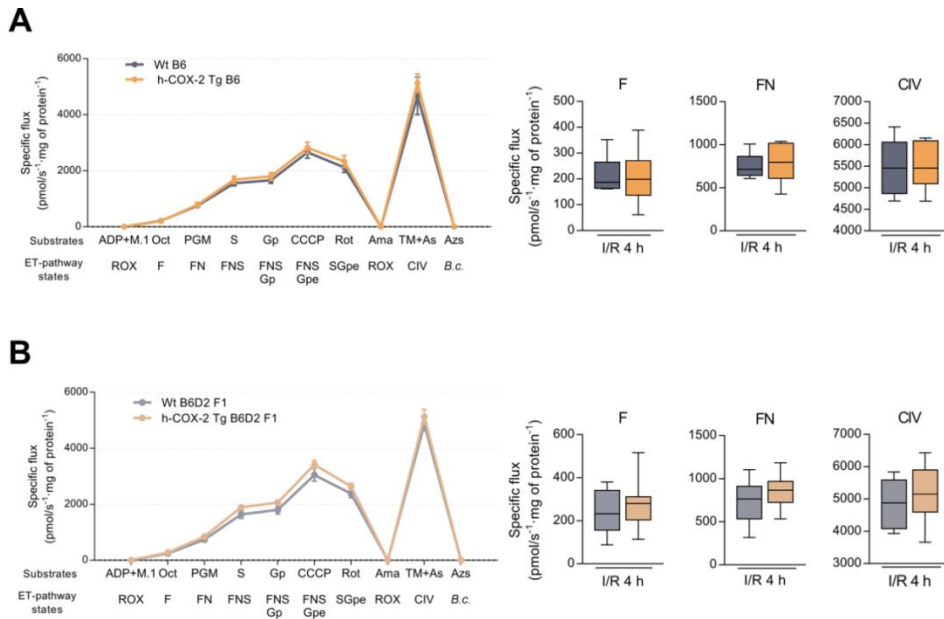


**Figure 26. Pure genetic and F1 hybrid backgrounds lose differences due to COX-2 expression with respect to mitochondrial respirometry.** Full SUIT2 protocol profile of isolated liver mitochondria from *Wt* and *h-COX-2 Tg* mice after I/R 4 h, and F, FN and CIV specific flux in detail from (A) B6 genetic background mice and (B) B6D2 F1 genetic background mice. Substrates and ET-pathway states are indicated. (n=8 per group). Abbreviations: SUIT, substrate-uncoupler-inhibitor titration; F, F-junction pathway; N, N-junction pathway; CIV, complex IV.

#### 4.2 Higher respiration in *h-COX-2 Tg* mitochondria is not due to an increase in ETC complexes expression

Reduced respiration at the level of complex I after I/R in *Wt* samples could be due to a reduced presence of complex I in the ETC of the mitochondria. To explore this possibility, isolated mitochondria were resolved on polyacrylamide gels and one subunit of each complex was detected in immunoblot. This analysis showed no differences in the presence of all ETC complexes comparing the four conditions (Figure 27A), therefore, the presence of complex I is not altered in *Wt* mitochondria after I/R, nor is its presence enhanced in *h-COX-2 Tg*-derived mitochondria.

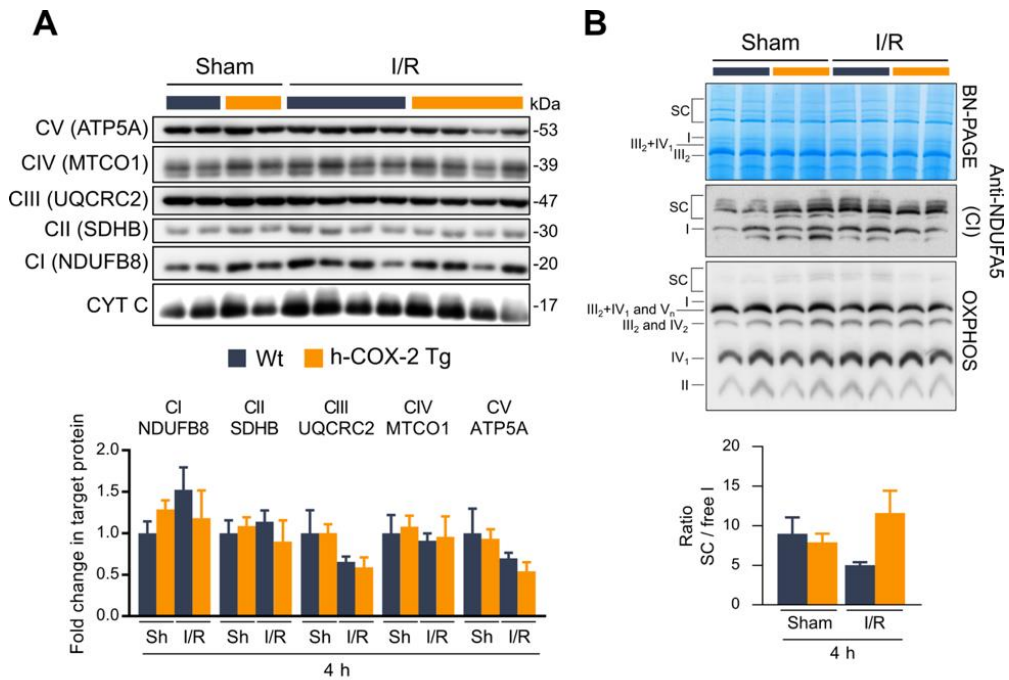


**Figure 27. Analysis of mitochondrial electron transfer chain (ETC) protein content.** (A) Representative Western blot and densitometric analysis of one subunit of each ETC complex (ATP5A for CV, MTCO1 for CIV, UQCRC for CIII, SDH for CII and NDUFB8 for CI), from isolated liver mitochondria from *Wt* and *h-COX-2 Tg* mice under Sham and I/R 4 h conditions. (B) ETC supercomplexes analysis of liver-derived mitochondria from *Wt* and *h-COX-2 Tg* mice under Sham and I/R 4 h conditions. Representative images of BN-PAGE and immunoblots, and its densitometric analysis, incubated with anti-complex I antibody (anti-NDUFA5) and anti-OXPPOS antibody. Data are represented as mean  $\pm$  SEM (n=4-9 per group). Abbreviations: CI, complex I; OXPPOS, oxidative phosphorylation; SC, supercomplexes; Sh, Sham.

ETC complexes do not move freely on the mitochondrial membrane, but interact with each other and form what are known as supercomplexes (SC). These SCs facilitate the transport of electrons from one complex to another, preventing the formation of ROS, as well as stabilising their folding and membrane presence. The presence and abundance of SC can be analysed by non-denaturing gels, and subsequent immunoblot analysis. In this case, mitochondria were permeabilised with digitonin that ensures the formation of pores in the mitochondrial membrane but

maintains the presence of the proteins anchored to it. They were then loaded onto gels under non-denaturing conditions and supercomplexes were resolved. Apparently, supercomplexes comprising complex I subunits are subtly more stabilised in *h-COX-2 Tg* mitochondria after I/R compared to *Wt* mitochondria (**Figure 27B**). Nevertheless, these results seem to be not strong enough to explain the increased respiration due to higher complex I activity but may be related to a lower contribution to ROS generation.

### 4.3 Ischemia-reperfusion causes lost in mitochondrial membrane potential and is prevented by COX-2 expression

Changes in mitochondrial respiration can be the cause or consequence of an alteration of the mitochondrial membrane potential ( $\Delta\Psi_m$ ). The  $\Delta\Psi_m$  is generated due to the accumulation of protons in the intermembrane space of mitochondria as electrons pass through the different ETC complexes. This chemical and energetic potential is used by ATP synthase to generate ATP from ADP and inorganic phosphate. Therefore, the analysis of the state of the  $\Delta\Psi_m$  is an indicator of the state of the mitochondria and subsequently, of the cell. To assess the state of mitochondrial membrane potential in liver mitochondria after I/R, liver homogenates were labelled with the TMRM probe and passed through a flow cytometer (**Figure 28A**). The TMRM probe will label anything that is positively charged, so in terms of mitochondria, it will label all mitochondria with an intact membrane potential. Indeed, mitochondria derived from *Wt* livers after I/R have a dissipated membrane potential, as indicated by number of positive TMRM events (**Figure 28B**) and the intensity of the TMRM signal (**Figure 28C**), which are both very low values. In contrast, *h-COX-2 Tg*-derived mitochondria have an intact membrane potential, as if it had not been lost after I/R.

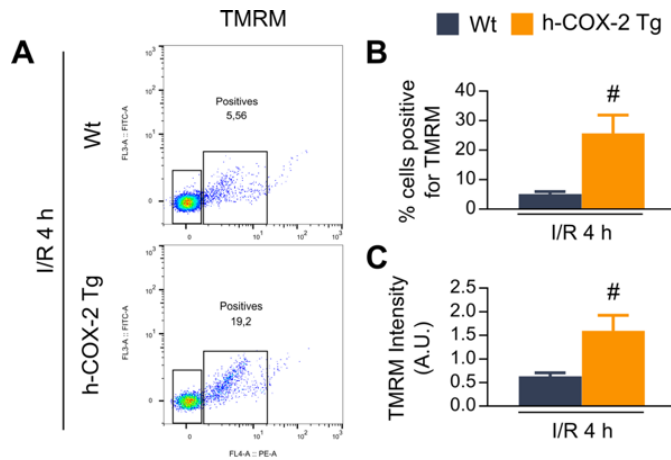


**Figure 28. Assessment of mitochondrial membrane potential.** (A) Representative flow cytometry images of TMRM probe-labelled mitochondria from *Wt* and *h-COX-2 Tg* liver homogenates after I/R 4 h. (B) Percentage of TMRM-positive cells and (C) TMRM intensity. Data are represented as mean  $\pm$  SEM (n=5-8 per group). #p<0,05 versus *Wt* I/R. Abbreviations: TMRM, Tetramethylrhodamine methyl ester; A.U., arbitrary units.

#### 4.4 Mitochondria number and phenotype are not altered because of the COX-2 expression

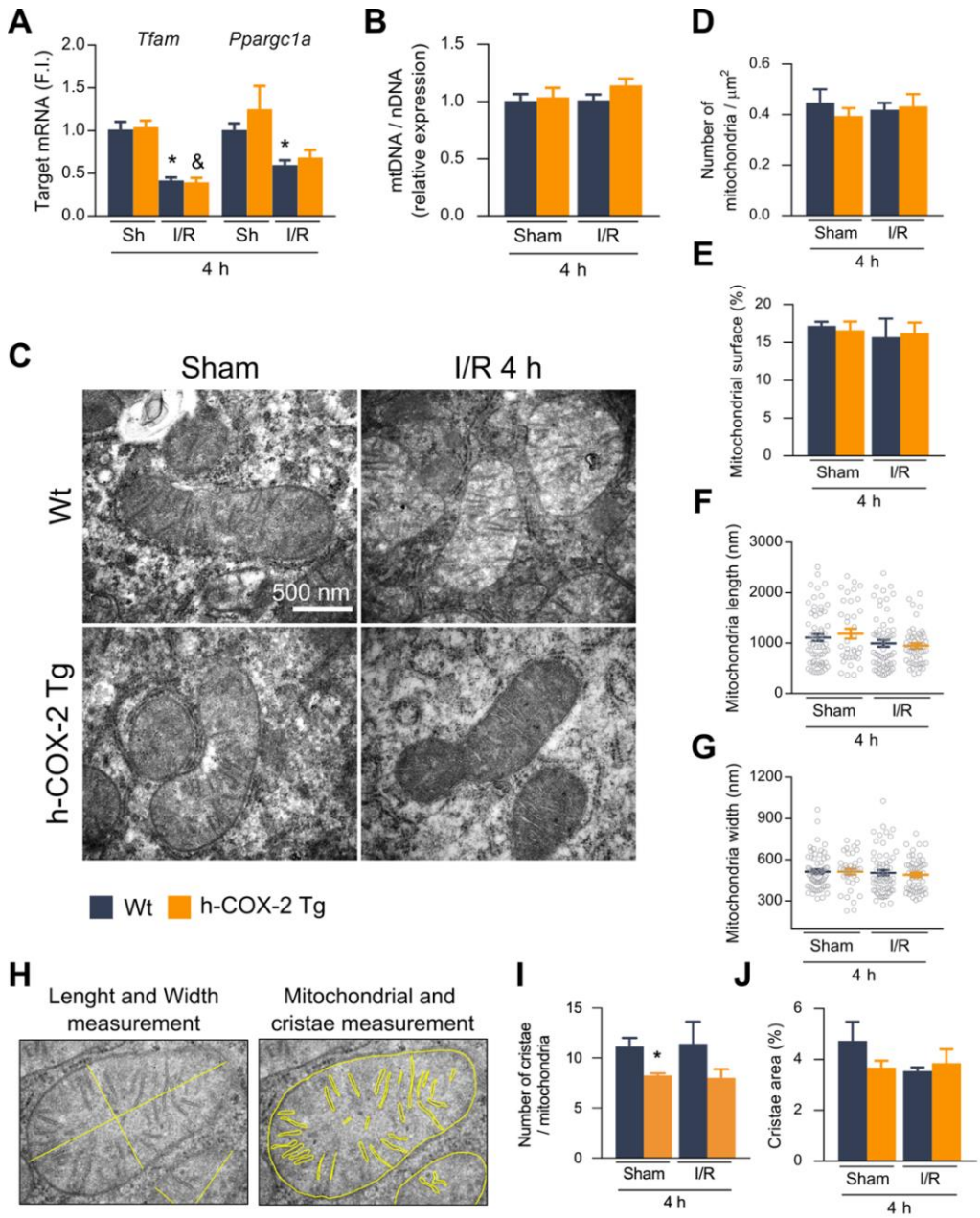
A lower respiration rates and a decrease in mitochondrial membrane potential in mitochondria after I/R could lead to major changes in the distribution of mitochondria in the tissue, altered morphology, disorganisation of cristae or even lower number of mitochondria. All these aspects were ruled out by comparing *Wt* and *h-COX-2 Tg* samples after Sham and I/R. First, mitochondrial biogenesis was analysed to assess whether it was altered during I/R or by the influence of the COX-2 enzyme. The transcriptions factors TFAM and PGC1 $\alpha$  (encoded by the gene *Ppargc1a*) are responsible for the expression of several mitochondrial genes and are therefore closely related to mitochondrial biogenesis. Both gene expressions decreased after I/R, but no differences were found when comparing *Wt* and *h-COX-2 Tg* samples (Figure 29A). Despite this decrease in mitochondrial biogenesis transcription factors after I/R, no differences were found when analysing the mitochondrial DNA copy number (Figure

**29B**). This analysis is usually assessed to reveal the number of mitochondria by comparing the ratio mtDNA/nDNA (mitochondrial to nuclear DNA). Furthermore, by counting the number of mitochondria in a representative number of electron microscopy micrographs (**Figure 29C**), no difference in the number of mitochondria is observed (**Figure 29D**). Moreover, the area of individual mitochondria is the same in all four conditions, measured by total area, length and width separately (**Figure 29E-G**).

Further analysis of the appearance of mitochondria was performed by analysing mitochondrial cristae. These structures are invaginations of the inner membrane that localise the entire ETC machinery, as well as other protein structures, and allow the generation of microenvironments to enhance mitochondrial respiration. The analysis of these cristae was performed by counting the number of cristae per mitochondria and the area (**Figure 29H**). The number of cristae is lower in *h-COX-2 Tg* mitochondria compared to *Wt* under Sham conditions, but no differences were found in I/R conditions, nor in the area of these cristae (**Figure 29I-J**).

**Figure 29. Mitochondrial number, morphology, and appearance analysis.** **(A)** Measurement of mRNA levels of genes related to mitochondrial biogenesis (*Tfam* and *Ppargc1a*), from liver extracts of *Wt* and *h-COX-2 Tg* mice under Sham and I/R 4 h conditions. **(B)** Mitochondrial DNA content (*CytB*) in relation to nuclear DNA content (*ApoB*) assessed by qPCR of liver extracts from *Wt* and *h-COX-2 Tg* mice under Sham and I/R 4 h conditions. **(C)** Representative transmission electron microscopic micrographs of liver sections from *Wt* and *h-COX-2 Tg* mice under Sham and I/R 4 h conditions. Number of mitochondria relative to area **(D)** and percentage of area occupied by mitochondria **(E)** quantified from TEM images. Measurement of mitochondrial length **(F)** and width **(G)** in TEM images, as indicated in **(H)**. Number of cristae per mitochondrion **(I)** and relative area occupied within the mitochondrion **(J)**, measured as indicated in **(H)**. Data are represented as mean  $\pm$  SEM (n=4-9 per group for (A) and (B); 5 images/animal, 3-5 per group for (D-J)). \*p<0,05 versus *Wt* Sham; & p<0,05 versus *h-COX-2 Tg* Sham. Abbreviations: mtDNA, mitochondrial DNA; nDNA, nuclear DNA; F.I., fold induction. (next page)





#### 4.5 Mitochondrial dynamics is altered after ischemia-reperfusion

Mitochondria are highly dynamic organelles that change their shape and distribution in the cell to respond to different stimuli [158]. During ischemia-reperfusion, mitochondria are heavily damaged, mainly by the generation of ROS and the opening of the mitochondrial transition pore. One mechanism by which the cell eliminates damaged mitochondria is through their fragmentation and subsequent selective autophagy, called mitophagy. The mitochondria found in *Wt* and *h-COX-2 Tg* tissues take a doughnut shape after ischemia and followed by 4 h of reperfusion, whereas under Sham conditions they remain with a filamentous phenotype (**Figure 30A**). This phenomenon has already been described and suggests that this peculiar remodelling of the mitochondrial network allows mitochondria to protect themselves from damage, fragmentation and elimination [159]. Interestingly, the lower damage observed in tissue and specifically in the mitochondria of *h-COX-2 Tg* mice after I/R is not sufficient to block the alteration of mitochondrial shape, as their mitochondrial network resembles that of *Wt* samples after I/R.

The changes in the mitochondrial network respond to changes in the dynamic processes of fusion and fission. Both mechanisms involve several cytosolic and mitochondrial proteins that are analysed in this study. The fission pathway involves the recruitment of the cytosolic factor DRP1 to the mitochondrial membrane. This small protein will interact with different receptors; including FIS1, and will oligomerise around the mitochondria, eventually forming a ring and constricting the mitochondria until finally dividing it. Despite what can be seen in the mitochondrial network images, where mitochondria appear to lose the filamentous conformation, DRP1 levels are lower in the *Wt* samples after I/R, while they remain unchanged in the *h-COX-2 Tg* samples (**Figure 30B**). FIS1 levels are unchanged in all conditions (**Figure 30C**).

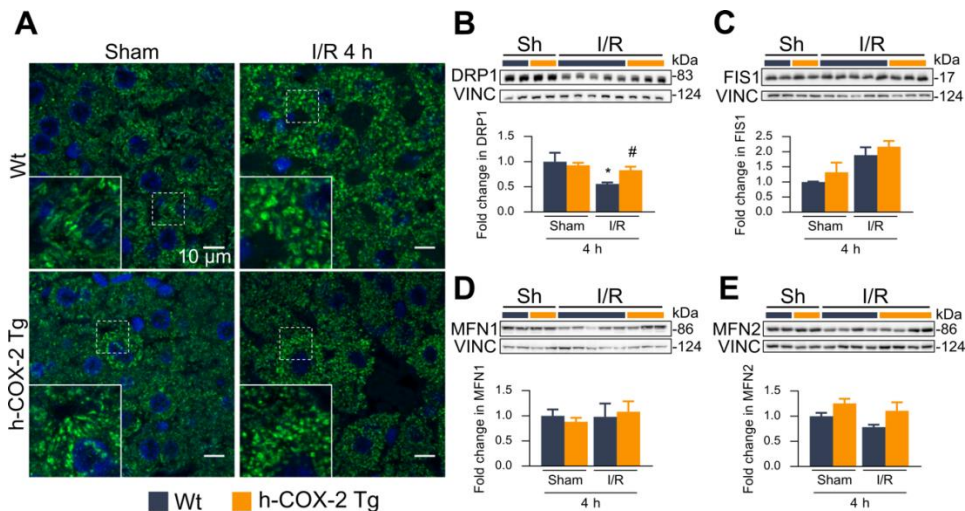


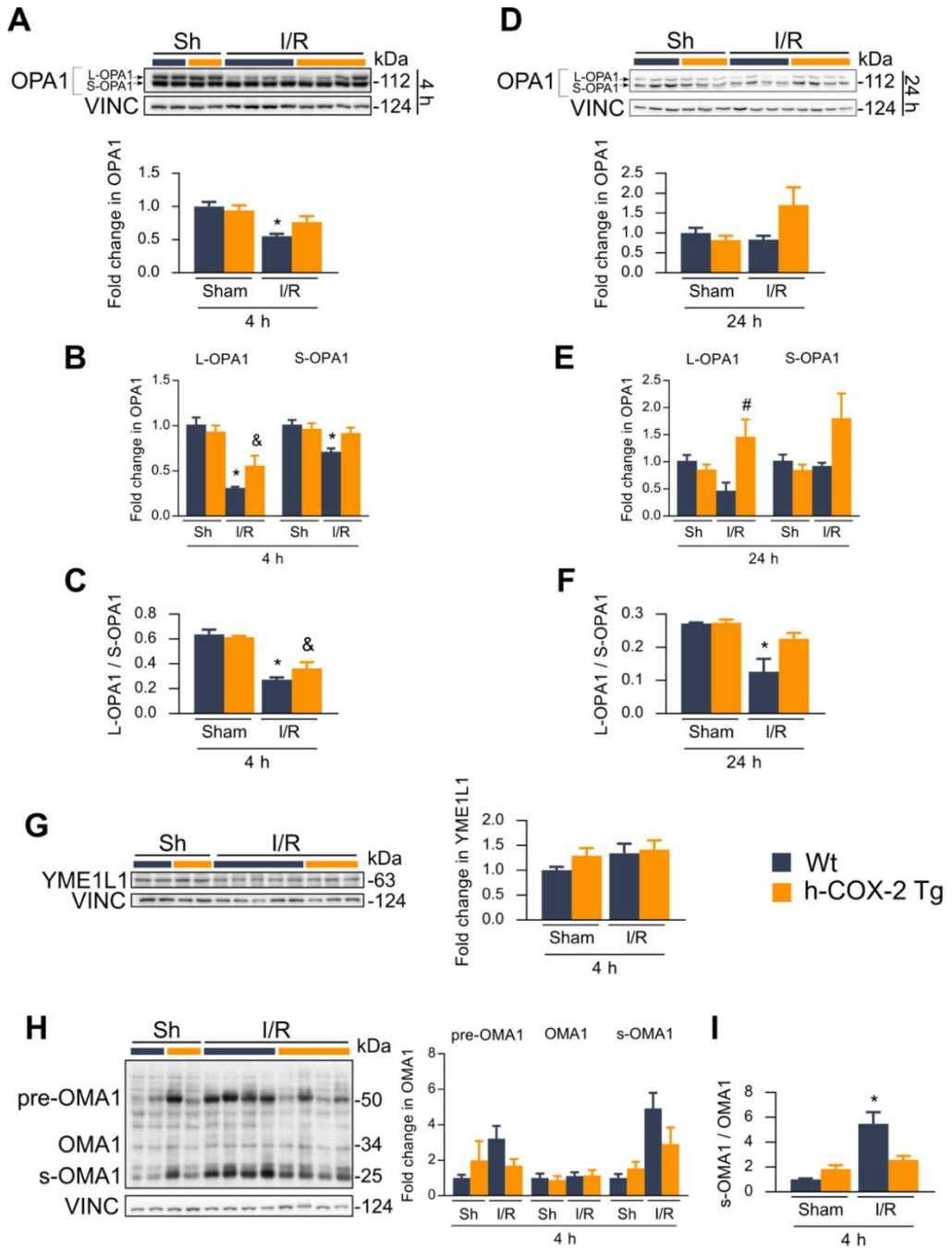
**Figure 30. Analysis of mitochondrial dynamic.** (A) Representative immunofluorescence images of liver sections from *Wt* and *h-COX-2 Tg* mice under Sham and I/R 4 h conditions, of HSP60 (mitochondrial marker) in green and DAPI (nucleus) in blue. (B-E) Representative Western blot and densitometric analysis of DRP1 (B), FIS1 (C), MFN1 (D), and MFN2 (E) proteins (normalised to VINCULIN), from *Wt* and *h-COX-2 Tg* liver extracts, under Sham and I/R 4 h conditions. Data are represented as mean  $\pm$  SEM ( $n=4-9$  per group) \* $p<0,05$  versus *Wt* Sham; # $p<0,05$  versus *Wt* I/R. Abbreviations: Sh, Sham; VINC, vinculin.

On the other side, the fusion pathway consists of a first approach and later fusion of the outer membrane and a second fusion of the inner mitochondrial membrane. Outer membrane fusion is mediated by mitofusins (MFN1 and MFN2) and inner membrane fusion is mediated by OPA1. In this regard, the expression of both MFN1 and MFN2 does not differ, neither by I/R nor the presence of COX-2 (Figure 30C-D). In contrast, the inner membrane fusion protein OPA1 is significantly less expressed in *Wt* livers after I/R, but is maintained in the *h-COX-2 Tg* livers (Figure 31A). These results show that the overall dynamics of mitochondria are not altered, but only OPA1, which has more functions in addition to mitochondrial fusion. Therefore, the observed changes in respiration, and even in mitochondrial membrane potential, could be due solely to changes in OPA1.

#### 4.6 OPA1 processing is enhanced by a higher activity of OMA1 in *Wt* mitochondria after ischemia-reperfusion

A detailed study of the expression of the OPA1 protein reveals that it can be found as different isoforms of different molecular weight. In fact, the OPA1 protein undergoes different proteolytic changes, and these different forms have different functions. The long forms interact with each other and are responsible for keeping the mitochondria cristae tight. When OPA1 is processed, shorter forms appear, and the interaction between the short and long forms is responsible for the fusion of the inner membranes of two fusing mitochondria. When analysing separately the two bands observed in Western blot analysis of OPA1, a consistent decrease of both long (L-OPA1) and short (S-OPA1) isoforms is observed in the *Wt* samples, while the *h-COX-2 Tg* samples have a minor decrease of the long form, and a fully maintained short form (**Figure 31B**). The ratio between L-OPA1 to S-OPA1 shows that under Sham condition both forms are close to be equal, and is the same in *Wt* and in *h-COX-2 Tg* samples, while in *Wt* after I/R the short form is predominant (**Figure 31C**). When the livers were left 24 h of reperfusion (**Figure 31D**), the predominance of the short form of OPA1 is maintained (**Figure 31E-F**), as in short periods of reperfusion (4 h).

**Figure 31. OPA1 expression and processing analysis.** (**A, D**) Representative Western blot and densitometric analysis of OPA1 protein (normalised to VINCULIN), from *Wt* and *h-COX-2 Tg* liver extracts under Sham and I/R 4 h conditions (**A**) and Sham and I/R 24 h conditions (**D**). (**B, E**) Differential densitometric analysis of L-OPA1 and S-OPA1 from Sham and I/R 4 h conditions (**B**) and Sham and I/R 24 h conditions (**E**). (**C, F**) Ratio between the two forms (L-OPA1 relative to S-OPA1) of Sham and I/R 4 h conditions (**C**) and Sham and I/R 24 h conditions (**F**). (**G**) Representative Western blot and densitometric analysis of YME1L1 protein (normalised to VINCULIN), from *Wt* and *h-COX-2 Tg* liver extracts under Sham and I/R 4 h conditions. (**H**) Representative Western blot and densitometric analysis of OMA1 protein and its different proteolytic forms (normalised to VINCULIN), from *Wt* and *h-COX-2 Tg* liver extracts under Sham and I/R 4 h conditions. (**I**) Ratio between the short form (s-OMA1) and the mature form (OMA1). Data are represented as mean  $\pm$  SEM (n=3-9 per group). \*p<0,05 versus *Wt* Sham; #p<0,05 versus *Wt* I/R; & p<0,05 versus *h-COX-2 Tg* Sham. Abbreviations: VINC, vinculin; L-OPA1, long-OPA1; s-OPA1, short-OPA1; s-OMA1, short OMA1; Sh, Sham. (next page)



The processing of OPA1 is mainly performed by two proteases. The YME1L1 protease acts basally and is responsible for the balance between the short and the long form, to maintain both cristae stability and mitochondrial fusion. OMA1, on the other hand, only acts under certain stimuli, for example when there is a drop in the mitochondrial membrane potential. Before being incorporated into the mitochondrial membrane, OMA1 appears as a pre-protein (pre-OMA1); this isoform undergoes proteolytic cleavage that allows it to be incorporated in the membrane (mature OMA1) where it remains inactive. When the membrane potential is lowered, a new cleavage occurs, giving rise to the short form of OMA1 (s-OMA1), which is the active form. When analysing the expression of both proteases, YME1L1 shows no difference in expression under any condition (**Figure 31G**), but OMA1 does. After I/R, *Wt* livers show a higher accumulation of s-OMA1, which correspond to the active form of the enzyme (**Figure 31H-I**). This result correlates with the predominant presence of the short form of OPA1 in *Wt* samples. Taken together, these results reveal that following I/R, loss of mitochondrial membrane potential can trigger OMA1 protease activation, leading to further processing of OPA1. The *h-COX-2 Tg* samples have similar levels of the different forms of OMA1 compared to the Sham conditions, in agreement with an intact membrane potential.

## 5. INCREASED PLASMATIC PGE<sub>2</sub> ARE ASSOCIATED WITH AN IMPROVEMENT IN LIVER FUNCTION

To translate all the results found in this study and validate them in a more physiological context, prostaglandin levels were measured in a retrospective study of a cohort of liver transplant (LT) patients. Liver transplantation is often the final stage of liver pathologies and is highly affected by ischemia-reperfusion injury. It involves a period of hypoxia when livers are resected from donors and have to face the period of reperfusion when they are transplanted into recipient patients. Therefore, the conditions under which ischemia-reperfusion occurs will determine the success of the transplantation or trigger graft dysfunction. Examples of different conditioning factors



are the time the graft spends on ice, the time before reperfusion occur, the conditions of the donor liver, such as whether the donor has a liver pathology like cirrhosis, hepatocellular carcinoma, viral infections, fatty liver or others. As demonstrated in the mouse model, COX-2 overexpression in hepatocytes plays an important role in the attenuation of I/R damage, so it can be assumed that its derived prostaglandins, PGE<sub>2</sub>, are mediating this effect. For this part of the study, PGE<sub>2</sub> levels collected from a cohort of 64 patients who had received LT were analysed. The cohort consisted of 41 men and 23 women; recipients ranged in age from 18 to 69 years and donors ranged in age from 14 to 81 years. The predominant cause of the need for liver transplantation was chronic cirrhosis (alcoholic or viral) and hepatocellular carcinoma. The preservation solution was Celsior solution (Genzyme Corporation, Naarden, The Netherlands) or University of Wisconsin solution (Du Pont Merck Pharmaceutical, Wilmington, DE, USA). The ischemia time was 563 min ± 164 min, of which 47 min ± 22 min correspond to warm ischemia and 544 min ± 161 min to cold ischemia. Other data, such as graft outcome and length of hospital stay, can be found in [Annex 1](#).

Arterial plasma was collected 60 min after reperfusion and several plasma parameters, including PGE<sub>2</sub> levels, were measured, and correlated with liver function parameters. Patients were divided according to whether or not they had experienced early graft dysfunction after transplantation based on ALT levels, coagulopathy and bile flow. Patients without early graft dysfunction, i.e. when transplantation was successful, have higher hepatic arterial plasma PGE<sub>2</sub> levels compared to those with early graft dysfunction, which have a lower presence of PGE<sub>2</sub> ([Figure 32A](#)). Furthermore, there is a negative correlation between the amount of PGE<sub>2</sub> detected and the length of hospital stay of the patients ([Figure 32B](#)), linking a shorter stay with higher prostaglandin levels, meaning that the presence of hepatic arterial plasma PGE<sub>2</sub> is indicative of a good prognosis in the liver transplant. These results point to a better acceptance of transplantation when prostaglandins are elevated in the patient's hepatic arterial plasma, validating the protective role of prostaglandins when the tissue is damaged by ischemia-reperfusion. Another parameter analysed in these patients was the duration of ischemia. In this case, a negative correlation was found when relating plasma PGE<sub>2</sub> levels and ischemia time during transplantation ([Figure 32C](#)). The

longer the ischemia; the less prostaglandins are detected in recipient patients. This may indicate that it is necessary to do the transplant in the shortest possible time, to ensure that prostaglandin levels are sufficient to exert their protective effect.

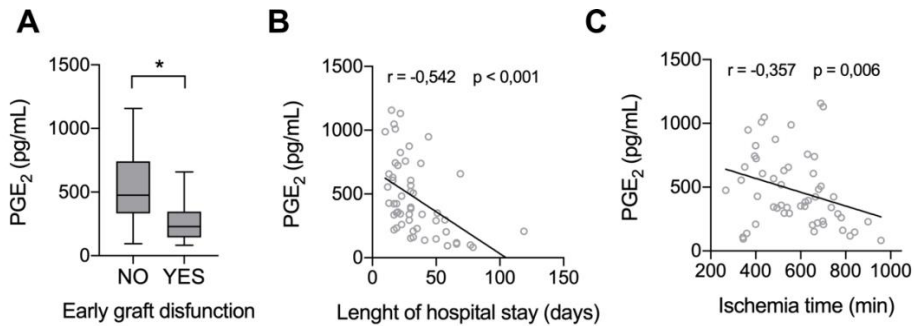


**Figure 32. Correlative studies of PGE<sub>2</sub> levels in plasma and graft function in patients receiving OLT. (A)** Correlation between PGE<sub>2</sub> levels and graft function, \* $p=0,026$ . **(B)** Correlation of PGE<sub>2</sub> levels and time spent in the hospital after receiving the transplant. **(C)** Correlation between PGE<sub>2</sub> levels and time of the ischemia. Both correlations (B, C), show a significantly negative correlation.



## V. DISCUSSION





Ischemia-reperfusion injury is generated when a tissue is subjected to hypoxia followed by a period of reperfusion, causing various damages and disorders at both the cellular and tissue level. Paradoxically, the necessary restoration of oxygen flow causes the most damage, leading to an oxidative response, inflammation, and ultimately cell death. In this study, the *h-COX-2 Tg* mouse model was used to evaluate the role of COX-2 in hepatic ischemia-reperfusion injury. In general, COX-2 expression in hepatocytes has a beneficial effect that mitigates liver damage following ischemia-reperfusion. The data obtained in the study support this claim at different levels which will be discussed below.

The use of a mouse strain with a specific genetic background is a controversial issue and a crucial point depending on the research being attempted [160], as is the selection of the sex of the animals [161]. Regarding sex selection, male individuals were selected for the present study to avoid hormonal modulation of endogenous prostaglandin levels [162][163]. Mouse strains are more difficult to choose because several aspects have to be considered, as mutations that differ from each other may determine the outcome of the results. In this study, the selection of a hybrid genetic background was a consequence of the methodology for the generation of the transgenic animal. Assuming that this hybrid genetic background could be the reason for the variability obtained in the results, two more homogenous backgrounds were obtained and several experiments were performed with these animals to test its susceptibility to IRI, as well as the variability between the individuals. The results clearly showed that, compared to the hybrid background mice, there was no damage in these two more homogenous strain mice, the pure C57BL/6JRcCHsd strain and the F1, a 50-50% mixture C57BL/6JRcCHsd and DBA. These results are surprising since many other studies have used pure genetic background mice to perform liver I/R and obtained the expected liver damage, but generally are different backgrounds than the ones used in this thesis, such as BALBc [164][165]. Even when using C57BL/6 as the strain of choice [166][167][168], is still a different strain from the one used in the present study (C57BL/6JRcCHsd), as is also the C57BL/6J [169][170]. These results are striking but not necessarily strange. Differences in I/R outcomes may be due to

differences in the mouse sub-strain used, but also due to the type of ischemia, ischemia time, and duration of reperfusion [171]. On the other hand, it has been reported that some mouse strains are not suitable for some models in research. For example, C57BL/6J animals do not progress to hepatocellular carcinoma [172], so the choice of another mouse strain is mandatory. Or even differences of two closely related mouse strains, such as C57BL/6J and C57BL/6N, are sufficient to behave differentially in models of MAFLD and NASH [173]. Therefore, after empirical demonstration of susceptibility and resistance to the I/R model in three different mouse strains, and although it is not clear why pure or F1 mixed strains do not behave the same way as the hybrid, selection and thus all subsequent studies were performed with the most susceptible mouse strain, which is the mixed strain.

When looking for the involvement of COX-2 in the initiation of inflammation or involution of disease, its inhibition is often found to be beneficial and administration of NSAIDs, that block its activity, are desirable to resolve the pathology of interest [38][174][175][176]. The overexpression model used in this thesis presents a contradiction of what is generally described (inhibition is better than induction), but several other studies have shown that PGE<sub>2</sub> are beneficial in different liver pathologies and have a protective role [177][178][179][180]. For example, the activation of the prostaglandin receptor EP<sub>4</sub> with agonists or its overexpression has been shown to improve liver function after I/R [181], reducing liver damage [182]. Moreover, the overexpression *h-COX-2 Tg* mouse model used in the present study has also been used in other liver pathologies such as acute liver damage, fatty liver disease, alcoholic liver disease and hyperglycaemia [47][48][183][184], which, although they are different pathologies and affect the liver at different levels, support the hypothesis of a protective role of COX-2. Therefore, the role of COX-2 in liver pathophysiology is still under debate.

Transgenic models of overexpression are not ideal in terms of translation to humans or the clinic, but they are very suitable tools for discovering and investigating the role and action of a protein when working with laboratory animals. In this case,

COX-2 expression specifically in the hepatocyte is constitutive, unlike in adult livers where its expression is inducible under stress signals and only in certain cell types [35]. But it has no further implications for liver development since COX-2 is expressed in embryonic stages, which does not imply any alteration in the normal development of the tissue.

After a period of ischemia, endogenous COX-2 is slightly expressed, suggesting that COX-2 expression is involved in the onset of inflammation, as reported by several authors [185]. But its induction need not be responsible for inflammation, but could be caused by it, in an attempt by the cell to protect itself from the damage that will be caused. In 2000, Clavien et al demonstrated that a short period of ischemia in the liver before the true period of ischemia, called preconditioning (PC), was beneficial for the tissue and ensured a better prognosis in the case of liver transplantation [186]. Of all the mechanisms activated in preconditioned livers, COX-2 expression is one of those that is significantly increased, leading to a rethinking of its role as a damage-causing factor, to consider it as a protective enzyme.

In recent years, many studies have tried to unravel the role of COX-2 in IRI in different tissues. In myocardial IRI, both endogenous and exogenous PGE<sub>2</sub> have been shown to protect cardiomyocytes after I/R [187], stimulate differentiation of progenitors to cardiomyocytes [188], and promote regeneration [189]. Moreover, COX-2 inhibition causes further cardiac damage and compromises cardiac function when subjected to ischemia-reperfusion [190][191]. In fact, a previous study using a model of COX-2 overexpression in cardiomyocytes showed that COX-2 confers a permanent cardioprotective stage against reperfusion injury [192]. The kidneys are other organs that may undergo transplantation and thus be subjected to ischemia and reperfusion. In renal IRI, PGE<sub>2</sub> has been shown to protect kidneys from IRI through upregulation of antioxidant, antiapoptotic, and anti-inflammatory pathways [193][194].

Based on this idea, the model of COX-2 overexpression in the hepatocyte has been used to address all the pathways responsible for COX-2-mediated reduction of

liver damage after IRI, creating a parallel with what happens when preconditioning is performed, and try to assign the correct role of COX-2 in this framework. To characterise the IRI model and validate the protective role of COX-2, several analysis and studies were performed and are described and discussed below.

First, *h-COX-2 Tg* mice subjected to I/R have lower levels of plasma transaminases (ALT and AST) compared to *Wt*, demonstrating less liver damage. Plasma transaminases are markers of acute liver damage as they are first released because of the rupture of cell membranes due to a necrotic state [195]. Thus, ALT and AST levels are higher after 4 h of reperfusion, when acute damage is generated, but their presence in plasma is decreased over time as no more cells die as a consequence of a first exacerbated reaction due to reperfusion. Furthermore, these transaminases will not remain in the bloodstream for long, according to the results of increased detection of transaminases at 4 h compared to 24 h of reperfusion. Like the release of liver transaminases, the detection of LDH in plasma is also an indicative of damage in response to the release of cytosolic enzymes that are only present in the bloodstream when cell membranes are disrupted. And like transaminases, LDH levels are lower in *h-COX-2 Tg* samples, supporting the idea of less liver damage in these animals. Although LDH could be released from any other tissue, not specifically from the liver like ALT and AST, the concordance of lower transaminases levels and the presence of fewer and smaller necrotic areas in transgenic samples lead to the conclusion that COX-2 expressing livers have less damage caused by I/R after 4 and 24 h of reperfusion.

One of the effects of this attenuated damage is a reduced activation of the inflammatory response. I/R in the liver causes global inflammation and can be observed by increased expression of pro-inflammatory genes (*Tnf*, *Il-6*, *Il-1b*) or release of proinflammatory cytokines into the bloodstream in *Wt* animals. In the presence of COX-2, the inflammatory response is attenuated after I/R, as can be seen by a lower expression of these proinflammatory genes, as well as by a lower presence of proinflammatory cytokines. In addition, the expression of the anti-inflammatory

cytokine IL-10 is increased in *h-COX-2 Tg* animals, consistent with an attenuated proinflammatory profile. COX-2 expression in hepatocytes has already been shown to be protective by attenuating inflammation in other liver pathologies, reinforcing the idea of an anti-inflammatory role of COX-2 [48][184]. Other inflammatory markers support the idea that COX-2 expression has a beneficial effect. Lower MPO activity is detected in COX-2 expressing samples, reflecting lower neutrophil infiltration, which is also observed in a lower presence of Ly6G<sup>+</sup> cells in transgenic samples.

Paradoxically, COX-2 inhibition has been a classic strategy to reduce inflammation, as prostaglandins are responsible for the main signs of inflammation, especially PGE<sub>2</sub> [31]. Several studies show that COX-2 inhibition with specific inhibitors (like NSAIDs) reduces the establishment of inflammation and promote the resolution of the pathology [39][43]. Hamada and colleagues described that global COX-2 deficiency enhances T helper 2 (Th2) immune function, reducing lymphocyte recruitment in the liver after I/R [40]. But, interestingly, the same authors later described that selective COX-2 inhibition in myeloid cells does not prevent liver injury after I/R, resulting in extensive necrosis and leukocyte infiltration [43], in addition to other studies that shown that signalling through PGI<sub>2</sub> (another COX-2 product besides PGE<sub>2</sub>) reduces inflammation by enhancing the production of the anti-inflammatory cytokine IL-10 in Th2 cells [196]. Indeed, what was observed is that COX-2 may have an anti-inflammatory role, depending on the expression of the enzyme at different times in the process. While at the onset of inflammation it plays a role in establishing inflammation, later it contributes to its resolution [44][197][198].

It should be noted that the model used in the present study has high basal levels of COX-2 expression, which could be assimilated to a situation close to the resolution of inflammation, when its expression has already been induced and is at its higher levels. Indeed, when *Wt* mice were preconditioned, the livers show attenuated inflammation compared to the *Wt* subjected to normal ischemia without PC. Actually, as mentioned above, liver preconditioning was described as protective in liver resections [186], and indeed preconditioned mice show overall less liver damage, less

necrosis and a lower antioxidant response, supporting the idea that COX-2 expression is beneficial in the setting of liver damage. In fact, and as also mentioned above, after I/R, *Wt* mice show a small increase in COX-2 expression, but after PC this increase is significantly higher, supporting the idea that the induction of COX-2 expression is beneficial in a context of liver damage. Furthermore, it validates the COX-2 overexpression mouse model to study the pathways that are activated or attenuated in PC livers and that contribute to tissue protection.

In addition, another fact that supports the idea of the role of COX-2 in the prevention of global injury is the results observed with the selective inhibition of the enzyme with DFU. In other studies, inhibition of 15-PGDH, the enzyme responsible for metabolising and reducing circulating PGE<sub>2</sub> levels, improves liver regeneration [38]. In the present study it is shown that inhibition of COX-2 in *h-COX-2 Tg* animals exacerbates liver damage, showing higher levels of liver damage, more necrosis, increased inflammatory response, and oxidative stress. Therefore, expression and activity of COX-2 enzyme is required to prevent exacerbated liver damage.

Necrotic areas are common after I/R, as observed by H&E staining. However, necrosis is not the only death pathway that leads cells to die after I/R, since apoptosis pathways are also activated [199]. Programmed cell death is activated after 90 min ischemia followed by 4 or 24 h of reperfusion, as can be seen in the increased activation of Caspase 3 and increased levels of BAX/BCL-2 ratio in *Wt* samples. In contrast, apoptosis markers do not increase in *h-COX-2 Tg* samples, demonstrating that pro-apoptotic signalling pathways are not activated in these cells. This anti-apoptotic effect of COX-2 has already been reported in models of fatty liver disease and acute liver injury [48][184].

In the context of reducing apoptosis, AKT and AMPK emerge as key players, as they are involved in several survival signalling pathways. Likewise, AKT and AMPK activations have been described to play a protective role in IRI [200]. AKT is known to be in the downstream signalling pathway of prostaglandin through binding to the EP<sub>2</sub>/EP<sub>4</sub> receptor dimer, and signalling through Gβγ factor and phosphoinositide 3-



kinases (PI3K) [201]. In hyperglycaemic mouse models with COX-2 overexpression, AKT phosphorylation is enhanced, promoting survival pathways [46][47]. Following I/R, transgenic samples also exhibit increased AKT phosphorylation compared to *Wt*, evidencing survival signalling. In addition, AMPK phosphorylation is also increased in the transgenic samples. In this case, in the Sham condition, p-AMPK appears already elevated in the transgenic samples, and after I/R it remains higher than in the *Wt* samples, where it is decreased. Indeed, inhibition of AMPK signalling leads to apoptosis [202], which reinforces the idea of an anti-apoptotic role of AMPK and suggests an interaction between COX-2, its derived prostaglandins and AMPK.

As mentioned above, AMPK is involved in several survival pathways, but also plays a role in the inflammation process. The higher p-AMPK/AMPK ratio observed in *h-COX-2 Tg* animals could explain the lower leukocyte infiltration, as it has been shown that AMPK can reduce the expression of adhesion molecules, inhibiting neutrophil infiltration, and inflammatory cytokines release [203]. Furthermore, activation of AMPK in preconditioning reduced liver injury by preserving ATP levels and reducing lactate accumulation [204].

Another pathway in which AMPK is actively involved is autophagy. Activation of AMPK is known to promote autophagy, and inhibition of AMPK-activating pathways leads to impaired autophagy [205][206][207]. In the context of ischemia, autophagy has been suggested to be impaired in liver IRI [208], and in particular a study showed that autophagy mediated by AMPK/mTOR signalling pathway reduces liver IRI in mice [209]. Indeed, increased autophagy is observed in *h-COX-2 Tg* samples after I/R, with an increase in autophagy initiating factor ATG7 and autophagosome protein LC3 II, compared to *Wt*. These results support the idea that COX-2 promotes AMPK-mediated autophagy. This connexion between COX-2 and autophagy is supported by other studies that reported in other cell types that up-regulation of COX-2 and PGE<sub>2</sub> induces autophagy [210], or that inhibition of autophagy and increased apoptosis are related to down-regulation of PGE<sub>2</sub> production [211]. Interestingly, levels of the cargo-marker protein p62 are higher in *Wt* after I/R,

compared to the transgenic samples which are lower, even before ischemia. Apparently, there are more cargoes marked for degradation in *Wt*, suggesting that more structures and materials are affected. Indeed, one study showed that increasing phosphorylation of AMPK at Thr172 leads to up-regulation of autophagy with decreased levels of p62, but increased levels of Beclin-1, ATG7, and LC3 [212]. Actually, autophagy is a well-known mechanism that is activated in cases of starvation [205][213], or in this case, in the absence of blood supply, which ultimately leads to nutrient deprivation. With these findings, it can be concluded that increased autophagy is a good mechanism to prevent liver damage after I/R and that COX-2 promotes it.

Cell death and apoptosis can also be promoted through the ER. Cellular stress, such as that caused by IRI, can alter ER function leading to the accumulation of misfolded proteins that will eventually trigger the UPR [77][214]. If this response fails to alleviate ER stress, the response itself will eventually drive the cells into apoptosis. Livers expressing COX-2 have an attenuated UPR compared to *Wt*, a fact that correlates with less apoptosis in these samples. Analysing the UPR from the beginning, *h-COX-2 Tg* samples have lower levels of the chaperone GPR78, indicating that there are fewer misfolded proteins to bind to. Chemical inhibition of chaperons has been shown to inhibit ER stress and protect against IRI [215], so lower chaperon expression or activity means less ER stress. Subsequently, although the *Atf6* gene appears up-regulated in the *h-COX-2 Tg* samples, the other two pathways, IRE1 and PERK pathways, remain attenuated in transgenic samples, compared to *Wt*. Following I/R, lower levels of *Atf4* and CHOP are indicative of reduced PERK factor activation. *Atf4* has been shown to be activated under different type of stress stimuli [216], which will stabilise CHOP expression and thus promote apoptosis [217][218]. In addition, IRE1 pathway is also attenuated, as observed by reduced JNK phosphorylation in the transgenic samples, as is *Xbp1* splicing. Reduced UPR activation is also related to AMPK activation, as can be seen in hypoxia studies in cardiomyocytes [219], a fact that could be extrapolated to these results since in the presence of COX-2, the activation of the AMPK pathway is promoted and there is less activation of the UPR. This ultimately translates into less reticulum stress and

ultimately less apoptosis. Indeed, Nakamura and colleagues demonstrated that antibiotic pre-treatment prior to transplantation activates the PGE<sub>2</sub>/EP<sub>4</sub> axis that regulates ER stress and autophagy and is beneficial in liver transplantation [220].

Reperfusion after an ischemic period is a source of cytokines and ROS that act as stress factors that will target the ER and activate the UPR [77][221]. It has already been shown in this work that in COX-2 expressing livers, less inflammation occurs, but also the overall presence of ROS is attenuated. The reduction of ROS may be a consequence of reduced ROS production, but also of increased antioxidant capacity of cells and tissues. The transcription factor NRF2 is a major player mediating the antioxidant response by inducing the expression of several antioxidant genes [222]. Previous studies demonstrated that NRF2 has a protective role against ischemia-induced hepatocellular damage [223], for example, pre-treatment of rats with an NRF2 inducer protects the animals against IRI [224]. The results in the present work show an increase of NRF2, both in gene and protein expression, as well as an increased localisation in the nucleus of hepatocytes in COX-2 expressing samples, indicating a favoured onset of antioxidant response. Thus, COX-2-derived prostaglandins would act as other metabolites that induce nuclear translocation of NRF2 [225], and reduce ROS levels in IRI models [226]. Some of the NRF2 target genes are antioxidant enzymes that detoxify tissue in the presence of ROS, such as *Sod*, *Hmox1*, *Catalase*, *Gr* or *Gpx* [227][228][229][230]. The expression and/or activities of these enzymes are higher in *h-COX-2 Tg* livers, consistent with a higher presence of NRF2 and the lower presence of ROS in these tissues. In fact, this data show on the one hand that *h-COX-2 Tg* livers have a better antioxidant response, with a higher antioxidant capacity, and on the other hand a lower oxidative stress, probably due to a lower ROS production. In any case, all these results reinforce the idea of an antioxidant role of COX-2.

Lipid peroxidation has been used as a biomarker of oxidative stress, and has also been linked to several conditions that generate oxidative stress, such as inflammation resulting from diabetes [231]. ROS not detoxified by an overwhelmed antioxidant

response can oxidise membrane-forming phospholipids and, over time, can form pores and allow the release of ROS into the cell and tissue, as well as damaging membrane-formed organelles, and cause damage to macromolecules, DNA, and proteins [232]. Ischemia-reperfusion cause lipid peroxidation as can be seen in the measurement of LPO in *Wt* samples, and again the presence of COX-2 mitigates this reaction, either as a consequence of increased scavenging of the ROS produced or directly by reduced ROS generation in these tissues.

Of all the cellular organelles that are affected by IRI, mitochondria are the most closely related to this phenomenon [57]. On the one hand, they participate to cell damage by contributing to ROS generation, but on the other hand they play an essential role in the antioxidant response through specific antioxidant enzymes [178][233]. General damage to mitochondria during IRI can determine the fate of the cell, changing its metabolism and affecting cellular energy status, or ultimately leading to cell death [57]. One of the key players mediating the antioxidant response in mitochondria is the mitochondrial isoform of superoxide dismutase (SOD2 or MnSOD) [234][235]. Both its expression and activity are increased in *h-COX-2 Tg* samples. In fact, its protein levels are already higher in control conditions, favouring the antioxidant response once the onset of oxidative stress occurs during I/R. Moreover, SOD2 expression is specific in the hepatocyte, supporting the idea of a hepatocyte-mediated antioxidant response under the effect of COX-2 expression.

As mentioned above, mitochondria are essential in the cellular response to IRI. Their direct dysfunction due to oxygen deprivation favours the generation of ROS and thus contributes to oxidative cell damage. Moreover, their preservation under hypoxic conditions is an indicator of cellular fitness [236] and proven therapy efficacy [237][238][239]. Due to the accumulating evidence demonstrating reduced I/R damage in COX-2 expressing livers, and the reported evidence that mitochondria play an essential role in the onset and resolution of cellular oxidative damage following I/R, an in-depth study of mitochondrial function was performed in this study.

One macroscopic effect caused by hypoxia is a change in the mitochondrial network. Mitochondrial morphology changes to adapt to specific cellular and tissue demands, and this remodelling influence different aspects such as ETC activity, apoptotic sensitivity and mitochondrial dynamics [240]. In general, large fused mitochondria are associated with increased ETC activity, mitophagy protection and resistance to apoptosis stimuli, whereas fragmented mitochondria are more susceptible to apoptosis and mitophagy [241]. Oxygen deprivation has been reported to cause mitochondrial fragmentation through increased mitochondrial fission [242]. Ong's team demonstrated that this hypoxia-induced fragmentation is mediated by DRP1 activity [133], and Bouche's group reported that pharmacological inhibition of DRP1 protected murine cardiomyocytes from IRI [243]. But, contrary to expectations, in the present study, *Wt* tissues have lower levels of DRP1 compared to *h-COX-2 Tg* samples after I/R, expecting lower mitochondrial fission. However, the mitochondrial network is altered after I/R, although the mitochondria do not appear fragmented but in a particular doughnut shape. A study by Liu and Hajnóczky showed that hypoxia can induce this network remodelling during reperfusion to protect mitochondria from fission and thus from mitophagy or apoptosis [159].

The fact that no further fission is observed in the samples after I/R is supported by the absence of changes in other mitochondrial aspects, such as the number or size of mitochondria. Thus, although the mitochondrial network appears to be modified towards doughnut-shaped morphology after IRI, neither the length nor the width of individual mitochondria is affected, and the number of mitochondria is the same in all conditions. Such contradictory results have already been described and are due to differences in the models used, in the *in vivo* or *in vitro* analysis, in the times chosen for ischemia and reperfusion, among other variables [244][245]. However, the mitochondrial copy number study, used to determine the number of mitochondria, shows no alteration in any condition, making it clear that there are no more mitochondria, i.e. no more fission.

Mitochondrial remodelling is carried out by several fission/fusion proteins such as OPA1 [246][247]. It has been reported that during hypoxia there is a decrease in OPA1 protein expression [242] and that its overexpression blocks fission [248]. Likewise, OPA1-mediated mitochondrial protection has been shown in models of cerebral and cardiac ischemia-reperfusion injury [135][249]. Indeed, this effect was observed in *Wt* livers after I/R, where there is a lower presence of OPA1. In this sense, COX-2 seems to stabilise OPA1 because its presence is maintained after I/R in *h-COX-2 Tg* samples. Moreover, OPA1 processing is also important in mitochondrial remodelling after I/R, as Duvezin-Caubet's team described that OPA1 processing increases after hypoxia [248]. Again, this increased processing is observed in *Wt* liver samples after I/R, and this effect is mitigated in the presence of COX-2. Furthermore, as detected in this study, the OPA1-related protective mechanism is independent of variations in MFN1 or MFN2 [250], which are normally altered when there are changes in mitochondrial fusion and fission dynamics [103].

OPA1 processing is required for a couple of basic functions. Basal processing by the YME1L1 protease ensures the presence of both short and long forms of OPA1 that will maintain balance in mitochondrial fusion, as the interaction of the two isoforms ensures the fusion of two fusing inner mitochondrial membranes[103][251][252]. On the other hand, the interaction of two long isoforms ensures the preservation of the cristae junctions, membrane unions at the end of these invaginations called mitochondrial cristae [253]. An imbalance of these two isoforms can cause cristae junctions to open and lead to a reduction in the rate of respiration, CytC release and ROS production [254][255][256]. Under hypoxia, OPA1 processing is imbalanced [257]. In particular, in the present study after I/R in liver, the L-OPA1/S-OPA1 ratio decreases, and S-OPA1 becomes the predominant isoform, indicating increased OPA1 processing. Since mitochondrial fragmentation does not seem to be affected, this result suggests that cristae would be less stabilized. However, this hypothesis could not be demonstrated because the analysis of cristae did not reveal changes in the number of cristae per mitochondria, nor in the area of cristae. Nevertheless, this part

of the study is based on TEM images, which lack sufficient depth to be fully representative of the situation of mitochondria in cells.

As mentioned above, YME1L1 is the protease responsible for the basal proteolysis of OPA1. This enzyme is not modified under any conditions, which means that the observed OPA1 processing is not mediated by YME1L1. But it has been described that OPA1 can be processed by a stress-induced protease called OMA1 [258][259][260]. OMA1 localises to the inner mitochondrial membrane and acts under stimuli such as loss of membrane potential [261]. In this case, it is more activated in *Wt* samples, while in *h-COX-2 Tg* samples remains less activated, as observed by Western blot analysis where less of the short form of the enzyme corresponding to the activated form is detected in the transgenic samples. In fact, OMA1 activation in *Wt* livers correlates with the low membrane potential detected in these samples. In this case, the presence of COX-2 preserves the membrane potential, which does not trigger OMA1 activation. Therefore, as described in the bibliography, under control conditions the loss of membrane potential triggers OMA1 activation and OPA1 processing; and this whole chain of events is prevented under the effect of COX-2 overexpression.

The drop in mitochondrial membrane potential is closely related to the opening of the mPTP, which occurs during periods of ischemia and subsequent reperfusion [262]. Opening of the mPTP leads to a fall in membrane potential, CytC release, and increased ROS production, events that are prevented by COX-2 overexpression. Furthermore, preconditioning prevents mPTP during reperfusion [262][263], supporting the idea that COX-2 protection could be through preservation of mitochondrial functionality, directly or indirectly.

In parallel, OMA1 activation has also been linked to mitochondrial stress through the interaction of the DAP3-binding cell death enhancer 1 (DELE1) and the eukaryotic translation initiation factor 2 alpha kinase 1 (HRI or EIF2AK1). DELE1 is an inner mitochondrial membrane protein related to apoptotic signalling pathways and HRI is an eIF2 $\alpha$ -type kinase present in the cytosol. When OMA1 is activated, due to

a drop of membrane potential, it cleaves the DELE1 protein releasing it to the cytosol and its accumulation will eventually activate the eIF2 kinase activity of HRI. This activation will promote translation inhibition on one hand and translation of *Atf4* on the other hand, thus activating stress signalling in the cell [154]. As described above, *Atf4* is less expressed in *h-COX-2 Tg* samples which, as just mentioned, reflects lower overall cellular stress.

Cristae disorganisation can lead to a reduction of the respiratory rate, ROS production, CytC release, as well as a reduction of the membrane potential [254][255][256]. In this case it is not possible to know exactly what triggers what, whether the loss of membrane potential causes OPA1 processing and thus further disorganisation of the cristae, or whether cristae opening is itself responsible for the drop of membrane potential. In either case, both situations generate a disorganisation of the components of the electron transfer chain, which has been described as leading to decreased respiration, generation of ROS, and reduced ATP production [264][265].

The electron transport chain is, together with the glycolysis and the tricarboxylic acid cycle, an essential step in maintaining the energetic demands on the cell. Its function is impaired after periods of hypoxia due to a lack of oxygen, the final electron acceptor of the chain. This alteration in its function causes ROS at the mitochondrial level [266], more in detail, due to the reverse electron transport (RET) that causes superoxide at level of Complex I [121]. Maintenance of respiration is compromised in *Wt* samples after I/R, compared to transgenic-derived mitochondria. The electron-feeding fatty acid pathway through the CETF is maintained in *h-COX-2 Tg* mitochondria after I/R, whereas *Wt*-derived mitochondria have a lower contribution of this pathway to the overall respiration. The NADH pathway (N-pathway) that uses substrates that feed the ETC with electrons from the NADH, such as malate, pyruvate and glutamate, is also maintained in *h-COX-2 Tg* mitochondria, revealing that *Wt* mitochondria have impaired mitochondrial respiration at CI level. Actually, an increase in CI activity has been shown to be protective in IRI [267].



Although ETC activity appears to be affected in *Wt* samples after I/R, no changes in ATP or AMP levels, nor in NADH levels, were observed compared to *Tg* samples. This observation is interesting because a lower ETC activity should translate into lower ATP production, but AMPK has been described to maintain ATP levels by promoting catabolic pathways, and inhibiting anabolic pathways to prevent ATP depletion [267].

The individual presence of ETC components does not reveal changes in any situation, not even after I/R or under COX-2 expression. This means that the reduction of respiration due to a reduced contribution of electrons feeding CI is not due to a reduction of CI expression. However, ETC complexes do not move freely in the membrane, but are described to be organised into SC [115][268]. This organisation ensures better respiration because it reduces the leakage of electrons when they are transferred from one complex to another [269][270], as well as being related to stress situations to ensure maintenance in respiration [264]. Furthermore, stabilisation of cristae affects the formation and activity of the SC [271], so it can be assumed that the observed changes in OPA1 will affect this balance. The analysis of SC points to a trend of destabilisation of the SC composed of CI in the *Wt* samples after I/R. These results could support the idea of reduced CI-dependent respiration, as the SC tend to be less organised. In relation to this result, it has been described that increased SC composed of complex I ensure higher respiration and lower ROS formation and when CI is predominately alone, more ROS are generated [270][272]. These results may also be related to the fact that *Wt* mitochondria have lost their membrane potential and mitochondrial cristae are opened. Indeed, the destabilisation of cristae may be due to a disorganisation of SC [253].

Overall, *h-COX-2 Tg*-derived mitochondria are less affected and show reduced damage after I/R compared to the *Wt*-derived mitochondria. This attenuated damage can be observed through a maintained respiratory capacity, preserved mitochondrial membrane potential and protection of mitochondrial structure (**Figure 33**).

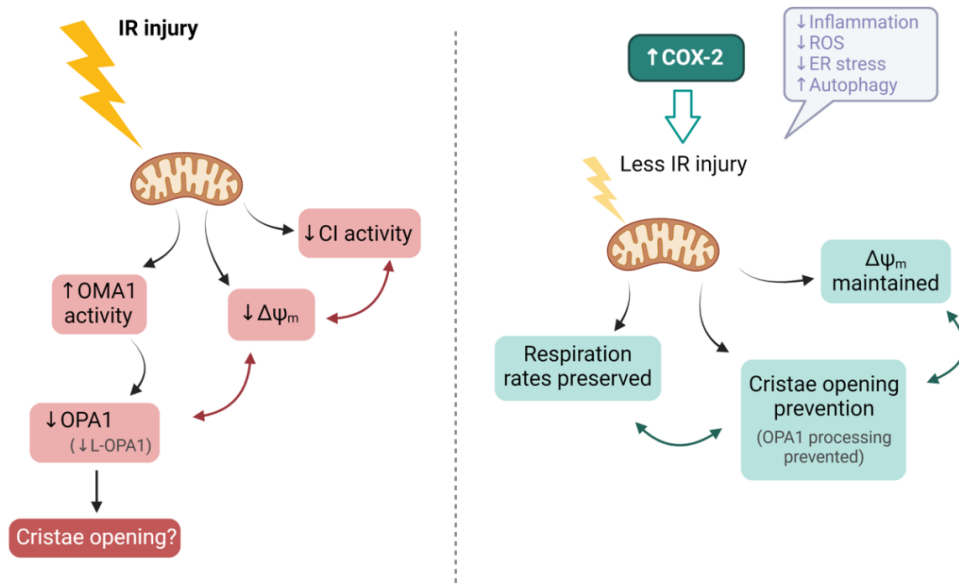


**Figure 33. Proposed model of mitochondrial damage after I/R and preservation of mitochondrial function in the context of COX-2 overexpression.** Under physiological conditions, I/R results in mitochondrial damage causing a decrease in Complex I activity, loss of membrane potential, and activation of the OMA1 protease. Activated OMA1 will further process OPA1, decreasing the presence of L-OPA1, leading to a destabilisation of the cristae, contributing to loss of membrane potential and dysfunction of respiration. When cellular and tissue damage is prevented under COX-2 overexpression (due to reduced inflammation, oxidative stress and ER stress, among other beneficial effects), mitochondria suffer less; they maintain membrane potential, OPA1 processing is prevented, leading to prevention of cristae opening and respiration rates are also preserved. *Created with Biorender.com*

Finally, the contribution of COX-2 to the prevention of tissue damage after I/R was analysed in the context of clinical translation. In this study, the relationship between plasma PGE<sub>2</sub> levels and clinical data of patients undergoing LT has been evaluated [273]. This analysis shows that the presence of PGE<sub>2</sub> in the plasma of recipients correlates with a better prognosis, while lower PGE<sub>2</sub> levels are associated with early graft dysfunction, assessed with a previously described scale [274].

These results support the data obtained with animal models and reinforces the idea of a protective role of COX-2 and its derived prostaglandins in the prevention of liver damage after I/R. Experimental results suggests that, even at levels in the physiological range, PGE<sub>2</sub> may be protective in patients receiving LT. In fact, it has been reported that when liver donors are subjected to preconditioning, thereby increasing PGE<sub>2</sub> prior to liver resection, liver protection is promoted and transplant outcome is improved [275].

An important detail that emerges from these results is that the protective function of COX-2 is effective when performed by the hepatocyte. In a common context of inflammation and oxidative response, it is the KCs that is responsible for the expression of COX-2 [276] and this cell-specific expression is correlated with a higher ROS production and therefore tissue damage [276]. But, when COX-2 expression is driven through the hepatocyte, either by overexpression or preconditioning, it is protective (**Figure 34**).

Taken together, COX-2 expression in hepatocytes appears to protect livers from ischemia-reperfusion injury. What all these results point to is an induction of COX-2 when liver damage occurs, and that this expression is beneficial. Under normal conditions, this expression is low and is not enough to generate any beneficial effect, leaving the tissue unprotected against the burst of liver damage caused by inflammation and oxidative stress. But, when COX-2 induction is higher, due to preconditioning or through transgenic overexpression, the role of COX-2 is clearly protective and prevents liver damage at several levels.

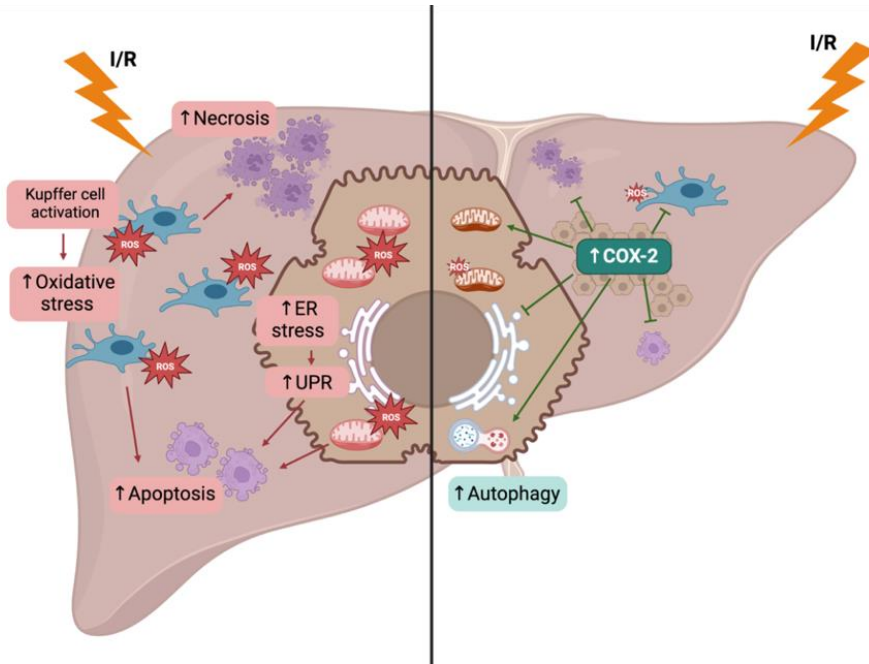


**Figure 34. Proposed model of cell and tissue injury by I/R and the role of COX-2 in protecting and reducing liver damage.** Under physiological conditions, I/R damage causes activation of Kupffer cells that generate a burst of oxidative stress that leads to cells death, via necrosis or apoptosis. Inside the cell, ROS produced by Kupffer cells join within ROS produced intracellularly, along with other cellular stresses such as UPR, to contribute to cell death. In the context of COX-2 overexpression, COX-2 and its derived prostaglandins prevent Kupffer cells from activating, reducing ROS generation; and together with an enhanced antioxidant response, cell death is prevented. In addition, autophagy is increased, aiding the maintenance and survival of cells in the tissue. *Created with Biorender.com*

## VI. CONCLUSIONS





Based on the results obtained during the research and in order to respond to the objectives set out at the beginning of this thesis, the following conclusions can be drawn:

1. Mice expressing COX-2 in hepatocytes show attenuated liver damage after I/R compared to *Wt* mice, showing decrease in markers of liver damage, markers of necrosis and necrotic areas.
2. To obtain a higher degree of damage and an adequate representation of the injury model, a mixed genetic background mouse line is required.
3. The reduction of liver damage in *h-COX-2 Tg* mice is specifically due to COX-2 expression, as demonstrated by COX-2 inhibition, where damage levels match those of a *Wt* mouse; as well as when a *Wt* mouse is preconditioned by inducing endogenous expression of *Ptgs2*, which shows protection from damage.
4. *h-COX-2 Tg* mice have a lower inflammatory response, showing a reduced NF- $\kappa$ B signalling pathway, a low pro-inflammatory profile, and reduced neutrophil infiltration.
5. Canonical cellular stress markers are reduced in *h-COX-2 Tg* mice, revealing decreased apoptosis, ER stress, and oxidative stress, while autophagy is promoted.
6. The antioxidant response is enhanced in *h-COX-2 Tg* mice through activation of the NRF2 transcription factor pathway, resulting in antioxidant gene expression increase.

7. Mitochondrial function is preserved in *h-COX-2 Tg* mice, maintaining mitochondrial respiration and membrane potential, through increased Complex I activity, without altering mitochondrial number and shape.
8. There is a tendency to stabilise supercomplexes composed of Complex I in mice overexpressing COX-2, without altering the expression of individual complexes.
9. Preservation of mitochondrial function in *h-COX-2 Tg* mice may be mediated by stabilisation of mitochondrial cristae through maintenance of OPA1 isoforms and reduced activation of the OPA1-processing enzyme, OMA1.
10. The presence of elevated plasma levels of PGE<sub>2</sub> in patients receiving OLT correlates with a good prognosis, reduced graft rejection and faster recovery. This result suggests that, even at physiological range levels, prostaglandins may have a protective role in patients receiving liver transplantation.



# VII. BIBLIOGRAPHY





- 
- [1] W. L. Smith, D. L. DeWitt, and R. M. Garavito, "Cyclooxygenases: structural, cellular, and molecular biology.," *Annu. Rev. Biochem.*, vol. 69, pp. 145–182, 2000, doi: 10.1146/annurev.biochem.69.1.145.
- [2] R. J. Coffey *et al.*, "Epidermal growth factor receptor activation induces nuclear targeting of cyclooxygenase-2, basolateral release of prostaglandins, and mitogenesis in polarizing colon cancer cells.," *Proc. Natl. Acad. Sci. U. S. A.*, vol. 94, no. 2, pp. 657–662, Jan. 1997, doi: 10.1073/pnas.94.2.657.
- [3] P. T. Bozza, W. Yu, J. F. Penrose, E. S. Morgan, A. M. Dvorak, and P. F. Weller, "Eosinophil lipid bodies: specific, inducible intracellular sites for enhanced eicosanoid formation.," *J. Exp. Med.*, vol. 186, no. 6, pp. 909–920, Sep. 1997, doi: 10.1084/jem.186.6.909.
- [4] J. Y. Liou, W. G. Deng, D. W. Gilroy, S. K. Shyue, and K. K. Wu, "Colocalization and interaction of cyclooxygenase-2 with caveolin-1 in human fibroblasts.," *J. Biol. Chem.*, vol. 276, no. 37, pp. 34975–34982, Sep. 2001, doi: 10.1074/jbc.M105946200.
- [5] J. C. Otto, D. L. DeWitt, and W. L. Smith, "N-glycosylation of prostaglandin endoperoxide synthases-1 and -2 and their orientations in the endoplasmic reticulum.," *J. Biol. Chem.*, vol. 268, no. 24, pp. 18234–18242, Aug. 1993.
- [6] N. Chandrasekharan and D. L. Simmons, "Protein family review The Smads," *Genome Biol.*, vol. 5, no. 9, p. 241, 2004.
- [7] G. Xiao, W. Chen, and R. J. Kulmacz, "Comparison of structural stabilities of prostaglandin H synthase-1 and -2.," *J. Biol. Chem.*, vol. 273, no. 12, pp. 6801–6811, Mar. 1998, doi: 10.1074/jbc.273.12.6801.
- [8] A. L. Blobaum and L. J. Marnett, "Structural and functional basis of cyclooxygenase inhibition," *J. Med. Chem.*, vol. 50, no. 7, pp. 1425–1441, 2007, doi: 10.1021/jm0613166.
- [9] R. N. Dubois *et al.*, "Cyclooxygenase in biology and disease.," *FASEB J. Off. Publ. Fed. Am. Soc. Exp. Biol.*, vol. 12, no. 12, pp. 1063–1073, Sep. 1998.
- [10] T. Tanabe and N. Tohnai, "Cyclooxygenase isozymes and their gene structures and expression," *Prostaglandins Other Lipid Mediat.*, vol. 68–69, pp. 95–114, 2002, doi: 10.1016/S0090-6980(02)00024-2.
- [11] L. H. Wang, A. Hajibeigi, X. M. Xu, D. Loose-Mitchell, and K. K. Wu, "Characterization of the promoter of human prostaglandin H synthase-1 gene.," *Biochem. Biophys. Res. Commun.*, vol. 190, no. 2, pp. 406–411, Jan. 1993, doi: 10.1006/bbrc.1993.1062.
- [12] Y. J. Kang, U. R. Mbonye, C. J. DeLong, M. Wada, and W. L. Smith, "Regulation of intracellular cyclooxygenase levels by gene transcription and protein degradation,"

## VII. BIBLIOGRAPHY

---

- Prog. Lipid Res.*, vol. 46, no. 2, pp. 108–125, 2007, doi: 10.1016/j.plipres.2007.01.001.
- [13] J. R. Vane and R. M. Botting, “The mechanism of action of aspirin.,” *Thromb. Res.*, vol. 110, no. 5–6, pp. 255–258, Jun. 2003, doi: 10.1016/s0049-3848(03)00379-7.
- [14] S. Bindu, S. Mazumder, and U. Bandyopadhyay, “Non-steroidal anti-inflammatory drugs (NSAIDs) and organ damage: A current perspective.,” *Biochem. Pharmacol.*, vol. 180, p. 114147, Oct. 2020, doi: 10.1016/j.bcp.2020.114147.
- [15] G. A. FitzGerald, “COX-2 and beyond: Approaches to prostaglandin inhibition in human disease.,” *Nat. Rev. Drug Discov.*, vol. 2, no. 11, pp. 879–890, Nov. 2003, doi: 10.1038/nrd1225.
- [16] R. M. Botting, “Vane’s discovery of the mechanism of action of aspirin changed our understanding of its clinical pharmacology.,” *Pharmacol. Rep.*, vol. 62, no. 3, pp. 518–525, 2010, doi: 10.1016/s1734-1140(10)70308-x.
- [17] N. R. Jana, “NSAIDs and apoptosis.,” *Cell. Mol. Life Sci.*, vol. 65, no. 9, pp. 1295–1301, May 2008, doi: 10.1007/s00018-008-7511-x.
- [18] M. W. Goldblatt, “A depressor substance in seminal fluid,” *J. Soc. Chem. Ind.*, vol. 52, pp. 1056 – 1057, 1933, [Online]. Available: <https://www.scopus.com/inward/record.uri?eid=2-s2.0-0001114268&partnerID=40&md5=9d01d9598360e2da3056fe459f29c31c>.
- [19] E. A. Dennis, S. G. Rhee, M. M. Billah, and Y. A. Hannun, “Role of phospholipase in generating lipid second messengers in signal transduction.,” *FASEB J. Off. Publ. Fed. Am. Soc. Exp. Biol.*, vol. 5, no. 7, pp. 2068–2077, Apr. 1991, doi: 10.1096/fasebj.5.7.1901288.
- [20] J. Nakano, E. Anggård, and B. Samuelsson, “15-Hydroxy-prostanoate dehydrogenase. Prostaglandins as substrates and inhibitors.,” *Eur. J. Biochem.*, vol. 11, no. 2, pp. 386–389, Dec. 1969, doi: 10.1111/j.1432-1033.1969.tb00784.x.
- [21] F. Catella-Lawson *et al.*, “Effects of specific inhibition of cyclooxygenase-2 on sodium balance, hemodynamics, and vasoactive eicosanoids.,” *J. Pharmacol. Exp. Ther.*, vol. 289, no. 2, pp. 735–741, May 1999.
- [22] S. S. Bhagwat, P. R. Hamann, W. C. Still, S. Bunting, and F. A. Fitzpatrick, “Synthesis and structure of the platelet aggregation factor thromboxane A<sub>2</sub>.,” *Nature*, vol. 315, no. 6019, pp. 511–513, Jun. 1985, doi: 10.1038/315511a0.
- [23] N. R. Ferreri, M. Schwartzman, N. G. Ibrahim, P. N. Chander, and J. C. McGiff, “Arachidonic acid metabolism in a cell suspension isolated from rabbit renal outer medulla.,” *J. Pharmacol. Exp. Ther.*, vol. 231, no. 2, pp. 441–448, Nov. 1984.

- [24] T. K. Chaudhury and E. D. Jacobson, "Prostaglandin cytoprotection of gastric mucosa.," *Gastroenterology*, vol. 74, no. 1, pp. 58–63, Jan. 1978.
- [25] M. R. Pourian, U. Kvist, L. Björndahl, and E. H. Oliw, "Rapid and slow hydroxylators of seminal E prostaglandins among men in barren unions.," *Andrologia*, vol. 27, no. 2, pp. 71–79, 1995, doi: 10.1111/j.1439-0272.1995.tb01075.x.
- [26] P. R. Colville-Nash and D. W. Gilroy, "COX-2 and the cyclopentenone prostaglandins - a new chapter in the book of inflammation?," *Prostaglandins Other Lipid Mediat.*, vol. 62, no. 1, pp. 33–43, Jun. 2000, doi: 10.1016/s0090-6980(00)00074-5.
- [27] K. Seibert *et al.*, "Pharmacological and biochemical demonstration of the role of cyclooxygenase 2 in inflammation and pain.," *Proc. Natl. Acad. Sci. U. S. A.*, vol. 91, no. 25, pp. 12013–12017, Dec. 1994, doi: 10.1073/pnas.91.25.12013.
- [28] V. L. Schuster, "Prostaglandin transport.," *Prostaglandins Other Lipid Mediat.*, vol. 68–69, pp. 633–647, Aug. 2002, doi: 10.1016/s0090-6980(02)00061-8.
- [29] E. Ricciotti and G. A. Fitzgerald, "Prostaglandins and inflammation," *Arterioscler. Thromb. Vasc. Biol.*, vol. 31, no. 5, pp. 986–1000, 2011, doi: 10.1161/ATVBAHA.110.207449.
- [30] S. B. Miller, "Prostaglandins in Health and Disease: An Overview," *Semin. Arthritis Rheum.*, vol. 36, no. 1, pp. 37–49, 2006, doi: 10.1016/j.semarthrit.2006.03.005.
- [31] C. D. Funk, "Prostaglandins and leukotrienes: advances in eicosanoid biology.," *Science*, vol. 294, no. 5548, pp. 1871–1875, Nov. 2001, doi: 10.1126/science.294.5548.1871.
- [32] D. P. Bogdanos, B. Gao, and M. E. Gershwin, "Liver immunology.," *Compr. Physiol.*, vol. 3, no. 2, pp. 567–598, Apr. 2013, doi: 10.1002/cphy.c120011.
- [33] K. Si-Tayeb, F. P. Lemaigre, and S. A. Duncan, "Organogenesis and Development of the Liver," *Dev. Cell*, vol. 18, no. 2, pp. 175–189, 2010, doi: 10.1016/j.devcel.2010.01.011.
- [34] M. Casado *et al.*, "Contribution of cyclooxygenase 2 to liver regeneration after partial hepatectomy," *FASEB J.*, vol. 15, no. 11, pp. 2016–2018, Jul. 2001, doi: 10.1096/fj.01-0158fje.
- [35] P. Martín-Sanz, N. A. Callejas, M. Casado, M. J. M. Díaz-Guerra, and L. Boscá, "Expression of cyclooxygenase-2 in foetal rat hepatocytes stimulated with lipopolysaccharide and pro-inflammatory cytokines," *Br. J. Pharmacol.*, vol. 125, no. 6, pp. 1313–1319, 1998, doi: 10.1038/sj.bjp.0702196.
- [36] N. A. Callejas, L. Boscá, C. S. Williams, R. N. DuBois, and P. Martín-Sanz,

- “Regulation of cyclooxygenase 2 expression in hepatocytes by CCAAT/enhancer-binding proteins,” *Gastroenterology*, vol. 119, no. 2, pp. 493–501, Aug. 2000, doi: 10.1053/gast.2000.9374.
- [37] P. Martín-Sanz, M. Casado, and L. Boscá, “Cyclooxygenase 2 in liver dysfunction and carcinogenesis: Facts and perspectives Paloma,” vol. 6124, no. 1, pp. 1–34, 2017, doi: 10.20959/wjpr2016-6447.
- [38] T. Zhang, Y. Ma, K. Q. Xu, and W. Q. Huang, “Pretreatment of parecoxib attenuates hepatic ischemia/reperfusion injury in rats,” *BMC Anesthesiol.*, vol. 15, no. 1, pp. 1–8, 2015, doi: 10.1186/s12871-015-0147-0.
- [39] N. Nishizawa *et al.*, “Inhibition of microsomal prostaglandin E synthase-1 facilitates liver repair after hepatic injury in mice,” *J. Hepatol.*, vol. 69, no. 1, pp. 110–120, 2018, doi: 10.1016/j.jhep.2018.02.009.
- [40] T. Hamada *et al.*, “Cyclooxygenase-2 deficiency enhances Th2 immune responses and impairs neutrophil recruitment in hepatic ischemia/reperfusion injury,” *J. Immunol.*, vol. 180, no. 3, pp. 1843–1853, Feb. 2008, doi: 10.4049/jimmunol.180.3.1843.
- [41] B. Li *et al.*, “COX-2 inhibition improves immune system homeostasis and decreases liver damage in septic rats,” *J. Surg. Res.*, vol. 157, no. 1, pp. 43–47, Nov. 2009, doi: 10.1016/j.jss.2008.12.020.
- [42] J. Chen *et al.*, “Celecoxib attenuates liver steatosis and inflammation in non-alcoholic steatohepatitis induced by high-fat diet in rats,” *Mol. Med. Rep.*, vol. 4, no. 5, pp. 811–816, 2011, doi: 10.3892/mmr.2011.501.
- [43] S. Duarte *et al.*, “Hepatic ischemia and reperfusion injury in the absence of myeloid cell-derived COX-2 in mice,” *PLoS One*, vol. 9, no. 5, pp. 1–11, 2014, doi: 10.1371/journal.pone.0096913.
- [44] O. Morteau *et al.*, “Impaired mucosal defense to acute colonic injury in mice lacking cyclooxygenase-1 or cyclooxygenase-2,” *J. Clin. Invest.*, vol. 105, no. 4, pp. 469–478, 2000, doi: 10.1172/JCI6899.
- [45] M. Casado *et al.*, “Protection against Fas-induced liver apoptosis in transgenic mice expressing cyclooxygenase 2 in hepatocytes,” *Hepatology*, vol. 45, no. 3, pp. 631–638, 2007, doi: 10.1002/hep.21556.
- [46] D. E. A. Francés *et al.*, “Cyclooxygenase-2 over-expression inhibits liver apoptosis induced by hyperglycemia,” *J. Cell. Biochem.*, vol. 114, no. 3, pp. 669–680, 2013, doi: 10.1002/jcb.24409.
- [47] D. E. Francés *et al.*, “Hepatic cyclooxygenase-2 expression protects against diet-induced steatosis, obesity, and insulin resistance,” *Diabetes*, vol. 64, no. 5, pp. 1522–1531, 2015, doi: 10.2337/db14-0979.

- [48] O. Motiño *et al.*, “Cyclooxygenase-2 expression in hepatocytes attenuates non-alcoholic steatohepatitis and liver fibrosis in mice,” *Biochim. Biophys. Acta - Mol. Basis Dis.*, vol. 1862, no. 9, pp. 1710–1723, 2016, doi: 10.1016/j.bbadis.2016.06.009.
- [49] P. C. Müller, G. Kabacam, E. Vibert, G. Germani, and H. Petrowsky, “Current status of liver transplantation in Europe,” *Int. J. Surg.*, vol. 82, no. May, pp. 22–29, 2020, doi: 10.1016/j.ijssu.2020.05.062.
- [50] U. Maggi and D. Azoulay, “Further Details From the First Human Liver Transplantation in Europe,” *Transplantation*, vol. 96, no. 6, pp. 47–48, 2013, doi: 10.1097/TP.0b013e3182a289db.
- [51] R. Adam *et al.*, “2018 Annual Report of the European Liver Transplant Registry (ELTR) – 50-year evolution of liver transplantation,” *Transpl. Int.*, vol. 31, no. 12, pp. 1293–1317, 2018, doi: 10.1111/tri.13358.
- [52] A. Casillas-Ramírez, I. Ben Mosbah, F. Ramalho, J. Roselló-Catafau, and C. Peralta, “Past and future approaches to ischemia-reperfusion lesion associated with liver transplantation,” *Life Sci.*, vol. 79, no. 20, pp. 1881–1894, 2006, doi: 10.1016/j.lfs.2006.06.024.
- [53] W. Milano, V. De Biasio, W. Di Munzio, G. Foggia, and A. Capasso, “Obesity: The New Global Epidemic Pharmacological Treatment, Opportunities and Limits for Personalized Therapy,” *Endocr. Metab. Immune Disord. Drug Targets*, vol. 20, no. 8, pp. 1232–1243, 2020, doi: 10.2174/1871530320666200515112853.
- [54] P. Marcellin and B. K. Kutala, “Liver diseases: A major, neglected global public health problem requiring urgent actions and large-scale screening,” *Liver Int.*, vol. 38, no. December 2017, pp. 2–6, 2018, doi: 10.1111/liv.13682.
- [55] R. W. Busuttil and K. Tanaka, “The utility of marginal donors in liver transplantation,” *Liver Transplant.*, vol. 9, no. 7, pp. 651–663, 2003, doi: 10.1053/jlts.2003.50105.
- [56] M. Selzner and P. A. Clavien, “Fatty liver in liver transplantation and surgery,” *Semin. Liver Dis.*, vol. 21, no. 1, pp. 105–113, 2001, doi: 10.1055/s-2001-12933.
- [57] T. Kalogeris, C. P. Baines, M. Krenz, and R. J. Korthuis, *Cell Biology of Ischemia/Reperfusion Injury*, 1st ed., vol. 298. Elsevier Inc., 2012.
- [58] M. Mendes-Braz, M. Elias-Miró, M. B. Jiménez-Castro, A. Casillas-Ramírez, F. S. Ramalho, and C. Peralta, “The current state of knowledge of hepatic ischemia-reperfusion injury based on its study in experimental models,” *J. Biomed. Biotechnol.*, vol. 2012, 2012, doi: 10.1155/2012/298657.
- [59] Z. Xia, H. Li, and M. G. Irwin, “Myocardial ischaemia reperfusion injury: the challenge of translating ischaemic and anaesthetic protection from animal models to humans,” *Br. J. Anaesth.*, vol. 117, pp. ii44–ii62, 2016, doi: 10.1093/bja/aew267.

## VII. BIBLIOGRAPHY

---

- [60] A. Casillas-Ramírez, I. Ben Mosbah, F. Ramalho, J. Roselló-Catafau, and C. Peralta, “Past and future approaches to ischemia-reperfusion lesion associated with liver transplantation,” *Life Sci.*, vol. 79, no. 20, pp. 1881–1894, 2006, doi: 10.1016/j.lfs.2006.06.024.
- [61] H. Hirao, K. Nakamura, and J. W. Kupiec-Weglinski, “Liver ischaemia–reperfusion injury: a new understanding of the role of innate immunity,” *Nat. Rev. Gastroenterol. Hepatol.*, vol. 19, no. 4, pp. 239–256, 2022, doi: 10.1038/s41575-021-00549-8.
- [62] G. Y. Chen and G. Nuñez, “Sterile inflammation: Sensing and reacting to damage,” *Nat. Rev. Immunol.*, vol. 10, no. 12, pp. 826–837, 2010, doi: 10.1038/nri2873.
- [63] M. Bilzer, F. Roggel, and A. L. Gerbes, “Role of Kupffer cells in host defense and liver disease,” *Liver Int.*, vol. 26, no. 10, pp. 1175–1186, 2006, doi: 10.1111/j.1478-3231.2006.01342.x.
- [64] P. Li, K. He, J. Li, Z. Liu, and J. Gong, “The role of Kupffer cells in hepatic diseases,” *Mol. Immunol.*, vol. 85, pp. 222–229, 2017, doi: 10.1016/j.molimm.2017.02.018.
- [65] M. Massip-salcedo, J. Roselló-Catafau, J. Prieto, M. A. Avila, and C. Peralta, “The response of the hepatocyte to ischemia,” *Liver Int.*, vol. 27, no. 1, pp. 6–16, 2007, doi: 10.1111/j.1478-3231.2006.01390.x.
- [66] J. Zhang *et al.*, “CCL2-CCR2 signaling promotes hepatic ischemia/reperfusion injury,” *J. Surg. Res.*, vol. 202, no. 2, pp. 352–362, 2016, doi: 10.1016/j.jss.2016.02.029.
- [67] D. Zheng, T. Liwinski, and E. Elinav, “Inflammasome activation and regulation: toward a better understanding of complex mechanisms,” *Cell Discov.*, vol. 6, no. 1, 2020, doi: 10.1038/s41421-020-0167-x.
- [68] J. M. Abais, M. Xia, Y. Zhang, K. M. Boini, and P. L. Li, “Redox Regulation of NLRP3 Inflammasomes: ROS as Trigger or Effector?,” *Antioxidants Redox Signal.*, vol. 22, no. 13, pp. 1111–1129, 2015, doi: 10.1089/ars.2014.5994.
- [69] P. Kubes and W. Z. Mehal, “Sterile inflammation in the liver.,” *Gastroenterology*, vol. 143, no. 5, pp. 1158–1172, Nov. 2012, doi: 10.1053/j.gastro.2012.09.008.
- [70] B. Lima, M. T. Forrester, D. T. Hess, and J. S. Stamler, “S-nitrosylation in cardiovascular signaling,” *Circ. Res.*, vol. 106, no. 4, pp. 633–646, 2010, doi: 10.1161/CIRCRESAHA.109.207381.
- [71] D. Nolfi-Donagan, A. Braganza, and S. Shiva, “Mitochondrial electron transport chain: Oxidative phosphorylation, oxidant production, and methods of measurement,” *Redox Biol.*, vol. 37, p. 101674, 2020, doi: 10.1016/j.redox.2020.101674.



- [72] H. Bugger and K. Pfeil, "Mitochondrial ROS in myocardial ischemia reperfusion and remodeling," *Biochim. Biophys. Acta - Mol. Basis Dis.*, vol. 1866, no. 7, p. 165768, 2020, doi: 10.1016/j.bbadis.2020.165768.
- [73] M. Elias-Miró, M. B. Jiménez-Castro, J. Rodés, and C. Peralta, "Current knowledge on oxidative stress in hepatic ischemia/reperfusion," *Free Radic. Res.*, vol. 47, no. 8, pp. 555–568, 2013, doi: 10.3109/10715762.2013.811721.
- [74] K. D. Poss and S. Tonegawa, "Reduced stress defense in heme oxygenase 1-deficient cells.," *Proc. Natl. Acad. Sci. U. S. A.*, vol. 94, no. 20, pp. 10925–10930, Sep. 1997, doi: 10.1073/pnas.94.20.10925.
- [75] A. Li, N. J. Song, B. P. Riesenber, and Z. Li, "The Emerging Roles of Endoplasmic Reticulum Stress in Balancing Immunity and Tolerance in Health and Diseases: Mechanisms and Opportunities," *Front. Immunol.*, vol. 10, no. February, pp. 1–15, 2020, doi: 10.3389/fimmu.2019.03154.
- [76] H. Nishitoh, "CHOP is a multifunctional transcription factor in the ER stress response," *J. Biochem.*, vol. 151, no. 3, pp. 217–219, 2012, doi: 10.1093/jb/mvr143.
- [77] T. Minamino, I. Komuro, and M. Kitakaze, "Endoplasmic reticulum stress as a therapeutic target in cardiovascular disease," *Circ. Res.*, vol. 107, no. 9, pp. 1071–1082, 2010, doi: 10.1161/CIRCRESAHA.110.227819.
- [78] Y. Ruan *et al.*, "Endoplasmic reticulum stress serves an important role in cardiac ischemia/reperfusion injury (Review)," *Exp. Ther. Med.*, vol. 20, no. 6, pp. 1–1, 2020, doi: 10.3892/etm.2020.9398.
- [79] Y. Han, M. Yuan, Y. S. Guo, X. Y. Shen, Z. K. Gao, and X. Bi, "Mechanism of Endoplasmic Reticulum Stress in Cerebral Ischemia," *Front. Cell. Neurosci.*, vol. 15, no. August, 2021, doi: 10.3389/fncel.2021.704334.
- [80] J. J. Martindale *et al.*, "Endoplasmic reticulum stress gene induction and protection from ischemia/reperfusion injury in the hearts of transgenic mice with a tamoxifen-regulated form of ATF6," *Circ. Res.*, vol. 98, no. 9, pp. 1186–1193, 2006, doi: 10.1161/01.RES.0000220643.65941.8d.
- [81] K. Shintani-Ishida, M. Nakajima, K. Uemura, and K. ichi Yoshida, "Ischemic preconditioning protects cardiomyocytes against ischemic injury by inducing GRP78," *Biochem. Biophys. Res. Commun.*, vol. 345, no. 4, pp. 1600–1605, 2006, doi: 10.1016/j.bbrc.2006.05.077.
- [82] K. Weigand, S. Brost, N. Steinebrunner, M. Bchler, P. Schemmer, and M. Müller, "Ischemia/Reperfusion injury in liver surgery and transplantation: Pathophysiology," *HPB Surg.*, vol. 2012, 2012, doi: 10.1155/2012/176723.
- [83] T. Hartley, M. Siva, E. Lai, T. Teodoro, L. Zhang, and A. Volchuk, "Endoplasmic

## VII. BIBLIOGRAPHY

---

- reticulum stress response in an INS-1 pancreatic  $\beta$ -cell line with inducible expression of a folding-deficient proinsulin,” *BMC Cell Biol.*, vol. 11, 2010, doi: 10.1186/1471-2121-11-59.
- [84] B. R. S. Broughton, D. C. Reutens, and C. G. Sobey, “Apoptotic mechanisms after cerebral ischemia,” *Stroke*, vol. 40, no. 5, 2009, doi: 10.1161/STROKEAHA.108.531632.
- [85] B. Kulsoom, T. S. Shamsi, N. A. Afsar, Z. Memon, N. Ahmed, and S. N. Hasnain, “Bax, Bcl-2, and Bax/Bcl-2 as prognostic markers in acute myeloid leukemia: Are we ready for bcl-2-directed therapy?,” *Cancer Manag. Res.*, vol. 10, pp. 403–416, 2018, doi: 10.2147/CMAR.S154608.
- [86] D. Moquin and F. K.-M. Chan, “The molecular regulation of programmed necrotic cell injury,” *Trends Biochem. Sci.*, vol. 35, no. 8, pp. 434–441, Aug. 2010, doi: 10.1016/j.tibs.2010.03.001.
- [87] C. C. T. Smith and D. M. Yellon, “Necroptosis, necrostatins and tissue injury,” *J. Cell. Mol. Med.*, vol. 15, no. 9, pp. 1797–1806, 2011, doi: 10.1111/j.1582-4934.2011.01341.x.
- [88] T. Bergsbaken, S. L. Fink, and B. T. Cookson, “Pyroptosis: Host cell death and inflammation,” *Nat. Rev. Microbiol.*, vol. 7, no. 2, pp. 99–109, 2009, doi: 10.1038/nrmicro2070.
- [89] A. Wree *et al.*, “NLRP3 inflammasome activation results in hepatocyte pyroptosis, liver inflammation, and fibrosis in mice,” *Hepatology*, vol. 59, no. 3, pp. 898–910, 2014, doi: 10.1002/hep.26592.
- [90] W. Li *et al.*, “Ferroptotic cell death and TLR4/Trif signaling initiate neutrophil recruitment after heart transplantation,” *J. Clin. Invest.*, vol. 129, no. 6, pp. 2293–2304, 2019, doi: 10.1172/JCI126428.
- [91] H. Takagi, Y. Matsui, S. Hirotsu, H. Sakoda, T. Asano, and J. Sadoshima, “AMPK mediates autophagy during myocardial ischemia in vivo,” *Autophagy*, vol. 3, no. 4, pp. 405–407, 2007, doi: 10.4161/auto.4281.
- [92] C. He and D. J. Klionsky, “Regulation mechanisms and signaling pathways of autophagy,” *Annu. Rev. Genet.*, vol. 43, pp. 67–93, 2009, doi: 10.1146/annurev-genet-102808-114910.
- [93] M. Hansen, D. C. Rubinsztein, and D. W. Walker, “Autophagy as a promoter of longevity: insights from model organisms,” *Nat. Rev. Mol. Cell Biol.*, vol. 19, no. 9, pp. 579–593, 2018, doi: 10.1038/s41580-018-0033-y.
- [94] G. Kroemer *et al.*, “Classification of cell death: Recommendations of the Nomenclature Committee on Cell Death 2009,” *Cell Death Differ.*, vol. 16, no. 1, pp.

- 3–11, 2009, doi: 10.1038/cdd.2008.150.
- [95] D. Glick, S. Barth, and K. F. Macleod, “Autophagy: Cellular and molecular mechanisms,” *J. Pathol.*, vol. 221, no. 1, pp. 3–12, 2010, doi: 10.1002/path.2697.
- [96] J. Cardinal, P. Pan, and A. Tsung, “Protective role of cisplatin in ischemic liver injury through induction of autophagy,” *Autophagy*, vol. 5, no. 8, pp. 1211–1212, 2009, doi: 10.4161/auto.5.8.9972.
- [97] M. Jiang, K. Liu, J. Luo, and Z. Dong, “Autophagy is a renoprotective mechanism during in vitro hypoxia and in vivo ischemia-reperfusion injury,” *Am. J. Pathol.*, vol. 176, no. 3, pp. 1181–1192, 2010, doi: 10.2353/ajpath.2010.090594.
- [98] S. Carloni, S. Girelli, C. Scopa, G. Buonocore, M. Longini, and W. Balduini, “Activation of autophagy and Akt/CREB signaling play an equivalent role in the neuroprotective effect of rapamycin in neonatal hypoxia-ischemia,” *Autophagy*, vol. 6, no. 3, pp. 366–377, 2010, doi: 10.4161/auto.6.3.11261.
- [99] Y. Zhong *et al.*, “Distinct regulation of autophagic activity by Atg14L and Rubicon associated with Beclin 1-phosphatidylinositol-3-kinase complex,” *Nat. Cell Biol.*, vol. 11, no. 4, pp. 468–476, 2009, doi: 10.1038/ncb1854.
- [100] W. Marin, D. Marin, X. Ao, and Y. Liu, “Mitochondria as a therapeutic target for cardiac ischemia-reperfusion injury (Review),” *Int. J. Mol. Med.*, vol. 47, no. 2, pp. 485–499, 2021, doi: 10.3892/ijmm.2020.4823.
- [101] R. Z. Zhao, S. Jiang, L. Zhang, and Z. Bin Yu, “Mitochondrial electron transport chain, ROS generation and uncoupling (Review),” *Int. J. Mol. Med.*, vol. 44, no. 1, pp. 3–15, 2019, doi: 10.3892/ijmm.2019.4188.
- [102] G. E. PALADE, “An electron microscope study of the mitochondrial structure.,” *J. Histochem. Cytochem. Off. J. Histochem. Soc.*, vol. 1, no. 4, pp. 188–211, Jul. 1953, doi: 10.1177/1.4.188.
- [103] M. Giacomello, A. Pyakurel, C. Glytsou, and L. Scorrano, “The cell biology of mitochondrial membrane dynamics,” *Nat. Rev. Mol. Cell Biol.*, vol. 21, no. 4, pp. 204–224, 2020, doi: 10.1038/s41580-020-0210-7.
- [104] J. Bereiter-Hahn, “Behavior of mitochondria in the living cell.,” *Int. Rev. Cytol.*, vol. 122, pp. 1–63, 1990, doi: 10.1016/s0074-7696(08)61205-x.
- [105] S. A. Detmer and D. C. Chan, “Functions and dysfunctions of mitochondrial dynamics,” *Nat. Rev. Mol. Cell Biol.*, vol. 8, no. 11, pp. 870–879, 2007, doi: 10.1038/nrm2275.
- [106] L. Tilokani, S. Nagashima, V. Paupe, and J. Prudent, “Mitochondrial dynamics:

## VII. BIBLIOGRAPHY

---

- Overview of molecular mechanisms,” *Essays Biochem.*, vol. 62, no. 3, pp. 341–360, 2018, doi: 10.1042/EBC20170104.
- [107] M. B. Hock and A. Kralli, “Transcriptional control of mitochondrial biogenesis and function,” *Annu. Rev. Physiol.*, vol. 71, pp. 177–203, 2009, doi: 10.1146/annurev.physiol.010908.163119.
- [108] P. Jensen, “ANTIMYCIN-INSENSITIVE OXIDATION OF SUCCINATE AND REDUCED N I C O T I N A M I D E - A D E N I N E DINUCLEOTIDE IN ELECTRON-TRANSPORT PARTICLES,” *Biochim. Biophys. Acta - Bioenerg.*, vol. 122, 1965.
- [109] P. Hernansanz-Agustín and J. A. Enríquez, “Generation of reactive oxygen species by mitochondria,” *Antioxidants*, vol. 10, no. 3, pp. 1–18, 2021, doi: 10.3390/antiox10030415.
- [110] G. Lenaz and M. L. Genova, “Structural and functional organization of the mitochondrial respiratory chain: a dynamic super-assembly.,” *Int. J. Biochem. Cell Biol.*, vol. 41, no. 10, pp. 1750–1772, Oct. 2009, doi: 10.1016/j.biocel.2009.04.003.
- [111] H. Schägger, “Respiratory chain supercomplexes,” *IUBMB Life*, vol. 52, no. 3–5, pp. 119–128, 2001, doi: 10.1080/15216540152845911.
- [112] N. V. Dudkina, R. Kouřil, K. Peters, H. P. Braun, and E. J. Boekema, “Structure and function of mitochondrial supercomplexes,” *Biochim. Biophys. Acta - Bioenerg.*, vol. 1797, no. 6–7, pp. 664–670, 2010, doi: 10.1016/j.bbabi.2009.12.013.
- [113] P. Jha, X. Wang, and J. Auwerx, “Analysis of Mitochondrial Respiratory Chain Supercomplexes Using Blue Native Polyacrylamide Gel Electrophoresis (BN-PAGE),” *Curr. Protoc. Mouse Biol.*, vol. 6, no. 1, pp. 1–14, 2016, doi: 10.1002/9780470942390.mo150182.
- [114] I. Vercellino and L. A. Sazanov, “The assembly, regulation and function of the mitochondrial respiratory chain,” *Nat. Rev. Mol. Cell Biol.*, vol. 23, no. 2, pp. 141–161, 2022, doi: 10.1038/s41580-021-00415-0.
- [115] R. Acín-Pérez, P. Fernández-Silva, M. L. Peleato, A. Pérez-Martos, and J. A. Enríquez, “Respiratory Active Mitochondrial Supercomplexes,” *Mol. Cell*, vol. 32, no. 4, pp. 529–539, 2008, doi: 10.1016/j.molcel.2008.10.021.
- [116] R. Acín-Pérez *et al.*, “Respiratory complex III is required to maintain complex I in mammalian mitochondria,” *Mol. Cell*, vol. 13, no. 6, pp. 805–815, 2004, doi: 10.1016/S1097-2765(04)00124-8.
- [117] F. Diaz, H. Fukui, S. Garcia, and C. T. Moraes, “Cytochrome c Oxidase Is Required for the Assembly/Stability of Respiratory Complex I in Mouse Fibroblasts ,” *Mol. Cell Biol.*, vol. 26, no. 13, pp. 4872–4881, 2006, doi: 10.1128/mcb.01767-05.

- [118] C. Anselmi, K. M. Davies, and J. D. Faraldo-Gómez, “Mitochondrial ATP synthase dimers spontaneously associate due to a long-range membrane-induced force,” *J. Gen. Physiol.*, vol. 150, no. 5, pp. 763–770, 2018, doi: 10.1085/jgp.201812033.
- [119] B. Westermann, “Mitochondrial fusion and fission in cell life and death,” *Nat. Rev. Mol. Cell Biol.*, vol. 11, no. 12, pp. 872–884, 2010, doi: 10.1038/nrm3013.
- [120] J. H. Xie, Y. Y. Li, and J. Jin, “The essential functions of mitochondrial dynamics in immune cells,” *Cell. Mol. Immunol.*, vol. 17, no. 7, pp. 712–721, 2020, doi: 10.1038/s41423-020-0480-1.
- [121] E. T. Chouchani *et al.*, “Ischaemic accumulation of succinate controls reperfusion injury through mitochondrial ROS,” *Nature*, vol. 515, no. 7527, pp. 431–435, 2014, doi: 10.1038/nature13909.
- [122] E. T. Chouchani *et al.*, “A unifying mechanism for mitochondrial superoxide production during ischemia-reperfusion injury,” *Cell Metab.*, vol. 23, no. 2, pp. 254–263, 2016, doi: 10.1016/j.cmet.2015.12.009.
- [123] E. L. Robb *et al.*, “Control of mitochondrial superoxide production by reverse electron transport at complex I,” *J. Biol. Chem.*, vol. 293, no. 25, pp. 9869–9879, 2018, doi: 10.1074/jbc.RA118.003647.
- [124] E. J. Lesnefsky, Q. Chen, B. Tandler, and C. L. Hoppel, “Mitochondrial Dysfunction and Myocardial Ischemia-Reperfusion: Implications for Novel Therapies.,” *Annu. Rev. Pharmacol. Toxicol.*, vol. 57, pp. 535–565, Jan. 2017, doi: 10.1146/annurev-pharmtox-010715-103335.
- [125] G. Paradies, G. Petrosillo, V. Paradies, and F. M. Ruggiero, “Role of cardiolipin peroxidation and Ca<sup>2+</sup> in mitochondrial dysfunction and disease.,” *Cell Calcium*, vol. 45, no. 6, pp. 643–650, Jun. 2009, doi: 10.1016/j.ceca.2009.03.012.
- [126] A. V. Kuznetsov, S. Javadov, R. Margreiter, M. Grimm, J. Hagenbuchner, and M. J. Ausserlechner, “The Role of Mitochondria in the Mechanisms of Cardiac Ischemia-Reperfusion Injury.,” *Antioxidants (Basel, Switzerland)*, vol. 8, no. 10, Oct. 2019, doi: 10.3390/antiox8100454.
- [127] L. S. Yang, L. L. Shan, A. Saxena, and D. L. Morris, “Liver transplantation: A systematic review of long-term quality of life,” *Liver Int.*, vol. 34, no. 9, pp. 1298–1313, 2014, doi: 10.1111/liv.12553.
- [128] V. R. Pell, E. T. Chouchani, C. Frezza, M. P. Murphy, and T. Krieg, “Succinate metabolism: a new therapeutic target for myocardial reperfusion injury.,” *Cardiovasc. Res.*, vol. 111, no. 2, pp. 134–141, Jul. 2016, doi: 10.1093/cvr/cvw100.
- [129] W. W. Sharp *et al.*, “Dynamin-related protein 1 (Drp1)-mediated diastolic dysfunction in myocardial ischemia-reperfusion injury: therapeutic benefits of Drp1 inhibition to

## VII. BIBLIOGRAPHY

---

- reduce mitochondrial fission.,” *FASEB J. Off. Publ. Fed. Am. Soc. Exp. Biol.*, vol. 28, no. 1, pp. 316–326, Jan. 2014, doi: 10.1096/fj.12-226225.
- [130] J. Wang, S. Toan, and H. Zhou, “New insights into the role of mitochondria in cardiac microvascular ischemia/reperfusion injury,” *Angiogenesis*, vol. 23, no. 3, pp. 299–314, 2020, doi: 10.1007/s10456-020-09720-2.
- [131] R. J. Giedt, C. Yang, J. L. Zweier, A. Matzavinos, and B. R. Alevriadou, “Mitochondrial fission in endothelial cells after simulated ischemia/reperfusion: Role of nitric oxide and reactive oxygen species,” *Free Radic. Biol. Med.*, vol. 52, no. 2, pp. 348–356, 2012, doi: 10.1016/j.freeradbiomed.2011.10.491.
- [132] H. Zhou, C. Shi, S. Hu, H. Zhu, J. Ren, and Y. Chen, “B11 is associated with microvascular protection in cardiac ischemia reperfusion injury via repressing Syk–Nox2–Drp1-mitochondrial fission pathways,” *Angiogenesis*, vol. 21, no. 3, pp. 599–615, 2018, doi: 10.1007/s10456-018-9611-z.
- [133] S. B. Ong, S. Subrayan, S. Y. Lim, D. M. Yellon, S. M. Davidson, and D. J. Hausenloy, “Inhibiting mitochondrial fission protects the heart against ischemia/reperfusion injury,” *Circulation*, vol. 121, no. 18, pp. 2012–2022, 2010, doi: 10.1161/CIRCULATIONAHA.109.906610.
- [134] K. Boengler, G. Lochnit, and R. Schulz, “Mitochondria ‘THE’ target of myocardial conditioning.,” *Am. J. Physiol. Heart Circ. Physiol.*, vol. 315, no. 5, pp. H1215–H1231, Nov. 2018, doi: 10.1152/ajpheart.00124.2018.
- [135] T. Varanita *et al.*, “The Opa1-dependent mitochondrial cristae remodeling pathway controls atrophic, apoptotic, and ischemic tissue damage,” *Cell Metab.*, vol. 21, no. 6, pp. 834–844, 2015, doi: 10.1016/j.cmet.2015.05.007.
- [136] M. Liu, X. Li, and D. Huang, “Mfn2 Overexpression Attenuates Cardio-Cerebrovascular Ischemia-Reperfusion Injury Through Mitochondrial Fusion and Activation of the AMPK/Sirt3 Signaling.,” *Front. cell Dev. Biol.*, vol. 8, p. 598078, 2020, doi: 10.3389/fcell.2020.598078.
- [137] W. Yin, A. P. Signore, M. Iwai, G. Cao, Y. Gao, and J. Chen, “Rapidly increased neuronal mitochondrial biogenesis after hypoxic-ischemic brain injury,” *Stroke*, vol. 39, no. 11, pp. 3057–3063, 2008, doi: 10.1161/STROKEAHA.108.520114.
- [138] J. Bi *et al.*, “Irisin alleviates liver ischemia-reperfusion injury by inhibiting excessive mitochondrial fission, promoting mitochondrial biogenesis and decreasing oxidative stress,” *Redox Biol.*, vol. 20, no. October 2018, pp. 296–306, 2019, doi: 10.1016/j.redox.2018.10.019.
- [139] N. Selzner, M. Selzner, W. Jochum, and P.-A. Clavien, “Ischemic preconditioning protects the steatotic mouse liver against reperfusion injury: an ATP dependent mechanism,” *J. Hepatol.*, vol. 39, no. 1, pp. 55–61, Jul. 2003, doi: 10.1016/S0168-

8278(03)00147-8.

- [140] C. Frezza, S. Cipolat, and L. Scorrano, "Organelle isolation: Functional mitochondria from mouse liver, muscle and cultured fibroblasts," *Nat. Protoc.*, vol. 2, no. 2, pp. 287–295, 2007, doi: 10.1038/nprot.2006.478.
- [141] C. Shackelford, G. Long, J. Wolf, C. Okerberg, and R. Herbert, "Qualitative and quantitative analysis of nonneoplastic lesions in toxicology studies," *Toxicol. Pathol.*, vol. 30, no. 1, pp. 93–96, 2002, doi: 10.1080/01926230252824761.
- [142] C. L. Scudamore, "Acquiring, recording, and analyzing pathology data from experimental mice: an overview.," *Curr. Protoc. Mouse Biol.*, vol. 4, no. 1, pp. 1–10, Mar. 2014, doi: 10.1002/9780470942390.mo130200.
- [143] T. Ishimoto *et al.*, "High-fat and high-sucrose (western) diet induces steatohepatitis that is dependent on fructokinase," *Hepatology*, vol. 58, no. 5, pp. 1632–1643, 2013, doi: 10.1002/hep.26594.
- [144] J. Lam *et al.*, "A universal approach to analyzing transmission electron microscopy with imagej," *Cells*, vol. 10, no. 9, 2021, doi: 10.3390/cells10092177.
- [145] J. L. Donahue, C. M. Okpodu, C. L. Cramer, E. A. Grabau, and R. G. Alscher, "Responses of antioxidants to paraquat in pea leaves: Relationships to resistance," *Plant Physiol.*, vol. 113, no. 1, pp. 249–257, 1997, doi: 10.1104/pp.113.1.249.
- [146] H. Ohkawa, N. Ohishi, and K. Yagi, "Assay for lipid peroxides in animal tissues by thiobarbituric acid reaction.," *Anal. Biochem.*, vol. 95, no. 2, pp. 351–358, Jun. 1979, doi: 10.1016/0003-2697(79)90738-3.
- [147] D. E. Francés *et al.*, "Role of reactive oxygen species in the early stages of liver regeneration in streptozotocin-induced diabetic rats.," *Free Radic. Res.*, vol. 45, no. 10, pp. 1143–1153, Oct. 2011, doi: 10.3109/10715762.2011.602345.
- [148] C. Doerrier, L. F. Garcia-Souza, G. Krumschnabel, Y. Wohlfarter, A. T. Mészáros, and E. Gnaiger, "High-Resolution FluoRespirometry and OXPHOS Protocols for Human Cells, Permeabilized Fibers from Small Biopsies of Muscle, and Isolated Mitochondria.," *Methods Mol. Biol.*, vol. 1782, pp. 31–70, 2018, doi: 10.1007/978-1-4939-7831-1\_3.
- [149] E. Gnaiger, "Mitochondrial pathways and respiratory control: An Introduction to OXPHOS Analysis. 5th ed.," 2020.
- [150] P. D. Greig *et al.*, "Prostaglandin E1 for primary nonfunction following liver transplantation.," *Transplant. Proc.*, vol. 21, no. 2, pp. 3360–3361, Apr. 1989.
- [151] S. Li *et al.*, "Characteristics of Changes in Inflammatory Cytokines as a Function of

## VII. BIBLIOGRAPHY

---

- Hepatic Ischemia-Reperfusion Injury Stage in Mice,” *Inflammation*, vol. 42, no. 6, pp. 2139–2147, 2019, doi: 10.1007/s10753-019-01078-y.
- [152] Y. Li, A. Palmer, L. Lupu, and M. Huber-Lang, “Inflammatory response to the ischaemia–reperfusion insult in the liver after major tissue trauma,” *Eur. J. Trauma Emerg. Surg.*, no. 0123456789, 2022, doi: 10.1007/s00068-022-02026-6.
- [153] H. Jaeschke, “Mechanisms of liver injury. II. Mechanisms of neutrophil-induced liver cell injury during hepatic ischemia-reperfusion and other acute inflammatory conditions,” *Am. J. Physiol. - Gastrointest. Liver Physiol.*, vol. 290, no. 6, pp. 1083–1088, 2006, doi: 10.1152/ajpgi.00568.2005.
- [154] X. Guo *et al.*, “Mitochondrial stress is relayed to the cytosol by an OMA1–DELE1–HRI pathway,” *Nature*, vol. 579, no. 7799, pp. 427–432, 2020, doi: 10.1038/s41586-020-2078-2.
- [155] A. Saraste, K. Pulkki, M. Kallajoki, K. Henriksen, M. Parvinen, and L. M. Voipio-Pulkki, “Apoptosis in human acute myocardial infarction,” *Circulation*, vol. 95, no. 2, pp. 320–323, Jan. 1997, doi: 10.1161/01.cir.95.2.320.
- [156] D. J. Thuerauf, M. Marcinko, N. Gude, M. Rubio, M. A. Sussman, and C. C. Glembotski, “Activation of the unfolded protein response in infarcted mouse heart and hypoxic cultured cardiac myocytes,” *Circ. Res.*, vol. 99, no. 3, pp. 275–282, 2006, doi: 10.1161/01.RES.0000233317.70421.03.
- [157] D. N. Granger and P. R. Kvietys, “Reperfusion injury and reactive oxygen species: The evolution of a concept,” *Redox Biol.*, vol. 6, pp. 524–551, 2015, doi: 10.1016/j.redox.2015.08.020.
- [158] S. Campello and L. Scorrano, “Mitochondrial shape changes: Orchestrating cell pathophysiology,” *EMBO Rep.*, vol. 11, no. 9, pp. 678–684, 2010, doi: 10.1038/embor.2010.115.
- [159] X. Liu and G. Hajnóczky, “Altered fusion dynamics underlie unique morphological changes in mitochondria during hypoxia-reoxygenation stress,” *Cell Death Differ.*, vol. 18, no. 10, pp. 1561–1572, 2011, doi: 10.1038/cdd.2011.13.
- [160] A. B. Rogers, “Stress of strains: Inbred mice in liver research,” *Gene Expr.*, vol. 19, no. 1, pp. 61–67, 2018, doi: 10.3727/105221618X15337408678723.
- [161] Y. Abe *et al.*, “Mouse model of liver ischemia and reperfusion injury: method for studying reactive oxygen and nitrogen metabolites in vivo,” *Free Radic. Biol. Med.*, vol. 46, no. 1, pp. 1–7, 2009, doi: 10.1016/j.freeradbiomed.2008.09.029.
- [162] A. K. Goff, “Steroid hormone modulation of prostaglandin secretion in the ruminant endometrium during the estrous cycle,” *Biol. Reprod.*, vol. 71, no. 1, pp. 11–16, 2004, doi: 10.1095/biolreprod.103.025890.



- [163] A. Sobrino *et al.*, “Estradiol selectively stimulates endothelial prostacyclin production through estrogen receptor- $\alpha$ ,” *J. Mol. Endocrinol.*, vol. 44, no. 4, pp. 237–246, 2010, doi: 10.1677/JME-09-0112.
- [164] Y. Jiang *et al.*, “Luteolin Pretreatment Attenuates Hepatic Ischemia-Reperfusion Injury in Mice by Inhibiting Inflammation, Autophagy, and Apoptosis via the ERK/PPAR  $\alpha$  Pathway,” *PPAR Res.*, vol. 2022, 2022, doi: 10.1155/2022/8161946.
- [165] Y. Wang *et al.*, “mice through ST2-dependent IL-13 production,” vol. 13, no. 579, pp. 1–21, 2021, doi: 10.1126/scitranslmed.abb6576.Eosinophils.
- [166] B. Dai *et al.*, “LncRNA AK054386 Functions as a ceRNA to Sequester miR-199 and Induce Sustained Endoplasmic Reticulum Stress in Hepatic Reperfusion Injury,” *Oxid. Med. Cell. Longev.*, vol. 2019, 2019, doi: 10.1155/2019/8189079.
- [167] Y. Du *et al.*, “The Dietary Supplement  $\gamma$ -Oryzanol Attenuates Hepatic Ischemia Reperfusion Injury via Inhibiting Endoplasmic Reticulum Stress and HMGB1/NLRP3 Inflammasome,” *Oxid. Med. Cell. Longev.*, vol. 2021, 2021, doi: 10.1155/2021/4628050.
- [168] S. Li *et al.*, “Dietary Inorganic Nitrate Protects Hepatic Ischemia-Reperfusion Injury Through NRF2-Mediated Antioxidative Stress,” *Front. Pharmacol.*, vol. 12, no. June, pp. 1–11, 2021, doi: 10.3389/fphar.2021.634115.
- [169] K. H. H. Liss *et al.*, “Monoacylglycerol Acyltransferase 1 Knockdown Exacerbates Hepatic Ischemia/Reperfusion Injury in Mice With Hepatic Steatosis,” *Liver Transplant. Off. Publ. Am. Assoc. Study Liver Dis. Int. Liver Transplant. Soc.*, vol. 27, no. 1, pp. 116–133, Jan. 2021, doi: 10.1002/lt.25886.
- [170] E. Yin *et al.*, “Anti-CD321 antibody immunotherapy protects liver against ischemia and reperfusion-induced injury,” *Sci. Rep.*, vol. 11, no. 1, pp. 1–10, 2021, doi: 10.1038/s41598-021-85001-2.
- [171] N. Nemeth *et al.*, “Hemorheological and microcirculatory factors in liver ischemia-reperfusion injury—an update on pathophysiology, molecular mechanisms and protective strategies,” *Int. J. Mol. Sci.*, vol. 22, no. 4, pp. 1–24, 2021, doi: 10.3390/ijms22041864.
- [172] R. R. Maronpot, “Biological basis of differential susceptibility to hepatocarcinogenesis among mouse strains,” *J. Toxicol. Pathol.*, vol. 22, no. 1, pp. 11–33, 2009, doi: 10.1293/tox.22.11.
- [173] E. Kawashita, K. Ishihara, M. Nomoto, M. Taniguchi, and S. Akiba, “A comparative analysis of hepatic pathological phenotypes in C57BL/6J and C57BL/6N mouse strains in non-alcoholic steatohepatitis models,” *Sci. Rep.*, vol. 9, no. 1, pp. 1–13, 2019, doi: 10.1038/s41598-018-36862-7.

## VII. BIBLIOGRAPHY

---

- [174] H. Fu *et al.*, “Flurbiprofen, a cyclooxygenase inhibitor, protects mice from hepatic ischemia/reperfusion injury by inhibiting GSK-3 $\beta$  signaling and mitochondrial permeability transition,” *Mol. Med.*, vol. 18, pp. 1128–1135, 2012, doi: 10.2119/molmed.2012.00088.
- [175] Z. Qi *et al.*, “Inhibition of COX-2 ameliorates murine liver schistosomiasis japonica through splenic cellular immunoregulation,” *Parasites and Vectors*, vol. 15, no. 1, pp. 1–12, 2022, doi: 10.1186/s13071-022-05201-1.
- [176] R. H. Tolba *et al.*, “Role of preferential cyclooxygenase-2 inhibition by meloxicam in ischemia/reperfusion injury of the rat liver,” *Eur. Surg. Res. Eur. Chir. Forschung. Rech. Chir. Eur.*, vol. 53, no. 1–4, pp. 11–24, 2014, doi: 10.1159/000362411.
- [177] V. S. Bhave, S. Donthamsetty, J. R. Latendresse, L. Muskhelishvili, and H. M. Mehendale, “Secretory phospholipase A2 mediates progression of acute liver injury in the absence of sufficient cyclooxygenase-2,” *Toxicol. Appl. Pharmacol.*, vol. 228, no. 2, pp. 225–238, 2008, doi: 10.1016/j.taap.2007.12.023.
- [178] V. S. Bhave, S. Donthamsetty, J. R. Latendresse, M. L. Cunningham, and H. M. Mehendale, “Secretory phospholipase A2-mediated progression of hepatotoxicity initiated by acetaminophen is exacerbated in the absence of hepatic COX-2,” *Toxicol. Appl. Pharmacol.*, vol. 251, no. 3, pp. 173–180, 2011, doi: 10.1016/j.taap.2011.01.013.
- [179] M. Hossain, H. Wakabayashi, K. Izuishi, K. Okano, S. Yachida, and H. Maeta, “The Role of Prostaglandins in Liver Ischemia-Reperfusion Injury,” *Curr. Pharm. Des.*, vol. 12, no. 23, pp. 2935–2951, 2006, doi: 10.2174/138161206777947678.
- [180] T. E. North *et al.*, “PGE2-regulated wnt signaling and N-acetylcysteine are synergistically hepatoprotective in zebrafish acetaminophen injury,” *Proc. Natl. Acad. Sci. U. S. A.*, vol. 107, no. 40, pp. 17315–17320, 2010, doi: 10.1073/pnas.1008209107.
- [181] Y. Kuzumoto *et al.*, “Role of EP4 prostaglandin E2 receptor in the ischemic liver,” *Transplant. Proc.*, vol. 37, no. 1, pp. 422–424, 2005, doi: 10.1016/j.transproceed.2004.11.085.
- [182] Y. Kuzumoto *et al.*, “Significance and therapeutic potential of prostaglandin E2 receptor in hepatic ischemia/reperfusion injury in mice,” *Hepatology*, vol. 42, no. 3, pp. 608–617, 2005, doi: 10.1002/hep.20827.
- [183] M. Chen *et al.*, “Hepatic COX-2 expression protects mice from an alcohol-high fat diet-induced metabolic disorder by involving protein acetylation related energy metabolism,” *Alcohol*, vol. 92, pp. 41–52, 2021, doi: 10.1016/j.alcohol.2020.08.007.
- [184] R. Mayoral, B. Mollá, J. M. Flores, L. Boscá, M. Casado, and P. Martín-Sanz, “Constitutive expression of cyclo-oxygenase 2 transgene in hepatocytes protects against liver injury,” *Biochem. J.*, vol. 416, no. 3, pp. 337–346, Dec. 2008, doi:

- 10.1042/BJ20081224.
- [185] E. Kirac, F. Özcan, H. Tuzcu, G. O. Elpek, and M. Aslan, “Analysis of polyunsaturated fatty acids and the omega-6 inflammatory pathway in hepatic ischemia/re-perfusion injury,” *Mol. Med. Rep.*, vol. 12, no. 3, pp. 4149–4156, 2015, doi: 10.3892/mmr.2015.3908.
- [186] P. A. Clavien, S. Yadav, D. Sindram, and R. C. Bentley, “Protective effects of ischemic preconditioning for liver resection performed under inflow occlusion in humans,” *Ann. Surg.*, vol. 232, no. 2, pp. 155–162, 2000, doi: 10.1097/00000658-200008000-00001.
- [187] Y. Guo *et al.*, “Inducible cardiac-specific overexpression of cyclooxygenase-2 (COX-2) confers resistance to ischemia/reperfusion injury,” *Basic Res. Cardiol.*, vol. 114, no. 5, pp. 1–11, 2019, doi: 10.1007/s00395-019-0741-2.
- [188] Y. C. Hsueh, J. M. F. Wu, C. K. Yu, K. K. Wu, and P. C. H. Hsieh, “Prostaglandin E2 promotes post-infarction cardiomyocyte replenishment by endogenous stem cells,” *EMBO Mol. Med.*, vol. 6, no. 4, pp. 496–503, 2014, doi: 10.1002/emmm.201303687.
- [189] M. L. FitzSimons *et al.*, “Cardiac injury modulates critical components of prostaglandin E2 signaling during zebrafish heart regeneration,” *Sci. Rep.*, vol. 10, no. 1, pp. 1–10, 2020, doi: 10.1038/s41598-020-59868-6.
- [190] J. A. Adams, A. Uryash, and J. R. Lopez, “Cyclooxygenase inhibition prior to ventricular fibrillation induced ischemia reperfusion injury impairs survival and outcomes,” *Med. Hypotheses*, vol. 135, no. August 2019, p. 109485, 2020, doi: 10.1016/j.mehy.2019.109485.
- [191] L. Timmers *et al.*, “Cyclooxygenase-2 inhibition increases mortality, enhances left ventricular remodeling, and impairs systolic function after myocardial infarction in the pig,” *Circulation*, vol. 115, no. 3, pp. 326–332, 2007, doi: 10.1161/CIRCULATIONAHA.106.647230.
- [192] J. Insete *et al.*, “Constitutive COX-2 activity in cardiomyocytes confers permanent cardioprotection. Constitutive COX-2 expression and cardioprotection,” *J. Mol. Cell. Cardiol.*, vol. 46, no. 2, pp. 160–168, 2009, doi: 10.1016/j.yjmcc.2008.11.011.
- [193] Y. A. Hong *et al.*, “Paricalcitol Pretreatment Attenuates Renal Ischemia-Reperfusion Injury via Prostaglandin E2 Receptor EP4 Pathway,” *Oxid. Med. Cell. Longev.*, vol. 2017, 2017, doi: 10.1155/2017/5031926.
- [194] H. S. Hwang *et al.*, “Pretreatment with paricalcitol attenuates inflammation in ischemia-reperfusion injury via the up-regulation of cyclooxygenase-2 and prostaglandin E2,” *Nephrol. Dial. Transplant.*, vol. 28, no. 5, pp. 1156–1166, 2013, doi: 10.1093/ndt/gfs540.

## VII. BIBLIOGRAPHY

---

- [195] M. R. McGill, "The past and present of serum aminotransferases and the future of liver injury biomarkers.," *EXCLI J.*, vol. 15, pp. 817–828, 2016, doi: 10.17179/excli2016-800.
- [196] Z. Jaffar, K.-S. Wan, and K. Roberts, "A Key Role for Prostaglandin I<sub>2</sub> in Limiting Lung Mucosal Th<sub>2</sub>, But Not Th<sub>1</sub>, Responses to Inhaled Allergen," *J. Immunol.*, vol. 169, no. 10, pp. 5997–6004, 2002, doi: 10.4049/jimmunol.169.10.5997.
- [197] C. Brenneis *et al.*, "Anti-inflammatory role of microsomal prostaglandin synthase-1 in a model of neuroinflammation," *J. Biol. Chem.*, vol. 286, no. 3, pp. 2331–2342, 2011, doi: 10.1074/jbc.M110.157362.
- [198] D. W. Gilroy, P. R. Colville-Nash, D. Willis, J. Chivers, M. J. Paul-Clark, and D. A. Willoughby, "Inducible cyclooxygenase may have anti-inflammatory properties," *Nat. Med.*, vol. 5, no. 6, pp. 698–701, 1999, doi: 10.1038/9550.
- [199] P. Cheng *et al.*, "Hydrogen sulfide ameliorates ischemia/reperfusion-induced hepatitis by inhibiting apoptosis and autophagy pathways," *Mediators Inflamm.*, vol. 2014, 2014, doi: 10.1155/2014/935251.
- [200] M. Bejaoui *et al.*, "Polyethylene Glycol Preconditioning: An Effective Strategy to Prevent Liver Ischemia Reperfusion Injury.," *Oxid. Med. Cell. Longev.*, vol. 2016, p. 9096549, 2016, doi: 10.1155/2016/9096549.
- [201] M. T. Rizzo, "Cyclooxygenase-2 in oncogenesis," *Clin. Chim. Acta*, vol. 412, no. 9–10, pp. 671–687, 2011, doi: 10.1016/j.cca.2010.12.026.
- [202] B. Wang *et al.*, "High glucose suppresses autophagy through the AMPK pathway while it induces autophagy via oxidative stress in chondrocytes," *Cell Death Dis.*, vol. 12, no. 6, 2021, doi: 10.1038/s41419-021-03791-9.
- [203] R. Vargas and L. A. Videla, "Thyroid hormone suppresses ischemia-reperfusion-induced liver NLRP3 inflammasome activation: Role of AMP-activated protein kinase," *Immunol. Lett.*, vol. 184, pp. 92–97, 2017, doi: 10.1016/j.imlet.2017.01.007.
- [204] C. Peralta *et al.*, "Adenosine monophosphate-activated protein kinase mediates the protective effects of ischemic preconditioning on hepatic ischemia-reperfusion injury in the rat," *Hepatology*, vol. 34, no. 6, pp. 1164–1173, 2001, doi: 10.1053/jhep.2001.29197.
- [205] J. Kim, M. Kundu, B. Viollet, and K. L. Guan, "AMPK and mTOR regulate autophagy through direct phosphorylation of Ulk1," *Nat. Cell Biol.*, vol. 13, no. 2, pp. 132–141, 2011, doi: 10.1038/ncb2152.
- [206] C. Lin *et al.*, "Inhibition of CAMKK2 impairs autophagy and castration-resistant prostate cancer via suppression of AMPK-ULK1 signaling," *Oncogene*, vol. 40, no. 9, pp. 1690–1705, 2021, doi: 10.1038/s41388-021-01658-z.

- [207] J. P. White, A. N. Billin, M. E. Campbell, A. J. Russell, K. M. Huffman, and W. E. Kraus, "The AMPK/p27Kip1 Axis Regulates Autophagy/Apoptosis Decisions in Aged Skeletal Muscle Stem Cells," *Stem Cell Reports*, vol. 11, no. 2, pp. 425–439, 2018, doi: 10.1016/j.stemcr.2018.06.014.
- [208] A. Liu *et al.*, "Baicalein pretreatment reduces liver ischemia/reperfusion injury via induction of autophagy in rats," *Sci. Rep.*, vol. 6, no. September 2015, pp. 1–12, 2016, doi: 10.1038/srep25042.
- [209] Z. Rao *et al.*, "Isoflurane Preconditioning Alleviated Murine Liver Ischemia and Reperfusion Injury by Restoring AMPK/mTOR-Mediated Autophagy," *Anesth. Analg.*, vol. 125, no. 4, pp. 1355–1363, 2017, doi: 10.1213/ANE.0000000000002385.
- [210] M. A. Pelissier-Rota, L. Pelosi, P. Meresse, and M. R. Jacquier-Sarlin, "Nicotine-induced cellular stresses and autophagy in human cancer colon cells: A supportive effect on cell homeostasis via up-regulation of Cox-2 and PGE2 production," *Int. J. Biochem. Cell Biol.*, vol. 65, pp. 239–256, 2015, doi: 10.1016/j.biocel.2015.06.013.
- [211] T. Li *et al.*, "Aggravation of acute kidney injury by mPGES-2 down regulation is associated with autophagy inhibition and enhanced apoptosis," *Sci. Rep.*, vol. 7, no. 1, pp. 1–15, 2017, doi: 10.1038/s41598-017-10271-8.
- [212] D. Z. Mohamed, A. E. D. E. S. El-Sisi, S. S. Sokar, A. M. Shebl, and S. E. S. Abu-Risha, "Targeting autophagy to modulate hepatic ischemia/reperfusion injury: A comparative study between octreotide and melatonin as autophagy modulators through AMPK/PI3K/AKT/mTOR/ULK1 and Keap1/Nrf2 signaling pathways in rats," *Eur. J. Pharmacol.*, vol. 897, no. February, p. 173920, 2021, doi: 10.1016/j.ejphar.2021.173920.
- [213] I. Tanida, T. Ueno, and E. Kominami, "LC3 and Autophagy.," *Methods Mol. Biol.*, vol. 445, pp. 77–88, 2008, doi: 10.1007/978-1-59745-157-4\_4.
- [214] E. Folch-Puy *et al.*, "Relevance of endoplasmic reticulum stress cell signaling in liver cold ischemia reperfusion injury," *Int. J. Mol. Sci.*, vol. 17, no. 6, pp. 1–12, 2016, doi: 10.3390/ijms17060807.
- [215] M. Vilatoba *et al.*, "Sodium 4-phenylbutyrate protects against liver ischemia reperfusion injury by inhibition of endoplasmic reticulum-stress mediated apoptosis.," *Surgery*, vol. 138, no. 2, pp. 342–351, Aug. 2005, doi: 10.1016/j.surg.2005.04.019.
- [216] P. M. Quirós *et al.*, "Multi-omics analysis identifies ATF4 as a key regulator of the mitochondrial stress response in mammals," *J. Cell Biol.*, vol. 216, no. 7, pp. 2027–2045, 2017, doi: 10.1083/jcb.201702058.
- [217] L. R. Palam, T. D. Baird, and R. C. Wek, "Phosphorylation of eIF2 facilitates ribosomal bypass of an inhibitory upstream ORF to enhance CHOP translation," *J. Biol. Chem.*, vol. 286, no. 13, pp. 10939–10949, 2011, doi: 10.1074/jbc.M110.216093.

## VII. BIBLIOGRAPHY

---

- [218] T. Verfaillie *et al.*, “PERK is required at the ER-mitochondrial contact sites to convey apoptosis after ROS-based ER stress,” *Cell Death Differ.*, vol. 19, no. 11, pp. 1880–1891, 2012, doi: 10.1038/cdd.2012.74.
- [219] K. Terai *et al.*, “AMP-Activated Protein Kinase Protects Cardiomyocytes against Hypoxic Injury through Attenuation of Endoplasmic Reticulum Stress,” *Mol. Cell. Biol.*, vol. 25, no. 21, pp. 9554–9575, 2005, doi: 10.1128/mcb.25.21.9554-9575.2005.
- [220] K. Nakamura *et al.*, “Antibiotic pretreatment alleviates liver transplant damage in mice and humans,” *J. Clin. Invest.*, vol. 129, no. 8, pp. 3420–3434, 2019, doi: 10.1172/JCI127550.
- [221] H. Toko *et al.*, “ATF6 is important under both pathological and physiological states in the heart.,” *J. Mol. Cell. Cardiol.*, vol. 49, no. 1, pp. 113–120, Jul. 2010, doi: 10.1016/j.yjmcc.2010.03.020.
- [222] Q. Ma, “Role of nrf2 in oxidative stress and toxicity.,” *Annu. Rev. Pharmacol. Toxicol.*, vol. 53, pp. 401–426, 2013, doi: 10.1146/annurev-pharmtox-011112-140320.
- [223] B. Ke *et al.*, “KEAP1-NRF2 complex in ischemia-induced hepatocellular damage of mouse liver transplants.,” *J. Hepatol.*, vol. 59, no. 6, pp. 1200–1207, Dec. 2013, doi: 10.1016/j.jhep.2013.07.016.
- [224] Y. Masuda *et al.*, “Salutary effect of pre-treatment with an Nrf2 inducer on ischemia reperfusion injury in the rat liver.,” *Gastroenterol. Hepatol.*, vol. 1, no. 1, pp. 1–7, 2014, doi: 10.3968/5206.Salutary.
- [225] E. Kansanen, A. M. Kivelä, and A. L. Levenon, “Regulation of Nrf2-dependent gene expression by 15-deoxy- $\Delta$ 12,14-prostaglandin J<sub>2</sub>,” *Free Radic. Biol. Med.*, vol. 47, no. 9, pp. 1310–1317, 2009, doi: 10.1016/j.freeradbiomed.2009.06.030.
- [226] K. Chen *et al.*, “15-Deoxy- $\Delta$ 12,14-prostaglandin J<sub>2</sub> alleviates hepatic ischemia-reperfusion injury in mice via inducing antioxidant response and inhibiting apoptosis and autophagy,” *Acta Pharmacol. Sin.*, vol. 38, no. 5, pp. 672–687, 2017, doi: 10.1038/aps.2016.108.
- [227] A. Banning, S. Deubel, D. Kluth, Z. Zhou, and R. Brigelius-Flohé, “The GI-GPx gene is a target for Nrf2,” *GBM Annu. Fall Meet. Berlin/Potsdam 2005*, vol. 2005, no. Fall, pp. 4914–4923, 2005, doi: 10.1240/sav\_gbm\_2005\_h\_001282.
- [228] C. J. Harvey *et al.*, “Nrf2-regulated glutathione recycling independent of biosynthesis is critical for cell survival during oxidative stress,” *Free Radic. Biol. Med.*, vol. 46, no. 4, pp. 443–453, 2009, doi: 10.1016/j.freeradbiomed.2008.10.040.
- [229] X. He and Q. Ma, “Redox regulation by nuclear factor erythroid 2-related factor 2: gatekeeping for the basal and diabetes-induced expression of thioredoxin-interacting

- protein.," *Mol. Pharmacol.*, vol. 82, no. 5, pp. 887–897, Nov. 2012, doi: 10.1124/mol.112.081133.
- [230] T. Rangasamy *et al.*, "Genetic ablation of Nrf2 enhances susceptibility to cigarette smoke-induced emphysema in mice," *J. Clin. Invest.*, vol. 114, no. 9, pp. 1248–1259, 2004, doi: 10.1172/JCI200421146.
- [231] F. Ito, Y. Sono, and T. Ito, "Measurement and clinical significance of lipid peroxidation as a biomarker of oxidative stress: Oxidative stress in diabetes, atherosclerosis, and chronic inflammation," *Antioxidants*, vol. 8, no. 3, 2019, doi: 10.3390/antiox8030072.
- [232] J. Van Der Paal, E. C. Neyts, C. C. W. Verlaack, and A. Bogaerts, "Effect of lipid peroxidation on membrane permeability of cancer and normal cells subjected to oxidative stress," *Chem. Sci.*, vol. 7, no. 1, pp. 489–498, 2016, doi: 10.1039/c5sc02311d.
- [233] D. C. Fuhrmann and B. Brüne, "Mitochondrial composition and function under the control of hypoxia," *Redox Biol.*, vol. 12, no. February, pp. 208–215, 2017, doi: 10.1016/j.redox.2017.02.012.
- [234] M. Elias-Miró, M. B. Jiménez-Castro, J. Rodés, and C. Peralta, "Current knowledge on oxidative stress in hepatic ischemia/reperfusion," *Free Radic. Res.*, vol. 47, no. 8, pp. 555–568, 2013, doi: 10.3109/10715762.2013.811721.
- [235] C. García-Ruiz and J. C. Fernández-Checa, "Mitochondrial Oxidative Stress and Antioxidants Balance in Fatty Liver Disease," *Hepatol. Commun.*, vol. 2, no. 12, pp. 1425–1439, 2018, doi: 10.1002/hep4.1271.
- [236] B. Zhuan *et al.*, "Hypoxia induces pulmonary artery smooth muscle dysfunction through mitochondrial fragmentation-mediated endoplasmic reticulum stress," *Aging (Albany. NY)*, vol. 12, no. 23, pp. 23684–23697, 2020, doi: 10.18632/aging.103892.
- [237] G. Li, J. Liu, X. Feng, B. Zhang, and R. Zhang, "Retigabine attenuates focal cerebral ischemic injury through inhibiting mitochondria-dependent apoptotic pathway," pp. 5018–5023, 2018.
- [238] M. Panel *et al.*, "Small-Molecule Inhibitors of Cyclophilins Block Opening of the Mitochondrial Permeability Transition Pore and Protect Mice From Hepatic Ischemia/Reperfusion Injury," *Gastroenterology*, no. September, pp. 1–15, 2019, doi: 10.1053/j.gastro.2019.07.026.
- [239] A. Rossetti *et al.*, "Unacylated ghrelin prevents mitochondrial dysfunction in a model of ischemia/reperfusion liver injury," *Cell Death Discov.*, vol. 3, no. 1, pp. 1–11, 2017, doi: 10.1038/cddiscovery.2017.77.
- [240] K. Labbé, A. Murley, and J. Nunnari, "Determinants and functions of mitochondrial

## VII. BIBLIOGRAPHY

---

- behavior,” *Annu. Rev. Cell Dev. Biol.*, vol. 30, no. 1, pp. 357–391, 2014, doi: 10.1146/annurev-cellbio-101011-155756.
- [241] Y. Zhou *et al.*, “Topology-dependent, bifurcated mitochondrial quality control under starvation,” *Autophagy*, vol. 16, no. 3, pp. 562–574, 2020, doi: 10.1080/15548627.2019.1634944.
- [242] L. Chen, Q. Gong, J. P. Stice, and A. A. Knowlton, “Mitochondrial OPA1, apoptosis, and heart failure,” *Cardiovasc. Res.*, vol. 84, no. 1, pp. 91–99, 2009, doi: 10.1093/cvr/cvp181.
- [243] L. Bouche *et al.*, “DRP1 haploinsufficiency attenuates cardiac ischemia/reperfusion injuries,” *PLoS One*, vol. 16, no. 3 March, pp. 1–15, 2021, doi: 10.1371/journal.pone.0248554.
- [244] H. Cheng, H. Huang, Z. Guo, Y. Chang, and Z. Li, “Role of prostaglandin E2 in tissue repair and regeneration,” *Theranostics*, vol. 11, no. 18, pp. 8836–8854, 2021, doi: 10.7150/thno.63396.
- [245] J. Vongsfak, W. Pratchayasakul, N. Apaijai, T. Vaniyapong, N. Chattipakorn, and S. C. Chattipakorn, “The alterations in mitochondrial dynamics following cerebral ischemia/reperfusion injury,” *Antioxidants*, vol. 10, no. 9, pp. 1–19, 2021, doi: 10.3390/antiox10091384.
- [246] L. Griparic, T. Kanazawa, and A. M. Van Der Blik, “Regulation of the mitochondrial dynamin-like protein Opa1 by proteolytic cleavage,” *J. Cell Biol.*, vol. 178, no. 5, pp. 757–764, 2007, doi: 10.1083/jcb.200704112.
- [247] Z. Song, H. Chen, M. Fiket, C. Alexander, and D. C. Chan, “OPA1 processing controls mitochondrial fusion and is regulated by mRNA splicing, membrane potential, and Yme1L,” *J. Cell Biol.*, vol. 178, no. 5, pp. 749–755, 2007, doi: 10.1083/jcb.200704110.
- [248] S. Duvezin-Caubet *et al.*, “Proteolytic processing of OPA1 links mitochondrial dysfunction to alterations in mitochondrial morphology,” *J. Biol. Chem.*, vol. 281, no. 49, pp. 37972–37979, 2006, doi: 10.1074/jbc.M606059200.
- [249] R. Quintana-Cabrera *et al.*, “The cristae modulator Optic atrophy 1 requires mitochondrial ATP synthase oligomers to safeguard mitochondrial function,” *Nat. Commun.*, vol. 9, no. 1, 2018, doi: 10.1038/s41467-018-05655-x.
- [250] N. Ishihara, Y. Fujita, T. Oka, and K. Mihara, “Regulation of mitochondrial morphology through proteolytic cleavage of OPA1,” *EMBO J.*, vol. 25, no. 13, pp. 2966–2977, 2006, doi: 10.1038/sj.emboj.7601184.
- [251] T. Ban *et al.*, “Molecular basis of selective mitochondrial fusion by heterotypic action between OPA1 and cardiolipin,” *Nat. Cell Biol.*, vol. 19, no. 7, pp. 856–863, 2017,



- doi: 10.1038/ncb3560.
- [252] S. Ehses *et al.*, “Regulation of OPA1 processing and mitochondrial fusion by m-AAA protease isoenzymes and OMA1,” *J. Cell Biol.*, vol. 187, no. 7, pp. 1023–1036, 2009, doi: 10.1083/jcb.200906084.
- [253] S. Cogliati, J. A. Enriquez, and L. Scorrano, “Mitochondrial Cristae: Where Beauty Meets Functionality,” *Trends Biochem. Sci.*, vol. 41, no. 3, pp. 261–273, 2016, doi: 10.1016/j.tibs.2016.01.001.
- [254] S. Cipolat *et al.*, “Mitochondrial Rhomboid PARL Regulates Cytochrome c Release during Apoptosis via OPA1-Dependent Cristae Remodeling,” *Cell*, vol. 126, no. 1, pp. 163–175, 2006, doi: 10.1016/j.cell.2006.06.021.
- [255] D. Hu *et al.*, “A Common Missense Variant in OMA1 Associated with the Prognosis of Heart Failure,” *Cardiovasc. Drugs Ther.*, vol. 34, no. 3, pp. 345–356, 2020, doi: 10.1007/s10557-020-06960-8.
- [256] K. P. Maremanda, I. K. Sundar, and I. Rahman, “Role of inner mitochondrial protein OPA1 in mitochondrial dysfunction by tobacco smoking and in the pathogenesis of COPD,” *Redox Biol.*, vol. 45, p. 102055, 2021, doi: 10.1016/j.redox.2021.102055.
- [257] Z. Wu *et al.*, “OMA1 reprograms metabolism under hypoxia to promote colorectal cancer development,” *EMBO Rep.*, vol. 22, no. 1, pp. 1–18, 2021, doi: 10.15252/embr.202050827.
- [258] M. J. Baker *et al.*, “Stress-induced OMA1 activation and autocatalytic turnover regulate OPA1-dependent mitochondrial dynamics,” *EMBO J.*, vol. 33, no. 6, pp. 578–593, 2014, doi: 10.1002/emboj.201386474.
- [259] B. Head, L. Griparic, M. Amiri, S. Gandre-Babbe, and A. M. Van Der Blik, “Inducible proteolytic inactivation of OPA1 mediated by the OMA1 protease in mammalian cells,” *J. Cell Biol.*, vol. 187, no. 7, pp. 959–966, 2009, doi: 10.1083/jcb.200906083.
- [260] K. Zhang, H. Li, and Z. Song, “Membrane depolarization activates the mitochondrial protease OMA1 by stimulating self-cleavage,” *EMBO Rep.*, vol. 15, no. 5, pp. 576–585, 2014, doi: 10.1002/embr.201338240.
- [261] H. McBride and V. Soubannier, “Mitochondrial Function: OMA1 and OPA1, the Grandmasters of Mitochondrial Health,” *Curr. Biol.*, vol. 20, no. 6, pp. R274–R276, 2010, doi: 10.1016/j.cub.2010.02.011.
- [262] A. P. Halestrap and A. P. Richardson, “The mitochondrial permeability transition: A current perspective on its identity and role in ischaemia/reperfusion injury,” *J. Mol. Cell. Cardiol.*, vol. 78, pp. 129–141, 2015, doi: 10.1016/j.yjmcc.2014.08.018.

## VII. BIBLIOGRAPHY

---

- [263] D. J. Hausenloy, D. M. Yellon, S. Mani-Babu, and M. R. Duchon, "Preconditioning protects by inhibiting the mitochondrial permeability transition," *Am. J. Physiol. - Hear. Circ. Physiol.*, vol. 287, no. 2 56-2, pp. 841–849, 2004, doi: 10.1152/ajpheart.00678.2003.
- [264] E. Balsa *et al.*, "ER and Nutrient Stress Promote Assembly of Respiratory Chain Supercomplexes through the PERK-eIF2 $\alpha$  Axis," *Mol. Cell*, vol. 74, no. 5, pp. 877–890.e6, 2019, doi: 10.1016/j.molcel.2019.03.031.
- [265] S. Cogliati *et al.*, "Mitochondrial cristae shape determines respiratory chain supercomplexes assembly and respiratory efficiency," *Cell*, vol. 155, no. 1, pp. 160–171, 2013, doi: 10.1016/j.cell.2013.08.032.
- [266] M. P. Murphy, "How mitochondria produce reactive oxygen species," *Biochem. J.*, vol. 417, no. 1, pp. 1–13, 2009, doi: 10.1042/BJ20081386.
- [267] S. J. Jiang, W. Li, and W. An, "Adenoviral gene transfer of hepatic stimulator substance confers resistance against hepatic ischemia-reperfusion injury by improving mitochondrial function," *Hum. Gene Ther.*, vol. 24, no. 4, pp. 443–456, 2013, doi: 10.1089/hum.2012.219.
- [268] J. A. Letts and L. A. Sazanov, "Clarifying the supercomplex: The higher-order organization of the mitochondrial electron transport chain," *Nat. Struct. Mol. Biol.*, vol. 24, no. 10, pp. 800–808, 2017, doi: 10.1038/nsmb.3460.
- [269] E. Lapuente-Brun *et al.*, "Supercomplex assembly determines electron flux in the mitochondrial electron transport chain," *Science (80-. )*, vol. 340, no. 6140, pp. 1567–1570, 2013, doi: 10.1126/science.1230381.
- [270] I. Lopez-Fabuel *et al.*, "Complex I assembly into supercomplexes determines differential mitochondrial ROS production in neurons and astrocytes," *Proc. Natl. Acad. Sci. U. S. A.*, vol. 113, no. 46, pp. 13063–13068, 2016, doi: 10.1073/pnas.1613701113.
- [271] I. Wittig, R. Carrozzo, F. M. Santorelli, and H. Schägger, "Supercomplexes and subcomplexes of mitochondrial oxidative phosphorylation," *Biochim. Biophys. Acta - Bioenerg.*, vol. 1757, no. 9–10, pp. 1066–1072, 2006, doi: 10.1016/j.bbambio.2006.05.006.
- [272] C. Greggio *et al.*, "Enhanced Respiratory Chain Supercomplex Formation in Response to Exercise in Human Skeletal Muscle," *Cell Metab.*, vol. 25, no. 2, pp. 301–311, 2017, doi: 10.1016/j.cmet.2016.11.004.
- [273] P. Martín-Sanz *et al.*, "Presence of a nitric oxide synthase inhibitor in the graft efflux during reperfusion in human liver transplantation.," *Clin. Transplant.*, vol. 13, no. 3, pp. 221–230, Jun. 1999, doi: 10.1034/j.1399-0012.1999.130302.x.

- [274] I. Garutti *et al.*, “Extravascular Lung Water and Pulmonary Vascular Permeability Index Measured at the End of Surgery Are Independent Predictors of Prolonged Mechanical Ventilation in Patients Undergoing Liver Transplantation,” *Anesth. Analg.*, vol. 121, no. 3, pp. 736–745, 2015, doi: 10.1213/ANE.0000000000000875.
- [275] M. Arai, X. X. Peng, R. T. Currin, R. G. Thurman, and J. J. Lemasters, “Protection of sinusoidal endothelial cells against storage/reperfusion injury by prostaglandin E2 derived from Kupffer cells.,” *Transplantation*, vol. 68, no. 3, pp. 440–445, Aug. 1999, doi: 10.1097/00007890-199908150-00017.
- [276] G. A. Wanner, P. Müller, W. Ertel, C. J. Busch, M. D. Menger, and K. Messmer, “Differential effect of cyclooxygenase metabolites on proinflammatory cytokine release by Kupffer cells after liver ischemia and reperfusion.,” *Am. J. Surg.*, vol. 175, no. 2, pp. 146–151, Feb. 1998, doi: 10.1016/S0002-9610(97)00275-4.



# VIII. ANNEXES





## ANNEX 1 – PATIENT INFORMATION TABLE

Gender-Recipient	Age (years) - Recipient	Weight (Kg) - Recipient	Aetiology <sup>1</sup> - Recipient	Preservation medium <sup>2</sup>	Ischemia time (min)	Warm ischemia time (min)	Cold ischemia time (min)	Early graft dysfunction	Length of hospital stay (days)	Mechanical ventilation (h)	Time of resuscitation (days)	PGE2 (pg/mL)	Age (years) - Donor
Man	29	70	PSC	W	322	42	322	Yes	39	12	3	1154	45
Man	57	70	AC	W	689	36	689	No	15	12	3	1157	73
Woman	48	58	AC	C	336	26	336	No	12	13	2	555,6	63
Woman	59	52	HCVC	C	366	30	366	No	44	9	2	949,3	39
Woman	44	73	HCVC + AC	W	787	45	787	No	32	96	6	161,4	32
Man	48	89	HCVC + AC	C	480	45	480	No	22	119	7	344	59
Woman	46	62	AC	W	747	57	747	No	19	116	8	423,5	48
Man	64	68	HBVC + HCC	C	634	40	634	No	30	24	10	395,8	54
Man	53	72	HCVC	W	620	45	620	No	30	5	2	384,8	60

<sup>1</sup> AC, Alcoholic Cirrhosis; HCVC, Hepatitis C Virus Cirrhosis; HBVC, Hepatitis B Virus Cirrhosis; AIC, Autoimmune Cirrhosis; OC, Other Cirrhosis; HCC, Hepatocellular Carcinoma; PSC, Primary Sclerosing Cholangitis; PBC, Primary Biliary Cholangitis; HC, Hemochromatosis; NA, not available

<sup>2</sup> W, Wisconsin; C, Celsior.

## VIII. ANNEXES

Gender-Recipient	Age (years) - Recipient	Weight (Kg) - Recipient	Aetiology <sup>1</sup> - Recipient	Preservation medium <sup>2</sup>	Ischemia time (min)	Warm ischemia time (min)	Cold ischemia time (min)	Early graft dysfunction	Length of hospital stay (days)	Mechanical ventilation (h)	Time of resuscitation (days)	PGE2 (pg/mL)	Age (years) - Donor
Man	41	84	AC	W	438	30	438	No	17	6	3	1049	70
Man	56	85	HCVC + AC	C	522	55	522	No	17	9	3	NA	60
Man	46	83	AC	C	656	20	656	No	16	10	3	607,2	41
Woman	63	60	NA	C	267	26	241	No	NA	176	9	475,1	71
Woman	60	76	AC	C	426	63	426	No	18	36	4	1011	77
Woman	63	60	AC	W	766	30	720	Yes	50	176	9	290,7	71
Man	42	76	HCVC + AC	W	297	NA	NA	No	17	14	2	2213	NA
Woman	58	66	HBVC	W	430	50	430	No	30	42	3	607	66
Man	41	70	HCVC	W	395	55	395	No	18	14	3	744,7	26
Woman	63	65	HCC	W	526	172	526	Yes	16	500	17	629,9	71
Woman	60	65	HCVC	C	631	31	631	No	26	6	4	757,5	71
Man	36	79	AC	W	600	47	600	Yes	19	40	60	351,8	43
Man	55	74	AC + HCC	W	545	58	487	No	13	17	3	656,6	47
Man	53	73	HCVC + AC	W	656	48	818	Yes	1	24	1	1609	73



Gender-Recipient	Age (years) - Recipient	Weight (Kg) - Recipient	Aetiology <sup>1</sup> - Recipient	Preservation medium <sup>2</sup>	Ischemia time (min)	Warm ischemia time (min)	Cold ischemia time (min)	Early graft dysfunction	Length of hospital stay (days)	Mechanical ventilation (h)	Time of resuscitation (days)	PGE2 (pg/mL)	Age (years) - Donor
Man	53	64	AC	W	495	50	495	No	17	21	3	337,7	27
Man	18	70	NA	W	402	48	412	No	20	62	5	724	14
Man	44	64	AC	W	665	30	665	No	17	9	3	424,2	77
Man	39	77	AC	W	698	48	698	No	19	14	4	232,7	74
Man	35	65	HCVC	W	356	36	236	No	22	9	3	2027	60
Woman	47	60	NA	W	701	58	643	No	NA	140	9	208,6	16
Man	38	76	HBVC + HCC	W	558	57	558	No	10	4	2	987,7	73
Man	67	110	HCVC + HCC	W	488	55	488	No	29	247	12	875,8	81
Man	61	85	HBVC + HCC	W	645	50	595	Yes	43	24	15	1047	50
Woman	67	79	HCVC	W	661	44	617	No	38	20	3	741	67
Man	56	88	AC	W	653	48	653	No	58	19	4	202,9	56
Woman	54	68	AC	W	539	65	530	Yes	29	75	6	340,1	62
Man	69	76	HC	W	736	59	677	No	39	21	12	340	59
Woman	29	55	NA	W	514	32	482	No	30	106	9	520	48

## VIII. ANNEXES

Gender-Recipient	Age (years) - Recipient	Weight (Kg) - Recipient	Aetiology <sup>1</sup> - Recipient	Preservation medium <sup>2</sup>	Ischemia time (min)	Warm ischemia time (min)	Cold ischemia time (min)	Early graft dysfunction	Length of hospital stay (days)	Mechanical ventilation (h)	Time of resuscitation (days)	PGE2 (pg/mL)	Age (years) - Donor
Man	52	90	OC	W	351	46	305	Yes	69	34	6	659,4	65
Woman	52	62	HCC	W	527	41	486	Yes	57	18	3	297,8	70
Man	57	103	HBVC	W	514	47	467	No	20	18	3	359,6	66
Man	43	77	HBVC	W	408	59	349	Yes	13	96	4	428,6	76
Man	59	53	HCVC + AC	W	343	24	319	No	66	16	3	109	67
Man	38	84	AC	W	840	NA	775	Yes	50	20	4	147,4	28
Woman	60	68	PBC	W	780	NA	689	Yes	23	6	6	261,2	69
Man	35	70	AC	W	900	NA	842	Yes	35	118	7	230,1	19
Woman	60	62	NA	W	618	NA	558	No	51	90	8	351,4	35
Man	41	84	HBVC	W	360	NA	320	Yes	41	68	12	138,8	46
Woman	20	54	OC	W	690	NA	655	No	32	5	3	508,1	21
Woman	54	53	AC	W	345	14	315	No	59	9	3	94,3	54
Man	62	64	AC	W	680	50	630	No	23	19	3	483,6	61
Man	63	85	AC	W	400	NA	358	No	32	16	2	209,6	50

Gender-Recipient	Age (years) - Recipient	Weight (Kg) - Recipient	Aetiology <sup>1</sup> - Recipient	Preservation medium <sup>2</sup>	Ischemia time (min)	Warm ischemia time (min)	Cold ischemia time (min)	Early graft dysfunction	Length of hospital stay (days)	Mechanical ventilation (h)	Time of resuscitation (days)	PGE2 (pg/mL)	Age (years) - Donor
Man	60	65	AC	W	400	NA	370	No	22	4	3	824,8	19
Woman	57	58	HCVC + AC	W	675	NA	645	Yes	17	8	17	220,4	73
Man	50	99	AC	W	957	NA	897	Yes	79	264	13	81,58	32
Man	65	69	AC	W	660	NA	613	Yes	NA	62	8	151,2	73
Man	58	74	AC	W	NA	60	NA	No	NA	6	5	406,1	65
Man	60	83	HCVC + HCC	W	NA	50	NA	Yes	30	144	7	153	44
Man	51	60	HCVC	W	550	36	510	No	29	10	1	295	54
Man	60	67	HCVC	W	NA	41	NA	No	323	19	2	329,7	57
Man	56	96	HCVC + HCC	W	NA	NA	NA	No	119	19	1	207,9	50
Man	50	90	AC	W	480	NA	420	No	30	12	2	567,6	60
Man	37	60	AC	W	820	70	730	Yes	66	24	4	119,2	49
Woman	NA	NA	AIC	W	700	NA	670	No	22	NA	NA	1132	17
Woman	NA	NA	PBC	W	NA	NA	NA	Yes	77	NA	NA	101,2	58



## ANNEX 2 – INDEX OF FIGURES

### INTRODUCTION FIGURES

<b>Figure 1.</b> Schematic representation of the cyclooxygenase enzyme.....	34
<b>Figure 2.</b> Metabolic pathway of conversion of arachidonic acid (AA) into different types of prostaglandins. ....	37
<b>Figure 3.</b> Liver circulation and structure .....	39
<b>Figure 4.</b> Role of COX-2 in different liver pathology models. ....	42
<b>Figure 5.</b> Intracellular pathways activated during ischemia and during reperfusion that cause cellular and tissue damage .....	46
<b>Figure 6.</b> Overview of the mitochondrial TCA cycle and OXPHOS .....	59
<b>Figure 7.</b> Mitochondrial dynamics .....	61

### MATERIALS AND METHODS FIGURES

<b>Figure 8.</b> Generation of the <i>h</i> -COX-2 <i>Tg</i> mouse line and maintenance of the colony .....	73
<b>Figure 9.</b> Schematic representation of the 70% liver ischemia model in mouse liver .....	77
<b>Figure 10.</b> Temporal diagram of the three different conditions of the experimental design.....	78
<b>Figure 11.</b> Summary of the high respirometry SUIT2 protocol .....	102

### RESULTS FIGURES

<b>Figure 12.</b> h-COX-2 expression evaluation in h-COX-2 <i>Tg</i> mice.....	110
<b>Figure 13.</b> Assessment of the liver damage after I/R.....	111

<b>Figure 14.</b> Pure genetic and F1 hybrid backgrounds don't reproduce the I/R model .....	113
<b>Figure 15.</b> Damage protection in <i>h-COX-2 Tg</i> mice is due to COX-2 activity .....	114
<b>Figure 16.</b> Endogenous expression of COX-2 confers protection to <i>Wt</i> mice following I/R.....	116
<b>Figure 17.</b> Whole transcriptome sequencing shows a differential gene expression profile in <i>h-COX-2 Tg</i> mice after I/R.....	119
<b>Figure 18.</b> Analysis of inflammatory-related genes and cytokines after I/R .....	121
<b>Figure 19.</b> Analysis of pro-inflammatory markers after I/R.....	123
<b>Figure 20.</b> Apoptotic markers analysis after I/R.....	125
<b>Figure 21.</b> Analysis of autophagy markers after I/R.....	127
<b>Figure 22.</b> Unfolded protein response (UPR) markers analysis after I/R.....	129
<b>Figure 23.</b> Oxidative stress and antioxidant response after I/R.....	133
<b>Figure 24.</b> Antioxidant response is increased in COX-2 expressing tissues .....	134
<b>Figure 25.</b> High-resolution mitochondrial respirometry analysis.....	137
<b>Figure 26.</b> Pure genetic and F1 hybrid backgrounds lose differences due to COX-2 expression with respect to mitochondrial respirometry .....	138
<b>Figure 27.</b> Analysis of mitochondrial electron transfer chain (ETC) protein content .....	139
<b>Figure 28.</b> Assessment of mitochondrial membrane potential.....	141
<b>Figure 29.</b> Mitochondrial number, morphology, and appearance analysis.....	142
<b>Figure 30.</b> Analysis of mitochondrial dynamic .....	145
<b>Figure 31.</b> OPA1 expression and processing analysis.....	146
<b>Figure 32.</b> Correlative studies of PGE <sub>2</sub> levels in plasma and graft function in patients receiving OLT .....	150

*DISCUSSION FIGURES*

**Figure 33.** Proposed model of mitochondrial damage after I/R and preservation of mitochondrial function in the context of COX-2 overexpression..... 168

**Figure 34.** Proposed model of cell and tissue injury by I/R and the role of COX-2 in protecting and reducing liver damage..... 170





## ANNEX 3 – INDEX OF TABLES

## MATERIALS AND METHODS TABLES

<b>Table 1.</b> Lysis Buffer for DNA extraction.....	75
<b>Table 2.</b> Primers for PCR genotyping of <i>PTGS2</i> .....	75
<b>Table 3.</b> PCR Master Mix.....	76
<b>Table 4.</b> PCR program for <i>PTGS2</i> detection .....	76
<b>Table 5.</b> Mitochondria Isolation Buffer (mIB).....	79
<b>Table 6.</b> Lysis Buffer for protein extraction .....	83
<b>Table 7.</b> Laemli sample Buffer .....	84
<b>Table 8.</b> Western blot buffers.....	85
<b>Table 9.</b> Buffers for the isolation of mitochondrial supercomplexes.....	86
<b>Table 10.</b> Primary Antibodies used for Western blot (WB) and Immunofluorescence (IF).....	86
<b>Table 11.</b> DNA Isolation Buffers.....	89
<b>Table 12.</b> Reverse Transcription (RT) program .....	90
<b>Table 13.</b> qPCR programs for SYBRGreen and TaqMan reagents .....	91
<b>Table 14.</b> Primers for qPCR.....	92
<b>Table 15.</b> Primers for <i>Xbp1</i> cDNA PCR and splicing detection .....	93
<b>Table 16.</b> PCR program for <i>Xbp1</i> splicing detection .....	93
<b>Table 17.</b> MiR05 medium composition .....	101
<b>Table 18.</b> Substrates, decoupling agents, and inhibitors for high-resolution respirometry protocols.....	102

*RESULTS TABLES*

**Table 19.** GR, GPX and CAT enzymatic activities. .... 133

## ANNEX 4 – PUBLICATIONS

Part of the results obtained and presented in this PhD thesis has been published in the following scientific articles:

- Motiño O, Francés DE, Casanova N, **Fuertes-Agudo M**, Cucarella C, Flores JM, Vallejo-Cremades MT, Olmedilla L, Pérez Peña J, Bañares R, Boscá L, Casado M, Martín-Sanz P. **Protective Role of Hepatocyte Cyclooxygenase-2 Expression Against Liver Ischemia-Reperfusion Injury in Mice**. *Hepatology*. 2019 Aug;70(2):650-665.  
[doi: 10.1002/hep.30241](https://doi.org/10.1002/hep.30241)
- **Fuertes-Agudo M**, Luque-Tévar M, Cucarella C, Brea R, Boscá L, Quintana-Cabrera R, Martín-Sanz P, Casado M. **COX-2 Expression in Hepatocytes Improves Mitochondrial Function after Hepatic Ischemia-Reperfusion Injury**. *Antioxidants (Basel)*. 2022 Aug 30;11(9):1724.  
[doi: 10.3390/antiox11091724](https://doi.org/10.3390/antiox11091724).